TAL
TECH

DOCTORAL THESIS

Co-Pyrolysis of Biomass and Oil Shale

Alejandro Lyons Cerón

TALLINNA TEHNIKAÜLIKOOL
TALLINN UNIVERSITY OF TECHNOLOGY
TALLINN 2024

Co-Pyrolysis of Biomass and Oil Shale

ALEJANDRO LYONS CERÓN

TALLINN UNIVERSITY OF TECHNOLOGY
School of Engineering
Department of Energy Technology
This dissertation was accepted for the defence of the degree 26/04/2024

Supervisor: Professor Alar Konist
                         School of engineering
                         Tallinn University of Technology
                         Tallinn, Estonia

Opponents: Professor Bo G Leckner
                         Energy Technology
                         Chalmers University of Technology
                         Gothenburg, Sweden

                         Professor Timo Kikas
                         Institute of Forestry and Engineering
                         Estonian University of Life Sciences
                         Tartu, Estonia

Defence of the thesis: 10/06/2024, Tallinn

Declaration:
Hereby I declare that this doctoral thesis, my original investigation, and achievement, submitted for the doctoral degree at Tallinn University of Technology has not been submitted for doctoral or equivalent academic degree.

Alejandro Lyons Cerón

----
                                                        signature

Lyons Ceron, A. (2024). Co-Pyrolysis of Biomass and Oil Shale [TalTech Press]. https://doi.org/10.23658/taltech.27/2024

TALLINNA TEHNIKAÜLIKOOL
DOKTORITÖÖ
27/2024

Biomassi ja põlevkivi koospürolüüs

ALEJANDRO LYONS CERÓN

TAL
TECH
KIRJASTUS

Contents

List of publications

The list of author's publications, based on which the thesis has been prepared:

I   **Cerón, A.L.**; Konist, A.; Lees, H.; Järvik, O. (2021). Current status of co-pyrolysis of oil shale and biomass. Oil Shale, 38 (3), 228–263. DOI: 10.3176/oil.2021.3.04.

II **Lyons Ceron, Alejandro**; Ochieng, Richard; Sarker, Shiplu; Järvik, Oliver; Konist, Alar (2024). Co-Pyrolysis of Woody Biomass and Oil Shale—A Kinetics and Modelling Study. Energies, 17 (5), #1055. DOI: 10.3390/en17051055.

III **Lyons Cerón, Alejandro**; Konist, Alar (2023). Co-Pyrolysis of Woody Biomass and Oil Shale in a Batch Reactor in CO2, CO2-H2O, and Ar Atmospheres. Energies, 16 (7), #3145. DOI: 10.3390/en16073145.

IV **(Accepted, to be published) Lyons Cerón, Alejandro**; Konist, Alar; Pihu, Tõnu (2024). Co-pyrolysis of biomass woodchips with Ca-rich oil shale fuel in a continuous feed reactor. Oil shale, Vol. 41, Issue 3, 2024.

Author's contributions to the publications

Contributions to the papers in this thesis are:

I   Identifying the research topic, performing a literature search, identifying gaps and novelty, organizing information, writing, and revision.

II   Design of the experiment, setting up experimental apparatus, sample preparation, conducting the experimental work, data collection, and analysis, collaboration on the computational model, writing, and revision.

III   Design of the experiment, setting up experimental apparatus, sample preparation, conducting the experimental work, data collection and analysis, writing and revision.

IV   Design of the experiment, setting up experimental apparatus, sample preparation, conducting the experimental work, data collection and analysis, writing and revision.

Introduction

Global climate concerns and the ever-increasing worldwide demand for energy have encouraged extensive research into clean alternative energy sources [1]. Moreover, the European Union aims to significantly reduce greenhouse gas emissions by 2050 through the EU Green Deal. The implementation of clean energy technologies is imperative to achieve these objectives. A promising approach to achieving carbon neutrality involves the co-conversion of renewable fuels and fossil fuels, such as biomass and oil shale. Both biomass and oil shale are utilized in thermochemical conversion processes, yielding solid, liquid, and gaseous products with various applications in the energy sector and chemical industry [2].

Biomass, a carbon-neutral renewable resource, is used extensively and has been investigated as a source of energy and for the production of valuable products, such as bio-oil, absorbent materials, biogas, and chemicals. Biomass resources could potentially meet up to 14% of the world's energy demands [1]. Furthermore, the use of biomass could contribute to a reduction of over one billion tons of carbon dioxide emissions [2], mitigating some of the environmental impact related to the utilization of traditional fossil fuels [3], [4]. Biomass is cleaner than coal and is the only renewable carbon resource that can be directly converted into fuel. Accordingly, biomass can contribute significantly to the world's energy needs if harnessed sustainably. However, there are certain problems associated with the thermal conversion of biomass, including its high moisture and oxygen contents, while bio-oil is subject to problems associated with its high-density viscosity, water content, and oxygenated-compound content, which decrease its energy density, shelf life, and stability, increase its corrosiveness, and necessitate additional processing and refining [5], [6].

Oil shale is an unconventional fossil fuel extracted from geological deposits found in various regions worldwide, including Estonia, the United States, Jordan, and China [7]. Oil shale is characterized by high contents of kerogen, inorganic matter, and ash. Kerogen, the organic component of oil shale, can be converted into valuable products such as shale oil, which is a valuable product for the chemical industry [8] owing to its high content of aliphatic hydrocarbons and its potential for conversion to shale gas through thermochemical processes [9]. However, there are also challenges in the thermal conversion of oil shale, including its low contents of C and H, high sulfur content (above 1.7 wt%), high ash content (above 50 wt%), and emissions of NO_x and SO_x [10], [11].

The co-pyrolysis of oil shale and biomass is a promising strategy to mitigate problems associated with the unfavourable properties of bio-oil while simultaneously decreasing the generation of unfavourable products and pollutants by oil shale pyrolysis. Oil shale and biomass share similarities in the operational and thermal conditions required during their pyrolysis, facilitating their co-conversion by co-pyrolysis, as well as study of the thermal behaviour and yields of the solid, liquid, and gaseous products [12]. During co-pyrolysis, oil shale can influence oxygen distribution in the biomass products, causing an increase of CO_2 and CO in the gaseous products and a reduction of unwanted oxygen-containing compounds in the biomass oil. Biomass, on the other hand, can participate in heat transfer mechanisms to improve pyrolysis of the oil shale.

Clearly, researching the co-pyrolytic behaviour of these two fuels has great potential. Specifically, the co-pyrolysis of oil shale and biomass may result in a more

environmentally friendly alternative for the production of energy and chemicals, reducing emissions from oil shale utilization and increasing the use of biomass waste resources [13]. The results of such research could be used to better understand the pyrolytic behaviour of oil shale and biomass blends for the proper design of industrial thermal conversion systems.

Figure 1 shows the yields of products from pyrolysis, as well as the advantages and disadvantages of oil shale and biomass utilization.

- 50-75 wt% liquids
- 20-25 wt% biogas
- 10-25 wt% solids
- Pyrolysis at 250-500 °C

Biomass

- 5-20 wt% Shale oil
- 5-20 wt% shale gas
- 60 wt% semicoke
- Pyrolysis at 450-550 °C

Oil shale

- High content of C, H and volatile matter
- LHV of 15-19 MJ/kg
- Low ash content (≈ 1wt% for woody biomass)
- Max yield of bio-oil at 500-550 °C

- High moisture content in biomass (5-20 wt%) dry basis
- High oxygen content
- High density bio-oil (1.0-1.2 kg/m3)
- High viscosity of bio-oil (40-100 mPa·s)
- High share of water in bio-oil (15-35 wt%)
- Oxygenated compounds (phenols, acids, ketones, aldehydes)

- Low moisture content (<2 wt%)
- Max yield of shale oils at 480-520 °C
- Shale oil with high C content (75-85 wt%)
- Shale oil with high H content (10-15 wt%)
- Low density of shale oil (0.80-0.95 kg/m3)
- Aliphatic hydrocarbons in shale oil (alkanes, alkenes, alkynes)

- Low content of C, H and volatile matter
- High sulfur content (>1.7 wt%)
- LHV of 5-20 MJ/kg
- High ash content (>50 wt%)
- Emissions of NOx and SOx
- Aromatic hydrocarbon in shale oil

Figure 1. Yields of products and advantages (green) and disadvantages (red) of biomass and oil shale

Research topics

Thermochemical conversion processes are widely used and essential for the production of heat, power, and valuable fuels and chemicals. An in-depth study of the thermal breakdown of the organic components of fuels into solid, liquid, and gaseous products allows the characterization of these products and the optimization of the process to achieve cleaner and more efficient conversion.

Pyrolysis is a thermochemical conversion process where fuel is decomposed under a controlled temperature and atmosphere environment to produce high-heating-value oils, gases, and solids.

Due to the similarity in their thermal and operational pyrolysis conditions, **biomass and oil shale** are potentially suitable for **co-pyrolysis** processes, as both biomass and oil shale pyrolysis occur in the same temperature range.

In the co-pyrolysis of biomass and oil shale, both fuels can interact and/or influence the **yields and quality of the co-pyrolysis products**. This results in products with combined properties, such as a reduction in the oxygen-containing compounds present in the bio-oil, increased yields of oil and gas, a reduction in the yield of solids (from the high ash content of oil shale), and a reduction in the sulphur content derived from oil shale, among others.

Aims and objectives

This research aims to investigate the co-pyrolytic behaviour of biomass and oil shale, as well as the co-pyrolysis products. The research objectives proposed are the following:

- Review important research on the co-pyrolysis of oil shale and biomass
- Conduct experiments on co-pyrolysis of oil shale and biomass under different operational conditions and at different experimental scales
- Characterize and study the products obtained from co-pyrolysis of oil shale and biomass

Through these objectives, the research aims to study:

- The feasibility of co-pyrolysis as well as the improvement of the pyrolysis process and of the yields and composition of the co-pyrolytic products
- The mitigation of problems associated with individual pyrolysis, including the undesirable properties of bio-oil and the environmental impact of oil shale pyrolysis
- Co-pyrolysis behaviour, i.e., possible interactions in co-pyrolysis through chemical reactions and heat-transfer mechanisms to yield products with enhanced properties

Research tasks

- **Publication I:** Conduct a literature overview of oil shale and biomass co-pyrolysis including:
    - Individual pyrolysis of oil shale and biomass
    - Co-pyrolysis processes and the effects of co-pyrolysis
    - Oil shale and biomass co-pyrolysis
    - Interactions in co-pyrolysis
    - Effects of fuel mixing ratios, hydrogen content, and catalytic effects
    - Yields and composition of co-pyrolysis products
    - Effects of temperature, heating rate, particle size, and different gas atmospheres
- **Publications II–IV**: Conduct laboratory-scale experiments on co-pyrolysis of oil shale and biomass, including:
    - Selection, preparation, and characterization of fuels
    - **Publication II:** Experiments with Thermogravimetric Analysis Equipment
    - **Publication III:** Experiments with a Batch Reactor
    - **Publication IV:** Experiments with a Continuous Feed Reactor
- Collect and characterize co-pyrolysis products
    - Characterize solid and liquid products in terms of elemental, proximate analysis, and calorimetry
    - Determine the chemical compounds present in co-pyrolysis oil, using analytical methods
- **Publication II**: Determine kinetics and model the process
    - Kinetic modelling of co-pyrolysis to determine apparent activation energies and activation energies at different conversion stages
    - A process model to predict the co-pyrolysis mass loss curves

Methodology

The methodology follows the structure of the research tasks, where the core of the research is based on the literature overview, from which the experiments are planned. The experimental conditions are derived from the optimal conditions required to maximize the yields and quality of co-pyrolysis products, as determined based on the literature on individual pyrolysis of oil shale and biomass, and from co-pyrolysis of oil shale, biomass, and other fuels. The literature overview identifies the research trends to propose a novel work. Based on the literature overview, the fuel characteristics are chosen, including particle size, mixing ratios, and fuel preparation. The co-pyrolysis experimental conditions are also chosen based on thorough research of the required operational parameters (temperature, heating rate, gas atmosphere, and residence time). The experiments are followed by characterization of the products and analysis of their yields and composition. The results from fuel decomposition (mass loss) obtained from thermogravimetric analysis studies are implemented in a model to determine the kinetic parameters and predict the mass-loss curves for co-pyrolysis. A schematic of the structure of the research methodology is shown in Figure 2.
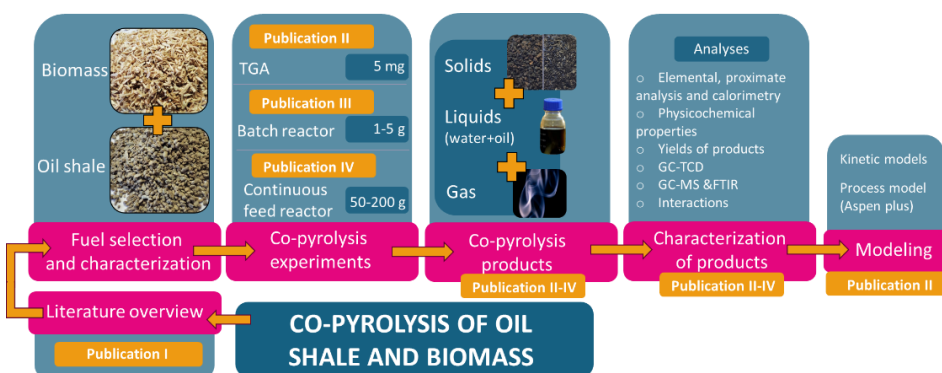

Figure 2. Structure of the methodology implemented in this doctoral research

Novelty

The current work was structured based on an in-depth literature overview. The purpose of the overview was to identify the main factors affecting the pyrolysis and co-pyrolysis of oil shale and biomass, and additionally to identify research gaps in the co-pyrolysis of oil shale and biomass. The framework of the experimental methodology was arranged based on this literature overview.

Previous research has focused on the study of interactions between fuels in co-pyrolysis, which can have a synergetic effect or an inhibiting effect on the pyrolysis decomposition or the yields and quality of products. While some studies have observed a synergetic behaviour, other research has demonstrated an additive behaviour in the yields and quality of co-products. This previous research has not had a conclusive result on interaction in co-pyrolysis (See **Publication I** for details). Therefore, thorough research is necessary to determine the existence of interactions and study the benefits of co-pyrolysis, i.e., whether the behaviour is additive or synergistic.

The current study is unique in its approach, employing three distinct experimental setups at three different scales, each utilizing specialized equipment and analytical

methods. This comprehensive approach enables an in-depth investigation of the co-pyrolysis of oil shale and biomass at multiple experimental scales. The experiments are conducted with the same operational conditions, optimized for high product yields (gas and liquid products). The research includes an analysis of interactions or additive behaviour in the three types of experiments, using various mixtures of oil shale and biomass, and a comparison of the results between the experiments. This contributes to obtaining more conclusive results on the existence or absence of interactions in oil shale/biomass co-pyrolysis.

The research comprises a comprehensive set of analyses to fully characterize the co-pyrolysis products. From thermogravimetric analysis with kinetic and process modelling and analysis of the composition of liquid and solid products to analytical methods to identify the chemical compounds and functional groups present in the co-pyrolysis liquid products.

A novel aspect of this research is the use of kinetic data and thermogravimetric results in a process model. Most kinetic studies on co-pyrolysis calculate kinetic parameters based on different models but do not proceed to apply these valuable results. The current research uses the thermogravimetric results and kinetic parameters in a process model to predict the mass loss (fuel decomposition) in co-pyrolysis. This allows the use of these results for design and optimization with larger-scale equipment.

The current work also studies the yields of co-pyrolysis at different residence times to identify the differences in the pyrolysis behaviour between oil shale and biomass. Moreover, various alternative co-pyrolysis atmospheres are tested to study the effect of different carrier gases in the decomposition process.

A detailed analysis of the composition of the products is conducted, especially of the liquid products, allowing the characterization and comparison of pyrolysis oils from oil shale and biomass, thus identifying the advantages of co-pyrolysis in terms of product composition. The study compares the results obtained with various characterization and analytical techniques to verify the characteristics of the oils and analyse the existence of interactions during co-pyrolysis.

The current study aims to demonstrate the benefits of oil shale and biomass co-pyrolysis, regardless of whether synergistic interactions exist between the fuels or if the process follows an additive behaviour. Several studies have concentrated on synergistic effects. However, a comprehensive study of oil shale and biomass co-pyrolysis behaviour and the yields and composition of its products is of great importance if we are to achieves sustainable and efficient biomass and oil shale valorisation and a valuable alternative to the thermochemical conversion of individual fossil or renewable fuels.

Approbation of the research results

I.   **Cerón, A.L.**; Konist, A.; Lees, H.; Järvik, O. (2021). Current status of co-pyrolysis of oil shale and biomass. Oil Shale, 38 (3), 228–263. DOI: 10.3176/oil.2021.3.04.

II. **Lyons Cerón, Alejandro**; Ochieng, Richard; Sarker, Shiplu; Järvik, Oliver; Konist, Alar (2024). Co-Pyrolysis of Woody Biomass and Oil Shale—A Kinetics and Modelling Study. Energies, 17 (5), #1055. DOI: 10.3390/en17051055.

III. **Lyons Cerón, Alejandro**; Konist, Alar (2023). Co-Pyrolysis of Woody Biomass and Oil Shale in a Batch Reactor in CO_2, CO_2-H_2O, and Ar Atmospheres. Energies, 16 (7), #3145. DOI: 10.3390/en16073145.

IV. **(Accepted, to be published) Lyons Cerón, Alejandro**; Konist, Alar; Pihu, Tõnu (2024). Co-pyrolysis of biomass woodchips with Ca-rich oil shale fuel in a continuous feed reactor. Oil shale, Vol. 41, Issue 3, 2024.

Participation in scientific conferences

I. **Lyons Ceron, A.**; Konist, A.; Lees, H.; Järvik, O. (2021). Effect of Estonian woody biomass gasification temperature on the composition of the producer gas. European Conference on Renewable Energy Systems, Turkey, 21-23 April 2021. Erciyes University, 135–139.

II. Konist, A.; Lees, H.; **Ceron, A. L**. (2021). Co-pyrolysis of woody biomass and oil shale in N_2, CO_2, and CO_2-H_2O atmospheres. Sustainable Energy & Environmental Protection: BOKU, Vienna, Austria. Ed. Christoph Pfeifer, Rafat Al Afif, Abdul Ghani Olabi. SEEP 2021 Conference, 67–71.

III. **Lyons Ceron, A.**; Konist, A. (2022). Co-pyrolysis of woody biomass and oil shale in a batch reactor in CO_2, CO_2-H_2O, and Ar atmospheres. Proceedings of the 25th Conference on Process Integration, Modelling and Optimisation for Energy Saving and Pollution Reduction, 5 September – 8 September 2022, Bol, Croatia.

IV. **Lyons Cerón, Alejandro**. (2023). Kinetics and modelling study of woody biomass and oil shale co-pyrolysis in N_2 and CO_2 atmospheres using TGA. Fuel and Research Forum Conference, 2nd European Conference on Fuel and Energy Research and its Applications. Sheffield, United Kingdom.

Abbreviations

A	Pre-exponential factor
BM	Biomass
CCUS	Carbon capture, utilization, and storage
E	Activation energy
FTIR	Fourier-transform infrared spectroscopy
GC-MS	Gas chromatography-mass spectrometry
GC-TCD	Gas chromatography with thermal conductivity detector
HHV	Gross calorific value
IR	Infrared
LHV	Net calorific value
OS	Oil shale
R^2	Coefficient of determination
RI	Refractive index
RSD	Relative standard deviation
TGA	Thermogravimetric analysis

1 Literature overview

This section contains a summary of the co-pyrolysis of biomass (BM) and oil shale (OS). The first publication (**Publication I**) is an extensive literature overview of all the most relevant aspects for consideration in OS and BM co-pyrolysis, including the pyrolysis of OS and BM individually, co-pyrolysis processes and the effects of co-pyrolysis, OS and BM co-pyrolysis, the effects of operational conditions and fuel characteristics, and interactions during co-pyrolysis.

1.1 Thermochemical conversion processes – Pyrolysis and co-pyrolysis

Pyrolysis is a type of thermochemical conversion process that occurs in a controlled inert atmosphere (absence of oxygen), where fuels are thermally decomposed. Decomposition of the large organic molecular structures in the fuel results in the production of solid, liquid, and gas products [12], [14]. The pyrolysis of fuels results in high-heating-value liquid oils, which are used in the energy and chemical industries for various applications, including, turbines, engines, and furnaces, and in the petrochemical industry [15]. Pyrolysis gas also has valuable applications as a high-energy-content gas with numerous uses in heat and power generation [16]. The solid products from pyrolysis have high carbon contents and high porosity, making them suitable for applications as adsorbent chars or biochar. Figure 3 shows the different products and applications of pyrolysis and other thermochemical conversion processes.
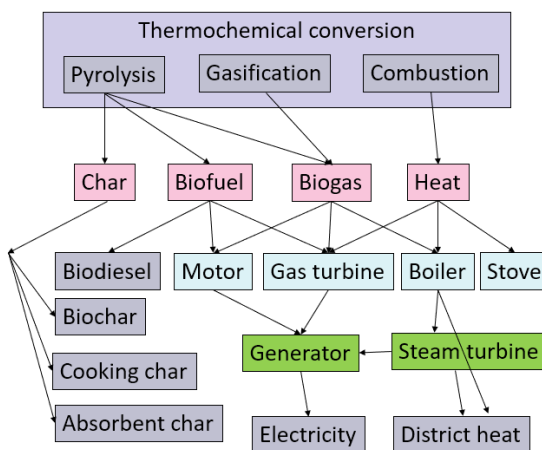

Figure 3. Schematic showing the products and applications of the thermochemical conversion of fuels

The co-conversion of fuels is a type of pyrolysis process whereby two or more fuels are pyrolyzed in the same reactor under the same operational conditions. The thermal degradation in co-pyrolysis occurs through several chemical reactions and heat transfer mechanisms [17], resulting in co-pyrolysis products with combined properties [12]. The study of co-pyrolysis allows the identification of possible interactions between the fuels as well as analysis of the yields and composition of the pyrolysis products. Co-pyrolysis can potentially result in products with improved properties, a sustainable solution for the use of waste residues, and a reduction of the environmental effects of

pyrolyzing fossil fuels [13], [18]. Thus, there is need to study the co-pyrolysis of fuels in terms of the effects of operational conditions and the yields and composition of co-pyrolysis products; which properties and yields are the result of additive behaviour or/and depend on interactions between the fuels; and which factors can promote or inhibit the co-pyrolysis process [19].

A valuable fuel with applications in co-pyrolysis is BM. BM has been studied as a fuel for use in co-pyrolysis with fossil fuels to reduce the environmental impact of the energy and fuel industries. BM has been implemented in co-pyrolysis to not only decrease the use of fossil fuels, but also to reduce emissions of gases such as CO_2, H_2S, NO_x, and SO_x [20], [21]. The composition of BM, including its H/C ratio, high volatile matter, and low ash content, can result in improved pyrolysis of fossil fuels, increasing the yields of desirable products and enhancing the pyrolytic process [22]–[25].

1.2 Utilization of solid fuels – Biomass

BM is a renewable resource that is considered carbon-neutral when sourced and used sustainably. BM is one of the most important renewable resources, as it can potentially supply 14% of the world's energy needs [1], [26], [27]. Its utilization has the potential to contribute to a decrease in use of fossil fuels, and thus a reduction of up to 1.3 billion tons of CO_2 emissions [2]–[4], [28]. BM has a high content of volatile matter, an LHV of 15–19 MJ/kg [29], and a low content of ash. These properties allow its use for the production of valuable bio-oils, biogas, fuels, chemicals, petroleum substitutes, semi coking products, and activated carbons [21], [30], [31].

As a sustainable fuel, BM can be utilized in various thermochemical conversion processes. Of these processes, the pyrolysis of BM is converts it into valuable solid, liquid, and gaseous products [32], [33]. BM is composed of hemicellulose, cellulose, and lignin. These three components define the pyrolysis decomposition behaviour of BM, as well as the yields and composition of the pyrolysis products [34]. Woody BM, a type of BM from wood resources, is mostly composed of hemicellulose and cellulose (50–80 wt%) [34]. Hemicellulose and cellulose pyrolysis occur at temperature ranges of 220–315 °C and 350–400 °C, respectively. Lignin, the remaining component of woody BM, decomposes at temperatures above 400 °C [35].

The yields and composition of the BM pyrolysis products depend upon, among other factors, the operational conditions (temperature, heating rate, particle size, type of reactor, etc). The effect of the operational parameters in BM pyrolysis has been widely studied [36], [37], [46]–[48], [38]–[45]. In addition to the operational parameters, the type of pyrolysis (torrefaction, carbonization, conventional pyrolysis, intermediate pyrolysis, fast pyrolysis, and flash pyrolysis) defines the yields and composition of products. Conventional pyrolysis results in 50 wt% of liquids, 20–25 wt% of gas, and 20–25 wt% of solids. Fast and flash pyrolysis favour the yields of liquids, with up to 75 wt% of liquids, below 20 wt% of gas, and 13–25 wt% of solids [49]. Pyrolysis temperature is one of the most important parameters defining the yields of products. For BM, a maximum yield of bio-oil is typically achieved at 520 °C [49]. Above this temperature, the process will result in lower yields of oils (favouring the yields of gas products), and with inferior quality due to higher moisture and oxygen contents [39].

Bio-oil is considered a valuable product from BM pyrolysis and it has various applications. It can be refined into biofuels like biodiesel and bioethanol. Additionally, its chemical compounds make it valuable for producing plastics, solvents, and adhesives. Bio-oil can also be burned directly for heat and power generation, used as a

soil amendment for agriculture, and processed into chemicals and carbon materials. Furthermore, it serves as a precursor for bio-based polymers [35], [50], [51]. Bio-oil is dark and viscous and it has certain unfavourable properties owing to its high contents of water (15–35 wt%) and oxygenated compounds, acids, ethers, and sugars [52]. Additionally, bio-oil is unstable, requiring further processing to reduce its unfavourable properties, such as high corrosiveness, chemical volatility, and viscosity [5], [6]. Thus, bio-oil requires refining and upgrading to enhance its suitability as a fuel and ensure compatibility with existing energy conversion technologies. Nevertheless, bio-oil has notable advantages, such as low toxicity and biodegradability.

1.3 Utilization of solid fuels – Oil shale

OS is a sedimentary rock found in geological formations that is composed of organic matter (kerogen), ash, and inorganic matter. There are large deposits of OS all over the world, exceeding those of crude oil reserves [53], [54]. The United States, China, Estonia, Morocco, Canada, Jordan, and Brazil are among the counties with the largest proven OS reserves [7], [55], [56]. Depending on the type of OS, it can have an LHV of 5–20 MJ/kg, an organic matter content from 5 to 80 wt%, and up to 70 wt% of ash [57].

The high content of organic matter in OS allows its use in thermochemical conversion processes, such as direct combustion, gasification, and pyrolysis, resulting in the production of heat and valuable products [9], [57]–[59]. During pyrolysis, the kerogen in OS is transformed into shale oil, shale gas, semicoke, and ashes [60]–[62] with yields of up to 20 wt% of shale oil, 5-20 wt% shale gas, and 60 wt% semicoke [63]. The yields and composition of OS pyrolysis products depend on the operational parameters [64], including temperature, heating rate, reactor, and particle size, among others. The effects of these parameters have been previously studied in depth [11], [17], [73]–[80], [65]–[72]

Shale oil is a valuable product obtained by the conversion of oil shale, with high energy content, versatility and stability, a viscosity and density comparable to those of crude oils, a high content of aliphatic hydrocarbons, high C and H contents, and a lower moisture content than that of BM [8], [81], [82]. However, there are challenges in the pyrolysis of OS. Some of these challenges include reducing its environmental effects, as the retorting of OS can produce high amounts of polluting gases, such as CO_2, while OS pyrolysis also produces a lot of ashes. Additionally, improving the quality and composition of the pyrolysis products is necessary [10], [11]. For instance, OS has certain unfavourable properties [10], [11], including high contents of nitrogen and sulphur, and emissions of NO_x and SO_x from its utilization [82]–[84]. Numerous initiatives have been taken to utilize the solid products from OS conversion and to shift from OS combustion to shale oil production [84]–[88] due to the decrease in the environmental impact and the increased profitability, compared to utilizing OS for power generation.

1.4 Oil shale and biomass co-pyrolysis

The co-pyrolysis of BM and OS has great potential to produce more sustainable and improved pyrolysis products. Co-pyrolysis of OS and BM is a more environmentally benign alternative for the production of fuels and chemicals due to the reduction of solid residues and emissions of pollutant gases, as well as the utilization of BM waste [13], [25], [70], [89]. During co-pyrolysis, the fuels go through degradation under the

same operational conditions, which can result in interactions from chemical reactions and heat-transfer mechanisms, improving the yields and quality of the products. The co-pyrolysis products can exhibit a combination of properties imparted by OS and BM pyrolysis [12]. The study of OS and BM co-pyrolysis is thus essential to understanding the its products and characteristics.

BM and OS share similarities in the thermal conditions required for their pyrolysis, allowing their use in co-pyrolysis. This co-compatibility allows for the use of BM in existing large-scale equipment used for OS conversion. Both fuels decompose at 350–520 °C to produce high yields of liquid products (bio-oil and shale oil) [70]. However, most BM pyrolysis occurs at lower temperatures than that required for OS pyrolysis (See Publication II), which can result in heat-transfer interactions that enhance the OS pyrolysis [33] in terms of the yields and properties of the pyrolysis products [74], [75]. BM's low ash content and high volatile-matter content result in OS-BM mixtures with lower yields of ash-containing solid products and higher yields of liquid and gaseous products [12]. Additionally, the high hydrogen content of BM allows it to act as a hydrogen donor, enhancing OS pyrolysis [90] and promoting thermal cracking [91]. Some studies on OS and BM co-pyrolysis have noted an increase in product yields, improved product properties, and enhanced thermal cracking [69], [75], [92]. However, improvements due to such interactions are not observed in all studies and appear to depend strongly on the co-pyrolysis conditions and the fuels utilized [93]. **Error! Reference source not found.** summarizes reported studies on the co-pyrolysis of OS and BM, including that of peanut shells, wheat straw, alkaline lignin, spirulina, pine sawdust, and corn stalks [92]–[98]. The effects of synergy, OS:BM ratios, catalysts, and hydrogen are shown in **Publication 1**.

*Table 1. Biomass and oil shale co-pyrolysis studies, fuels utilized, yields of products, and observations (From **Publication 1**)*

BM type	OS type	Blend ratio BM:OS	Oil yield (%wt)	Gas yield (%wt)	Water yield (%wt)	Solid yield (%wt)	Main co-pyrolysis observations
E. rigida [10]	Seyitomer (Turkey)	1:0	25–30	50–55 (water+gas)		15–20	- Higher oil yields - No synergy*
		1:1	15–20	55–60 (water+gas)		20–25	
		0:1	5–10	40–55 (water+gas)		30–35	
Terebinth berries [74]	Goynuk (Turkey)	1:0	40–41 (total liquid)	22–26	-	32–37	- Improved oil quality - No synergy
		1:1	38–44 (total liquid)	18–25	-	36–44	
		0:1	37–46 (total liquid)	10–16	-	37–52	
Spent mushroom [75]	Huadian (China)	1:0	9–11	37–40	9–14	36–50	- Synergy - Higher yields of usable product
		1:1	7–17	24–40	2–4	50–61	
		0:1	7–17	15–20	0–2	65–76	
Wheat	Huadian	1:0	17	12.5	9	61	- Improved oil

BM type	OS type	Blend ratio BM:OS	Oil yield (%wt)	Gas yield (%wt)	Water yield (%wt)	Solid yield (%wt)	Main co-pyrolysis observations
straw grain [69]	(China)	3:1	18	10	8.5	63	quality - Synergy - OS acted as a catalyst
		1:1	18	8	8	64	
		1:3	19	7	7.5	65	
		0:1	20	5	7	66	
Wood pellet [70]	Huadian (China)	1:0	8	65	10	27	- Improved oil quality - Synergy - Higher oil yields up to 520 °C
		3:1	10	42	8	40	
		1:1	13	30	6	50	
		1:3	17	20	4	60	
		0:1	20	13	1	67	
Pine and spruce [64]	Kukersite (Estonia)	1:0	16–26	20–21	24–26	28–39	- Significant differences in OS and BM pyrolysis oils
		0:1	28	8	6	58	
C. vulgaris Microalgae [99]	Guandong Maoming (China)	1:0	89 (liquid+gas)			10	- Synergy - Solid residues acted as catalysts - Higher yields of usable product
		9:1	78 (liquid+gas)			21	
		7:3	68 (liquid+gas)			32	
		1:1	59 (liquid+gas)			41	
		0:1	30 (liquid+gas)			70	

*Existence of promotion or inhibition effects due to interactions between fuels. Synergy existed in experiments where there was a difference in the experimental and calculated yields of products. The yields displayed are from experimental results.

2 Materials and methods

The experimental studies were organized in a structure that allows analysis and comparison of the co-pyrolysis of BM and OS at different experimental scales. These co-pyrolysis experiments apply different OS and BM mixtures in thermogravimetric analysis equipment **(Publication II)**, a batch reactor **(Publication II),** and a continuous feed reactor **(Publication III)**. Table 2 Displays the scale of experiments conducted on each type of equipment.

Table 2. Co-pyrolysis experiments conducted

Experimental Equipment		Fuel used	Capacity
(Publication II)	Thermogravimetric analyser	Woody BM and OS	5–20 mg
(Publication III)	Batch reactor	Woody BM and OS	1–5 g
(Publication IV)	Continuous feed reactor	Woodchips and OS	0.01–0.5 kg/h

A detailed methodology for each type of experiment is shown in **Publications II, III,** and **IV**. Overall, for each experimental setting, the research methodology was divided into:

- Materials
    - Selection and preparation of fuels: Grinding, sieving, mixing, storage
    - Fuel characterization: Elemental and proximate composition, and calorimetry
- Experimental setup
    - Operational conditions: Temperature, heating rate, particle size, carrier gas, residence time
    - Collection of pyrolysis products: Mass balance, yields, condensations
- Characterization of pyrolysis products:
    - Elemental and proximate composition, and calorimetry
    - Physicochemical properties
    - GC-TCD, GC-MS, FTIR
    - Analysis of interactions: calculation of theoretical yields
- Kinetics and computational modelling (**Publication II**)
    - Kinetic analysis
    - Input of model parameters
    - Model validation and prediction of mass-loss curves

2.1 Materials

Two types of fuel were used in co-pyrolysis: OS and BM. For BM, woodchips and woody BM species including Norway spruce *(Picea abies)*, grey alder (*Alnus incana*), Scots pine (*Pinus sylvestris*), and silver birch (*Betula pendula*) were used as a BM mixture. For OS, Estonian OS was used.

2.1.1 Selection and preparation of fuels

BM and OS samples were ground and sieved to the required particle size. The prepared samples were dried to remove moisture and mixed into the specified mixing ratios. The prepared samples were stored in airtight bags. Details on the sample preparation and the standards followed can be read in **Publications II–IV.** Table 3 **s**hows the sample preparation conditions used for each case.

Table 3. Sample preparation

Experimental equipment	BM				OS	Particle size	Drying	Mixing deviation
Thermogravimetric analyser	Spruce (25 wt%)	Alder (25 wt%)	Pine (25 wt%)	Birch (25 wt%)	OS 100 wt%	< 0.125 mm	105 °C for 3 h	±1%
Batch reactor	Spruce (25 wt%)	Alder (25 wt%)	Pine (25 wt%)	Birch (25 wt%)	OS 100 wt%	0.5–1 mm	105 °C for 3 h	±2%
Continuous feed reactor	Woodchips				OS 100 wt%	0.25–1.3 mm	105 °C for 3 h	±2%

2.1.2 Fuel characterization

OS and BM were characterized in terms of elemental composition (C, H, N, S) using a Vario MACRO CHNS Cube system Proximate analyses (ash content, moisture content, fixed carbon, and volatile matter) and calorimetry (HHV and LHV) were performed using bomb calorimeters (IKA 2000C, and IKA 5000C).

2.2 Experimental set-up

The co-pyrolysis experiments were conducted in three different types of reactors with different capacities. All experiments were conducted in temperature ranges of 500–550 °C, a temperature range previously identified as providing the maximum yield of liquid products for OS and BM [71]. As mentioned above, higher temperatures can increase the yields of gas and decrease the yields of liquid products [99], [49]. The purpose of each type of experiment is explained as follows:

- **Thermogravimetric analysis** equipment: TGA experiments were conducted to:
  - Understand the **decomposition behaviour** of **OS, BM**, and **OS:BM** mixtures. These experiments allow the study of mass loss as the temperature increases at a constant rate
  - Identify the **differences** in pyrolytic behaviour **between OS and BM**
  - Identify the temperature peaks of decomposition for both OS and BM, i.e., where most of the decomposition occurs
  - Study the effect of different carrier gases (N_2 and CO_2) in co-pyrolysis
  - Determine the **kinetic properties** of OS and BM
  - **Model the mass loss** of OS:BM mixtures
- **Bath reactor**: Co-pyrolysis in the batch reactor was carried out to:
  - Produce and collect gas and solid products from pyrolysis and co-pyrolysis
  - Study the **effect of the residence time** in pyrolysis and co-pyrolysis
  - Study the effect of different carrier gases (CO_2, $H_2O:CO_2$ 1:1, Ar) in co-pyrolysis
  - Study the **possible interactions** due to co-pyrolysis in the yield of solid products
  - Characterize **the solid products** in terms of elemental composition and surface area
  - Determine the **composition of the main gases** present in the gas products

- **Continuous feed reactor**: Experiments on the continuous feed reactor were conducted to:
  - Produce a sufficiently **large sample of solid and liquid** pyrolysis products for characterization
  - Determine the **yields of products** in pyrolysis and co-pyrolysis
  - Characterize **solid products** in terms of elemental composition, proximate analysis, and calorimetry
  - Characterize **liquid products** in terms of viscosity, density, refractive index, and elemental composition
  - Determine the **organic compounds** and **functional groups** present in the liquid products

2.2.1 Operational conditions

As shown in Table 2, co-pyrolysis of OS and BM was conducted in three different apparatuses, TGA equipment, a batch reactor, and a continuous feed reactor. The operational conditions chosen include temperature, heating rate, particle size, carrier gas, reaction time, and mixing ratio of OS:BM. Table 4 displays the operational conditions for the co-pyrolysis of OS and BM.

Table 4. Co-pyrolysis operational conditions

Operational conditions	Experimental Equipment		
	Thermogravimetric analyser	Batch reactor	Continuous feed reactor
Equipment description	Netzsch STA 449F3 thermal analyser	Prototype batch reactor with gas cleaning and cooling and GC-TCD	Cylindrical retort (feed hopper, screw feeder agitator) with cooling + condensing system
OS:BM mixing ratios	1:0, 9:1, 7:3, 1:1, 3:7, 0:1	1:0, 9:1, 7:3, 0:1	0:1, 7:3, 1:1, 3:7, 1:0
Sample size	5 mg ±0.4 mg	1.5 g ± 5.5 %	0.05-0.2 kg/h 40-60 min
Particle size	< 0.125 mm	0.5 – 1.0 mm	0.25 - 1.30 mm
Temperature	80-630 °C	520 °C	520 °C
Reaction time	55 min	20 min 0.5, 1, 3, 5, 7, 10, 20 min	40-60 min
Carrier gas	N_2 and O_2	CO_2, H_2O-CO_2, Ar	CO_2
Parallel experiments	2	2	2
Products obtained	-	Gas Solid	Liquid Solid

2.2.2 Collection of pyrolysis products

The TGA experiments did not provide sufficient amounts of products (<5 mg) to collect samples for characterization. However, the solid and gas products from the batch reactor experiments and the liquid and solid products from the continuous feed reactor experiments were collected.

For the batch reactor experiments, the solid products were collected from the sample holder at the end of each experiment. The pyrolysis gas was collected and stored in Tedlar® bags after it exited the batch reactor.

The products from co-pyrolysis in the continuous feed reactor were collected after each experiment. Solid products including char, ash, and semicoke gathered in the cylindrical retort were collected, while liquid products were collected from the condenser. The continuous reactor allowed calculation of the mass balance and yield of products by determining the fuel consumption (OS+BM) and by adding up the yield of solid and liquid products to determine the yield of gas.

2.3 Characterization of pyrolysis products

The co-pyrolysis products required the use of different characterization equipment depending on the type of products generated.

2.3.1 Batch reactor

The schematics of the batch reactor are shown in Figure 4. The gas products were analysed in terms of composition, while the liquid products were analysed in terms of elemental composition and surface area.

The concentration of H_2, CO, and CH_4 in the producer gas was determined using a GC-TCD gas analyser, with two columns for H_2, CO, and CH_4 detection. The equipment was calibrated, and the concentration of gas species in vol% was determined using the software Clarity.
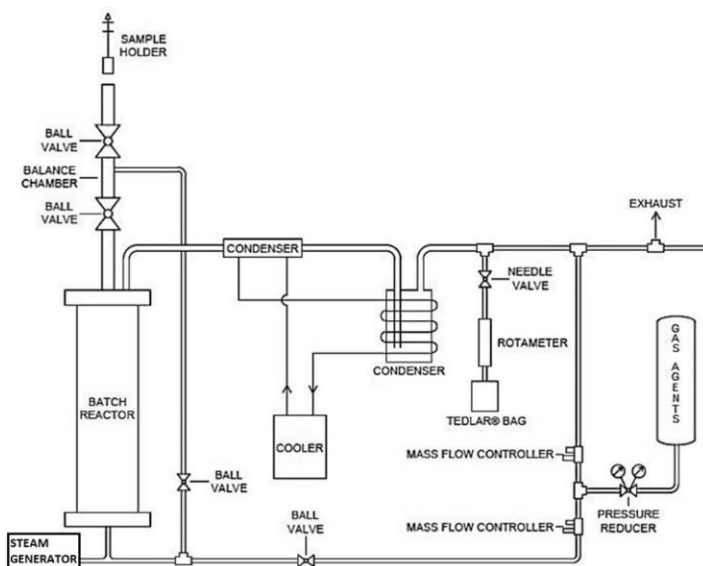

Figure 4. Schematics of the batch reactor (from **Publication III**)

2.3.2 Continuous feed reactor

The schematics of the continuous feed reactor are shown in Figure 5. The continuous feed reactor has the following components: 1. Feed; 2. Motor; 3. Screw feeder; 4. Carrier gas; 5. Controller; 6. Reactor; 7. Heater; 8. Chiller; 9. Coolant bath; 10. Condenser.

The solid products were analysed in terms of elemental composition, proximate analysis, and calorimetry, while the liquid products were analysed in terms of elemental composition, physicochemical properties (density, viscosity, and refractive index), organic compounds, and functional groups.
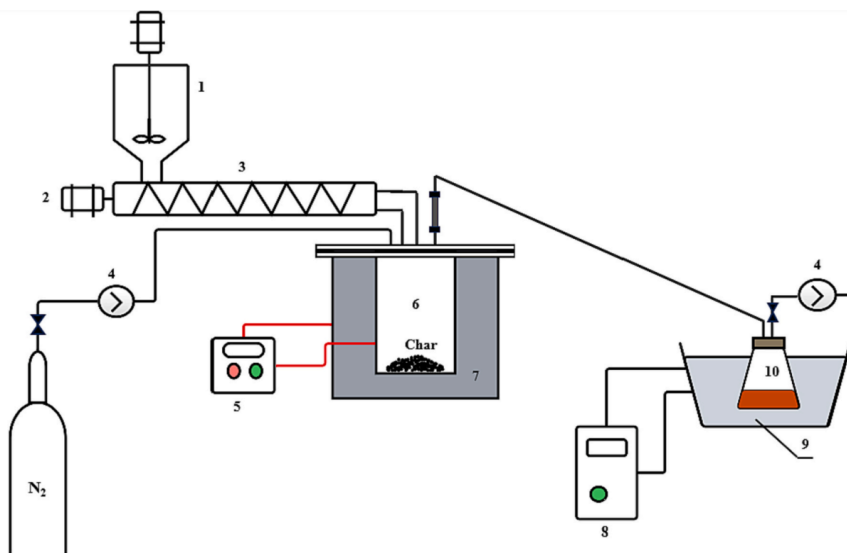

*Figure 5. Schematics of continuous feed reactor (from **Publication IV** and* [100]*).*

Table 5 shows the equipment and conditions used for characterization of the products from co-pyrolysis in the batch reactor and the continuous feed reactor. More detailed conditions are given in **Publications II–IV**.

Table 5. Characterization techniques used for co-pyrolysis products

Characterization technique	Equipment	Analysis on Batch reactor	Analysis on Continuous feed reactor
Elemental analysis	Vario MACRO CHNS Cube system	CHNS of Solid products	CHNS of Solid and liquid products
Proximate analysis	Nabertherm RT120 drying oven Nabertherm L9 muffle furnace	Ash content, fixed carbon, and volatile matter of solid products	Ash content, fixed carbon, and volatile matter of solid and liquid products
Calorimetry	IKA 2000C and IKA 5000C bomb calorimeter	HHV and LHV of Solid products	HHV and LHV of Solid products
Surface area	Anton Paar Quantachrome Autosorb iQ-C surface area and a pore size analyser	BET surface area of Solid products	*n.m.*
Gas composition	Gazohrom 3101 gas analyser	H_2, CO, and CH_4	n.m.
Density	Anton Paar DMA 5000 M density meter	*n.m.*	Density of liquid products at 21°C
Viscosity	Anton Paar MCR 72 Modular Compact Rheometer	*n.m.*	Viscosity of liquid products at 40 °C

Characterization technique	Equipment	Analysis on Batch reactor	Analysis on Continuous feed reactor
Refractive index	Anton Paar Abbemat HT refractometer	*n.m.*	RI of liquid products wavelength of 589.3 nm
GC-MS	Interspectrum Interspec 301-X portable spectrometer	*n.m.*	Chemical composition of the liquid products
FTIR	Agilent 7890B Gas Chromatograph	*n.m.*	Functional groups from IR spectra of the liquid products

*n.m. not measured

2.3.3 Analysis of interactions

The possible interactions during co-pyrolysis of OS and BM were studied by comparing the theoretical and experimental yields. The theoretical yields were calculated from experimental data obtained during the pyrolysis of OS and BM individually. This comparison allowed the identification of interactions, in the yields of products, including inhibitory and promoting effects, arising from the co-pyrolysis of OS and BM.

Theoretical and experimental yields were determined using a linear correlation that considers the proportions of OS and BM. This correlation was established based on experimental yields obtained from individual pyrolysis of both OS and WC, as depicted in **Error! Reference source not found.**, where x is the share of OS, m_{BM} is the theoretical yields of OS:BM mixtures, while m_{OS} and m_{BM} are the experimental yields. The data of mass loss over temperature were used for TGA. For the batch reactor, the yields of solid products were used, while for the continuous feed reactor, the yields of all products (solid, liquid, and gas) were used.

$$m_{theo} = m_{OS}x + m_{BM}(1 - x)$$ *(1)*

2.4 Kinetics and computational modelling

The TGA data allowed a detailed study of the decomposition behaviour of OS, BM, and OS:BM mixtures. Based on these data, different kinetic models were utilized to determine the activation energies. Additionally, these kinetic parameters combined with the TGA data allowed the development of a computational model to determine the mass loss curves in the co-pyrolysis of OS and BM.
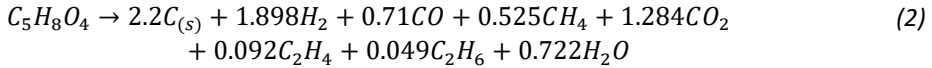
The TGA data were used to determine the kinetic parameters from pyrolysis and co-pyrolysis experiments, including the total apparent activation energy, the activation energy vs. stages of conversion, and the average activation energy at different stages of conversion. The initial kinetic model used was the Coat Redfern model [101], using a reaction order range from 0 to 2, at a step increase of 0.1. The Kissinger model [102] and additionally isoconversional models including Friedman [103] and Vyazovkin [104] were implemented to study the activation energy at different stages of conversion. Details of the equations and procedures for the kinetic studies are available in **Publication II**.

A model was developed using Aspen Plus®, based on the calculated kinetic parameters and the TGA data. The model uses the activation energy and the pre-exponential factors for OS and BM. For BM, the model uses the structural components hemicellulose, cellulose, and lignin (Lignin-C, Lignin-H, and Lignin-O) based
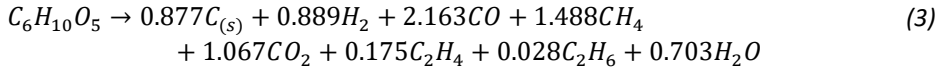
on stoichiometric equations for the pyrolysis of each one of the components. This was based on the approaches in Ranzi et al. and Baliban et al. [105], [106].

For OS, the model uses stoichiometry based on the composition of OS from the elemental and proximate analyses from section 2.1.2. The stoichiometric formula for OS pyrolysis is calculated based on the approach in Baliban et al. [106], and the composition of pyrolysis gas species in Mozaffari et al. [107], to calculate the CO/CO_2, CO_2/CH_4, and CO/H_2 ratios. A detailed description of Aspen Plus® is available in **Publication II**. (2(3(4(5, (6, and(7 display the stoichiometric OS and BM reactions used for the model.
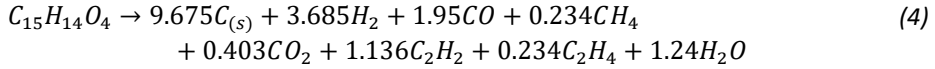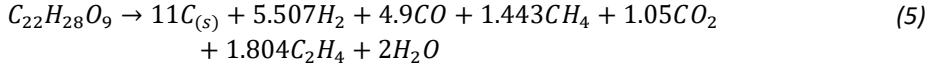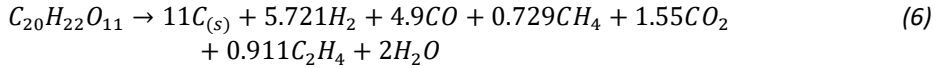
Hemicellulose:
$$C_5H_8O_4 \rightarrow 2.2C_{(s)} + 1.898H_2 + 0.71CO + 0.525CH_4 + 1.284CO_2 \qquad (2)$$
$$+ 0.092C_2H_4 + 0.049C_2H_6 + 0.722H_2O$$

Cellulose:
$$C_6H_{10}O_5 \rightarrow 0.877C_{(s)} + 0.889H_2 + 2.163CO + 1.488CH_4 \qquad (3)$$
$$+ 1.067CO_2 + 0.175C_2H_4 + 0.028C_2H_6 + 0.703H_2O$$

Lig-C:
$$C_{15}H_{14}O_4 \rightarrow 9.675C_{(s)} + 3.685H_2 + 1.95CO + 0.234CH_4 \qquad (4)$$
$$+ 0.403CO_2 + 1.136C_2H_2 + 0.234C_2H_4 + 1.24H_2O$$

Lig-H:
$$C_{22}H_{28}O_9 \rightarrow 11C_{(s)} + 5.507H_2 + 4.9CO + 1.443CH_4 + 1.05CO_2 \qquad (5)$$
$$+ 1.804C_2H_4 + 2H_2O$$

Lig-O:
$$C_{20}H_{22}O_{11} \rightarrow 11C_{(s)} + 5.721H_2 + 4.9CO + 0.729CH_4 + 1.55CO_2 \qquad (6)$$
$$+ 0.911C_2H_4 + 2H_2O$$

OS:
$$C_{4.265}H_{5.232}O_{2.472}N_{0.0134}S_{0.117} \rightarrow 1.6744\ C_{(s)} + 0.3058\ CO + $$
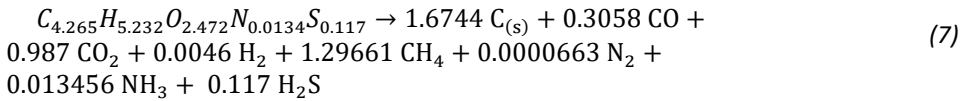$$0.987\ CO_2 + 0.0046\ H_2 + 1.29661\ CH_4 + 0.0000663\ N_2 + \qquad (7)$$
$$0.013456\ NH_3 + \ 0.117\ H_2S$$

3 Results

The experimental results are arranged in a structure that allows analysis and comparison of the co-pyrolysis of BM and OS at different experimental scales, as well as analysis of interactions in the yields of co-pyrolysis. The experiment results are derived from pyrolysis and co-pyrolysis in TGA **(Publication II)**, the batch reactor **(Publication II),** and the continuous feed reactor **(Publication III)**.

3.1 Fuel properties

Table 6 shows the compositions of BM and OS used in co-pyrolysis. The results shown in Table 6 are divided into elemental composition (C, H, N, S, O) proximate analysis properties (ash, moisture content, fixed carbon, and volatile matter), and calorific values (HHV and LHV). For the TGA and batch reactor studies, Table 6 shows the average composition of the woody BM species used (spruce, alder, pine, and birch) as these were pyrolyzed as a mixture and the variation in their composition is notably low (See **Publications II** and **III**). For the continuous reactor, the BM composition results shown are from woodchips.

The BM composition results are in agreement with other studies on woody BM [108]. These BM species are characterized by a low ash content (<1.5 wt%), high carbon and oxygen contents, and a high content of volatile matter (>80 wt%). These properties indicate the potential of using BM in thermochemical conversion processes [34]. OS composition differs greatly from that of the BM used, especially in terms of the higher contents of ashes (>51 wt%) and sulphur (>1.7 wt%) and the lower contents of volatile matter and fixed carbon. Accordingly, different results in the yields and composition of pyrolysis products, as well as in the pyrolysis behaviour, were expected.

*Table 6. Characterization of co-pyrolysis products (Adapted from **Publications II-IV**)*

Characterization		TGA		Batch reactor		Continuous feed reactor	
		BM	OS	BM	OS	BM	OS
Elemental analysis, wt%	C	**49.9**	27.2	**49.9**	27.2	**51.7**	27.0
	H	**6.6**	2.8	**6.6**	2.8	**6.4**	2.5
	N	0.2	<0.1	0.1	<0.1	0.4	0.1
	S	*n.d.*	**2.0**	n.d.	**2.0**	<0.1	**1.7**
	O**	**43.2**	15.4	**43.2**	15.4	**41.5**	15.4
Proximate analysis, wt%	Ash content	**0.3**	**52.4**	**0.3**	**52.4**	1.5	**51.4**
	Moisture	7.7	0.9	7.7	0.9	6.4	0.9
	Fixed carbon	13.9	1.5	13.9	1.5	10.6	1.5
	Volatile matter	**85.8**	46.1	**85.8**	46.1	**81.5**	47.1
Calorific value, MJ/kg	LHV	18.4	8.7	18.4	8.7	18.8	8.7
	HHV	19.5	9.7	19.9	9.7	20.2	9.7

** Calculated, *n.d. not detected

A comparison of the BM used in TGA and batch reactor (blends of spruce, alder, pine, and birch), with the woodchips used in the continuous feed reactor, indicates very high similarities between the woody BM mixture and the woodchips used in terms of elemental composition, proximate analysis, and calorimetry. Accordingly, all BM samples used are considered woody BM and can be compared to each other in pyrolysis experiments.

3.2 Pyrolysis behaviour

The thermal behaviours of OS, BM, and OS:BM mixtures are shown in Figure 6. These analyses facilitate an understanding of the thermochemical decomposition in individual pyrolysis and co-pyrolysis. The temperature range selected was based on previous studies on OS and BM, where the individual pyrolysis ranges from 250–550 °C for BM [49] and 350–550 °C for OS [71].
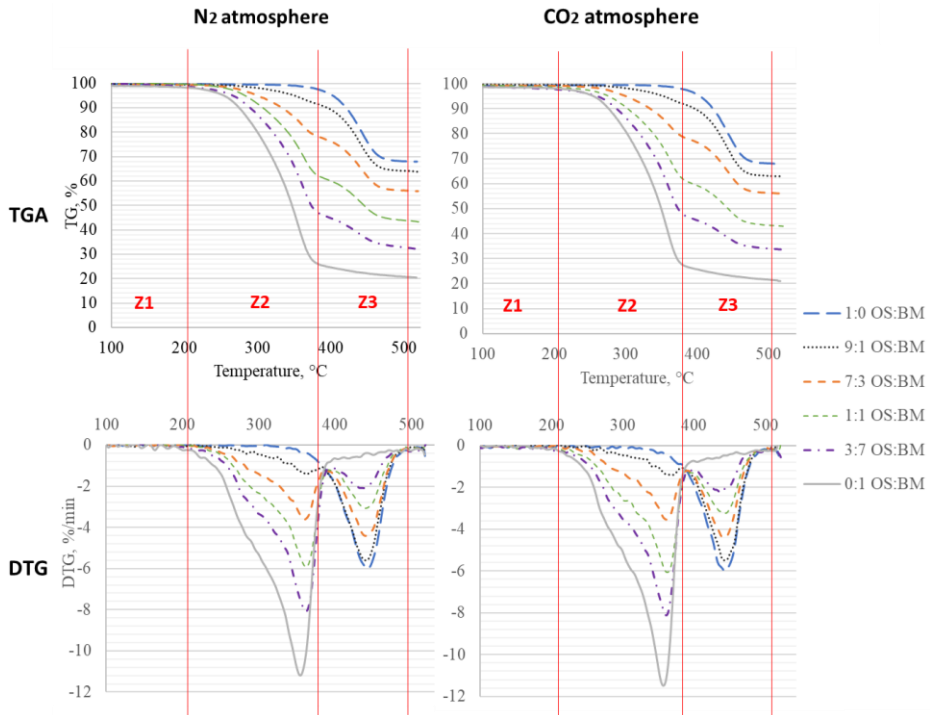

*Figure 6. TGA and DTG of OS and BM co-pyrolysis in N_2 and CO_2 (Adapted from **Publication II**)*

An analysis of BM and OS pyrolysis individually indicates a clear difference in the decomposition temperatures for both fuels. The majority of BM decomposition occurs in the temperature range 200–400 °C. This is due to the biochemical components of BM, i.e., cellulose and hemicellulose, which decompose in this temperature range [35]. The remaining mass losses above 500 °C are related to pyrolysis of lignin and residues from pyrolysis [34]. The TGA results for BM are in agreement with those from other studies [39]. Conversely, the majority of OS decomposition occurs in the range 400–500 °C and is related to kerogen transformation into volatile ash and semicoke [109]. Above this temperature range, there is mostly decomposition of inorganic matter and carbonates [58], [110]. The OS TGA results agree with those from other studies [63], [111].

As shown in Figure 6 there are three clear pyrolysis zones in all cases:

- Zone 1: from 100–200 °C, related to drying and pre-pyrolysis
- Zone 2: from **200–400 °C**, where most **BM pyrolysis** occurs
- Zone 3: from **400–500 °C**, where most **OS pyrolysis** occurs

Figure 6 shows how the co-pyrolysis of OS and BM also occurs in the same three zones as the individual pyrolysis, with a zone where most BM pyrolysis occurs, and one where most OS pyrolysis occurs. This behaviour is supported by the DTG results observed in Figure 6, where the co-pyrolysis of OS and BM results in a combined decomposition, where the higher the share of BM, the more similar behaviour to BM pyrolysis, and the higher the share of OS, the more similar behaviour to OS pyrolysis. From these results, it can be inferred that the co-pyrolysis behaviour is additive, with two well-defined pyrolysis zones, one for BM and one for OS. These observations of linear additive behaviour have been made in other co-pyrolysis studies of OS and BM [10].

The addition of BM increases the proportion of decomposition due to its higher content of volatile matter and lower content of ash. Nevertheless, the co-pyrolysis can result in enhanced decomposition of OS, as BM pyrolysis occurs in a lower temperature range. Thus, BM (and its volatiles) can accelerate decomposition due to heat transfer to the OS [69], [75] and reduce the activation energy of the process [17]. Figure 7 shows additional evidence of the possible heat interactions between BM and OS in co-pyrolysis.
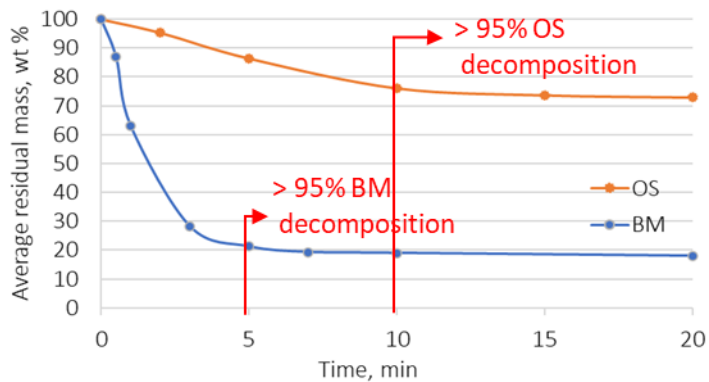

Figure 7. Residual mass from pyrolysis of OS and BM at different pyrolysis times (Adapted from **Publication III***)*

The DTG peaks from Figure 6 and additional studies using the batch reactor (Figure 7) indicate how BM pyrolysis occurs in a lower temperature range. The residual masses at different pyrolysis times in the batch reactor, as shown in Figure 7, show that BM pyrolysis occurs considerably faster than OS pyrolysis, with most decomposition occurring within 5 min, compared to 10 min for OS. The faster decomposition of BM can result in heat transfer interactions from the BM volatiles released, which can enhance the pyrolysis of OS and shift its pyrolysis to a lower temperature region [92]. The DTG results for OS:BM mixtures shown in Figure 6 also indicate a shift of OS pyrolysis to a lower temperature region by as much as 3–10 °C compared to that required for individual pyrolysis of OS.

The TGA and DTG curves for experiments conducted under H_2 and CO_2 atmospheres are almost identical, with less than 0.7 wt% difference between their residual masses.

3.3 Yields of products

The yields of products were measured for all experiments. For TGA, the yield of solid products was determined (uncertainty of ±1 wt%), for the batch reactor, the yield of solid products were determined (RSD 0.35%–3.99%), and for the continuous feed reactor, the yields of solid and liquid products were determined (RSDs 3.41%–8.73% and 1.43%–6.88%, respectively), with the yield of gaseous products being calculated by difference.

3.3.1 Yields of solid products

Table 7 compares the yields of solid products obtained from TGA, the batch reactor, and the continuous feed reactor, using different carrier gases, i.e., N_2, CO_2, Ar, and CO_2/H_2O. Due to the observed additive behaviour in TGA results, not all the mixtures of OS:BM were used in all co-pyrolysis experiments.

*Table 7. Yields of solid products in pyrolysis with different gas carriers (Adapted from **Publications II–IV**)*

OS:BM	Yield of solid products, wt%					
	TGA		Batch reactor			Continuous feed reactor
	N_2	CO_2	Ar	CO_2	H_2O/CO_2	CO_2
1:0 (OS)	67.9	67.7	74.5	74.1	74.6	74.4
9:1	65.0	63.8	70.3	68.0	71.6	*n.m.*
7:3	55.9	56.1	60.0	57.4	57.5	55.1
1:1	42.8	43.0	*n.m.*	n.m.	n.m.	46.3
3:7	33.5	33.3	*n.m.*	*n.m.*	*n.m.*	36.6
0:1 (BM)	20.5	21.3	18.2	18.4	19.7	21.0

*n.m. not measured

The yields of solids obtained agree with the TGA data and the expected yield of solids obtained from pyrolysis of woody BM [112] and Estonian OS [64], [113]. BM pyrolysis results in 18.2–21.3 wt% of solid products, while OS pyrolysis results in 67.7–74.6 wt% of solid products. A comparison of the results for pyrolysis under different gas atmospheres shows that the effect of the carrier gas is almost negligible, with less than 1.0 wt% difference in TGA experiments (lower than the measurement uncertainty) and below 3.6 wt% in batch reactor experiments (close to the experimental RSD). A stronger effect of non-inert atmospheres such as CO_2 and H_2O is likely to be observed at higher reaction temperatures (above 500 °C), when these gas species contribute to gasification reactions, resulting in higher yields of gas and enhanced thermal cracking [114], [115]. Figure 8 shows a comparison of the average yields of products for each type of experiment.
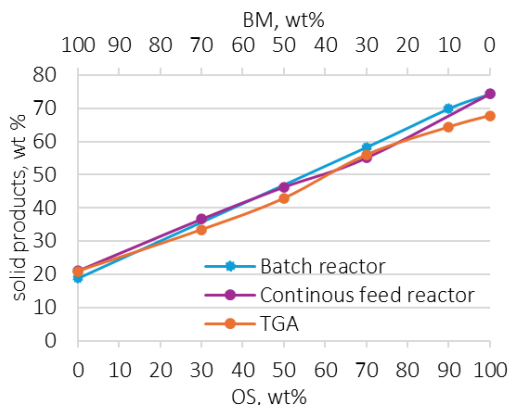
*Figure 8. Yields of solid products (Adapted from **Publication II–IV**)*

Figure 8 confirms additive behaviour for co-pyrolysis in all experimental setups, as the yield of solid products increases parallelly to the increase in the share of OS. For all cases, the yield of solid products has a linear additive behaviour, with linear coefficients of determination (R^2) of 0.9947, 0.9996, and 0.9955 for TGA, the batch reactor, and the continuous feed reactor experiments, respectively.

3.3.2 Yields of solid, liquid, and gas products

The continuous feed reactor allows the collection and measurement of solid and liquid yields. The yields of pyrolysis and co-pyrolysis products are shown in Figure 9.
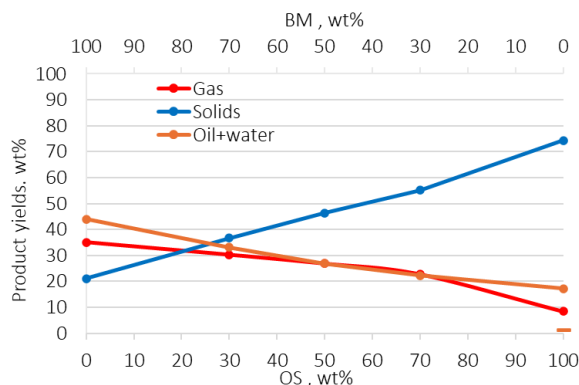

*Figure 9. Yields of solid, liquid, and gas products (Adapted from **Publication IV**)*

From Figure 9, BM pyrolysis yields 21.0, 43.9, and 35.1 wt%, while OS yields 74.4, 17.3, and 8.4 wt% of solids, liquids, and gas products, respectively. The obtained results are in agreement with those of other studies on intermediate pyrolysis of BM [38], [116]–[118]. The yields of products from OS pyrolysis are in agreement with those for the pyrolysis of Estonian OS [64]. For co-pyrolysis mixtures, increasing the share of BM results in higher yields of gas and liquid products and lower yields of solids. As with the yields of solids shown in Figure 8, the liquid products also follow a linear behaviour, with a coefficient of determination (R^2) of 0.9704.

33

3.4 Chemical composition of solid products

The characterizations of the solid products produced in the batch reactor and the continuous reactor are shown in Table 8 (Elemental composition) and Table 9 (Proximate analysis and calorimetry). The solid products for BM are composed mostly of char (>80 wt% C) alongside a low ash content (<8 wt%). Those for OS are composed of a high proportion of ashes (>65 wt%) with a low content of carbon (<13 wt%). Both the OS and BM results are in agreement in those for the batch reactor and continuous reactor and with the average composition of char from BM pyrolysis [112], [119], and semicoke from OS pyrolysis [85].

*Table 8. Elemental composition of solid products (Adapted from **Publications III and IV**)*

OS:BM	Elemental analysis, wt%							
	Batch reactor				Continuous feed reactor			
	C	H	N	S	C	H	N	S
1:0 **(OS)**	11.4	0.2	<0.1	**1.0**	12.9	0.3	<0.1	**1.5**
9:1	12.1	0.2	<0.1	0.9	n.m.	n.m.	n.m.	n.m.
7:3	15.1	0.3	<0.1	0.8	18.8	0.5	<0.1	1.4
1:1	*n.m.	n.m.	n.m.	n.m.	23.3	0.7	0.1	1.3
3:7	n.m.	n.m.	n.m.	n.m.	31.7	1.1	0.2	1.1
0:1 **(BM)**	**78.4**	**3.4**	0.4	**n.d.	**81.1**	**3.1**	0.6	0.1

*n.m. not measured, **n.d. not detected

The co-pyrolysis solid products comprise a mixture of the properties of OS and BM, with higher C and H contents as BM share increases, and higher ash and sulphur as OS share raises. Due to the high ash content of OS, it has a more significant role in the composition of co-pyrolysis solid products. For all cases, especially for OS-containing mixtures, the volatile matter (Table 9) indicates an incomplete degradation in pyrolysis [120]. Adding BM to OS results in solid products with improved characteristics, such as higher C and H contents, higher HHV and LHV values, and lower ash and sulphur contents. These improved properties result in solid products with enhanced thermal properties, higher heating values, and higher aromaticity and stability. This is highly beneficial for its potential application as absorbent materials and biochar [52], [121]. Similarly to TGA behaviour and product yields, the composition of solid products in co-pyrolysis follows an additive behaviour.

*Table 9. Proximate analysis and calorific values of solid products (Adapted from **Publications IV**)*

OS:BM	Proximate analysis, wt%				Calorific value, MJ/kg	
	Ash content	Moisture	Fixed carbon*	Volatile matter	LHV	HHV
1:0 **(OS)**	**67.7**	**0.7**	5.3	26.2	1.9	2.0
7:3	62.1	1.7	9.5	26.7	3.8	4.0
1:1	58.1	2.9	10.2	28.8	5.7	5.8
3:7	49.9	5.5	15.0	29.6	9.1	9.3
0:1 **(BM)**	7.4	11.4	**62.5**	18.7	29.5	30.2

3.5 Composition of liquid products

The compositions of the liquid products were obtained from various experiments.

Table 10 displays the results for elemental composition and physicochemical properties (density, viscosity, and refractive index). Figure 10 and
Table 11 show the results of the chemical compounds present and their classification in terms of functional groups obtained from GC-MS. Figure 11 displays the FTIR results divided into wavenumber regions that indicate the presence of certain functional groups.

3.5.1 Elemental composition and physicochemical properties

OS and BM oil have different properties and characteristics. **BM oil is brown, viscous, and dense**, while **OS oil is lighter and of a darker brown colour**. The elemental compositions of OS and BM agree with the results of previous literature studies [51], [84], [122], [123].

BM has a density of 1.06 g/cm^3 (1.0–1.2 kg/m^3, a typical range for bio-oil), which is higher than those of conventional liquid fuels [51], and a viscosity of 51.1 mPa·s (40–100 mPa·s being the typical range for bio-oil) due to the high molecular weight of lignin-derived compounds [51], [124]. The BM density, viscosity, and refractive index results agree with those from other studies [124]–[127].

Compared with BM, OS has a lower density and viscosity of 0.95 g/cm^3 and 12.3 mPa·s, respectively (values that are lower than the average values for petroleum-derived oils), and a higher sulphur content - but one that is comparable to the average sulphur content for crude oil (0.01–4.20 wt%) [51]. The density, viscosity, and refractive index of OS liquid products agree with those from previous studies [123], [128].

*Table 10. Elemental composition and physicochemical properties of liquid products **(Adapted from Publication IV**)*

OS:BM	Viscosity, mPa·s	Density, g/cm^3	Refractive index, *n.D.	Elemental analysis, wt%			
				C	H	N	S
1:0 **(OS)**	12.3	0.95	1.53	**80.6**	**9.2**	0.2	0.9
7:3	17.3	1.01	1.53	78.7	9.4	0.3	0.8
1:1	29.5	1.02	1.54	65.8	8.5	0.3	0.7
3:7	38.8	1.05	1.54	68.3	8.8	0.3	0.4
0:1 **(BM)**	51.1	1.06	1.52	58.5	8.8	0.4	**0.3**

*n.D. adimensional

As with solid products, the co-pyrolysis liquid products represent a combination of the properties of OS and BM, with higher C, H, and S contents as the OS proportion increases, and higher viscosity and density as the BM proportion increases. OS:BM mixtures result in combined enhanced properties; the addition of BM reduces the sulphur content, while the addition of OS increases the C and H concentrations. A more detailed analysis of the composition of the oils based on GC-MS analysis is shown in Figure 10 and
Table 11.

3.5.2 GC-MS – FTIR chemical compounds and functional groups

The chromatograms for the liquid products obtained from GC-MS are shown in Figure 10. The data was analysed with the MassHunter Qualitative Analysis Software, based on two parallel runs per sample and selecting the compounds present in both parallel runs

and with a matching score above 70. BM has more and larger peaks at lower retention times (15–25 min), and OS at higher retention times (30–50 min). Co-pyrolysis mixtures show additive behaviour (a combination of OS and BM chromatograms). Further details of the compounds detected are available in **Publication IV.**
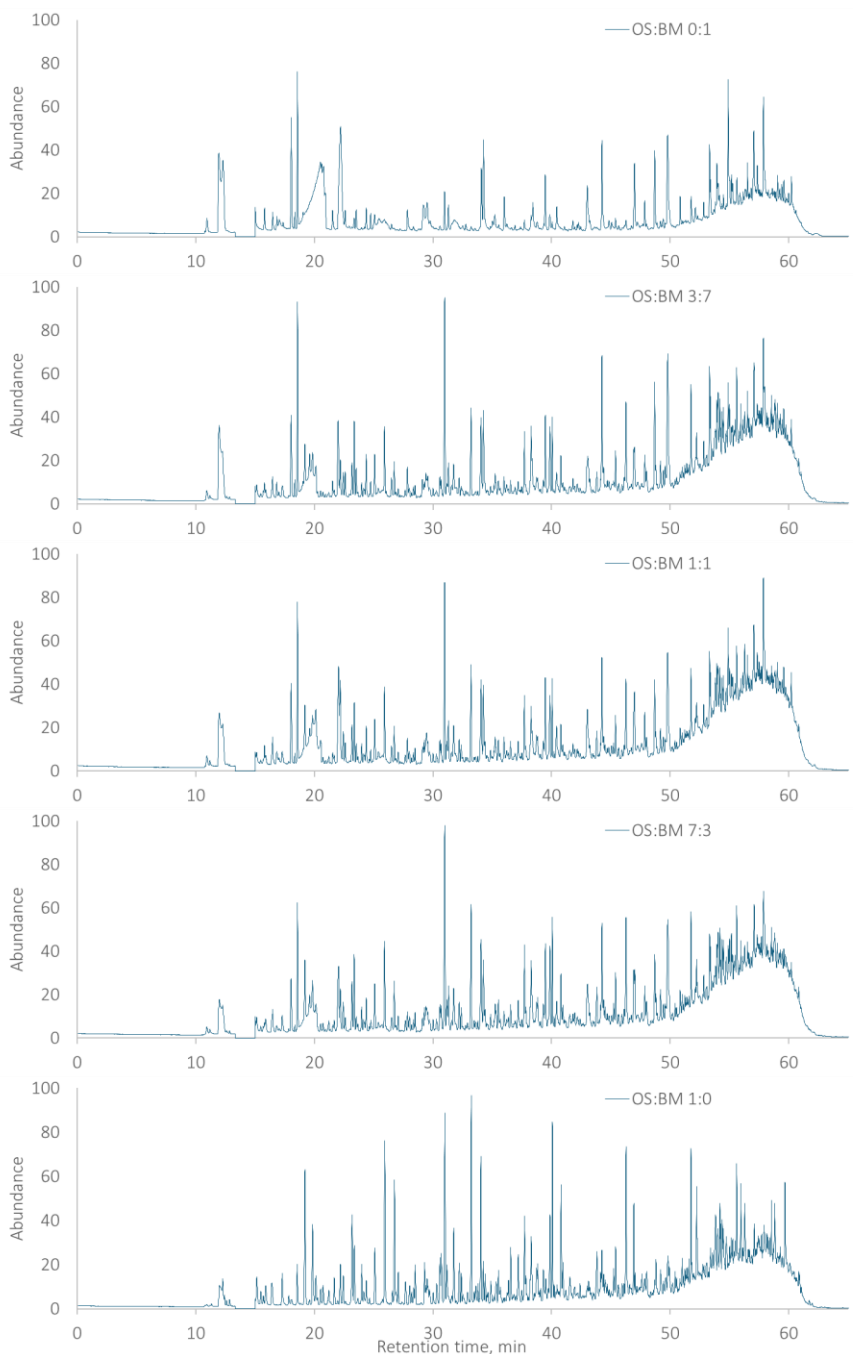

*Figure 10. Chromatogram for the liquid products from co-pyrolysis of OS and BM (From **Publication IV**)*

BM liquid products contain mostly compounds from the functional groups of ketones (C=O), carboxylic acids, aromatic hydrocarbons, and phenols (OH), especially oxygenated compounds, due to BM elemental composition (Table 6Table 5). Most compounds are light (C_2 to C_8). The chromatogram and compounds identified agree with those from literature studies of woody BM pyrolysis, which report high contents of light-oxygenated compounds [116], [129]–[133].

OS liquid products contain mostly compounds bearing the functional groups of aromatic hydrocarbons, aliphatic hydrocarbons, aliphatic alcohols, cycloalkanes, and polycyclic compounds, with the majority being aliphatic (alkenes, alkanes, and alkynes) and aromatic hydrocarbons (benzene, toluene, and o-xylene) from C_6 to C_{11}. The identified compound results agree with those from literature studies on shale oil, which identify aliphatic and aromatic hydrocarbons [10], [74], [122].

OS:BM liquid products comprise a combination of the compounds present in OS and BM liquid products (Table 11). The amount of oxygenated compounds increases with BM proportion, while the amount of hydrocarbon compounds increases with OS proportion. As with the previous results, the co-pyrolysis behaviour can be described as additive, as also observed in Kiliç at al. [10]. Nevertheless, the co-pyrolysis liquid products exhibit improved properties, such as a decrease in the amount of oxygenated compounds when increasing the proportion of OS, and a decrease in the amount of aromatic hydrocarbons as BM proportion is increased.

*Table 11. Functional group distribution in the liquid products from co-pyrolysis of OS and BM (From **Publication IV**)*

OS:BM	Functional groups				
	Ketones	Aromatic Hydrocarbons	Aliphatic Hydrocarbons	Phenols	Cycloalkanes
1:0 **(OS)**	2	10	19	1	12
7:3	6	9	9	6	0
1:1	7	9	6	6	0
3:7	7	7	5	6	0
0:1 **(BM)**	8	1	0	8	0

The results from the GC-MS measurements were confirmed with FTIR analysis (Figure 11). The IR spectra identified different vibration ranges: O-H stretching from phenols, C–H stretching and bending from aliphatic hydrocarbons, C=O stretching from ketones and alkenes, and C–O stretching from phenols. As with the chromatogram, the IR spectra identified more intense vibration signals for phenols and ketones in the BM liquid products and more intense vibration signals for aliphatic hydrocarbons in the OS liquid products. The results agree with the IR spectra of OS and BM pyrolysis and co-pyrolysis [10], [75], [123].
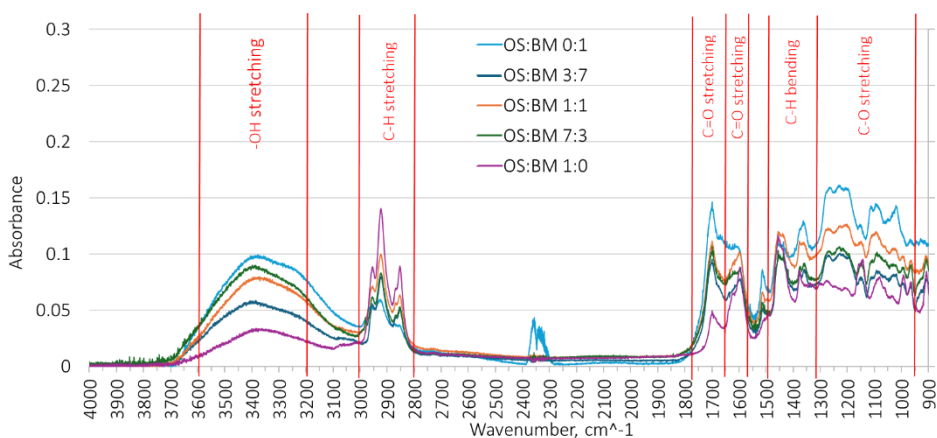
*Figure 11. IR spectra of co-pyrolysis of OS and BM (From **Publication IV**)*

3.6 Interactions in co-pyrolysis

Table 12 shows a comparison of the experimental and theoretical solid and liquid product yields for co-pyrolysis. For all cases (TGA, batch reactor, and continuous feed reactor) the differences in experimental and theoretical yields are not significant enough to conclude any synergistic behaviour between OS and BM, considering the experimental RSD and uncertainties shown in section 3.3. This lack of synergy can also be strongly supported by the additive behaviour identified in the TGA data, the yields of products, the composition of solids and liquids, and the chemical and physicochemical compositions of liquid products. All these experiments demonstrate an additive rather than synergistic behaviour in OS:BM co-pyrolysis. Similar observations have been made in other research [74], [93], where an additive behaviour and minimal to no synergistic effects were observed. Nevertheless, a more detailed analysis was performed based on the TGA data to evaluate the differences in experimental and theoretical data at different stages of decomposition (Figure 12).

*Table 12. Comparison of experimental and theoretical yields of solid and liquid products (From **Publications II–IV**)*

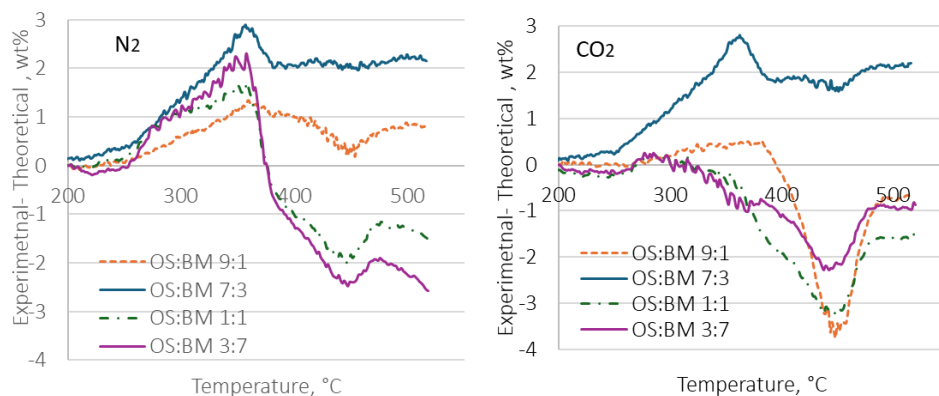|	Experimental-Theoretical yields of solid products, wt%						Experimental-Theoretical yields of liquid products, wt%
OS:BM	TGA		Batch reactor			Continuous feed reactor	
	N_2	CO_2	Ar	CO_2	H_2O-CO_2	CO_2	
9:1	1.8	0.7	1.5	-0.5	2.4	n.m.	n.m.
7:3	2.2	2.3	2.5	0.0	-0.7	-3.3	-3.0
1:1	-1.4	-1.5	*n.m.	n.m.	n.m.	-1.4	-3.7
3:7	-1.2	-1.9	n.m.	n.m.	n.m.	-0.4	-2.8

* n.m. not measured

*Figure 12. Experimental-theoretical TGA curves for OS:BM co-pyrolysis (From **Publication II**)*

Figure 12 shows the differences in the experimental and theoretical TGA curves for pyrolysis and co-pyrolysis of OS and BM. The following was observed: Below 250 °C there are negligible interactions, but there are stronger interactions at 350–370 °C and 440–460 °C, which coincide with the DTG peaks for BM and OS, where the most significant decomposition occurs.

3.7 Kinetics and modelling

The results in this section detail the kinetic features of BM and OS pyrolysis, as well as OS:BM co-pyrolysis. The kinetic parameters were calculated using the TGA results, proceeded by a process model based on kinetic parameters and TGA data.

3.7.1 Kinetics

A detailed description of the kinetic models and their respective equations used, as well as the determination of the apparent activation energies, is available in **Publication II.** The kinetic parameters were calculated using four models: Coats–Redferns models with reaction orders from 0 to 2, Kissinger models for determining apparent activation energies, and Friedman and Vyazovkin isoconversional models for determining apparent activation energies and activation energies at different stages of conversion. The results are shown in Table 13.

*Table 13. Activation energies in the co-pyrolysis of OS and BM (From **Publication II**)*

OS:BM	Coats-Redfern	Kissinger	Friedman		Vyazovkin
	E, kJ/mol	E, kJ/mol	E, kJ/mol	A, min^{-1}	E, kJ/mol
1:0	58.9	160.2	167.4	2.34E+09	171.5
9:1	66.1	172.9	153.6	2.94E+08	153.4
7:3	69.9	145.9	197.3	7.39E+11	193
1:1	77.4	152.9	164.3	5.25E+11	163.1
3:7	85.3	179.4	154.7	5.95E+09	156.8
0:1	96.7	147.4	139.3	2.95E+09	140.4

Table 13 displays the apparent activation energies determined using four different models. The Kissinger, Friedman, and Vyazovkin models result in similar results, with activation energies from 139–147 and 160–172 kJ/mol for BM and OS, respectively,

which are in agreement with those from other studies [69], [92], [113], [134], [135]. The Coats–Redfern model resulted in values that differ from those of the other three models. The activation energies obtained for OS:BM mixtures range between 145 and 193 kJ/mol. There is, however, a higher activation energy obtained for OS:BM 7:3. Figure 13 shows the apparent activation energies at different stages of conversion.
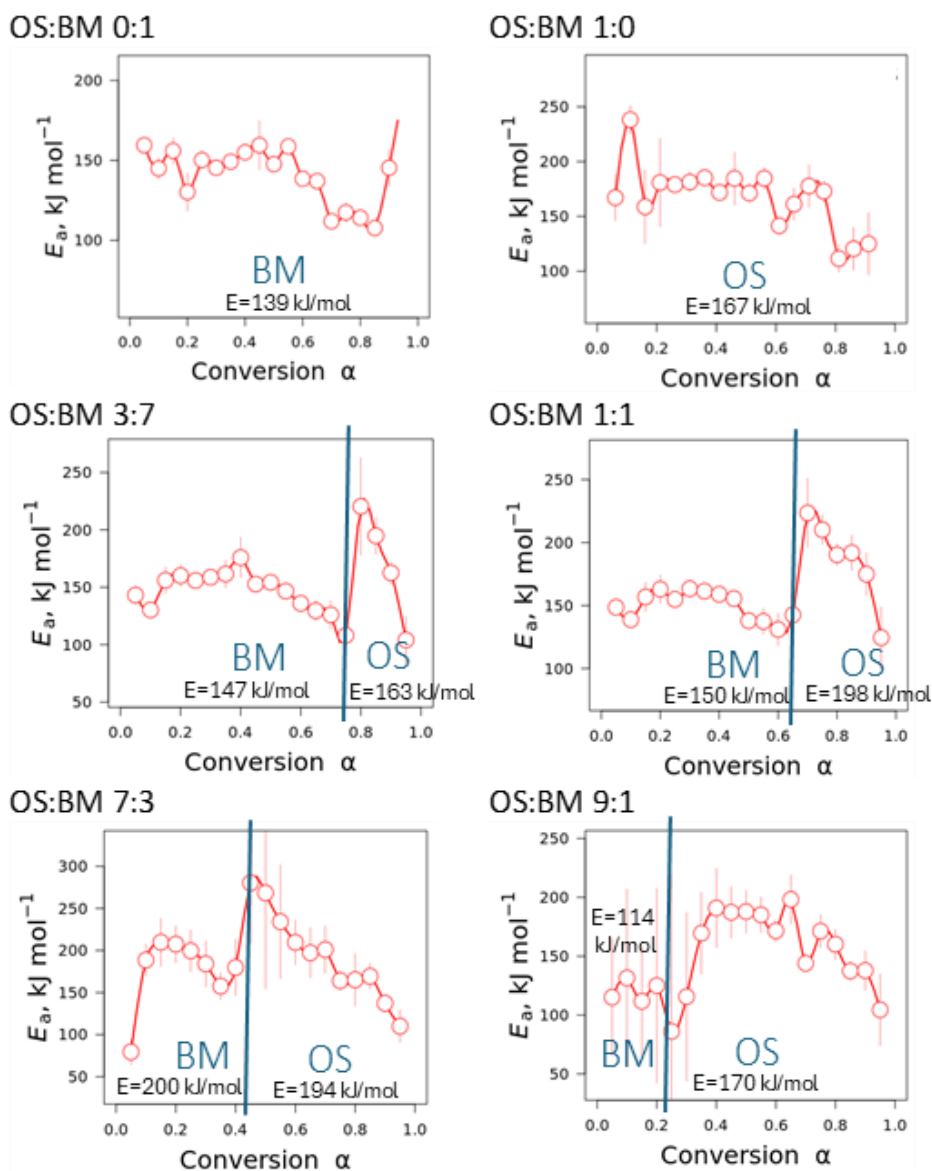

Figure 13. Apparent activation energies forn the co-pyrolysis of OS and BM at different conversion stages (From **Publication II**)

A more detailed study with the isoconversional models (Figure 13) identified two separate regions for the co-pyrolysis mixtures, one for BM pyrolysis and one for OS pyrolysis. This indicates a clear two-stage additive decomposition, which is supported by the previous TGA results, the yields of products, the composition of products, and the interactions. The two-stage decomposition allowed the identification of apparent activation energies for OS (170–198 kJ/mol) and BM (114–201 kJ/mol) in co-pyrolysis mixtures.

3.7.2 Modelling

An Aspen Plus® simulation was modelled based on the stoichiometric equations obtained for BM and OS, and the associated kinetic parameters determined. OS is considered a non-conventional component, while BM is considered as its biochemical components (hemicellulose, cellulose and lignin-C, lignin-H, and lignin-O), based on Debiagi et al. [136]. The estimated mass-loss curves for OS:BM mixtures are shown in Figure 14.
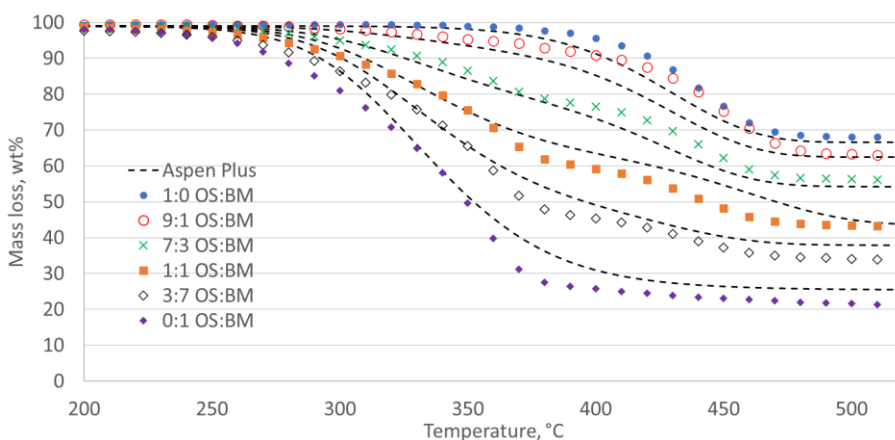

*Figure 14. TGA behaviour vs. mass-loss curve in co-pyrolysis of OS and BM modelled in Aspen Plus® (From **Publication II**)*

Figure 14 shows a close match between the TGA data and the Aspen Plus®-modelled results, with mean absolute errors between 1.8% and 3.8% for all OS:BM mixtures. The sensitivity analysis showed how the pre-exponential factor and the reaction order have a greater influence on the predicted mass losses for OS and BM pyrolysis and OS:BM co-pyrolysis.

4 Conclusions

This study investigated the co-pyrolysis of BM and OS. First, a comprehensive literature review was performed to explore the current status of research on the co-pyrolysis of BM and OS. This review encompassed the most significant studies, with a focus on co-pyrolysis parameters, interactions, and products.

Second, an experimental section included kinetic modelling and analyses of co-pyrolysis with optimized operational parameters.

Co-pyrolysis of OS and BM is a promising alternative for reducing the technical challenges associated with properties of bio-oil and the environmental effect of OS utilization, as well as being a means to increase its yields of liquid and gaseous products.

Considering the similarities in the thermal decomposition behaviour of OS and BM, implementing the currently available large-scale processing technologies used in OS conversion is a feasible alternative for their co-pyrolysis.

The operational parameters for co-pyrolysis, such as temperature, heating rate, particle size, reactor, and gas atmosphere, among others, are of the greatest importance, significantly affecting the yield and quality of the pyrolysis products. It is essential to optimize these parameters for each specific case in order to maximize the yield and quality of co-pyrolysis products, whether the priority is oil, char, or gas production.

Alternative atmospheres, such as steam and CO_2 can enhance the decomposition of fuels, acting as heat and volatile carriers. However, the effects of these atmospheres is not significant (minimal) at pyrolysis temperatures below 520 °C. Alternative atmospheres, such as CO_2, obtained sustainably from CCUS technologies, can be used as a substitute for inert atmospheres in co-pyrolysis without affecting the pyrolysis process.

Due to its higher decomposition temperature, the pyrolysis of OS occurs more slowly than BM decomposition, as evidenced in experiments performed using a batch reactor and thermogravimetric analysis experiments. As BM reaches an isothermal condition more rapidly, it can enhance OS pyrolysis through heat-transfer mechanisms, accelerating its decomposition. Shifts of up to 10 °C in the thermal decomposition peaks of the OS share in co-pyrolysis mixtures are evidence of this enhanced pyrolysis.

The co-pyrolysis of OS and BM follow a linear additive behaviour and a two-stage decomposition (first BM, followed by OS) without significant promoting or inhibiting interactions in the yield or quality of products. The yields of solid, gaseous, and liquid products are additive in all the studied scenarios, i.e., those using thermogravimetric analysis, a batch reactor, and a continuous feed reactor.

The kinetic studies confirmed an additive behaviour in co-pyrolysis, as the apparent activation energies and the activation energies at different stages of conversion (from the Friedman model) confirmed two-stage pyrolysis.

The compositions of the co-pyrolysis oils also confirmed an additive behaviour, with oxygenated compounds derived from BM bio-oil and aromatic and aliphatic hydrocarbons derived from OS.

The additive behaviour in co-pyrolysis can result in improved pyrolysis, as blending BM and OS results in pyrolysis products with improved properties and a lower yield of solid residues and sulphur in the pyrolysis products.

Adding BM to OS can contribute to addressing the environmental impact of OS utilization, while adding OS to BM can increase the energy density of the mixture and decrease the unfavourable properties of the resultant bio-oils. This improvement in co-pyrolysis products demonstrates the potential of using this process as a more sustainable alternative to produce valuable fuels and chemicals.

The liquid fraction obtained from BM pyrolysis oils primarily consists of oxygenated compounds (ketones and phenols), whereas that from OS consists of aromatics, aliphatic hydrocarbons, and cycloalkanes. When BM and OS are co-pyrolyzed, the resulting liquid fraction is a blend of compounds from both sources. Incorporating OS into BM decreases the production of oxygenated compounds, while adding BM to OS decreases the production of aromatic compounds. Co-pyrolysis can yield a liquid fraction with improved characteristics, including enhanced stability and heating value, making it suitable for potential applications as a fuel or chemical.

The use of thermogravimetric data in kinetic studies and process modelling, such as that using Aspen Plus, allows prediction of the decomposition behaviour in co-pyrolysis. A combination of experimental and thermal data with these types of tools provides the opportunity to use actual experimental data in reactor design.

The following suggestions are beneficial for future research:
- Many studies have already been conducted based on TGA and kinetic analysis. Studies that make use of the kinetic data for computational modelling and reactor design will contribute to defining the most optimal conditions required for co-pyrolysis
- The effects of alternative atmospheres in co-pyrolysis at temperatures above 520 °C may evidence a promoting effect in the co-pyrolysis process
- The catalytic effect of the inorganic components of OS and BM should be studied in more depth, as these can result in enhanced pyrolysis and its products
- As shown in this work, the scale of the equipment affects the yield and composition of pyrolysis products. The use of larger-scale equipment such as fluidized bed reactors and fixed bed reactors is suggested as the next step in studying co-pyrolysis and its products
- Future research could involve exploring variations in process parameters such as temperature, residence time, and catalyst usage
- While qualitative analysis of the liquid fraction in co-pyrolysis provides highly valuable data, a detailed quantitative analysis of co-pyrolysis oils will contribute to an understanding of the co-pyrolytic behaviour, interactions, and composition of the oils
- Study of the pyrolysis gases is also recommended as a means to obtain a more comprehensive analysis of the whole process
- Conducting economic and environmental evaluations as well as lifecycle assessments will better assess the viability and environmental impact of the co-pyrolysis of OS and BM for commercial purposes

List of figures

List of tables

References

[1] M. A. Mehmood *et al.*, "Pyrolysis and kinetic analyses of Camel grass (Cymbopogon schoenanthus) for bioenergy," *Bioresour. Technol.*, vol. 228, pp. 18–24, 2017, doi: 10.1016/j.biortech.2016.12.096.

[2] M. Antar, D. Lyu, M. Nazari, A. Shah, X. Zhou, and D. L. Smith, "Biomass for a sustainable bioeconomy: An overview of world biomass production and utilization," *Renew. Sustain. Energy Rev.*, vol. 139, no. April 2020, p. 110691, 2021, doi: 10.1016/j.rser.2020.110691.

[3] A. Erkiaga, G. Lopez, M. Amutio, J. Bilbao, and M. Olazar, "Influence of operating conditions on the steam gasification of biomass in a conical spouted bed reactor," *Chem. Eng. J.*, vol. 237, pp. 259–267, 2014, doi: 10.1016/j.cej.2013.10.018.

[4] M. Van de Velden, J. Baeyens, A. Brems, B. Janssens, and R. Dewil, "Fundamentals, kinetics and endothermicity of the biomass pyrolysis reaction," *Renew. Energy*, vol. 35, no. 1, pp. 232–242, 2010, doi: 10.1016/j.renene.2009.04.019.

[5] Q. Wang, X. Li, K. Wang, and Y. Zhu, "Commercialization and Challenges for the Next Generation of Biofuels: Biomass Fast Pyrolysis," in *2010 Asia-Pacific Power and Energy Engineering Conference*, 2010, pp. 1–4.

[6] M. Sharifzadeh *et al.*, "The multi-scale challenges of biomass fast pyrolysis and bio-oil upgrading: Review of the state of art and future research directions," *Prog. Energy Combust. Sci.*, vol. 71, pp. 1–80, 2019, doi: 10.1016/j.pecs.2018.10.006.

[7] T. R. S. Oil and U.S. Energy Information Administration, "Shale Gas Resources: An Assessment of 137 Shale Formations in 41 Countries Outside the United States," 2013.

[8] Z. S. Baird, V. Oja, and O. Järvik, "The composition of kukersite shale oil," *Oil Shale*, vol. 40, no. 1, pp. 25–43, 2023, doi: 10.3176/oil.2023.1.02.

[9] J. P. Foltin, A. C. L. Lisboa, and A. De Klerk, "Oil Shale Pyrolysis: Conversion Dependence of Kinetic Parameters," *Energy and Fuels*, vol. 31, no. 7, pp. 6766–6776, 2017, doi: 10.1021/acs.energyfuels.7b00578.

[10] M. Kiliç, A. E. Pütün, B. B. Uzun, and E. Pütün, "Converting of oil shale and biomass into liquid hydrocarbons via pyrolysis," *Energy Convers. Manag.*, vol. 78, pp. 461–467, 2014, doi: 10.1016/j.enconman.2013.11.002.

[11] J. M. Nazzal, "The influence of grain size on the products yield and shale oil composition from the Pyrolysis of Sultani oil shale," *Energy Convers. Manag.*, vol. 49, no. 11, pp. 3278–3286, 2008, doi: 10.1016/j.enconman.2008.03.028.

[12] Q. Jin *et al.*, "Synergistic effects during co-pyrolysis of biomass and plastic: Gas, tar, soot, char products and thermogravimetric study," *J. Energy Inst.*, vol. 92, no. 1, pp. 108–117, 2019, doi: 10.1016/j.joei.2017.11.001.

[13] E. Ganev, B. Ivanov, N. Vaklieva-Bancheva, E. Kirilova, and Y. Dzhelil, "A multi-objective approach toward optimal design of sustainable integrated biodiesel/diesel supply chain based on first-and second-generation feedstock with solid waste use," *Energies*, vol. 14, no. 8, 2021, doi: 10.3390/en14082261.

[14] A. Demirbaş, "Recovery of chemicals and gasoline-range fuels from plastic wastes via pyrolysis," *Energy Sources*, vol. 27, no. 14, pp. 1313–1319, 2005, doi: 10.1080/009083190519500.

[15] A. V. Bridgwater, "Review of fast pyrolysis of biomass and product upgrading," *Biomass and Bioenergy*, vol. 38, pp. 68–94, 2012, doi: 10.1016/j.biombioe.2011.01.048.

[16] N. Ahmed, M. Zeeshan, N. Iqbal, M. Z. Farooq, and S. A. Shah, "Investigation on bio-oil yield and quality with scrap tire addition in sugarcane bagasse pyrolysis," *J. Clean. Prod.*, vol. 196, pp. 927–934, 2018, doi: 10.1016/j.jclepro.2018.06.142.

[17] G. Özsin and A. E. Pütün, "TGA/MS/FT-IR study for kinetic evaluation and evolved gas analysis of a biomass/PVC co-pyrolysis process," *Energy Convers. Manag.*, vol. 182, no. January, pp. 143–153, 2019, doi: 10.1016/j.enconman.2018.12.060.

[18] B. Moghtaderi, C. Meesri, and T. F. Wall, "Pyrolytic characteristics of blended coal and woody biomass," *Fuel*, vol. 83, no. 6, pp. 745–750, 2004, doi: 10.1016/j.fuel.2003.05.003.

[19] L. Kong, G. Li, L. Jin, and H. Hu, "Pyrolysis behaviors of two coal-related model compounds on a fixed-bed reactor," *Fuel Process. Technol.*, vol. 129, pp. 113–119, 2015, doi: 10.1016/j.fuproc.2014.09.009.

[20] A. Demirbaş and A. Demirbas, "Sustainable cofiring of biomass with coal," *Energy Convers. Manag.*, vol. 44, no. 9, pp. 1465–1479, 2003, doi: 10.1016/S0196-8904(02)00144-9.

[21] M. F. Demirbas and M. Balat, "Recent advances on the production and utilization trends of bio-fuels: A global perspective," *Energy Convers. Manag.*, vol. 47, no. 15–16, pp. 2371–2381, 2006, doi: 10.1016/j.enconman.2005.11.014.

[22] A. G. Collot, Y. Zhuo, D. R. Dugwell, and R. Kandiyoti, "Co-pyrolysis and co-gasification of coal and biomass in bench-scale fixed-bed and fluidized bed reactors," *Fuel*, vol. 78, no. 6, pp. 667–679, 1999, doi: 10.1016/S0016-2361(98)00202-6.

[23] C. Y. H. Chao, P. C. W. Kwong, J. H. Wang, C. W. Cheung, and G. Kendall, "Co-firing coal with rice husk and bamboo and the impact on particulate matters and associated polycyclic aromatic hydrocarbon emissions," *Bioresour. Technol.*, vol. 99, no. 1, pp. 83–93, 2008, doi: 10.1016/j.biortech.2006.11.051.

[24] H. Haykiri-Acma and S. Yaman, "Synergy in devolatilization characteristics of lignite and hazelnut shell during co-pyrolysis," *Fuel*, vol. 86, no. 3, pp. 373–380, 2007, doi: 10.1016/j.fuel.2006.07.005.

[25] H. Haykiri-Acma and S. Yaman, "Interaction between biomass and different rank coals during co-pyrolysis," *Renew. Energy*, vol. 35, no. 1, pp. 288–292, 2010, doi: 10.1016/j.renene.2009.08.001.

[26] C. Frau, F. Ferrara, A. Orsini, and A. Pettinau, "Characterization of several kinds of coal and biomass for pyrolysis and gasification," *Fuel*, vol. 152, pp. 138–145, 2015, doi: 10.1016/j.fuel.2014.09.054.

[27] J. Akhtar and N. A. S. Amin, "A review on process conditions for optimum bio-oil yield in hydrothermal liquefaction of biomass," *Renew. Sustain. Energy Rev.*, vol. 15, no. 3, pp. 1615–1624, 2011, doi: 10.1016/j.rser.2010.11.054.

[28] Y. A. Strizhakova and T. V. Usova, "Current trends in the pyrolysis of oil shale: A review," *Solid Fuel Chem.*, vol. 42, no. 4, pp. 197–201, 2008, doi: 10.3103/S0361521908040022.

[29] L. Zhang, C. (Charles) Xu, and P. Champagne, "Overview of recent advances in thermo-chemical conversion of biomass," *Energy Convers. Manag.*, vol. 51, no. 5, pp. 969–982, 2010, doi: 10.1016/j.enconman.2009.11.038.

[30] X. Wang *et al.*, "Synergetic effect of sewage sludge and biomass co-pyrolysis: A combined study in thermogravimetric analyzer and a fixed bed reactor," *Energy Convers. Manag.*, vol. 118, pp. 399–405, 2016, doi: 10.1016/j.enconman.2016.04.014.

[31] R. K. Singh and B. Ruj, "Time and temperature depended fuel gas generation from pyrolysis of real world municipal plastic waste," *Fuel*, vol. 174, pp. 164–171, 2016, doi: 10.1016/j.fuel.2016.01.049.

[32] G. Duman and J. Yanik, "Two-step steam pyrolysis of biomass for hydrogen production," *Int. J. Hydrogen Energy*, vol. 42, no. 27, pp. 17000–17008, 2017, doi: 10.1016/j.ijhydene.2017.05.227.

[33] W. Lan, G. Chen, X. Zhu, X. Wang, and B. Xu, "Progress in techniques of biomass conversion into syngas," *J. Energy Inst.*, vol. 88, no. 2, pp. 151–156, 2015, doi: 10.1016/j.joei.2014.05.003.

[34] S. Wang and Z. Luo, "Pyrolysis of biomass," in *GREEN Alternative Energy Resources*, Walter de Gruyter GmbH, 2017, p. 268.

[35] A. Akhtar, V. Krepl, and T. Ivanova, "A Combined Overview of Combustion, Pyrolysis, and Gasification of Biomass," *Energy and Fuels*, vol. 32, no. 7, pp. 7294–7318, 2018, doi: 10.1021/acs.energyfuels.8b01678.

[36] A. A. Lappas, V. S. Dimitropoulos, E. V. Antonakou, S. S. Voutetakis, and I. A. Vasalos, "Design, construction, and operation of a transported fluid bed process development unit for biomass fast pyrolysis: Effect of pyrolysis temperature," *Ind. Eng. Chem. Res.*, vol. 47, no. 3, pp. 742–747, 2008, doi: 10.1021/ie060990i.

[37] R. J. M. Westerhof, D. W. F. Brilman, W. P. M. Van Swaaij, and S. R. A. Kersten, "Effect of temperature in fluidized bed fast pyrolysis of biomass: Oil quality assessment in test units," *Ind. Eng. Chem. Res.*, vol. 49, no. 3, pp. 1160–1168, 2010, doi: 10.1021/ie900885c.

[38] A. Demirbas, "Effect of temperature on pyrolysis products from biomass," *Energy Sources, Part A Recover. Util. Environ. Eff.*, vol. 29, no. 4, pp. 329–336, 2007, doi: 10.1080/009083190965794.

[39] M. Garcia-Perez *et al.*, "Fast pyrolysis of oil mallee woody biomass: Effect of temperature on the yield and quality of pyrolysis products," *Ind. Eng. Chem. Res.*, vol. 47, no. 6, pp. 1846–1854, 2008, doi: 10.1021/ie071497p.

[40] M. Z. Stummann *et al.*, "Hydrogen assisted catalytic biomass pyrolysis. Effect of temperature and pressure," *Biomass and Bioenergy*, vol. 115, pp. 97–107, 2018, doi: 10.1016/j.biombioe.2018.04.012.

[41] A. Dufour, P. Girods, E. Masson, Y. Rogaume, and A. Zoulalian, "Synthesis gas production by biomass pyrolysis: Effect of reactor temperature on product distribution," *Int. J. Hydrogen Energy*, vol. 34, no. 4, pp. 1726–1734, 2009, doi: 10.1016/j.ijhydene.2008.11.075.

[42] A. Zolghadr, J. J. Biernacki, and R. J. Moore, "Biomass fast pyrolysis using a novel microparticle microreactor approach: Effect of particles size, biomass type, and temperature," *Energy and Fuels*, vol. 33, no. 2, pp. 1146–1156, 2019, doi: 10.1021/acs.energyfuels.8b03395.

[43] K. R. Gaston, M. W. Jarvis, P. Pepiot, K. M. Smith, W. J. Frederick, and M. R. Nimlos, "Biomass pyrolysis and gasification of varying particle sizes in a fluidized-bed reactor," *Energy and Fuels*, vol. 25, no. 8, pp. 3747–3757, 2011, doi: 10.1021/ef200257k.

[44]   H. Bennadji, K. Smith, M. J. Serapiglia, and E. M. Fisher, "Effect of particle size on low-temperature pyrolysis of woody biomass," *Energy and Fuels*, vol. 28, no. 12, pp. 7527–7537, 2014, doi: 10.1021/ef501869e.

[45]   D. Angin, "Effect of pyrolysis temperature and heating rate on biochar obtained from pyrolysis of safflower seed press cake," *Bioresour. Technol.*, vol. 128, pp. 593–597, 2013, doi: 10.1016/j.biortech.2012.10.150.

[46]   J. L. Klinger *et al.*, "Effect of biomass type, heating rate, and sample size on microwave-enhanced fast pyrolysis product yields and qualities," *Appl. Energy*, vol. 228, no. June, pp. 535–545, 2018, doi: 10.1016/j.apenergy.2018.06.107.

[47]   S. A. El-Sayed and M. Khairy, "Effect of heating rate on the chemical kinetics of different biomass pyrolysis materials," *Biofuels*, vol. 6, no. 3–4, pp. 157–170, 2015, doi: 10.1080/17597269.2015.1065590.

[48]   M. Somerville and A. Deev, "The effect of heating rate, particle size and gas flow on the yield of charcoal during the pyrolysis of radiata pine wood," *Renew. Energy*, vol. 151, pp. 419–425, 2020, doi: 10.1016/j.renene.2019.11.036.

[49]   M. N. Uddin *et al.*, "An overview of recent developments in biomass pyrolysis technologies," *Energies*, vol. 11, no. 11, p. 3115, 2018, doi: 10.3390/en11113115.

[50]   X. Hu and M. Gholizadeh, "Biomass pyrolysis: A review of the process development and challenges from initial researches up to the commercialisation stage," *J. Energy Chem.*, vol. 39, no. x, pp. 109–143, 2019, doi: 10.1016/j.jechem.2019.01.024.

[51]   D. Lachos-Perez *et al.*, "Review on Biomass Pyrolysis with a Focus on Bio-Oil Upgrading Techniques," *Analytica*, vol. 4, no. 2, pp. 182–205, 2023, doi: 10.3390/analytica4020015.

[52]   B. Igliński, W. Kujawski, and U. Kiełkowska, "Pyrolysis of Waste Biomass: Technical and Process Achievements, and Future Development—A Review," *Energies*, vol. 16, no. 4, 2023, doi: 10.3390/en16041829.

[53]   T. V. Le Doan, N. W. Bostrom, A. K. Burnham, R. L. Kleinberg, A. E. Pomerantz, and P. Allix, "Green river oil shale pyrolysis: Semi-open conditions," *Energy and Fuels*, vol. 27, no. 11, pp. 6447–6459, 2013, doi: 10.1021/ef401162p.

[54]   J. L. Hillier and T. H. Fletcher, "Pyrolysis kinetics of a green river oil shale using a pressurized TGA," *Energy and Fuels*, vol. 25, no. 1, pp. 232–239, 2011, doi: 10.1021/ef101115u.

[55]   E. Akalin *et al.*, "Co-hydrothermal Liquefaction of Lignocellulosic Biomass with Kukersite Oil Shale," *Energy and Fuels*, vol. 33, no. 8, pp. 7424–7435, 2019, doi: 10.1021/acs.energyfuels.9b01473.

[56]   E. Knaus, J. Killen, K. Biglarbigi, and P. Crawford, "An overview of oil shale resources," *ACS Symp. Ser.*, vol. 1032, pp. 3–20, 2010, doi: 10.1021/bk-2010-1032.ch001.

[57]   X. Han, I. Kulaots, X. Jiang, and E. M. Suuberg, "Review of oil shale semicoke and its combustion utilization," *Fuel*, vol. 126, pp. 143–161, 2014, doi: 10.1016/j.fuel.2014.02.045.

[58]   Q. Q. Liu, X. X. Han, Q. Y. Li, Y. R. Huang, and X. M. Jiang, "TG-DSC analysis of pyrolysis process of two Chinese oil shales," *J. Therm. Anal. Calorim.*, vol. 116, no. 1, pp. 511–517, 2014, doi: 10.1007/s10973-013-3524-2.

[59]   V. Oja and E. M. Suuberg, "Oil Shale oil shale Processing oil shale processing, Chemistry and Technology," in *Encyclopedia of Sustainability Science and Technology*, Springer New York, 2012, pp. 7457–7491.

[60] M. A. Raja, Y. Zhao, X. Zhang, C. Li, and S. Zhang, "Practices for modeling oil shale pyrolysis and kinetics," *Rev. Chem. Eng.*, vol. 34, no. 1, pp. 21–42, 2017, doi: 10.1515/revce-2016-0038.

[61] J. Boak, "Shale-Hosted Hydrocarbons and Hydraulic Fracturing," in *Future Energy: Improved, Sustainable and Clean Options for our Planet*, 2013, pp. 117–143.

[62] J. G. Speight, *Origin and Properties of Oil Shale*. 2012.

[63] F. Bai, Y. Sun, Y. Liu, Q. Li, and M. Guo, "Thermal and kinetic characteristics of pyrolysis and combustion of three oil shales," *Energy Convers. Manag.*, vol. 97, pp. 374–381, 2015, doi: 10.1016/j.enconman.2015.03.007.

[64] H. Luik, L. Luik, L. Tiikma, and N. Vink, "Parallels between slow pyrolysis of Estonian oil shale and forest biomass residues," *J. Anal. Appl. Pyrolysis*, vol. 79, no. 1-2 SPEC. ISS., pp. 205–209, 2007, doi: 10.1016/j.jaap.2006.12.003.

[65] I. Johannes, K. Kruusement, and R. Veski, "Evaluation of oil potential and pyrolysis kinetics of renewable fuel and shale samples by Rock-Eval analyzer," *J. Anal. Appl. Pyrolysis*, vol. 79, no. 1-2 SPEC. ISS., pp. 183–190, 2007, doi: 10.1016/j.jaap.2006.12.001.

[66] M. V. Kök, "Evaluation of Turkish oil shales - Thermal analysis approach," *Oil Shale*, vol. 18, no. 2, pp. 131–138, 2001.

[67] M. V. Kök and R. Pamir, "Pyrolysis kinetics of oil shales determined by DSC and TG/DTG," *Oil Shale*, vol. 20, no. 1, pp. 57–68, 2003.

[68] M. V. KöK, G. Guner, and S. Bagci, "Combustion kinetics of oil shales by reaction cell experiments," *Oil Shale*, vol. 25, no. 1, pp. 5–16, 2008, doi: 10.3176/oil.2008.1.02.

[69] B. Chen, X. Han, M. Mu, and X. Jiang, "Studies of the Co-pyrolysis of Oil Shale and Wheat Straw," *Energy and Fuels*, vol. 31, no. 7, pp. 6941–6950, 2017, doi: 10.1021/acs.energyfuels.7b00871.

[70] B. Chen *et al.*, "Studies of fast co-pyrolysis of oil shale and wood in a bubbling fluidized bed," *Energy Convers. Manag.*, vol. 205, no. September 2019, p. 112356, 2020, doi: 10.1016/j.enconman.2019.112356.

[71] X. X. Han, X. M. Jiang, and Z. G. Cui, "Studies of the effect of retorting factors on the yield of shale oil for a new comprehensive utilization technology of oil shale," *Appl. Energy*, vol. 86, no. 11, pp. 2381–2385, 2009, doi: 10.1016/j.apenergy.2009.03.014.

[72] A. M. Khalil, "Oil shale pyrolysis and effect of particle size on the composition of shale oil," *Oil Shale*, vol. 30, no. 2, pp. 136–146, 2013, doi: 10.3176/oil.2013.2.04.

[73] W. Sha, J. Liu, X. Jiang, X. Han, and J. Tong, "Effect of heating rate on products yield and characteristics of non-condensable gases and shale oil obtained by retorting Dachengzi oil shale," *Oil Shale*, vol. 30, no. 1, pp. 27–47, 2013, doi: 10.3176/oil.2013.1.04.

[74] J. Yanik *et al.*, "Low-temperature pyrolysis and co-pyrolysis of Göynük oil shale and terebinth berries (Turkey) in an autoclave," *Oil Shale*, vol. 28, no. 4, pp. 469–486, 2011, doi: 10.3176/oil.2011.4.02.

[75] H. Jiang *et al.*, "Preliminary Study on Copyrolysis of Spent Mushroom Substrate as Biomass and Huadian Oil Shale," *Energy and Fuels*, vol. 30, no. 8, pp. 6342–6349, 2016, doi: 10.1021/acs.energyfuels.6b01085.

[76] N. Jamal M and W. Paul T, "Influence of temperature and steam on the products from the flash pyrolysis of Jordan oil shale," *Int. J. Energy Res.*, vol. 26, no. 14, pp. 1207–1219, 2002.

[77] J. G. Na, C. H. Im, S. H. Chung, and K. B. Lee, "Effect of oil shale retorting temperature on shale oil yield and properties," *Fuel*, vol. 95, pp. 131–135, 2012, doi: 10.1016/j.fuel.2011.11.029.

[78] O. S. Al-Ayed, A. Al-Harahsheh, A. M. Khaleel, and M. Al-Harahsheh, "Oil shale pyrolysis in fixed-bed retort with different heating rates," *Oil Shale*, vol. 26, no. 2, pp. 139–147, 2009, doi: 10.3176/oil.2009.2.06.

[79] M. À. Olivella and F. X. C. De Las Heras, "Evaluation of linear kinetic methods from pyrolysis data of spanish oil shales and coals," *Oil Shale*, vol. 25, no. 2, pp. 227–245, 2008, doi: 10.3176/oil.2008.2.05.

[80] A. Aboulkas, T. Makayssi, L. Bilali, K. El Harfi, M. Nadifiyine, and M. Benchanaa, "Co-pyrolysis of oil shale and plastics: Influence of pyrolysis parameters on the product yields," *Fuel Process. Technol.*, vol. 96, pp. 209–213, 2012, doi: 10.1016/j.fuproc.2011.12.001.

[81] O. Järvik and V. Oja, "Molecular weight distributions and average molecular weights of pyrolysis oils from oil shales: Literature data and measurements by size exclusion chromatography (SEC) and atmospheric solids analysis probe mass spectroscopy (ASAP MS) for oils from four di," *Energy and Fuels*, vol. 31, no. 1, pp. 328–339, 2017, doi: 10.1021/acs.energyfuels.6b02452.

[82] B. A. Akash and J. O. Jaber, "Characterization of shale oil as compared to crude oil and some refined petroleum products," *Energy Sources*, vol. 25, no. 12, pp. 1171–1182, 2003, doi: 10.1080/00908310390233612.

[83] O. Gavrilova, R. Vilu, and L. Vallner, "A life cycle environmental impact assessment of oil shale produced and consumed in Estonia," *Resour. Conserv. Recycl.*, vol. 55, no. 2, pp. 232–245, 2010, doi: 10.1016/j.resconrec.2010.09.013.

[84] N. D. Ristic, M. R. Djokic, A. Konist, K. M. Van Geem, and G. B. Marin, "Quantitative compositional analysis of Estonian shale oil using comprehensive two dimensional gas chromatography," *Fuel Process. Technol.*, vol. 167, pp. 241–249, 2017, doi: 10.1016/j.fuproc.2017.07.008.

[85] B. Maaten, O. Järvik, O. Pihl, A. Konist, and A. Siirde, "Oil shale pyrolysis products and the fate of sulfur," *Oil Shale*, vol. 37, no. 1, pp. 51–69, 2020, doi: 10.3176/oil.2020.1.03.

[86] H. Pikkor, B. Maaten, Z. S. Baird, O. Järvik, A. Konist, and H. Lees, "Surface area of oil shale and its solid pyrolysis products depending on the particle size," *Chem. Eng. Trans.*, vol. 81, no. 2010, pp. 961–966, 2020, doi: 10.3303/CET2081161.

[87] H. Lees, O. Järvik, A. Konist, A. Siirde, and B. Maaten, "Comparison of the ecotoxic properties of oil shale industry by-products to those of coal ash," *Oil Shale*, vol. 39, no. 1, pp. 1–19, 2022, doi: 10.3176/oil.2022.1.01.

[88] T. Pihu, A. Konist, E. Puura, M. Liira, and K. Kirsimäe, "Properties and environmental impact of oil shale ash landfills," *Oil Shale*, vol. 36, no. 2, pp. 257–270, 2019, doi: 10.3176/oil.2019.2.01.

[89] S. Li, X. Chen, A. Liu, L. Wang, and G. Yu, "Co-pyrolysis characteristic of biomass and bituminous coal," *Bioresour. Technol.*, vol. 179, pp. 414–420, 2015, doi: 10.1016/j.biortech.2014.12.025.

[90] C. Quan, S. Xu, Y. An, and X. Liu, "Co-pyrolysis of biomass and coal blend by TG and in a free fall reactor," *J. Therm. Anal. Calorim.*, vol. 117, no. 2, pp. 817–823, 2014, doi: 10.1007/s10973-014-3774-7.

[91] S. Krerkkaiwan, C. Fushimi, A. Tsutsumi, and P. Kuchonthara, "Synergetic effect during co-pyrolysis/gasification of biomass and sub-bituminous coal," *Fuel Process. Technol.*, vol. 115, pp. 11–18, 2013, doi: 10.1016/j.fuproc.2013.03.044.

[92] M. Dai, Z. Yu, S. Fang, and X. Ma, "Behaviors, product characteristics and kinetics of catalytic co-pyrolysis spirulina and oil shale," *Energy Convers. Manag.*, vol. 192, no. March, pp. 1–10, 2019, doi: 10.1016/j.enconman.2019.04.032.

[93] I. Johannes, L. Tiikma, and H. Luik, "Synergy in co-pyrolysis of oil shale and pine sawdust in autoclaves," *J. Anal. Appl. Pyrolysis*, vol. 104, pp. 341–352, 2013, doi: 10.1016/j.jaap.2013.06.015.

[94] J. Bai, X. Chen, J. Shao, C. Jia, and Q. Wang, "Study of breakage of main covalent bonds during co-pyrolysis of oil shale and alkaline lignin by TG-FTIR integrated analysis," *J. Energy Inst.*, vol. 92, no. 3, pp. 512–522, 2019, doi: 10.1016/j.joei.2018.04.007.

[95] Y. Zhai, T. Yang, Y. Zhang, and Y. Zhu, "Co-pyrolysis characteristics of raw / torrefied corn stalk and oil shale," *J. Anal. Appl. Pyrolysis*, vol. 171, no. March, p. 105967, 2023, doi: 10.1016/j.jaap.2023.105967.

[96] S. Cui, T. Yang, Y. Zhai, Y. Zhu, Z. Yu, and X. Kai, "Investigation on the characteristics and interaction of co-pyrolysis of oil shale and peanut shell," *Fuel*, vol. 340, no. November 2022, p. 127502, 2023, doi: 10.1016/j.fuel.2023.127502.

[97] B. Chen *et al.*, "Simulation analysis of Co-Pyrolysis of oil shale and wheat straw based on the combination of chain reaction kinetics and improved CPD models," *Energy Convers. Manag.*, vol. 243, no. March, p. 114405, 2021, doi: 10.1016/j.enconman.2021.114405.

[98] Y. Zhai, Y. Zhu, S. Cui, Y. Tao, X. Kai, and T. Yang, "Study on the co-pyrolysis of oil shale and corn stalk : Pyrolysis characteristics , kinetic and gaseous product analysis," *J. Anal. Appl. Pyrolysis*, vol. 163, no. January, p. 105456, 2022, doi: 10.1016/j.jaap.2022.105456.

[99] Z. Hu, X. Ma, and L. Li, "The synergistic effect of co-pyrolysis of oil shale and microalgae to produce syngas," *J. Energy Inst.*, vol. 89, no. 3, pp. 447–455, 2016, doi: 10.1016/j.joei.2015.02.009.

[100] R. Ochieng, A. L. Cerón, A. Konist, and S. Sarker, "Experimental and modeling studies of intermediate pyrolysis of wood in a laboratory-scale continuous feed retort reactor," *Bioresour. Technol. Reports*, vol. 24, no. August, 2023, doi: 10.1016/j.biteb.2023.101650.

[101] R. Ebrahimi-Kahrizsangi and M. H. Abbasi, "Evaluation of reliability of Coats-Redfern method for kinetic analysis of non-isothermal TGA," *Trans. Nonferrous Met. Soc. China (English Ed.)*, vol. 18, no. 1, pp. 217–221, 2008, doi: 10.1016/S1003-6326(08)60039-4.

[102] H. E. Kissinger, "Reaction Kinetics in Differential Thermal Analysis," *Anal. Chem.*, vol. 29, no. 11, pp. 1702–1706, Nov. 1957, doi: 10.1021/ac60131a045.

[103] H. Friedman, "Kinetics of Thermal Degradation of Char-Forming Plastics From Thermogravimetry. Application to Phenolic Plastic," *J. Polym. Sci. Part C Polym. Symp.*, vol. 6, pp. 183–195, Mar. 2007, doi: 10.1002/polc.5070060121.

[104] S. Vyazovkin, "Modification of the Integral Isoconversional Method to Account for Variation in Activation Energy," *J. Comput. Chem.*, vol. 22, pp. 178–183, Jan. 2001, doi: 10.1002/1096-987X(20010130)22:23.0.CO;2-#.

[105] E. Ranzi *et al.*, "Chemical kinetics of biomass pyrolysis," *Energy and Fuels*, vol. 22, no. 6, pp. 4292–4300, Nov. 2008, doi: 10.1021/EF800551T/SUPPL_FILE/EF800551T_SI_001.PDF.

[106] R. C. Baliban, J. A. Elia, and C. A. Floudas, "Toward novel hybrid biomass, coal, and natural gas processes for satisfying current transportation fuel demands, 1: Process alternatives, gasification modeling, process simulation, and economic analysis," *Ind. Eng. Chem. Res.*, vol. 49, no. 16, pp. 7343–7370, Aug. 2010, doi: 10.1021/IE100063Y/SUPPL_FILE/IE100063Y_SI_001.XLS.

[107] S. Mozaffari, O. Järvik, and Z. S. Baird, "Composition of gas from pyrolysis of Estonian oil shale with various sweep gases," vol. 38, no. 3, pp. 215–227, 2021, doi: 10.3176/oil.2021.3.03.

[108] A. L. Cerón, A. Konist, H. Lees, and O. Järvik, "Effect of woody biomass gasification process conditions on the composition of the producer gas," *Sustainability (Switzerland)*, vol. 13, no. 21. 2021, doi: 10.3390/su132111763.

[109] Q. Wang, B. Sun, A. Hu, J. Bai, and S. Li, "Pyrolysis characteristics of Huadian oil shales," *Oil Shale*, vol. 24, no. 2, pp. 147–157, 2007.

[110] P. Tiwari and M. Deo, "Compositional and kinetic analysis of oil shale pyrolysis using TGA-MS," *Fuel*, vol. 94, pp. 333–341, 2012, doi: 10.1016/j.fuel.2011.09.018.

[111] P. Tiwari and M. Deo, "Detailed Kinetic Analysis of Oil Shale Pyrolysis TGA Data," *AIChE J.*, vol. 58, no. 2, pp. 505–515, 2012, doi: 10.1002/aic.

[112] A. Bieniek, W. Jerzak, and A. Magdziarz, "Experimental studies of intermediate pyrolysis of woody and agricultural biomass in a fixed bed reactor," *E3S Web Conf.*, vol. 323, pp. 1–6, 2021, doi: 10.1051/e3sconf/202132300003.

[113] B. Maaten, L. Loo, A. Konist, D. Nešumajev, T. Pihu, and I. Külaots, "Decomposition kinetics of American, Chinese and Estonian oil shales kerogen," *Oil Shale*, vol. 33, no. 2, pp. 167–183, 2016, doi: 10.3176/oil.2016.2.05.

[114] J. Ye, J. Xiao, X. Huo, Y. Gao, J. Hao, and M. Song, "Effect of CO2 atmosphere on biomass pyrolysis and in-line catalytic reforming," *Int. J. Energy Res.*, vol. 44, no. 11, pp. 8936–8950, 2020, doi: 10.1002/er.5602.

[115] T. S. Farrow, C. Sun, and C. E. Snape, "Impact of CO2 on biomass pyrolysis, nitrogen partitioning, and char combustion in a drop tube furnace," *J. Anal. Appl. Pyrolysis*, vol. 113, pp. 323–331, 2015, doi: 10.1016/j.jaap.2015.02.013.

[116] G. Özbay, "Catalytic Pyrolysis of Pine Wood Sawdust to Produce Bio-oil: Effect of Temperature and Catalyst Additives," *J. Wood Chem. Technol.*, vol. 35, no. 4, pp. 302–313, 2015, doi: 10.1080/02773813.2014.958240.

[117] E. Grieco and G. Baldi, "Analysis and modelling of wood pyrolysis," *Chem. Eng. Sci.*, vol. 66, no. 4, pp. 650–660, 2011, doi: 10.1016/j.ces.2010.11.018.

[118] L. Fagernäs, E. Kuoppala, K. Tiilikkala, and A. Oasmaa, "Chemical composition of birch wood slow pyrolysis products," *Energy and Fuels*, vol. 26, no. 2, pp. 1275–1283, 2012, doi: 10.1021/ef2018836.

[119] Y. Yang, J. G. Brammer, A. S. N. Mahmood, and A. Hornung, "Intermediate pyrolysis of biomass energy pellets for producing sustainable liquid, gaseous and solid fuels," *Bioresour. Technol.*, vol. 169, pp. 794–799, Oct. 2014, doi: 10.1016/J.BIORTECH.2014.07.044.

[120] G. Ningbo, L. Baoling, L. Aimin, and L. Juanjuan, "Continuous pyrolysis of pine sawdust at different pyrolysis temperatures and solid residence times," *J. Anal. Appl. Pyrolysis*, vol. 114, pp. 155–162, 2015, doi: 10.1016/j.jaap.2015.05.011.

[121] D. B. Wiedemeier *et al.*, "Aromaticity and degree of aromatic condensation of char," *Org. Geochem.*, vol. 78, pp. 135–143, 2015, doi: 10.1016/j.orggeochem.2014.10.002.

[122] N. Olukcu, J. Yanik, M. Saglam, and M. Yuksel, "Liquefaction of beypazari oil shale by pyrolysis," *J. Anal. Appl. Pyrolysis*, vol. 64, no. 1, pp. 29–41, 2002, doi: 10.1016/S0165-2370(01)00168-1.

[123] S. Mozaffari, O. Järvik, and Z. S. Baird, "Effect of N2 and CO2 on shale oil from pyrolysis of Estonian oil shale," *Int. J. Coal Prep. Util.*, vol. 00, no. 00, pp. 1–15, 2021, doi: 10.1080/19392699.2021.1914025.

[124] M. F. Demirbas, "Characterization of bio-oils from spruce wood (Picea orientalis L.) via pyrolysis," *Energy Sources, Part A Recover. Util. Environ. Eff.*, vol. 32, no. 10, pp. 909–916, 2010, doi: 10.1080/15567030903059970.

[125] F. Tinwala, P. Mohanty, S. Parmar, A. Patel, and K. K. Pant, "Intermediate pyrolysis of agro-industrial biomasses in bench-scale pyrolyser: Product yields and its characterization," *Bioresour. Technol.*, vol. 188, pp. 258–264, Jul. 2015, doi: 10.1016/J.BIORTECH.2015.02.006.

[126] E. Okoroigwe, Z. Li, T. Stuecken, C. Saffron, and S. Onyegegbu, "Pyrolysis of Gmelina arborea wood for bio-oil/bio-char production: Physical and chemical characterisation of products," *Journal of Applied Sciences*, vol. 12, no. 4. pp. 369–374, 2012, doi: 10.3923/jas.2012.369.374.

[127] A. Y. Yadykova and S. O. Ilyin, "Compatibility and rheology of bio-oil blends with light and heavy crude oils," *Fuel*, vol. 314, p. 122761, Apr. 2022, doi: 10.1016/J.FUEL.2021.122761.

[128] O. Järvik and V. Oja, "Molecular weight distributions and average molecular weights of pyrolysis oils from oil shales: Literature data and measurements by size exclusion chromatography (SEC) and atmospheric solids analysis probe mass spectroscopy (ASAP MS) for oils from four different deposits," *Energy and Fuels*, vol. 31, no. 1, pp. 328–339, Jan. 2017, doi: 10.1021/ACS.ENERGYFUELS.6B02452/SUPPL_FILE/EF6B02452_SI_001.PDF.

[129] F. Jin, P. Liu, L. Chen, D. Hua, and X. Yi, "Study on the thermal stability of the bio-oil components by Py-GC/MS," *Energy Reports*, vol. 9, pp. 280–288, 2023, doi: 10.1016/j.egyr.2023.04.001.

[130] S. Yorgun and D. Yildiz, "Slow pyrolysis of paulownia wood: Effects of pyrolysis parameters on product yields and bio-oil characterization," *J. Anal. Appl. Pyrolysis*, vol. 114, pp. 68–78, 2015, doi: 10.1016/j.jaap.2015.05.003.

[131] J. Zandersons *et al.*, "Pyrolysis and smoke formation of grey alder wood depending on the storage time and the content of extractives," *J. Anal. Appl. Pyrolysis*, vol. 85, no. 1–2, pp. 163–170, 2009, doi: 10.1016/j.jaap.2008.11.036.

[132] L. Zhang, C. Shen, and R. Liu, "GC-MS and FT-IR analysis of the bio-oil with addition of ethyl acetate during storage," *Front. Energy Res.*, vol. 2, no. JAN, p. 75175, Jan. 2014, doi: 10.3389/FENRG.2014.00003/BIBTEX.

[133] A. L. dos Santos *et al.*, "Quantitative GC-MS Analysis of Sawdust Bio-Oil," *J. Braz. Chem. Soc.*, vol. 34, no. 11, pp. 1581–1591, 2023, doi: 10.21577/0103-5053.20230060.

[134] M. Baqain, D. Neshumayev, and A. Konist, "TG-MS analysis and kinetic study of co-combustion of ca-rich oil shale with biomass in air and oxy-like conditions," *Carbon Capture Sci. Technol.*, vol. 10, no. November 2023, p. 100162, 2024, doi: 10.1016/j.ccst.2023.100162.

[135]   R. Ochieng, A. L. Cerón, A. Konist, and S. Sarker, "A combined analysis of the drying and decomposition kinetics of wood pyrolysis using non-isothermal thermogravimetric methods," *Energy Convers. Manag. X*, vol. 20, no. March, 2023, doi: 10.1016/j.ecmx.2023.100424.

[136]   P. E. A. Debiagi *et al.*, "Extractives Extend the Applicability of Multistep Kinetic Scheme of Biomass Pyrolysis," *Energy and Fuels*, vol. 29, no. 10, pp. 6544–6555, Oct. 2015, doi: 10.1021/ACS.ENERGYFUELS.5B01753/SUPPL_FILE/EF5B01753_SI_002.PDF.

Acknowledgments

Abstract

Co-pyrolysis of biomass and oil shale

Substituting fossil fuels partially with biomass offers a promising alternative for generating cleaner and more sustainable energy and fuels. Biomass and oil shale co-pyrolysis offers a feasible means for the shift toward carbon neutrality. Considering the similarities in their thermochemical behaviour in pyrolysis, the existing infrastructure from conventional shale oil production has the potential to be used for co-pyrolysis with biomass, reducing oil shale usage and mitigating its environmental impact. Furthermore, co-pyrolysis of oil shale and biomass yields products with enhanced yields and improved properties.

This study investigates the potential benefits of the co-pyrolysis of biomass and oil shale, as well as their interactions. Starting from a comprehensive review of recent co-pyrolysis studies, it analyses various experimental and operational parameters, as well as the yields and composition of co-pyrolytic products. The overview extends to the effects of co-pyrolysis on different fuel blends and the effects of different pyrolysis parameters—such as alternative atmospheres, heating rate, reaction temperature, and particle size—on enhancing the pyrolysis process and its product quality. Co-pyrolysis demonstrates the potential to achieve higher yields of products with improved properties while mitigating the environmental impacts associated with fossil fuel usage.

Experimental analyses were conducted using thermogravimetric analysis equipment, a batch reactor, and a continuous feed reactor. The co-pyrolysis behaviour; the yields and composition of solid, gaseous, and liquid products; and possible interactions between biomass and oil shale were studied.

A comparison between theoretical and experimental residual mass yields of oil shale-biomass mixtures demonstrated an additive behaviour, indicating no significant interactions between the fuels. In thermogravimetric studies, the use of biomass in oil shale mixtures led to a reduction of up to 34.4 wt% in solid residues compared to individual oil shale pyrolysis. Additionally, as the biomass ratio increased, the thermal decomposition curves shifted to lower temperatures by up to 10 °C. Kinetic analyses confirmed a two-stage pyrolysis process, where the most significant decomposition of biomass and oil shale occurs at different stages of conversion. Aspen Plus® was utilized with kinetic data derived from thermogravimetric analysis from co-pyrolysis. The model closely matched experimental thermogravimetric data, with absolute errors ranging from 1.7% to 3.8%, highlighting the significance of thermal analysis in simulating co-pyrolysis processes and reactor design.

In the batch reactor experiments, the differences between the experimental and theoretical mass balances of the fuel blends were found to be less than 2.5 wt% (close to the experimental uncertainty), indicating an additive behaviour and minimal interactions between the fuels. The use of biomass and alternative atmospheres was observed to enhance pyrolysis by promoting increased fuel decomposition, a higher proportion of combustible gases, and a reduced fraction of residual mass.

In the continuous feed reactor experiments, the highest yields of liquids and gases were achieved with increasing proportions of biomass, reaching 43.9 and 35.1 wt%, respectively. The maximum yield of solids was observed with higher proportions of oil shale, reaching 74.3 wt%. Analysis of elemental composition, as well as FTIR and GC-MS data, confirmed an additive rather than synergistic behaviour in the yields and composition of co-pyrolysis products. The combined properties of co-pyrolysis resulted

in improved liquid products, characterized by reduced oxygenated compounds (ketones and phenols) from biomass and decreased aromatic hydrocarbons from oil shale. Co-pyrolysis liquids contained more aliphatic hydrocarbons ranging from C_6 to C_{11}, contributing to enhanced stability and heating value of the liquid products.

Overall, this work succeeded in furthering our understanding of the co-pyrolysis of biomass and oil shale, potentially contributing to a paradigmatical shift in the way these valuable resources are utilized. The thesis was divided into two sections. First, an overview to study the developments, findings, and advancements in biomass and oil shale co-pyrolysis. The second section consisted of experimental, kinetic, and modelling work on the co-pyrolysis of oil shale and biomass, in optimized operational parameters using experimental equipment over three different scales. This allowed the characterization of the pyrolytic behaviour and the characterization of the co-pyrolysis products.

Lühikokkuvõte

Biomassi ja põlevkivi koospürolüüs

Fossiilkütuste osaline asendamine biomassiga pakub võimalusi puhtama ja säästvama energia ning kütuste tootmiseks. Biomassi ja põlevkivi koospürolüüs võib pakkuda üht võimalikku lahendust süsinikdioksiidi neutraalsusele üleminekuks. Võttes arvesse nende lähtematerjalide termokeemilise käitumise sarnasust pürolüüsil, on võimalik juba olemasolevat infrastruktuuri, mis pärineb tavapärasest põlevkiviõli tootmisest, kasutada biomassi koospürolüüsiks, vähendades põlevkivi kasutamist ja leevendades selle keskkonnamõju. Põlevkivi ja biomassi koospürolüüsil on võimalik saada tooteid millel on paremad omadused ja suurem saagikus.

Käesolevas doktoritöös uuritakse biomassi ja põlevkivi koospürolüüsi võimalikke eeliseid ja koostoimet. Alustades hiljutiste koospürolüüsiuuringute põhjalikust ülevaatest, uuring analüüsib erinevaid katse- ja tööparameetreid ning koospürolüüsil saadavate produktide saagikust ja koostist. Ülevaade hõlmab ka koospürolüüsi mõju erinevatele kütusesegudele ning erinevate pürolüüsiparameetrite – näiteks alternatiivsete atmosfääride, kuumutamiskiiruse, reaktsioonitemperatuuri ja osakeste suuruse – mõju pürolüüsiprotsessi ja -produktide kvaliteedi parandamisele. Koospürolüüs näitab potentsiaali, et sellega on võimalik saada suurema saagikuse ja paremate omadustega õlisid, vähendades samal ajal fossiilsete kütuste kasutamisega seotud keskkonnamõjusid.

Katsed viidi läbi termogravimeetrilises analüüsiseadmes, portsjonreaktoris ja pidevvoolureaktoris. Uuriti biomassi ja põlevkivi käitumist koospürolüüsil, tahkete, gaasiliste ja vedelate produktide saagikust ja koostist ning pürolüüsivõimalikke sünergilisi efekte.

Põlevkivi ja biomassi segude teoreetilise ja eksperimentaalse jääkmassi saagikuse võrdlus näitas aditiivset käitumist, mis näitab, et kütuste vahel ei ole olulisi vastastikmõjusid. Termogravimeetrilistes uuringutes vähendas biomassi kasutamine koos põlevkivi tahkeid jääke kuni 34.4 massiprotsendi võrra võrreldes puhta põlevkivi pürolüüsiga. Lisaks sellele nihkusid biomassi osakaalu suurenemisel termilise lagunemise kõverad kuni 10 °C võrra madalamale temperatuurile. Kineetiline analüüs kinnitas kaheetapilist pürolüüsiprotsessi, kus biomassi ja põlevkivi kõige olulisem lagunemine toimub eri muundamisetappides. Töös kasutati Aspen Plus® tarkvarakoos termogravimeetrilisest analüüsist saadud koospürolüüsi kineetiliste andmetega. Valminud mudel vastas täpselt eksperimentaalsetele termogravimeetrilistele andmetele, kusjuures absoluutsed vead olid vahemikus 1.7-3.8%, mis rõhutab termilise analüüsi tähtsust koospürolüüsiprotsesside ja reaktori projekteerimise simuleerimisel.

Portsjonreaktori katsetes leiti, et kütusesegude eksperimentaalse ja teoreetilise massibilansi erinevused olid vähem kui 2.5 massiprotsenti (mis on lähedane eksperimentaalsele määramatusele).See näitab, et kütused käituvad aditiivselt ja nende vastastikmõju on minimaalne. Täheldati, et biomassi ja alternatiivsete atmosfääride kasutamine tõhustab pürolüüsi, soodustades kütuse suuremat lagunemist, suuremat põlevate gaaside osakaalu ja väiksemat jääkmassi osakaalu.

Pidevvoolureaktori katsetes saavutati suurim vedelike ja gaaside saagis biomassi osakaalu suurendamisel, ulatudes vastavalt 43.9 massiprotsendi ja 35.1 massiprotsendini. Maksimaalne tahkete ainete saagis saavutati suurema põlevkivi osakaalu korral, ulatudes 74.3 massiprotsendini. Elementkoostise analüüs ning FTIR- ja GC-MS-andmed kinnitasid, et koospürolüüsitoodete saagis ja koostis on pigem aditiivne

kui sünergiline. Koospürolüüsi kombineeritud omaduste tulemusena saadi paremaid vedelaid tooteid, mida iseloomustab biomassi hapnikuühendite (ketoonide ja fenoolide) vähenemine ja põlevkivi aromaatsete süsivesinike vähenemine. Koospürolüüsi vedelikes oli rohkem alifaatseid süsivesinikke vahemikus C_6 kuni C_{11}, mis aitas kaasa vedelate toodete stabiilsuse ja kütteväärtuse suurenemisele.

Üldiselt oli käesoleva doktoritöö eesmärk uurida biomassi ja põlevkivi koospürolüüsi. Uurimistöö oli jagatud kahte ossa. Esiteks ülevaade, et uurida biomassi ja põlevkivi koospürolüüsi arenguid, järeldusi ja edusamme. Ülevaade hõlmas kõige olulisemaid uuringuid, keskendudes koospürolüüsi parameetrite tähtsusele, koostoimetele koospürolüüsis ja koospürolüüsi toodetele. Teine osa koosnes põlevkivi ja biomassi koospürolüüsi eksperimentaalsetest, kineetilistest ja modelleerimist käsitlevatest töödest, kolme erineva suurusega proovide optimeeritud tööparameetritega katseseadmetes. See võimaldas iseloomustada pürolüüsi käitumist ja iseloomustada koospürolüüsi tooteid.

Appendix (Publications)

Publication I

Current status of co-pyrolysis of oil shale and biomass

Alejandro Lyons Cerón*, Alar Konist, Heidi Lees, Oliver Järvik

Department of Energy Technology, Tallinn University of Technology, Ehitajate tee 5, 19086 Tallinn, Estonia

Abstract. *The use of biomass (BM) and oil shale (OS) blends for the production of cleaner and improved fuels and chemicals through co-pyrolysis has recently attracted attention. The potential benefits, synergetic effects, interactions and promotion and inhibition effects of co-pyrolysis of BM and OS are reviewed and analyzed in this article based on an overview of various recent studies of co-pyrolysis, including the experimental and operational parameters and the yield and composition of the products. The effects of co-pyrolysis on different feedstock blends are discussed to guide future research on BM and OS co-pyrolysis. The effects of different pyrolysis parameters that can improve the pyrolysis process and quality of products are also reviewed. These parameters include CO_2 and steam atmospheres, heating rate, reaction temperature and particle size. Overall, in most cases reviewed, co-pyrolysis can enhance the yields of bio-oils, producer gas and chars as well as improve their properties while reducing the environmental effects of fossil fuels.*

Keywords: oil shale, biomass, co-pyrolysis, gas atmosphere, operational parameters.

1. Introduction

The current accelerating increase in energy consumption, shortage of natural resources, environmental pollution and depletion of conventional fossil fuels around the world have urged the research and implementation of clean, alternative and renewable sources for energy generation and production of fuels [1, 2]. The use of conventional fossil fuels as a source of energy and petrochemical products has increased the emissions of CO_2 significantly and altered the carbon balance on Earth [3, 4]. A promising economically feasible and cleaner alternative to the production of improved biofuels and chemicals is the co-pyrolysis of carbon-neutral fuels, such as biomass (BM), and alternative fuels, such as oil shale (OS) [5–7].

* Corresponding author: e-mail *allyon@taltech.ee*

Oil shale is a sedimentary rock found in different geological formations, which is composed of organic matter, ash and inorganic matter. OS is considered an alternative fossil fuel whose organic matter (kerogen) can be converted into oil and gaseous products, such as shale oil and shale gas, through different processes, including pyrolysis, combustion, gasification and liquefaction under supercritical conditions [8–11]. There are OS deposits in many regions of the world, exceeding the crude oil reserves [12, 13] and making OS one of the most important alternative fossil fuels. The United States has the largest proven reserves, but OS can also be found in Brazil, China, Russia, Estonia, Jordan, Morocco, Australia, Canada, Italy and Congo [14–16]. Pyrolysis is one of the most frequently used technological processes for the retorting of OS, and it is used to convert the organic matter kerogen into bitumen and bitumen into shale gas, shale oil and semicoke [17, 18]. There are still various challenges in the OS conversion process and the usage of its products. Some of these challenges include reducing the environmental effects, improving the quality and composition of the products [19, 20] and reducing the yields of solid residues.

Biomass is a renewable, carbon-neutral resource with the potential to supply approximately 14% of the world's energy consumption [21–23], making it one of the most important energy sources of its kind. BM can decrease the dependence on fossil fuels [24, 25], as well as emissions of CO_2 and other pollutant gases [26]. Owing to its different characteristics, such as high volatile matter content and low ash content [27], BM can be processed into bio-oil, biogas, char and activated carbons, among other products [28]. Thermochemical, biochemical and mechanical conversion processes are the most commonly used processes for BM conversion [29, 30]. Among the thermochemical processes, pyrolysis has been widely used to convert BM into products because of the favorable conditions for converting solid carbonaceous feedstock (FS). However, the obtention of BM products from individual pyrolysis still needs further improvement and research owing to technical and economic challenges, such as low calorific values and high moisture content [31].

Pyrolysis is a thermochemical conversion process in which FS undergoes thermal degradation in the absence of oxygen, breaking large molecular structures and producing gas, liquid oil and solids [32, 33]. High-heating-value liquid oils obtained through pyrolysis are used in furnaces, turbines, engines, and the petrochemical industry [34]. Other products obtained from pyrolysis are high energy content gases used for heat and power generation [35], and high carbon content and adsorbent chars. Pyrolysis can also be an intermediate process, as it is a part of other thermochemical conversion processes, such as gasification and torrefaction. The yields and composition of products obtained from pyrolysis depend on different parameters, including the type of FS and its physical and chemical composition (organic and mineral content, particle size, moisture content, heating value), the reactor used, and the operational

parameters, such as reaction temperature, heating rate, residence time and gas atmosphere (N_2, CO_2, H_2O, H_2, CH_4, CO_2).

Co-processing of FS has been studied to analyze the interactions between fuels, improve the quality of fuel and reduce its environmental impact, thus producing improved and cleaner liquid and gaseous fuels [36]. Co-pyrolysis is a process in which the thermal degradation of two fuels occurs through a set of chemical reactions, heat and mass transfer mechanisms, and interactions between the fuels [37]. The yield and composition of liquid, solid and gaseous products obtained from co-pyrolysis cumulatively depend on the products from individual pyrolysis, the synergetic effects that may promote or inhibit the yield and quality of the products, the interactions between the organic and mineral matter of both fuels, and the operational parameters [38].

This work aims to present different developments, findings and advancements in BM and OS co-pyrolysis processes. Various studies are reviewed and compared. First, an overview of the most relevant operational parameters used for each co-pyrolysis experiment is provided, followed by a presentation of the main findings, improvements, synergetic effects, interactions, and characteristics of the products obtained from co-pyrolysis of different feedstocks. The present study also reviews the main operational parameters of OS pyrolysis, including the effects of the gas atmosphere, heating rate, particle size, and reaction temperature.

2. Overview

2.1. Individual pyrolysis of oil shale and biomass

Through different industrial retorting processes, OS has been used to obtain shale oil, shale gas and semicoke with different yields (5–20 wt% of shale oil, 5–20 wt% of shale gas and > 60 wt% of semicoke) and compositions. The yields of products depend, among other factors, on the type of OS, the retorting reactor used and the operational parameters [39]. Different OS types from various worldwide regions give different product yields, as the organic matter and lower heating value (LHV) in OS can vary from 5 to 80% [40] and from 5 to 20 MJ/kg, respectively. OS retorting processes have been studied to improve the quality and increase the yield of usable products [4, 19, 41]. However, there are still different issues to be resolved from the individual retorting of OS. For instance, semicoke, as a product of OS retorting, is sent to landfills. Additionally, the high molecular weight, viscosity, nitrogen and sulfur content, along with the low stability of shale oil, can cause environmental effects (emission of NO_x and SO_x) [42–44] and may require further improvement and refining of the oil [19, 20]. Moreover, the individual retorting of OS can produce high amounts of polluting gaseous carbon, such as CO_2, leading to environmental contamination.

Biomass has been widely used to produce bio-oils, semi-coking products, fuels, chemicals and petroleum substitutes [45]. The yields of products obtained from BM pyrolysis vary depending on the type of pyrolysis process used, such as torrefaction, carbonization, conventional pyrolysis, fast pyrolysis and flash pyrolysis. Conventional pyrolysis yields approximately 50 wt% of liquids, 20–25 wt% of gas and 20–25 wt% of solids. Fast and flash pyrolysis yields up to 75 wt% of liquids, less than 20 wt% of gas and 13–25 wt% of solids [6]. However, the individual pyrolysis of BM still poses different challenges, such as the low energy density (10–40% of that in most fossil fuels), high moisture content and low heating value of BM (15–19 MJ/kg) [5, 46]. As a resource, biomass is highly diverse; the different types of BM significantly differ in composition, making the characterization of the matter a challenge and requiring individual techniques for the pretreatment and processing of its various types [47]. For some types of BM, FS availability is a constraint in specific regions or due to seasonal and environmental conditions, leading to challenges in transporting the types of BM available and limiting their use in specific locations and environments [48]. The properties and quality of the products obtained from BM pyrolysis can also challenge their usage. Products such as bio-oil can have undesirable properties, including high corrosiveness, thermal instability and a variable composition of the bio-oil depending on the type of BM and pyrolysis conditions [49]. As with shale oil, bio-oil needs refining and upgrading to use it as a fuel and make it compatible with current energy conversion technologies. Moreover, the application of BM pyrolysis is usually economically and technologically limited to prototype and small-scale processes [50]. The individual pyrolysis characteristics and products obtained from BM conversion have been widely studied [51–53].

2.2. Co-pyrolysis

Co-pyrolysis has been studied to enhance the properties and products of individual pyrolysis. BM has been used in co-pyrolysis to decrease the consumption of fossil fuels, reduce environmental problems, such as the CO_2 emissions and pollutant gases (H_2S, NO_x, SO_x) produced from conventional usage of solid fuels [45, 54], and address operational challenges in processing fuels, such as the fused-ash slagging that forms inside reactors [55]. The differences in the composition of BM, including the fraction of oxygenated species, H/C and O/C ratios, ash composition, and volatile matter [56, 57], can potentially promote beneficial synergetic effects and interactions during co-pyrolysis. Other possible positive effects include reducing pollutants from solid fossil fuel conversion, improving the product yields and composition, and enhancing the thermal reactivity of the fuels [58, 59].

Various studies have been conducted on the co-pyrolysis of BM and other fuels, including switch grass, rice straw, sawdust, crystalline cellulose and lignin with bituminous coal [60–62], olive stone, wheat straw, almond shells

and pine sawdust with coal [63], corncob wood waste, wheat straw, rice straw, sawdust and pine with subbituminous coal [64–69], and corncob and hazelnut shells with lignite [59, 70]. Plastics have also been co-pyrolyzed with BM, resulting in improvements in the properties of pyrolysis products while using plastic residues as an alternative. Plastics, for example, have been used to upgrade hydrocarbon mixtures [35, 71] by donating hydrogen and increasing the quality and yield of bio-oil [72, 73]. Some studies using plastics include those by Jin et al. [32] on the synergetic effects in the co-pyrolysis of wheat straw and polyurethane, and by Özsin and Pütün [37] who conducted kinetic studies of the co-pyrolysis of cherry seeds and polyvinyl chloride. Further, co-pyrolysis of BM and OS with residues such as waste tires and sewage sludge can produce a valuable, improved bio-oil while reducing the amount of waste that creates environmental problems and health risks as these residues are non-biodegradable or require a challenging waste recycling process [74–77]. Moreover, the individual pyrolysis of waste produces extensive amounts of ash and produces gas-rich CO_2 with a low heating value [78]. Co-pyrolysis can use waste and residues while producing usable products such as bio-oil. A relevant example is the co-pyrolysis of sewage sludge and wheat straw investigated by Wang et al. [27].

2.3. Effects of co-pyrolysis

Several positive effects have been observed in the quality and yield of products from co-pyrolysis due to interactions and synergetic and catalytic effects between the FS blends. FS with a high hydrogen content and high H/C ratios, such as BM and plastics, can play an essential role in co-pyrolysis, acting as hydrogen donors and promoting FS decomposition and cracking of fuel blends, which can increase the yield of oil and decrease that of solids [59, 60, 62, 66–68, 70]. The alkaline and alkali earth metals present in different feedstocks, such as BM, plastics, tires and sewage sludge, can act as catalysts and enhance the co-pyrolysis process, therefore increasing the fuel conversion and yields of usable products and promoting secondary cracking and dehydrogenation. FS ash can also have similar catalytic effects in co-pyrolysis [27, 32, 66, 67].

For example, BM in co-pyrolysis can promote the solids decomposition and increase the co-pyrolysis decomposition rate because of its high volatile content and low fixed carbon, resulting in higher yields of gas and oil and lower yields of solid products [60–62, 64, 69]. Co-pyrolysis using BM can also produce a gas with a higher concentration of CO, as the CO_2 produced can react in the Boudouard reaction between char and CO_2, increasing the yield of CO and decreasing that of CO_2 [67, 68]. Co-processing can also shift the pyrolysis temperature and reduce the activation energy of the blend [37, 60, 65]. Co-pyrolysis using BM, plastics and tires, among other materials, can improve the fuel properties of oil. Some improved properties include lower water and oxygen content, higher calorific value, higher carbon and hydrogen content [32, 74], lower fractions of heavy aromatics and heterocyclic compounds, and higher fractions of light tars and light aromatic tars [32, 61].

However, the synergetic effects of co-pyrolysis could not be generalized. Several studies have observed a promotion or inhibition effect on the yield of products, including the yield of oils, gas, non-condensable gases and solids [64, 67, 68]. Some studies have found inhibitory effects on the pyrolysis rate and activation energy due to a decrease in the heat transfer, while other studies have proved the promotion effects on the oil yield, a decrease in the solids yields as well as in the reaction temperatures [32, 37, 62]. The synergetic effects have also been observed to depend on the blend mixture ratio and reactor type. For example, co-pyrolysis in fluidized- or fixed-bed reactors has shown improved synergetic effects, unlike that in Thermogravimetric Analysis (TGA) [27], while higher pyrolysis temperatures (> 500 °C) favor interactions between feedstocks [63, 69]. Other studies have found that co-pyrolysis products behave as additive products from the individual pyrolysis of FS, indicating no synergetic effects [65, 70].

Although co-pyrolysis has many advantages and positive effects, various challenges must be considered. For example, many experimental data from co-pyrolysis have been obtained from pilot-scale equipment and TGA [65]. Co-pyrolysis can also cause technical and operational issues and require modifications to the power plants to operate them with FS mixtures, thereby reducing the generation capacity [63]. However, these modification costs can be compensated for by the decrease in fuel cost when using BM, residues or waste [70]. The modifications required for pyrolysis plants to operate in co-pyrolysis require fewer investments than new plants for individual pyrolysis of renewable FS, such as BM, or waste, such as plastic residue [65].

2.4. Oil shale and biomass co-pyrolysis

Co-processing of OS and BM has the potential to reduce various challenges from individual pyrolysis while producing higher yields of bio-oil with improved composition [60]. BM for char, oil and gas production is pyrolyzed at temperatures of 350–500 °C, which are within the same temperature range of OS retorting [79]. The bio-oils obtained from BM pyrolysis have very different characteristics from those of shale oil. For example, bio-oil is lighter than shale oil and contains more oxygenated compounds [80]. It is mostly water-soluble differently from the mainly benzene-soluble shale oil [81]. Co-processing of BM and OS is a promising option for improving the retorting of OS, bettering its pyrolysis characteristics and providing environmental benefits such as the reduction of CO_2 emissions [81, 82]. The different characteristics of BM, OS and their pyrolysis products have been discussed as possessing potential synergetic effects, resulting in improved co-pyrolysis products. However, these synergies are not generally the same in all cases and have been observed to depend on the type of BM [82], reactor, fossil fuel and pyrolysis conditions [83]. Table 1 presents the main operational parameters used in various studies on the co-pyrolysis of BM and OS.

Table 1. Experimental operational parameters used in the studies on oil shale and biomass co-pyrolysis

Biomass	Oil shale	Experiment type	Temperature range, °C	Heating rate, °C/min	Residence time	Atmosphere	Sample mass	Particle size, mm
E. rigida (flowering plant) [19]	Syitomer (Turkey)	TGA	25–1000	10	–	0.1 l/min N_2	5–15 mg	BM 0.425-1.250, OS 0.425-0.600
		Fixed bed reactor	450, 500, 550	10	–	0.1 l/min N_2	–	
Spirulina (algae) [84]	Fushun (China)	TGA	20–950	20, 30, 40, 50	–	0.08 l/min N_2	5 mg	< 0.177
		Py-GC-MS	–	20 °C/ms	20 s	N_2	0.5 mg	
Terebinth berries [81]	Goynuk (Turkey)	Autoclave	340, 360, 380, 400, 420	100 min heating time	120 min	Dry pyrolysis Hydrous pyrolysis 4 and 6 ml	4 g	< 0.120
Spent mushroom [82]	Huadian (China)	TGA	25–750	10	–	0.05 l/min N_2	8 mg	< 0.9
		Retorting reactor	490, 590	–	–	0.2 l/min N_2	50 g 0.52 g/min	< 0.9
Wheat straw grain [80]	Huadian (China)	Cylindrical retort	520	10	20 min	0.3 l/min argon	24 g	< 3
Wood pellet [79]	Huadian (China)	Bubbling fluidized bed reactor	430, 460, 490, 520, 550, 600	–	–	N_2	100 g (feeding speed 24.3 r/min)	3
Pine sawdust [83]	Kukersite (Estonia)	Autoclave	360, 380, 400	–	60, 120, 180 min	–	10 g	BM < 1.0, OS < 0.1
Pine and spruce [39]	Kukersite (Estonia)	Fischer assay	25–520	5	–	–	50 g	0.04-0.10
C.vulgaris Microalgae [85]	Guandong Maoming (China)	Quartz tube reactor	500, 600, 700, 800, 900	–	15 min	0.08 m³/h N_2	0.2 g	< 0.2
Alkaline lignin [86]	Tongchuan (China)	TGA	30–900	30	–	0.05 l/min N_2	–	< 0.074

”_” data not available

2.4.1. Effect of synergy

Co-pyrolysis can promote the yield of products through synergetic effects owing to the interactions between OS and BM. In various studies, these interactions resulted in non-linear changes in yields, unlike the linear changes in yields from the individual pyrolysis of FS. The interactions also increased the yield of oil and its H/C ratio, as observed by Chen et al. [79], and the yield of gas while reducing that of solid residues [80, 82, 84–86]. The synergetic effect of co-pyrolysis can depend on the blend ratio of BM:OS, as shown by Dai et al. [84], who demonstrated a maximum synergy at 30 wt% blends of OS using microalgae and OS. The synergetic effects were also observed to reduce the activation energy of the mixtures, which decreased mainly at low temperatures (< 400 °C). This was observed by Chen et al. [80] and Dai et al. [84] in the co-pyrolysis of OS with wheat straw grain and microalgae, respectively. However, the synergetic effects noticed in co-pyrolysis cannot be generalized, as a study by Kiliç et al. [19] with OS and *E. rigida* and that by Janik et al. [81] with OS and Terebinth berries found that co-pyrolysis behaved as an additive process, resulting in additive yields of products from the individual FS pyrolysis. Though, a study by Johannes et al. [83] with pine sawdust and OS has described minimal synergetic effects and only at the initial stage of decomposition.

2.4.2. Effect of BM:OS blend ratios

The blend ratio of BM:OS was also seen to affect the product yields and composition and thermal decomposition, with an accelerating or delaying effect on the decomposition and a change in the activation energy of the process [19]. Chen et al. [80] used wheat straw grain and OS, proving that higher wheat straw quantities in the blend with OS increased the yields of oil and semicoke unlike those from the individual pyrolysis of OS. For microalgae and OS, higher OS amounts delayed thermal decomposition [84]. A study by Chen et al. [79] on wood pellets and OS blends showed that BM:OS ratios of 3:1 and 1:1 resulted in a decrease in oil yield (from 19.7 wt% for pure OS to 10–13 wt% for BM:OS ratios of 3:1 and 1:1), inhibition of the production of heteroatomic hydrocarbons and promotion of that of unsaturated hydrocarbons. For the alkaline lignin and OS co-pyrolysis studied by Bai et al. [86], a small amount of alkaline lignin promoted OS pyrolysis. It produced more methane by breaking the main covalent bonds of OS. In addition, at higher alkaline to lignin ratios, the promotion effect was significantly reduced. The co-pyrolysis of microalgae and OS carried out by Hu et al. [85] established that with higher BM quantities, the pyrolysis process was postponed while increasing the yields of H_2 and CO, as well as the heating value of gas, and decreasing the solid residues yield from 41.50 wt% at 1:9 BM:OS to 22.55 wt% at 1:1 BM:OS.

2.4.3. Catalytic effect

Different elements present in BM and OS can potentially act as catalysts, promoting the pyrolysis and decomposition of FS and increasing the yields of oil and gas. These elements include alkali and alkaline earth metals, and inorganic non-metallic elements which in BM express a promotion effect and in OS ash an inhibition effect. Dai et al. [84] discovered that during the co-pyrolysis of microalgae and OS at 400 °C, the ash alkaline earth metals present in the FS ash had a catalytic effect, being revealed by the enhancement of the decomposition of organic matter, promotion of the carbonization process and increase of the aliphatic hydrocarbons fraction from 9.57 to 17.48%. In the co-pyrolysis of spent mushroom and OS, Jiang et al. [82] noted that alkali and alkaline earth metals (e.g., potassium) in BM produced a catalytic effect on the decomposition of OS, improving its pyrolysis characteristics. While studying the co-pyrolysis of microalgae *C. vulgaris* and OS, Hu et al. [85] established that the solid residues of BM acted as catalysts, promoting the production of gas and oil from OS. However, the ash particles in OS inhibited the production of oil and gas in the microalgae.

2.4.4. Hydrogen content

The higher hydrogen content of BM contributes to the participation of hydrogen-free radicals in co-pyrolysis, which can increase the oil yield and promote the cracking of kerogen and bitumen, resulting in oil with a higher H/C ratio. Chen et al. [80] found that in the co-pyrolysis of wheat straw grain and OS, the hydrogen-free radicals present in BM contributed to cracking the bridge bonds in kerogen, leading to a higher H/C in the oil obtained. Bai et al. [86] discovered that in the co-pyrolysis of alkaline lignin and OS, the early decomposition of the former promoted the pyrolysis of OS, providing hydrogen-free radicals and producing more CH_4.

2.4.5. Yields and composition of products

The composition of products can be affected by OS-BM co-pyrolysis, resulting in products with additive compositions or enhanced contents of products due to synergetic effects. For oil, the hydrogen and carbon contents increased while that of oxygen decreased. The oil obtained from co-pyrolysis contains lower quantities of heteroatomic compounds and higher amounts of aromatic hydrocarbons as well as higher fractions of intermediate and heavy compounds compared to the oil from individual pyrolyses. For example, the oil from the co-pyrolysis of wheat straw grain and OS contained lower amounts of light compounds and higher quantities of medium compounds, while there was but a slight difference in the amount of heavy compounds between the two types of oil [80]. The oil obtained by Jiang et al. [82] from the co-pyrolysis of spent mushroom and OS had a higher content of carbon and hydrogen and a lower content of oxygen compared to the oil from individual pyrolyses. The product

yields from the co-pyrolysis of OS and BM obtained in different studies are listed in Table 2.

2.5. Co-pyrolysis of oil shale and other feedstocks

Other feedstocks and residues, such as different types of waste plastics or residues from OS retorting, can be used in co-pyrolysis processes with OS. Recycling waste plastics through thermochemical conversion processes, such as co-pyrolysis, is a promising approach for utilizing waste to produce liquid fuels or petrochemical products [87]. Plastics have a high H/C ratio, being similar to that of alkanes, which can produce a liquid fuel with a high H/C ratio [88–90]. Co-processing plastics with other fossil fuels has been proposed to enhance fuel conversion into liquid products, and because of their high hydrogen content, these materials can serve as a hydrogen source in the conversion of OS into improved liquid fuel [91–93]. Moreover, adding plastics to OS makes the processing of the mixture more feasible than converting plastics individually [94]. Different studies have achieved high processing efficiencies [92, 95], but it has also been observed that the feasibility of co-pyrolysis depends on the type of OS, type of plastic used and pyrolysis conditions [93]. Table 3 presents the results of various studies on the co-pyrolysis of OS with plastics and shale oil sludge.

Hong et al. [97] demonstrated synergetic effects in the co-pyrolysis of OS and shale oil sludge from discrepancies in the product yields compared to the additive yields from individual pyrolysis, promoting the solid residue decomposition and gas yield. Other beneficial interactions of co-pyrolysis were observed by Aboulkas et al. [96] using polystyrene and OS. In this study, the decomposition of OS accelerated the weight loss of organic matter, the thermal stability of the co-pyrolysis process increased and the peak rates of mass losses shifted to higher temperatures. In the co-pyrolysis of low-density polyethylene with OS carried out by Tiikma et al. [91], the differences between the experimental and calculated yields proved interactions to take place, as plastics provided hydrogen in the processing of OS and enhanced the oil yield. However, other studies have not found clear evidence of synergetic effects when comparing additive individual pyrolysis products with co-pyrolysis products. This lack of synergy was observed in the case of co-pyrolysis of Kukersite OS and plastics conducted by Alboukas et al. [93], where the differences between the experimental and calculated results were irregular and below the accuracy of the experiments. This was also noted by Bozoglu et al. [92] in the co-pyrolysis of blends of polyethylene (LDPE) and OS where no synergetic effects were observed.

Co-pyrolysis of OS with plastics can improve the quality and yield of products because plastics can act as catalysts in the decomposition of OS, and the yields of oil and gas can increase while the solids yield decreases. Alboukas et al. [93] reported that using OS and different plastics (LDPE,

Table 2. Yields of products from co-pyrolysis of oil shale and biomass

Biomass	Oil shale	Blend ratio BM:OS	Oil yield, %wt	Gas yield, %wt	Water yield, %wt	Solids yield, %wt	Main co-pyrolysis observations
E. rigida [19]	Seyitomer (Turkey)	1:0	25–30	50–55 (water + gas)		15–20	Higher oil yields No synergy*
		1:1	15–20	55–60 (water + gas)		20–25	
		0:1	5–10	40–55 (water + gas)		30–35	
Terebinth berries [81]	Goynuk (Turkey)	1:0	40–41 (total liquid)	22–26	–	32–37	Improved oil quality No synergy
		1:1	38–44 (total liquid)	18–25	–	36–44	
		0:1	37–46 (total liquid)	10–16	–	37–52	
Spent mushroom [82]	Huadian (China)	1:0	9–11	37–40	9–14	36–50	Synergy Higher yields of usable product
		1:1	7–17	24–40	2–4	50–61	
		0:1	7–17	15–20	0–2	65–76	
Wheat straw grain [80]	Huadian (China)	1:0	17	12.5	9	61	Improved oil quality Synergy OS acted as a catalyst
		3:1	18	10	8.5	63	
		1:1	18	8	8	64	
		1:3	19	7	7.5	65	
		0:1	20	5	7	66	

Table 2 (continued)

Biomass	Oil shale	Blend ratio BM:OS	Oil yield, %wt	Gas yield, %wt	Water yield, %wt	Solids yield, %wt	Main co-pyrolysis observations
Wood pellet [79]	Huadian (China)	1:0	8	65	10	27	Improved oil quality / Synergy / Higher oil yields up to 520 °C
		3:1	10	42	8	40	
		1:1	13	30	6	50	
		1:3	17	20	4	60	
		0:1	20	13	1	67	
Pine and spruce [39]	Kukersite (Estonia)	1:0	16–26	20–21	24–26	28–39	Significant differences in OS and BM pyrolysis oils
		0:1	28	8	6	58	
C. vulgaris Microalgae [85]	Guandong Maoming (China)	1:0		89 (liquid + gas)		10	Synergy / Solid residues acted as catalysts / Higher yields of usable product
		9:1		78 (liquid + gas)		21	
		7:3		68 (liquid + gas)		32	
		1:1		59 (liquid + gas)		41	
		0:1		30 (liquid + gas)		70	

* Existence of promotion or inhibition effects due to interactions between fuels. Synergy existed in experiments where there was a difference in the experimental and calculated yields of products. Yields displayed are from experimental results.

"–" data not available

Table 3. Experimental parameters of co-pyrolysis of oil shale and other feedstocks

Feedstock	Oil shale	Experiment type	Temperature range, °C	Heating rate, °C/min	Residence time	Atmosphere	Sample mass	Particle size, mm
Low-density polyethylene [91]	Kukersite and Dictyonema (Estonia)	Autoclave	420, 540	–	20–120 min	–	4 g	0.04
Polystyrene [96]	Tarfaya (Morocco)	TGA	20–1000	2, 10, 20, 50, 100	–	0.06 l/min N_2	20 mg	FS 0.1–0.2, OS 0.1
Polyethylene (LDPE) [92]	Goynuk (Turkey)	TGA	25–800	10	–	0.2 l/min N_2	10 mg	FS 3.2, OS 1.0
		Fixed bed reactor	600	5	60 min	0.025 l/min N_2	100 g	
Polyethylene (LDPE and HDPE) and polypropylene [93]	Tarfaya (Morocco)	Autoclave	25–500 400, 450, 500, 525, 550, 600	2–10, 20	15 min	N_2	–	0.1
Shale oil sludge [97] a scanning electron microscope (SEM	Longkou (China)	TGA	50–900	10, 30, 50	–	0.05 l/min N_2	20 mg	0.2

",," data not available

polyethylene HDPE, polypropylene) with high oil conversion and low char production led to co-pyrolysis products with a considerably higher yield of oil compared to that of OS. The quality and composition of the products were also noticed to change; for instance, the co-pyrolysis of LDPE improved the fuel properties of oil, somewhat decreased the content of sulfur and significantly decreased that of oxygen and polar compounds [92]. The co-pyrolysis oil obtained in this study was also reported to have a higher content of carbon and aliphatic hydrocarbons fractions, as well as improved fuel properties. Similar developments were also observed by Tiikma et al. [91]. The yields of liquids, gases and solids obtained from co-pyrolysis of OS and various feedstocks in different studies are presented in Table 4.

Table 4. Yields of products from co-pyrolysis of oil shale and various feedstocks

Feedstock	Oil shale	Blend ratio FS:OS	Oil yield, %wt	Gas yield, %wt	Water yield, %wt	Solids yield, %wt
Low-density polyethylene [91]	Kukersite (Estonia)	1:0	86	13	–	0.5
		1:1	55	10	–	32.9
		0:1	16	11	–	72
Polyethylene (LDPE) [92]	Goynuk (Turkey)	1:0	79.0	20.8	–	0.2
		1:3	71.3	16.0	4.3	8.4
		1:1	53.3	27.8	2.0	16.9
		3:1	37.0	26.1	8.8	28.1
		0:1	23.7	31.7	6.5	38.1
Polyethylene (LDPE and HDPE) and polypropylene [93]	Tarfaya (Morocco)	1:0	89–92	7-11	–	0.3–0.7
		1:1	51–54	5–7	–	41–43
		0:1	7.6	4.8	–	87.6

"–" data not available

3. Pyrolysis operational parameters

Determining the operational parameters is crucial for thermochemical conversion processes independent of the type of FS or reactor used. For pyrolysis, the atmosphere (inert or reactive), reaction temperature, FS particle size and heating rate affect the yield and composition of liquid, gaseous and solid products, as well as the efficiency of the process. These parameters also af-

fect heat transfer, the temperature gradients between particles and between the particles' surface and core, and the residence time, among other factors. The effects of pyrolysis temperature [98–103], particle size [104–106] and heating rate [107–110] on the fast, intermediate and slow pyrolysis of BM have been widely studied in different types of reactors and for different BM species. There have also been carried out numerous studies on the effects of temperature, particle size and heating rate on pyrolysis [111–117].

3.1. Steam atmosphere

The retorting of OS for the production of shale oil and shale gas has been studied using inert gas atmospheres (nitrogen, argon, or helium) for different purposes, such as kinetic analysis and modeling, TGA, product yield and composition analysis, and studies on the effects of different operational parameters [118–124]. Research on the pyrolysis of OS in different gas atmospheres (steam, H_2, CO_2) is scarce, even though the presence of steam as a gas atmosphere can potentially provide free hydrogen radicals, which can promote the decomposition of OS and increase the yield of shale oil [125].

Steam has been used with BM for different processes, such as liquefaction, torrefaction and carbon activation, and for improving the fuel properties of BM [126]. However, BM pyrolysis has been mostly studied in inert gas atmospheres, with only a few studies using gases such as steam, H_2, CO_2 and CH_4. Pyrolysis under steam atmosphere has been used to produce activated carbon, chemicals, liquid fuels [127, 128], hydrogen from bio-oil [129–131], and synthesis gas. The use of steam in pyrolysis has been proven to increase the yield of bio-oil and improve its quality, as well as the adsorption characteristics of activated carbons [132, 133]. Steam atmospheres influence the yields of products, especially liquid products [134, 135], owing to the efficient penetration of steam into the solids particles, which enhances the decomposition and removal of volatiles [136]. Steam works as a heat carrier, potentially reducing the need for external heating during pyrolysis [137]. Pyrolysis under steam atmospheres needs to be further studied as most of the research has been conducted only in fixed-bed reactors and has resulted in a limited production of liquid products on a commercial scale [34, 138]. Table 5 provides an overview of the studies on the pyrolysis of OS and BM using steam atmospheres.

The quality and composition of the products are improved in steam atmospheres compared to those in inert atmospheres. Different studies on the pyrolysis of OS under steam atmospheres demonstrated an increase in oil yield and weight loss (less solid residues) differently from N_2 atmospheres [125, 139, 140]. Steam was observed to affect the decomposition of OS positively, promoting the evaporation of oils from the shale particles, increasing the organic matter conversion, lowering the retorting temperature and minimizing the retrogressive reactions which lead to char formation. Higher steam flow

rates also promoted shale oil yield. Razvigorova et al. [125] noticed that in steam environments, the produced shale oil had a higher H/C ratio, higher fractions of neutral oil and heteroatomic compounds, light hydrocarbons, aliphatic compounds, asphaltenes and lower polar compounds. While studying the influence of steam on OS pyrolysis, Nazzal and Williams [140] noted steam to increase the contents of H_2, CO, CO_2, hydrocarbons, alkanes and alkene gases in the producer gas. El Harfi et al. [139] observed that not only the content of solid residue, but also that of sulfur in the semicoke decreased in steam atmospheres. However, the effect of steam atmosphere on OS pyrolysis needs to be further studied.

In the pyrolysis of BM, steam atmospheres decreased the yield of solid products and increased that of oil and gas unlike N_2 and static pyrolyses, as found by Özbay et al. [144] while comparing different atmospheric conditions. The pyrolysis of bamboo powder and woody BM in steam was studied by Kantarelis [141] and Kantarelis et al. [142] who noted divergences in the decomposition mechanisms, a faster decomposition rate, inhibition of the adsorption of tar vapors on char surfaces, and prevention of secondary tar cracking. Steam pyrolysis also contributed to the removal of low-molecular-weight compounds, thus reducing pore-clogging. The effects of steam were observed by Duman and Yanik [29] and Giudicianni et al. [136] to change with reaction temperature. High temperatures (> 500 °C) favor gas production and inhibit that of solids. Steam:BM ratios can also affect product yields. Kantarelis et al. [143] established that intermediate steam ratios promoted oil production, whereas high steam ratios inhibited oil yield.

The composition of BM and interactions between its components under steam atmospheres can affect the pyrolysis behavior, as observed from the individual and blended pyrolysis of lignin, hemicellulose and cellulose [136]. Lignin afforded the highest yield of char, cellulose the highest yield of liquid and hemicellulose the highest yield of gas, while in blends, the cellulose-lignin interactions strongly increased the yield of liquid and reduced that of char. The composition of the products can also change under steam atmosphere. Bio-oil can have a lower content of oxygen, a lower O/C ratio and a lower fraction of polar compounds, as well as a higher H/C ratio and higher fractions of aliphatic compounds and alkanes. Some researchers have found that the producer gas can generate higher yields of H_2 and CO_2 (due to the water-gas shift reaction), as well as of CH_4 and CO gas species, and give a higher high heating value (HHV) [143]. Moreover, the gas from steam pyrolysis increases the yields of H_2, CH_4 and CO, and also HHV, as it is not diluted with N_2 [142].

Overall, for BM and OS, steam atmospheres can act as reactive agents, hydrogen donors and heat and volatile carriers as they penetrate the solids particles and contribute to the desorption and removal of volatiles [144]. These atmospheres can produce positive effects during pyrolysis on the decomposition rate, heat transfer and heating rate, and trigger the prevention of secondary tar cracking and adsorption of tar by char particles.

Table 5. Experimental parameters of pyrolysis of oil shale and biomass in steam atmospheres

Feedstock	Experiment type	Temperature range, °C	Heating rate, °C/min	Residence time	Atmosphere	Sample mass	Particle size, mm
Tarfaya OS (Morocco) [139]	Fischer assay	550	10	20 min	150 cm^3/min N$_2$, or steam	20 g	1.00–1.25
Krasava OS (Bulgaria) [125]	Hydrothermal treatment	400	30	25–30 min	steam	25 g	< 0.2
Sultani OS (Jordan) [140]	Fluidized-bed reactor	400, 450, 520, 570, and 650	–	45 min	N$_2$ or steam	–	1.20–3.33
Bamboo powder [141, 142]	Fixed-bed reactor	525, 875	–	9–12 min	1 Nm^3/h N$_2$, 7.85 g/min steam	–	0.2–0.5
Pine and spruce [141,143]	Bubbling fluidized-bed reactor	500	–	300 min	20.8 l/min N$_2$, 0.5–1.0 kg/h steam	1.5–2.65 kg/h	1–1.4
Cellulose, hemicellulose, and lignin[136]	TGA	30–600	5	–	0.02 l/min N$_2$	1.5 mg	–
	Chamber test reactor	200–700	5–40	1.5–3 s	steam	6 g	–
Apricot pulp [144]	Fixed-bed reactor	550	5	–	100 cm^3/min N$_2$, 2 cm^3/min steam	10 g	–
Apricot pulp [145]	Fixed-bed reactor	300, 400, 450, 500, 550	5	30 min	2.5 cm^3/min steam	10 g	~1.122

Table 5 (continued)

Feedstock	Experiment type	Temperature range, °C	Heating rate, °C/min	Residence time	Atmosphere	Sample mass	Particle size, mm
Pine, abies, maple and peach stones [146]	Box furnace	100–1000	–	30 min	0.02 l/min steam	250	Crushed
Cellulose, hemicellulose, lignin and Sugi (Japanese cedar) [134]	Superheated steam pyrolysis reactor	700	5–10	120 min	9 l/h water evaporated to steam	20–50 g	2.5 x 2.5 x 2.5, 0.01–0.10
Olive pomace [29]	Semi-batch reactor	500, 700	5	60 min	0.03 l/min N_2, 0.002 l/min steam	50 g	0.1–0.6

",," data not available

3.2. CO_2 atmosphere

There have been carried out studies on reducing, capturing and utilizing the CO_2 produced from industrial, agricultural and domestic human activities, considering the detrimental effects of its emissions on the atmosphere [2, 147]. Pyrolysis of BM and OS using CO_2 atmospheres is an alternative to produce liquid bio-oil in enhanced atmospheres. CO_2 can influence the yield and quality of products [148, 149] and affect the behavior of FS during thermochemical conversion in terms of devolatilization and reforming of char and ash [150, 151]. In the pyrolysis of OS, CO_2 atmospheres can improve the properties of the products, such as the H_2/CO ratio in the producer gas [152]. There is not much research on the pyrolysis of OS using CO_2 atmospheres. Meanwhile, BM conversion in CO_2 environments has been studied, especially in BM gasification, where CO_2 can improve thermal efficiency, enhance tar cracking and promote dehydrogenation [149, 153]. CO_2 atmospheres have been observed to enhance the thermal efficiency of the process, unlike inert gas atmospheres [154, 155], while also increasing the CO production during fast pyrolysis [156] and decreasing the char production and CO_2 yield [157]. Table 6 lists experimental parameters used in various studies on the pyrolysis of OS and BM in CO_2 atmospheres.

The conversion of OS under CO_2 in pyrolysis or gasification processes has rarely been studied. Tang et al. [162] used CO_2 atmospheres for the pyrolysis of different types of Chinese OS. It was observed that the activation energy decreased in CO_2 atmospheres, contrary to N_2 atmospheres, and that the interactions between OS minerals, organic matter and CO_2 atmosphere resulted in a positive synergetic effect. Xie et al. [158] pyrolyzed Huadian OS in a CO_2 atmosphere, which resulted in a decrease of the solids yields. Differently from N_2, OS in CO_2 underwent further decomposition due to the gasification of carbon, which was transformed into CO. Moreover, CO_2 produced shale oil with large fractions of aliphatic hydrocarbons and long-chain hydrocarbons (C_{16}–C_{23}). The CO_2 atmosphere can promote interactions between the organic and mineral components present in OS as well as between the two former and the atmosphere itself.

Compared to N_2 pyrolysis, CO_2 pyrolysis of BM can yield higher quantities of non-condensable gases and lower quantities of solids and oils, as shown by Zhang et al. [157] in the pyrolysis of corncob, and by Ye et al. [159] in the pyrolysis of sawdust. The yield of gases increased in most of the studies carried out with different types of BM owing to the contribution of CO_2 in char gasification reactions, such as methane reforming, reverse water-gas shift and char gasification, which can enhance the thermal cracking of volatile organic compounds and favor reactions involving CO_2 and volatile organic compounds [156, 160]. Other benefits are observed in lower yields of CO_2 and higher yields of CO and H_2 owing to the cracking and reforming of oil under a CO_2 atmosphere. The bio-oil obtained has a higher HHV and a higher stability

Table 6. Experimental parameters of pyrolysis of biomass and oil shale in CO_2 atmospheres

Feedstock	Experiment type	Temperature range, °C	Heating rate, °C/min	Residence time	Atmosphere	Sample mass	Particle size, mm
Huadian OS (China) [158]	TGA	30–1200	20	–	0.08 l/min N_2 or CO_2	5 mg	< 0.28
	Fixed-bed reactor	30–500	10–20	–	0.1 l/min N_2 or CO_2	20 g	5–10
Corncob [157]	Fluidized-bed reactor	550	–	10 min	N_2, CO_2, CO, CH_4, and H_2	6 g	1–2
Pine sawdust [159]	Fixed-bed reactor	600, 800	–	15 min	0-80 vol% CO_2	1 g	< 2
Woodchips [156]	M-TG Horizontal tubular reactor	850	–	–	100 vol% N_2, 20 vol% CO_2 and 80 vol% N_2	0.5 g	4–5
Sawdust and pinewood [160]	Drop tube furnace	900, 1100, 1300, 1450	–	500–600 ms	1 l/min N_2 or CO_2	5–10 g/h	0.125–0.250
Coffee, corn, oak, seaweed and *C. vulgaris* [161] oak wood, corn stover, macroalgae, microalgae, cellulose, hemicellulose, and lignin	TGA	25–800	20–400	–	0.06 l/min N_2 or CO_2	10 mg	< 2

"–" data not available

with large fractions of monoaromatic substances, polycyclic aromatics and phenols for the liquid products. For solids, the residual chars can have a higher porosity and a different morphology, increasing the access of reactants into the particles and promoting OS decomposition [160, 161].

3.3. Effect of temperature, heating rate and particle size on OS pyrolysis

The OS retorting process requires controlling different parameters to maximize the yield and quality of shale oil and shale gas and minimize residues. The pyrolysis reaction temperature, OS particle size and heating rate are among the most critical operational parameters that determine the quality, yield and efficiency of the retorting process [163–165]. Optimizing the pyrolysis parameters has contributed to reducing the amount of energy required for the retorting process and producing higher yields of products, especially shale oil [113]. The product yield is significantly affected by the heat transfer and heating conditions during the process. Some studies have focused on optimizing the shale oil production during OS pyrolysis [166, 167]. The effects of the pyrolysis reaction temperature, particle size and heating rate have been mostly studied through TGA and kinetic analysis [168–170]. Other studies have focused on the pyrolysis kinetics and reaction mechanisms of OS under different operational conditions [171–173]. The experimental parameters used in the studies of their effect on OS pyrolysis are listed in Table 7.

3.3.1. Temperature

Temperature has a significant effect on the product yield and residence time during pyrolysis (shorter residence time at higher temperatures). The yield of shale oil has been studied by Jaber et al. [177] and Olukcu et al. [178] at different temperatures in the 500–700 °C range. This temperature range has been used in numerous studies of the OS conversion process [39, 79, 80, 113, 164, 175, 176]. Several studies have found that temperature affects the yield of OS, resulting in a maximum yield in the range of 450–550 °C, with 520–525 °C being optimal for producing the highest shale oil yield [79, 93, 111, 113, 140, 174]. At temperatures over 550 °C, the pyrolysis process favors the gas yield owing to the secondary cracking or shale oil [81, 82, 140, 174]. Higher temperatures (above 550 °C) produce lower yields of semicoke and shale oil because of the catalytic effect of K, Na, Ca and Fe present in OS, which act as catalysts in the presence of steam, promoting the gasification of OS [85, 111]. Shale oil composition has also been observed to change with pyrolysis temperature. Higher temperatures (up to 525 °C) can produce oil with fewer fractions of asphaltenes and higher fractions of alkanes and aromatics, while decreasing the H/C ratio of shale oil [174].

Table 7. The effect of particle size, heating rate and pyrolysis temperature on the pyrolysis of oil shale

Oil shale	Experiment type	Temperature range, °C	Heating rate, °C/min	Residence time	Atmosphere	Sample mass	Particle size, mm
Huadian (China) [113]	Retorting system	25–430, 460, 490, and 520	3.67–9.57	40 min	–	50 g	0.0–3.0, 0.0–1.2, 0.0–0.6, 0.0–0.28
US Western OS [174]	Batch reactor	400, 450, 500	10	–	0.06 l/min N_2	200 g	–
Sultani (Jordan) [20]	Fluidized-bed reactor	520	–	45 min	Steam and N_2, 25–28 s residence time	0.75 kg/h (feeding rate)	0.20–0.60, 0.60–1.20, 1.20–3.33, 3.33–5.60
El-Lajjun (Jordan) [175]	Fixed-bed reactor	550	2–3	–	50 cm³/min N_2	400 g	4–10
Huadian (China) [176]	Cylindrical retort	25–520	5, 8.5, 12, and 20	20 min	0.3 l/min argon	50 g	0–3
Tarfaya (Morocco) [111]	Fischer assay	400–600	12	–	0.15 l/min N_2 or steam	20 g	1.00–1.25
El-Lajjun (Jordan) [164]	Fixed-bed reactor	530	2, 5, 10, 15, 20, and 30	60 min	N_2 and steam (30 s residence time for steam)	–	1.20–3.33
El-Lajjun (Jordan) [115]	Fixed-bed reactor	340–600	0.2–2.8, 2.2–5.0, 7.0–13.0	–	N_2	500 g	0.5–2.1

"–" data not available

3.3.2. Particle size

The OS particle size affects several factors, such as the yield and composition of products, residence time, heat transfer and decomposition rate. The shale decomposition and the oil retained in the shale are inversely proportional to the particle size: large particles require longer residence times, resulting in higher yields of oil and non-hydrocarbon gases and lower yields of hydrocarbon gases. Moreover, the shale oil from OS of larger particle sizes has a higher content of carbon and hydrogen and a lower content of nitrogen, as well as higher quantities of aliphatic compound fractions and lower quantities of aromatic compound fractions due to the aromatization of oils, as observed by Nazzal [20]. However, a study by Khalil [175] shows how excessively large particles are affected by the heat diffusion from their surface to the core, leading to incomplete decomposition due to the slow heat transfer, requiring longer residence times and affecting the product yields. Meanwhile, small particles can provide a lower devolatilization of OS particle pores. The particle size is also dependent on the type of reactor; for example, fluidized-bed reactors require smaller particle sizes than fixed-bed reactors.

3.3.3. Heating rate

The heating rate in OS pyrolysis affects the product yields and can shift the main pyrolysis zone towards other temperature ranges. Different heating rates also affect the residence times, the penetration of thermal gradients towards the core of the particles and the decomposition of OS [37]. Wang et al. [176] observed a clear relationship between an increase in the heating rate from 5 to 12 °C/min and the final yield of shale oil. It was found that a heating rate above 12 °C/min resulted in a decrease in shale oil yield as higher heating rates impeded a sufficient sweep of the atmosphere gas to enhance the decomposition of OS. Another study, the one by Han et al. [113], found that an increase in heating rate up to 10 °C/min resulted in higher shale oil yields, which decreased when using heating rates higher than 10 °C/min, as it can result in the secondary cracking of shale oil. This observation was also confirmed by Nazzal [164] in the pyrolysis of Jordan OS where increasing the heating rate over 10 °C/min resulted in a slight decrease in oil yield.

The maximum yield of shale oil can be achieved at intermediate heating rates of 10–12 °C/min. Above these values, the shale oil yield decreases and the pyrolysis process enhances the yield of hydrocarbon and non-hydrocarbon gases due to secondary cracking and dehydrogenation reactions. Low heating rates require longer residence times for complete pyrolysis to take place. Lower heating rates can also lead to higher decomposition degrees as the particles are maintained at the same temperature for a longer time. Conversely, high heating rates may impede a complete pyrolysis process as the atmosphere gas does not have the required time to react with the OS particles and properly sweep the volatiles. At high heating rates, the oils cannot diffuse from the

OS pores, as found by Al-Ayed et al. [115]. At higher heating rates, the OS products are produced faster, thus being unable to diffuse out of the pores of the particles, leading to an increase in secondary tar cracking reactions and a decrease in product yields, especially shale oil's [164].

The shale oil composition is affected by the heating rate as high heating rates result in oil with a higher content of carbon, a lower content of hydrogen, and lower O/C and H/C ratios. High heating rates decrease the content of oxygen (more oxygen is transformed into non-condensable gases or char [176]) and sulfur in oil, producing lighter oil with a high content of asphaltenes, aromatics and benzene fractions. At higher heating rates, the content of the lighter fraction (light naphtha) in oil increased, resulting in a much lighter oil than crude oil. For the producer gas, as the heating rate increases, the contents of all the measured gases, including hydrocarbon and non-hydrocarbon gases, increase due to secondary cracking reactions [164, 176].

4. Conclusions

Co-pyrolysis of oil shale and biomass is a promising alternative for reducing environmental effects and improving the quality and yields of liquid and gaseous products. Co-pyrolysis using the currently available processing technologies is technologically and economically feasible, considering the similarities to the technology used in individual pyrolysis, as well as the economic, environmental and technical challenges of the individual pyrolysis of fuels. This study reviewed the different findings of recent co-pyrolysis studies, including the operational parameters, interactions, and yields and composition of co-pyrolysis products. The effects of the pyrolysis operational parameters on individual pyrolysis were also reviewed to serve as a guide for optimizing the co-pyrolysis of OS and BM.

The existence of interactions between OS and BM in co-pyrolysis is not definitive, as in some cases, the co-pyrolysis product yields prove synergy, while in other cases, co-pyrolysis behaves as an additive process of the pyrolysis of individual feedstocks. However, regardless of the existence of synergetic effects, co-pyrolysis of BM and OS results in products with improved quality and yield. These include a lower yield of solid products and a higher yield of oils with higher hydrogen and carbon contents and H/C ratios, and lower oxygen and sulfur contents. Co-pyrolysis triggers thermal decomposition and increases reaction temperature and activation energy. The main interactions in co-pyrolysis take place between FS ash, volatiles, inorganic elements present in FS and free hydrogen radicals (from BM), which promote the cracking of fuels. The improved co-pyrolysis products demonstrate the potential of using this process as a more sustainable alternative to producing valuable fuels and chemicals.

The effect of the operational parameters in the pyrolysis of OS and BM

proves that their optimization also plays an essential role in producing higher yields of improved products. Steam and CO_2 atmospheres speed up the decomposition of fuels, acting as reactive agents, heat carriers and volatile carriers and promoting the fuel cracking and interactions between the organic and mineral components. Temperature, particle size and heating rate strongly affect the decomposition and yields of OS and should be selected to ensure a complete decomposition of the fuel and release of all the volatiles.

The following suggestions would be beneficial for future research:

•   While various studies have already been conducted based on themogravimetric analysis, the co-pyrolysis of BM and OS and the effect of operational parameters on a larger scale, using equipment such as prototype reactors and small-scale reactors, should be studied.
•   The effects of reactive gases (CO_2 and H_2O) on the co-pyrolysis of OS and BM should be determined.
•   The effects of catalysts on the co-pyrolysis of OS and BM should also be investigated.

Acknowledgments

REFERENCES

1.   Sikarwar, V. S., Zhao, M., Clough, P., Yao, J., Zhong, X., Memon, M. Z., Shah, N., Anthony, E. J., Fennell, P. S. An overview of advances in biomass gasification. *Energy Environ. Sci.*, 2016, **9**, 2939–2977.
2.   Rogelj, J., Den Elzen, M., Höhne, N., Fransen, T., Fekete, H., Winkler, H., Schaeffer, R., Sha, F. Riahi, K., Meinshausen, M. Paris Agreement climate proposals need a boost to keep warming well below 2 °C. *Nature*, 2016, **534**, 631–639.
3.   Powell, T. W. R., Lenton, T. M. Future carbon dioxide removal *via* biomass energy constrained by agricultural efficiency and dietary trends. *Energy Environ. Sci.*, 2012, **5**, 8116–8133.
4.   Wang, Q., Ma, Y., Li, S., Hou, J., Shi, J. Exergetic life cycle assessment of Fushun-type shale oil production process. *Energy Convers. Manag.*, 2018, **164**, 508–517.
5.   Zhang, L., Xu, C. (Charles), Champagne, P. Overview of recent advances in thermo-chemical conversion of biomass. *Energy Convers. Manag.*, 2010, **51**(5), 969–982.
6.   Uddin, M. N., Techato, K., Taweekun, J., Rahman, M. M., Rasul, M. G., Mahlia, T. M. I., Ashrafur, S. M. An overview of recent developments in biomass pyrolysis technologies. *Energies*, 2018, **11**(11), 3115.

7. Akhtar, A., Krepl, V., Ivanova, T. A combined overview of combustion, pyrolysis, and gasification of biomass. *Energy Fuels*, 2018, **32**(7), 7294–7318.

8. Foltin, J. P., Lisboa, A. C. L., De Klerk, A. Oil shale pyrolysis: conversion dependence of kinetic parameters. *Energy Fuels*, 2017, **31**(7), 6766–6776.

9. Han, X., Kulaots, I., Jiang, X., Suuberg, E. M. Review of oil shale semicoke and its combustion utilization. *Fuel*, 2014, **126**, 143–161.

10. Liu, Q. Q., Han, X. X., Li, Q. Y., Huang, Y. R., Jiang, X. M. TG-DSC analysis of pyrolysis process of two Chinese oil shales. *J. Therm. Anal. Calorim.*, 2014, **116**, 511–517.

11. Oja ,V., Suuberg, E. M. Oil shale processing, chemistry and technology. In: *Encyclopedia of Sustainability Science and Technology* (Meyers, R. A., ed.). Springer, New York, 2012, 7457–7491.

12. Le Doan, T. V., Bostrom, N. W., Burnham, A. K., Kleinberg, R. L., Pomerantz, A. E., Allix, P. Green River oil shale pyrolysis: semi-open conditions. *Energy Fuels*, 2013, **27**(11), 6447–6459.

13. Hillier, J. L., Fletcher, T. H. Pyrolysis kinetics of a Green River oil shale using a pressurized TGA. *Energy Fuels*, 2011, **25**(1), 232–239.

14. Akalin, E., Kim, Y. M., Alper, K., Oja, V., Tekin, K., Durukan, I., Siddiqui, M. Z., Karagöz, S. Co-hydrothermal liquefaction of lignocellulosic biomass with Kukersite oil shale. *Energy Fuels*, 2019, **33**(8), 7424–7435.

15. U.S. Energy Information Administration. *Technically Recoverable Shale Oil and Shale Gas Resources: An Assessment of 137 Shale Formations in 41 Countries Outside the United States*, Washington, DC, 2013.

16. Knaus, E., Killen, J., Biglarbigi, K., Crawford, P. An overview of oil shale resources. In: *Oil Shale: A Solution to the Liquid Fuel Dilemma* (Ogunsola, O. I., Hartstein, A. M., Ogunsola, O., eds.), ACS Symp. Ser., 2010, **1032**, 3–20.

17. Boak, J. Shale-hosted hydrocarbons and hydraulic fracturing. In: *Future Energy (Second Edition): Improved, Sustainable and Clean Options for Our Planet*, 2014, 117–143.

18. Speight, J. G. Origin and properties of oil shale. In: *Shale Oil Production Processes*. Gulf Professional Publishing, 2012, 1–33.

19. Kiliç, M., Pütün, A. E., Uzun, B. B., Pütün, E. Converting of oil shale and biomass into liquid hydrocarbons via pyrolysis. *Energy Convers. Manag.*, 2014, **78**, 461–467.

20. Nazzal, J. M.. The influence of grain size on the products yield and shale oil composition from the pyrolysis of Sultani oil shale. *Energy Convers. Manag.*, 2008, **49**(11), 3278–3286.

21. Frau, C., Ferrara, F., Orsini, A., Pettinau, A. Characterization of several kinds of coal and biomass for pyrolysis and gasification. *Fuel*, 2015, **152**, 138–145.

22. Akhtar, J., Amin, N. A. S. A review on process conditions for optimum bio-oil yield in hydrothermal liquefaction of biomass. *Renew. Sust. Energ. Rev.*, 2011, **15**(3), 1615–1624.

23. Mehmood, M. A., Ye, G., Luo, H., Liu, C., Malik, S., Afzal, I., Xu, J., Ahmad, M. S. Pyrolysis and kinetic analyses of Camel grass (*Cymbopogon schoenanthus*) for bioenergy. *Bioresour. Technol.*, 2017, **228**, 18–24.

24. Erkiaga, A., Lopez, G., Amutio, M., Bilbao, J., Olazar, M. Influence of operating conditions on the steam gasification of biomass in a conical spouted bed reactor. *Chem. Eng. J.*, 2014, **237**, 259–267.

25. Van de Velden, M., Baeyens, J., Brems, A., Janssens, B., Dewil, R. Fundamentals, kinetics and endothermicity of the biomass pyrolysis reaction. *Renew. Energ.*, 2010, **35**(1), 232–242.

26. Strizhakova, Yu. A., Usova, T. V. Current trends in the pyrolysis of oil shale: A review. *Solid Fuel Chem.*, 2008, **42**, 197–201.

27. Wang, X., Deng, S., Tan, H., Adeosun, A., Vujanović, M., Yang, F., Duić, N. Synergetic effect of sewage sludge and biomass co-pyrolysis: A combined study in thermogravimetric analyzer and a fixed bed reactor. *Energy Convers. Manag.*, 2016, **118**, 399–405.

28. Singh, R. K., Ruj, B. Time and temperature depended fuel gas generation from pyrolysis of real world municipal plastic waste. *Fuel*, 2016, **174**, 164–171.

29. Duman, G., Yanik, J. Two-step steam pyrolysis of biomass for hydrogen production. *Int. J. Hydrogen Energy*, 2017, **42**(27), 17000–17008.

30. Lan, W., Chen, G., Zhu, X., Wang, X., Xu, B. Progress in techniques of biomass conversion into syngas. *J. Energy Inst.*, 2015, **88**(2), 151–156.

31. Wu, C., Liu, R. Carbon deposition behavior in steam reforming of bio-oil model compound for hydrogen production. *Int. J. Hydrogen Energy*, 2010, **35**(14), 7386–7398.

32. Jin, Q., Wang X., Li, S., Mikulčić, H., Bešenić, T., Deng, S., Vujanović, M., Tan, H., Kumfer, B. M. Synergistic effects during co-pyrolysis of biomass and plastic: Gas, tar, soot, char products and thermogravimetric study. *J. Energy Inst.*, 2019, **92**(1), 108–117.

33. Demirbaş, A. Recovery of chemicals and gasoline-range fuels from plastic wastes via pyrolysis. *Energ. Source.*, 2005, **27**(14), 1313–1319.

34. Bridgwater, A. V. Review of fast pyrolysis of biomass and product upgrading. *Biomass Bioenerg.*, 2012, **38**, 68–94.

35. Ahmed, N., Zeeshan, M., Iqbal, N., Farooq, M. Z., Shah, S. A. Investigation on bio-oil yield and quality with scrap tire addition in sugarcane bagasse pyrolysis. *J. Clean. Prod.*, 2018, **196**, 927–934.

36. Moghtaderi, B., Meesri, C., Wall, T. F. Pyrolytic characteristics of blended coal and woody biomass. *Fuel*, 2004, **83**(6), 745–750.

37. Özsin, G., Pütün, A. E. TGA/MS/FT-IR study for kinetic evaluation and evolved gas analysis of a biomass/PVC co-pyrolysis process. *Energy Convers. Manag.*, 2019, **182**, 143–153.

38. Kong, L., Li, G., Jin, L., Hu, H. Pyrolysis behaviors of two coal-related model compounds on a fixed-bed reactor. *Fuel Process. Technol.*, 2015, **129**, 113–119.

39. Luik, H., Luik, L., Tiikma, L., Vink, N. Parallels between slow pyrolysis of Estonian oil shale and forest biomass residues. *J. Anal. Appl. Pyrolysis*, 2007, **79**(1–2), 205–209.

40. Urov, K., Sumberg, A. Characteristic of oil shales and shale-like rocks of known deposits and outcrops. Monograph. *Oil Shale*, 1999, **16**(3S), 1–64.

41. Bai, F., Sun, Y., Liu, Y., Li, Q., Guo, M. Thermal and kinetic characteristics of pyrolysis and combustion of three oil shales. *Energy Convers. Manag.*, 2015, **97**, 374–381.
42. Akash, B. A., Jaber, J. O. Characterization of shale oil as compared to crude oil and some refined petroleum products. *Energ. Source.*, 2003, **25**(12), 1171–1182.
43. Gavrilova, O., Vilu, R., Vallner, L. A life cycle environmental impact assessment of oil shale produced and consumed in Estonia. *Resour. Conserv. Recy.*, 2010, **55**(2), 232–245.
44. Ristic, N. D., Djokic, M. R., Konist, A., Van Geem, K. M., Marin, G. B. Quantitative compositional analysis of Estonian shale oil using comprehensive two dimensional gas chromatography. *Fuel Process. Technol.*, 2017, **167**, 241–249.
45. Demirbas, M. F., Balat, M. Recent advances on the production and utilization trends of bio-fuels: A global perspective. *Energy Convers. Manag.*, 2006, **47**(15–16), 2371–2381.
46. Li, S., Chen, X., Liu, A., Wang, L., Yu, G. Study on co-pyrolysis characteristics of rice straw and Shenfu bituminous coal blends in a fixed bed reactor. *Bioresour. Technol.*, 2014, **155**, 252–257.
47. Wang, Q., Li, X., Wang, K., Zhu, Y., Wang, S. Commercialization and challenges for the next generation of biofuels: Biomass fast pyrolysis. In: *2010 Asia-Pacific Power and Energy Engineering Conference*, Chengdu, China, 28–31 March 2010, IEEE, 2010, 1–4.
48. Hu, X., Gholizadeh, M. Biomass pyrolysis: A review of the process development and challenges from initial researches up to the commercialisation stage. *J. Energy Chem.*, 2019, **39**, 109–143.
49. Sharifzadeh, M., Sadeqzadeh, M., Guo, M., Borhani, T. N., Murthy Konda, N. V. S. N., Garcia, M. C., Wang, L., Hallett, J., Shah, N. The multi-scale challenges of biomass fast pyrolysis and bio-oil upgrading: Review of the state of art and future research directions. *Prog. Energy Combust. Sci.*, 2019, **71**, 1–80.
50. Wu, C., Liu, R. Carbon deposition behavior in steam reforming of bio-oil model compound for hydrogen production. *Int. J. Hydrogen Energy*, 2010, **35**(14), 7386–7398.
51. Veksha, A., McLaughlin, H., Layzell, D. B., Hill, J. M. Pyrolysis of wood to biochar: Increasing yield while maintaining microporosity. *Bioresour. Technol.*, 2014, **153**, 173–179.
52. Maguyon, M. C. C., Capareda, S. C. Evaluating the effects of temperature on pressurized pyrolysis of *Nannochloropsis oculata* based on products yields and characteristics. *Energy Convers. Manag.*, 2013, **76**, 764–773.
53. Wang, S., Luo, Z., *Pyrolysis of Biomass*, In: GREEN – Alternative Energy Resources, Walter de Gruyter GmbH, 2017, 268.
54. Demirbaş, A. Sustainable cofiring of biomass with coal. *Energy Convers. Manag.*, 2003, **44**(9), 1465–1479.
55. Armesto, L., Bahillo, A., Cabanillas, A., Veijonen, K., Otero, J., Plumed, A., Salvador, L. Co-combustion of coal and olive oil industry residues in fluidised bed. *Fuel*, 2003, **82**(8), 993–1000.

56. Collot, A.-G., Zhuo, Y., Dugwell, D. R., Kandiyoti, R. Co-pyrolysis and co-gasification of coal and biomass in bench-scale fixed-bed and fluidized bed reactors. *Fuel*, 1999, **78**(6), 667–679.

57. Chao, C. Y. H., Kwong, P. C. W., Wang, J. H., Cheung, C. W., Kendall, G. Co-firing coal with rice husk and bamboo and the impact on particulate matters and associated polycyclic aromatic hydrocarbon emissions. *Bioresour. Technol.*, 2008, **99**(1), 83–93.

58. Haykiri-Acma, H., Yaman, S. Synergy in devolatilization characteristics of lignite and hazelnut shell during co-pyrolysis. *Fuel*, 2007, **86**(3), 373–380.

59. Haykiri-Acma, H., Yaman, S. Interaction between biomass and different rank coals during co-pyrolysis. *Renew. Energ.*, 2010, **35**(1), 288–292.

60. Li, S., Chen, X., Liu, A., Wang, L., Yu, G. Co-pyrolysis characteristic of biomass and bituminous coal. *Bioresour. Technol.*, 2015, **179**, 414–420.

61. Weiland, N. T., Means, N. C., Morreale, B. D. Product distributions from iso-thermal co-pyrolysis of coal and biomass. *Fuel*, 2012, **94**, 563–570.

62. Li, S., Chen, X., Wang, L., Liu, A., Yu, G. Co-pyrolysis behaviors of saw dust and Shenfu coal in drop tube furnace and fixed bed reactor. *Bioresour. Technol.*, 2013, **148**, 24–29.

63. Cordero, T., Rodríguez-Mirasol, J., Pastrana, J., Rodríguez, J. J. Improved solid fuels from co-pyrolysis of a high-sulphur content coal and different lignocellulosic wastes. *Fuel*, 2004, **83**(11–12), 1585–1590.

64. Wang, J., Yan, Q., Zhao, J., Wang, Z., Huang, J., Gao, S., Song, S., Fang, Y. Fast co-pyrolysis of coal and biomass in a fluidized-bed reactor. *J. Therm. Anal. Calorim.*, 2014, **118**, 1663–1673.

65. Vuthaluru, H. B. Thermal behaviour of coal/biomass blends during co-pyrolysis. *Fuel Process. Technol.*, 2004, **85**(2–3), 141–155.

66. Park, D. K., Kim, S. D., Lee, S. H., Lee, J. G. Co-pyrolysis characteristics of sawdust and coal blend in TGA and a fixed bed reactor. *Bioresour. Technol.*, 2010, **101**(15), 6151–6156.

67. Krerkkaiwan, S., Fushimi, C., Tsutsumi, A., Kuchonthara, P. Synergetic effect during co-pyrolysis/gasification of biomass and sub-bituminous coal. *Fuel Process. Technol.*, 2013, **115**, 11–18.

68. Quan, C., Xu, S., An, Y., Liu, X. Co-pyrolysis of biomass and coal blend by TG and in a free fall reactor. *J. Therm. Anal. Calorim.*, 2014, **117**, 817–823.

69. Soncini, R. M., Means, N. C., Weiland, N. T. Co-pyrolysis of low rank coals and biomass: Product distributions. *Fuel*, 2013, **112**, 74–82.

70. Sonobe, T., Worasuwannarak, N., Pipatmanomai, S. Synergies in co-pyrolysis of Thai lignite and corncob. *Fuel Process. Technol.*, 2008, **89**(12), 1371–1378.

71. Sajdak, M., Muzyka, R., Hrabak, J., Słowik, K. Use of plastic waste as a fuel in the co-pyrolysis of biomass: Part III: Optimisation of the co-pyrolysis process. *J. Anal. Appl. Pyrolysis*, 2015, **112**, 298–305.

72. Zhou, L., Wang, Y., Huang, Q., Cai, J. Thermogravimetric characteristics and kinetic of plastic and biomass blends co-pyrolysis. *Fuel Process. Technol.*, 2006, **87**(11), 963–969.

73. Brebu, M., Ucar, S., Vasile, C., Yanik, J. Co-pyrolysis of pine cone with synthetic polymers. *Fuel*, 2010, **89**(8), 1911–1918.

74. Martínez, J. D., Veses, A., Mastral, A. M., Murillo, R., Navarro, M. V., Puy, N., Artigues, A., Bartroli, J., Garcia, T. Co-pyrolysis of biomass with waste tyres: Upgrading of liquid bio-fuel. *Fuel Process. Technol.*, 2014, **119**, 263–271.

75. Rofiqul Islam, M., Haniu, H., Rafiqul Alam Beg, M. Liquid fuels and chemicals from pyrolysis of motorcycle tire waste: Product yields, compositions and related properties. *Fuel*, 2008, **87**(13–14), 3112–3122.

76. Ilkiliç, C., Aydin, H. Fuel production from waste vehicle tires by catalytic pyrolysis and its application in a diesel engine. *Fuel Process. Technol.*, 2011, **92**(5), 1129–1135.

77. Smith, K. M., Fowler, G. D., Pullket, S., Graham, N. J. D. Sewage sludge-based adsorbents: A review of their production, properties and use in water treatment applications. *Water Res.*, 2009, **43**(10), 2569–2594.

78. Shao, J., Yan, R., Chen, H., Wang, B., Lee, D. H., Liang, D. T. Pyrolysis characteristics and kinetics of sewage sludge by thermogravimetry Fourier transform infrared analysis. *Energy Fuels*, 2008, **22**(1), 38–45.

79. Chen, B., Han, X., Tong, J., Mu, M., Jiang, X., Wang, S., Shen, J., Ye, X. Studies of fast co-pyrolysis of oil shale and wood in a bubbling fluidized bed. *Energy Convers. Manag.*, 2020, **205**, 112356.

80. Chen, B., Han, X., Mu, M., Jiang, X. Studies of the co-pyrolysis of oil shale and wheat straw. *Energy Fuels*, 2017, **31**(7), 6941–6950.

81. Yanik, J., Seçim, P., Karakaya, S., Tiikma, L., Luik, H., Krasulina, J., Raik, P., Palu, V. Low-temperature pyrolysis and co-pyrolysis of Göynük oil shale and terebinth berries (Turkey) in an autoclave. *Oil Shale*, 2011, **28**(4), 469–486.

82. Jiang, H., Deng, S., Chen, J., Zhang, L., Zhang, M., Li, J., Li, S., Li, J. Preliminary study on copyrolysis of spent mushroom substrate as biomass and Huadian oil shale. *Energy Fuels*, 2016, **30**(8), 6342–6349.

83. Johannes, I., Tiikma, L., Luik, H. Synergy in co-pyrolysis of oil shale and pine sawdust in autoclaves. *J. Anal. Appl. Pyrolysis*, 2013, **104**, 341–352.

84. Dai, M., Yu, Z., Fang, S., Ma, X. Behaviors, product characteristics and kinetics of catalytic co-pyrolysis spirulina and oil shale. *Energy Convers. Manag.*, 2019, **192**, 1–10.

85. Hu, Z., Ma, X., Li, L. The synergistic effect of co-pyrolysis of oil shale and microalgae to produce syngas. *J. Energy Inst.*, 2016, **89**(3), 447–455.

86. Bai, J., Chen, X., Shao, J., Jia, C., Wang, Q. Study of breakage of main covalent bonds during co-pyrolysis of oil shale and alkaline lignin by TG-FTIR integrated analysis. *J. Energy Inst.*, 2019, **92**(3), 512–522.

87. Ballice, L., Reimert, R. Temperature-programmed co-pyrolysis of Turkish lignite with polypropylene. *J. Anal. Appl. Pyrolysis*, 2002, **65**(2), 207–219.

88. Pinto, F., Costa, P., Gulyurtlu, I., Cabrita, I. Pyrolysis of plastic wastes. 1. Effect of plastic waste composition on product yield. *J. Anal. Appl. Pyrolysis*, 1999, **51**(1–2), 39–55.

89. Al-Salem, S. M., Antelava, A., Constantinou, A., Manos, G., Dutta, A. A review

on thermal and catalytic pyrolysis of plastic solid waste (PSW). *J. Environ. Manage.*, 2017, **197**, 177–198.

90. Kumagai, S., Yoshioka, T. Feedstock recycling via waste plastic pyrolysis. *J. Jpn. Petrol. Inst.*, 2016, **59**(6), 243–253.

91. Tiikma, L., Luik, H., Pryadka, N. Co-pyrolysis of Estonian shales with low-density polyethylene. *Oil Shale*, 2004, **21**(1), 75–85.

92. Bozoglu, C., Karayildirim, T., Yanik, J. Utilization of products obtained from copyrolysis of oil shale and plastic. *Oil Shale*, 2009, **26**(4), 475–490.

93. Aboulkas, A., Makayssi, T., Bilali, L., El Harfi, K., Nadifiyine, M., Benchanaa, M. Co-pyrolysis of oil shale and plastics: Influence of pyrolysis parameters on the product yields. *Fuel Process. Technol.*, 2012, **96**, 209–213.

94. Gersten, J., Fainberg, V., Garbar, A., Hetsroni, G., Shindler, Y. Utilization of waste polymers through one-stage low-temperature pyrolysis with oil shale. *Fuel*, 1999, **78**(8), 987–990.

95. Ballice, L. Classification of volatile products evolved from the temperature-programmed co-pyrolysis of Turkish oil shales with atactic polypropylene (APP). *Energy Fuels*, 2001, **15**(3), 659–665.

96. Aboulkas, A., El Harfi, K., Nadifiyine, M., Benchanaa, M. Pyrolysis behaviour and kinetics of Moroccan oil shale with polystyrene. *Int. J. Energy Eng.*, 2011, **1**(1), 1–11.

97. Hong, Q., Lei, Z., Lidong, Z., Hongpeng, L., Chunxia, J., Qing, W., Meiduan, C. Synergy analysis for co-pyrolysis of oil shale and shale oil sludge. *Oil Shale*, 2019, **36**(3), 370–391.

98. Lappas, A. A., Dimitropoulos, V. S., Antonakou, E. V., Voutetakis, S. S., Vasalos, I. A. Design, construction, and operation of a transported fluid bed process development unit for biomass fast pyrolysis: Effect of pyrolysis temperature. *Ind. Eng. Chem. Res.*, 2008, **47**(3), 742–747.

99. Westerhof, R. J. M., Brilman, D. W. F., Van Swaaij, W. P. M., Kersten, S. R. A. Effect of temperature in fluidized bed fast pyrolysis of biomass: Oil quality assessment in test units. *Ind. Eng. Chem. Res.*, 2010, **49**(3), 1160–1168.

100. Demirbas, A. Effect of temperature on pyrolysis products from biomass. *Energ. Source. Part A*, 2007, **29**(4), 329–336.

101. Garcia-Perez, M., Wang, X. S., Shen, J., Rhodes, M. J., Tian, F., Lee W. J., Wu, H., Li, C. Z. Fast pyrolysis of oil mallee woody biomass: Effect of temperature on the yield and quality of pyrolysis products. *Ind. Eng. Chem. Res.*, 2008, **47**(6), 1846–1854.

102. Stummann, M. Z., Høj, M., Schandel, C. B., Hansen, A. B., Wiwel, P., Gabrielsen, J., Jensen, P. A., Jensen, A. D. Hydrogen assisted catalytic biomass pyrolysis. Effect of temperature and pressure. *Biomass Bioenerg.*, 2018, **115**, 97–107.

103. Dufour, A., Girods, P., Masson, E., Rogaume, Y., Zoulalian, A. Synthesis gas production by biomass pyrolysis: Effect of reactor temperature on product distribution. *Int. J. Hydrogen Energy*, 2009, **34**(4), 1726–1734.

104. Zolghadr, A., Biernacki, J. J., Moore, R. J. Biomass fast pyrolysis using a novel

microparticle microreactor approach: Effect of particles size, biomass type, and temperature. *Energy Fuels*, 2019, **33**(2), 1146–1156.

105. Gaston, K. R., Jarvis, M. W., Pepiot, P., Smith, K. M., Frederick, W. J., Nimlos, M. R. Biomass pyrolysis and gasification of varying particle sizes in a fluidized-bed reactor. *Energy Fuels*, 2011, **25**(8), 3747–3757.

106. Bennadji, H., Smith, K., Serapiglia, M. J., Fisher, E. M. Effect of particle size on low-temperature pyrolysis of woody biomass. *Energy Fuels*, 2014, **28**(12), 7527–7537.

107. Angin, D. Effect of pyrolysis temperature and heating rate on biochar obtained from pyrolysis of safflower seed press cake. *Bioresour. Technol.*, 2013, **128**, 593–597.

108. Klinger, J. L., Westover, T. L., Emerson, R. M., Williams, C. L., Hernandez, S., Monson, G. D., Ryan, J. C. Effect of biomass type, heating rate, and sample size on microwave-enhanced fast pyrolysis product yields and qualities. *Appl. Energ.*, 2018, **228**, 535–545.

109. El-Sayed, S. A., Khairy, M. Effect of heating rate on the chemical kinetics of different biomass pyrolysis materials. *Biofuels*, 2015, **6**(3–4), 157–170.

110. Somerville, M., Deev, A. The effect of heating rate, particle size and gas flow on the yield of charcoal during the pyrolysis of radiata pine wood. *Renew. Energ.*, 2020, **151**, 419–425.

111. El Harfi, K., Mokhlisse, A., Ben Chanâa, M. Yields and composition of oil obtained by isothermal pyrolysis of the Moroccan (Tarfaya) oil shales with steam or nitrogen as carrier gas. *J. Anal. Appl. Pyrolysis*, 2000, **56**(2), 207–218.

112. Kok, M. V., Senguler, I., Hufnagel, H., Sonel, N. Thermal and geochemical investigation of Seyitomer oil shale. *Thermochim. Acta*, 2001, **371**(1–2), 111–119.

113. Han, X. X., Jiang, X. M., Cui, Z. G. Studies of the effect of retorting factors on the yield of shale oil for a new comprehensive utilization technology of oil shale. *Appl. Energy*, 2009, **86**(11), 2381–2385.

114. Wang, Q., Sun, B., Hu, A., Bai, J., Li, S. Pyrolysis characteristics of Huadian oil shales. *Oil Shale*, 2007, **24**(2), 147–157.

115. Al-Ayed, O. S., Al-Harahsheh, A., Khaleel, A. M., Al-Harahsheh, M. Oil shale pyrolysis in fixed-bed retort with different heating rates. *Oil Shale*, 2009, **26**(2), 139–147.

116. Al-Ayed, O. S., Suliman, M. R., Rahman, N. A. Kinetic modeling of liquid generation from oil shale in fixed bed retort. *Appl. Energy*, 2010, **87**(7), 2273–2277.

117. Al-Harahsheh, A., Al-Ayed, O., Al-Harahsheh, M., Abu-El-Halawah, R. Heating rate effect on fractional yield and composition of oil retorted from El-lajjun oil shale. *J. Anal. Appl. Pyrolysis*, 2010, **89**(2), 239–243.

118. Tiwari, P., Deo, M. Compositional and kinetic analysis of oil shale pyrolysis using TGA-MS. *Fuel*, 2012, **94**, 333–341.

119. Tiwari, P., Deo, M. Detailed kinetic analysis of oil shale pyrolysis TGA data. *AIChE J.*, 2012, **58**(2), 505–515.

120. Kök, M. V., Pamir, M. R. Comparative pyrolysis and combustion kinetics of oil shales. *J. Anal. Appl. Pyrolysis*, 2000, **55**(2), 185–194.

121. Torrente, M. C., Galán, M. A. Kinetics of the thermal decomposition of oil shale from Puertollano (Spain). *Fuel*, 2001, **80**(3), 327–334.

122. Jiang, X. M., Han, X. X., Cui, Z. G. New technology for the comprehensive utilization of Chinese oil shale resources. *Energy*, 2007, **32**(5), 772–777.

123. Syed, S., Qudaih, R., Talab, I., Janajreh, I. Kinetics of pyrolysis and combustion of oil shale sample from thermogravimetric data. *Fuel*, 2011, **904**(4), 1631–1637.

124. Lü, X., Sun, Y., Lu, T., Bai, F., Viljanen, M. An efficient and general analytical approach to modelling pyrolysis kinetics of oil shale. *Fuel*, 2014, **135**, 182–187.

125. Razvigorova, M., Budinova, T., Petrova, B., Tsyntsarski, B., Ekinci, E., Ferhat, M. F. Steam pyrolysis of Bulgarian oil shale kerogen. *Oil Shale*, 2008, **25**(1), 27–36.

126. Pach, M., Zanzi, R., Björnbom, E. Torrefied biomass a substitute for wood and charcoal. In: *Proceedings of the 6th Asia-Pacific International Symposium on Combustion and Energy Utilization*, Kuala Lumpur, Malaysia, May 20–22, 2002, 6.

127. Önal, E. P., Uzun, B. B., Pütün, A. E. Steam pyrolysis of an industrial waste for bio-oil production. *Fuel Process. Technol.*, 2011, **92**(5), 879–885.

128. Trane, R., Dahl, S., Skjøth-Rasmussen, M. S., Jensen, A. D. Catalytic steam reforming of bio-oil. *Int. J. Hydrogen Energy*, 2012, **37**(8), 6447–6472.

129. Gil, M. V., Fermoso, J., Rubiera, F., Chen, D. H_2 production by sorption enhanced steam reforming of biomass-derived bio-oil in a fluidized bed reactor: An assessment of the effect of operation variables using response surface methodology. *Catal. Today*, 2015, **242**, 19–34.

130. Xie, H., Yu, Q., Zuo, Z., Han, Z., Yao, X., Qin, Q. Hydrogen production via sorption-enhanced catalytic steam reforming of bio-oil. *Int. J. Hydrogen Energy*, 2016, **41**(4), 2345–2353.

131. Xie, H., Yu, Q., Yao, X., Duan, W., Zuo, Z., Qin, Q. Hydrogen production via steam reforming of bio-oil model compounds over supported nickel catalysts. *J. Energy Chem.*, 2015, **24**(3), 299–308.

132. Pütün, A., Özbay, N., Pütün, E. Effect of steam on the pyrolysis of biomass. *Energ. Source. Part A*, 2006, **28**(3), 253–262.

133. Pütün, E., Ateş, F., Pütün, A. E. Catalytic pyrolysis of biomass in inert and steam atmospheres. *Fuel*, 2008, **87**(6), 815–824.

134. Sagehashi, M., Miyasaka, N., Shishido, H., Sakoda, A. Superheated steam pyrolysis of biomass elemental components and *Sugi* (Japanese cedar) for fuels and chemicals. *Bioresour. Technol.*, 2006, **97**(11), 1272–1283.

135. Mullen, C. A., Boateng, A. A., Goldberg, N. M., Lima, I. M., Laird, D. A., Hicks, K. B. Bio-oil and bio-char production from corn cobs and stover by fast pyrolysis. *Biomass Bioenerg.*, 2010, **34**(1), 67–74.

136. Giudicianni, P., Cardone, G., Ragucci, R. Cellulose, hemicellulose and lignin slow steam pyrolysis: Thermal decomposition of biomass components mixtures. *J. Anal. Appl. Pyrolysis*, 2013, **100**, 213–222.

137. Umeki, K., Yamamoto, K., Namioka, T., Yoshikawa, K. High temperature steam-only gasification of woody biomass. *Appl. Energy*, 2010, **87**, 791–798.

138. Tennant, M. F., Mazyck, D. W. Steam-pyrolysis activation of wood char for superior odorant removal. *Carbon*, 2003, **41**(12), 2195–2202.

139. El Harfi, K., Mokhlisse, A., Ben Chanâa, M. Effect of water vapor on the pyrolysis of the Moroccan (Tarfaya) oil shale. *J. Anal. Appl. Pyrolysis*, 1999, **48**(2), 65–76.

140. Nazzal, J. M., Williams, P. T. Influence of temperature and steam on the products from the flash pyrolysis of Jordan oil shale. *Int. J. Energ. Res.*, 2002, **26**(14), 1207–1219.

141. Kantarelis, E. *Catalytic Steam Pyrolysis of Biomass for Production of Liquid Feedstock*. Ph.D. Thesis. Royal Institute of Technology, Stockholm, 2014.

142. Kantarelis, E., Liu, J., Yang, W., Blasiak, W. Sustainable valorization of bamboo via high-temperature steam pyrolysis for energy production and added value materials. *Energy Fuels*, 2010, **24**(11), 6142–6150.

143. Kantarelis, E., Yang, W., Blasiak, W. Production of liquid feedstock from biomass *via* steam pyrolysis in a fluidized bed reactor. *Energy Fuels*, 2013, **27**(8), 4748–4759.

144. Özbay, N., Uzun B. B., Varol, E. A., Pütün, A. E. Comparative analysis of pyrolysis oils and its subfractions under different atmospheric conditions. *Fuel Process. Technol.*, 2006, **87**(11), 1013–1019.

145. Özbay, N., Pütün, A. E. Characterization of chars from steam pyrolysis of apricot pulp. *Energ. Source. Part A*, 2011, **33**(16), 1504–1513.

146. Hapazari, I., Ntuli, V., Parawira, W. Evaluation of single-step steam pyrolysis-activated carbons from Lesotho agro-forestry residues. *Tanz. J. Sci.*, 2011, **37**, 120–128.

147. Turner, J., Lu, H., White, I., King, J. C., Phillips, T., Hosking, J. S., Bracegirdle, T. J., Marshall, G. J., Mulvaney, R., Deb, P. Absence of 21st century warming on Antarctic Peninsula consistent with natural variability. *Nature*, 2016, **535**, 411–415.

148. Jindarom, C., Meeyoo, V., Rirksomboon, T., Rangsunvigit, P. Thermochemical decomposition of sewage sludge in CO_2 and N_2 atmosphere. *Chemosphere*, 2007, **67**(8), 1477–1484.

149. Lee, J., Yang , X., Cho, S. H., Kim, J. K., Lee, S. S., Tsang, D. C. W., Ok, Y. S., Kwon, E. E. Pyrolysis process of agricultural waste using CO_2 for waste management, energy recovery, and biochar fabrication. *Appl. Energy*, 2017, **185**, Part 1, 214–222.

150. Messenböck, R. C., Dugwell, D. R., Kandiyoti, R. CO_2 and steam-gasification in a high-pressure wire-mesh reactor: The reactivity of Daw Mill coal and combustion reactivity of its chars. *Fuel*, 1999, **78**(7), 781–793.

151. Naredi, P., Pisupati, S. Effect of CO_2 during coal pyrolysis and char burnout in oxy-coal combustion. *Energy Fuels*, 2011, **25**, 2452–2459.

152. Lahijani, P., Zainal, Z. A., Mohammadi, M., Mohamed, A. R. Conversion of the greenhouse gas CO_2 to the fuel gas CO via the Boudouard reaction: A review. *Renew. Sustain. Energy Rev.*, 2015, **41**, 615–632.

153. Prabowo, B., Umeki, K., Yan, M., Nakamura, M. R., Castaldi, M. J., Yoshikawa, K. CO_2-steam mixture for direct and indirect gasification of rice straw in a downdraft gasifier: Laboratory-scale experiments and performance prediction. *Appl. Energy*, 2014, **113**, 670–679.

154. Cho, S. H., Lee, J., Kim, K. H., Jeon, Y. J., Kwon, E. E. Carbon dioxide assisted co-pyrolysis of coal and ligno-cellulosic biomass. *Energy Convers. Manag.*, 2016, **118**, 243–252.

155. Lee, J., Yang, X., Song, H., Ok, Y. S., Kwon, E. E. Effects of carbon dioxide on pyrolysis of peat. *Energy*, 2017, **120**, 929–936.

156. Guizani, C., Escudero Sanz, F. J., Salvador, S. Effects of CO_2 on biomass fast pyrolysis: Reaction rate, gas yields and char reactive properties. *Fuel*, 2014, **116**, 310–320.

157. Zhang, H., Xiao, R., Wang, D., He, G., Shao, S., Zhang, J., Zhong, Z. Biomass fast pyrolysis in a fluidized bed reactor under N_2, CO_2, CO, CH_4 and H_2 atmospheres. *Bioresour. Technol.*, 2011, **102**(5), 4258–4264.

158. Xie, F. F., Wang, Z., Lin, W. G., Song, W. L. Study on thermal conversion of Huadian oil shale under N_2 and CO_2 atmospheres. *Oil Shale*, 2010, **27**(4), 309–320.

159. Ye, J., Xiao, J., Huo, X., Gao, Y., Hao, J., Song, M. Effect of CO_2 atmosphere on biomass pyrolysis and in-line catalytic reforming. *Int. J. Energ. Res.*, 2020, **44**(11), 8936–8950.

160. Farrow, T. S., Sun, C., Snape, C. E. Impact of CO_2 on biomass pyrolysis, nitrogen partitioning, and char combustion in a drop tube furnace. *J. Anal. Appl. Pyrolysis*, 2015, **113**, 323–331.

161. Lee, J., Oh, J. I., Ok, Y. S., Kwon, E. E. Study on susceptibility of CO_2-assisted pyrolysis of various biomass to CO_2. *Energy*, 2017, **137**, 510–517.

162. Tang, L., Yan, Y., Meng, Y., Wang, J., Jiang, P., Pang, C. H., Wu, T. CO_2 gasification and pyrolysis reactivity evaluation of oil shale. *Energy Procedia*, 2019, **158**, 1694–1699.

163. Yağmur, S., Durusoy, T. Kinetics of the pyrolysis and combustion of Göynük oil shale. *J. Therm. Anal. Calorim.*, 2006, **86**(2), 479–482.

164. Nazzal, J. M. Influence of heating rate on the pyrolysis of Jordan oil shale. *J. Anal. Appl. Pyrolysis*, 2002, **62**(2), 225–238.

165. Olivella, M. À., De Las Heras, F. X. C. Evaluation of linear kinetic methods from pyrolysis data of Spanish oil shales and coals. *Oil Shale*, 2008, **25**(2), 227–245.

166. Gersten, J., Fainberg, V., Hetsroni, G., Shindler, Y. Kinetic study of the thermal decomposition of polypropylene, oil shale, and their mixture. *Fuel*, 2000, **79**(13), 1679–1686.

167. Johannes, I., Kruusement, K., Veski, R. Evaluation of oil potential and pyrolysis kinetics of renewable fuel and shale samples by Rock-Eval analyzer. *J. Anal. Appl. Pyrolysis*, 2007, **79**(1–2), 183–190.

168. Qian, J., Wang, J., Li, S. Oil shale development in China. *Oil Shale*, 2003, **20**(3S), 356–359.

169. Li, S., Yue, C. Study of pyrolysis kinetics of oil shale. *Fuel*, 2003, **82**(3), 337–342.

170. Williams, P. T., Ahmad, N. Investigation of oil-shale pyrolysis processing conditions using thermogravimetric analysis. *Appl. Energy*, 2000, **66**(2), 113–133.

171. Kök, M. V. Evaluation of Turkish oil shales - Thermal analysis approach. *Oil Shale*, 2001, **18**(2), 131–138.

172. Kök, M. V., Pamir, R. Pyrolysis kinetics of oil shales determined by DSC and TG/DTG. *Oil Shale*, 2003, **20**(1), 57–68.

173. Kök, M. V., Guner, G., Bagci, S. Combustion kinetics of oil shales by reaction cell experiments. *Oil Shale*, 2008, **25**(1), 5–16.

174. Na, J. G., Im, C. H., Chung, S. H., Lee, K. B. Effect of oil shale retorting temperature on shale oil yield and properties. *Fuel*, 2012, **95**, 131–135.

175. Khalil, A. M. Oil shale pyrolysis and effect of particle size on the composition of shale oil. *Oil Shale*, 2013, **30**(2), 136–146.

176. Wang, S., Liu, J., Jiang, X., Han, X., Tong, J. Effect of heating rate on products yield and characteristics of non-condensable gases and shale oil obtained by retorting Dachengzi oil shale. *Oil Shale*, 2013, **30**(1), 27–47.

177. Jaber, J. O., Probert, S. D., Williams, P. T. Evaluation of oil yield from Jordanian oil shales. *Energy*, 1999, **24**(9), 761–781.

178. Olukcu, N., Yanik, J., Saglam, M., Yuksel, M. Liquefaction of beypazari oil shale by pyrolysis. *J. Anal. Appl. Pyrolysis*, 2002, **64**(1), 29–41.

Publication II

Article

Co-Pyrolysis of Woody Biomass and Oil Shale—A Kinetics and Modelling Study

Alejandro Lyons Ceron [1], **Richard Ochieng** [2], **Shiplu Sarker** [2,*], **Oliver Järvik** [1] and **Alar Konist** [1]

1   Department of Energy Technology, Tallinn University of Technology, 19086 Tallinn, Estonia;
    allyon@taltech.ee (A.L.C.); oliver.jarvik@taltech.ee (O.J.); alar.konist@taltech.ee (A.K.)
2   Department of Manufacturing and Civil Engineering, Faculty of Engineering, Norwegian University of
    Science and Technology, 2815 Gjøvik, Norway; richard.ochieng@ntnu.no
*   Correspondence: shiplu.sarker@ntnu.no

Abstract: The co-pyrolysis of biomass and fossil fuels has been the subject of studies on sustainable energy. Co-feeding oil shale with woody biomass can contribute to a transition into carbon neutrality. The present study analysed the thermal decomposition behaviour of oil shale and biomass blends (0:1, 3:7, 1:1, 7:3, 9:1, and 1:0) through thermogravimetric analysis (TGA) at 80–630 °C with a heating rate of 10 °C/min in CO_2 and N_2 atmospheres. A comparison of theoretical and experimental residual mass yields of oil shale–biomass mixtures indicated no significant interactions between the fuels. The blends contributed to a decrease of up to 34.4 wt% in solid residues compared to individual pyrolysis of oil shale, and the TGA curves were shifted from up to 10 °C to a lower temperature when the biomass ratio increased. The use of a CO_2 atmosphere resulted in the production of solid residues, comparable to the one obtained with the N_2 atmosphere. CO_2 atmosphere can be used in oil shale–biomass co-pyrolysis, without affecting the decomposition process or increasing the yield of residues. A kinetic model method is proposed based on TGA data at 10, 20, and 30 °C/min. The apparent activation energies for a temperature range of 200–520 °C were in the order of 139, 155, 164, 197, 154, and 167 kJ/mol for oil shale–biomass 0:1, 3:7, 1:1, 7:3, 9:1, and 1:0 blends, respectively. From the isoconversional kinetic analysis, a two-stage pyrolysis was observed, which separated biomass and oil shale pyrolysis. A simulation of biomass and oil shale co-pyrolysis was conducted in Aspen Plus® using TGA-derived kinetic data. The model prediction resulted in a close match with the experimental thermogravimetric data with absolute errors from 1.75 to 3.78%, which highlights the relevance of TGA analysis in simulating co-pyrolysis processes.

Keywords: co-pyrolysis; kinetics; modelling; oil shale; woody biomass

1. Introduction

The production of clean and sustainable fuels is one of the current worldwide priorities for the mitigation of climate change, the reduction of the human-made environmental impact, and the depletion of natural resources. Conventional energy technologies and fossil fuels have led to an increase in emissions of CO_2 and other pollutant gases [1]. Co-feeding renewable, conventional, and alternative fuels is a technologically feasible solution expected to continue into a transition to full implementation of renewable technologies. Co-feeding biomass (BM) (a carbon-neutral fuel) and oil shale (OS) can provide a partial solution to the sustainable energy need in countries where these fuels are abundant. Particularly, employing a thermochemical conversion such as co-pyrolysis of OS and BM is one good example, which can contribute heavily to achieving some of the sustainable development goals [2].

BM, generally a highly volatile and low ash-content fuel, can be thermochemically converted into bio-oil, biogas, and activated carbon, and, as a renewable carbon-neutral resource, it can potentially provide around 14% of the world's energy demand [3]. Pyrolysis

of BM yields a high share of bio-oil (50–75% yield of liquids), permanent gases (20–25%), and solids (10–25%) [2]. On the other hand, OS, a sedimentary rock, composed of a share of kerogen (organic matter) is found in deposits all over the world—in China, Estonia, Jordan, and the United States, among others—exceeding the crude oil reserves. OS can be converted into shale oil (5–20%) and shale gas (5–20%) through thermochemical conversion processes, including pyrolysis [4,5]. The individual conversion of each fuel has been widely studied. BM pyrolysis has vast potential to produce sustainable fuel and energy. However, there have been some challenges in its conversion, particularly with regards to its physical and chemical properties such as low energy density due to high moisture content, and high diversity of available species, which eventually require diverse conversion techniques, followed by the upgrading and refining of the produced fuels due to stability issues [6]. Similarly, pyrolysis of OS leads to a high share of semicoke and ashes (>60%), which commonly results in waste and causes adverse environmental effects through high sulphur and CO_2 production [7,8]. As with the upgrading and refining requirement of BM-derived fuels, shale oil also requires additional upgrading or refining prior to utilisation, depending on the purpose. Additionally, different oil shales yield different shale oil. The main difference comes from the concentration of different heteroatoms [9].

During the co-pyrolysis of OS and BM, the two fuels can go through thermal degradation while interacting with different stages of chemical reactions and heat transfer to yield products with enhanced properties, as compared to the individual pyrolysis of each fuel. Co-feeding BM with fossil fuels, including OS, can result in a reduction in the emission of pollutant gases while improving the decomposition of the fuels and the yield and composition of the co-pyrolytic products [10]. The high hydrogen content and H/C ratio of BM allow the fuel to act as a hydrogen donor, enhancing pyrolysis decomposition [11], and reducing the activation energy of the co-pyrolysis blend [12]. BM and OS pyrolysis process typically occurs within the temperature range of 200–500 °C [13]. While the largest part of woody BM pyrolyzes at 200–400 °C for OS, the main pyrolysis occurs in the temperature range of 350–550 °C [14]. Co-pyrolysis of OS and BM has been observed to enhance the decomposition process, reduce the environmental impact, and enhance the yield and properties of pyrolysis products [15,16].

Thermogravimetric analysis is a commonly used method to study the thermochemical behaviour of fuels and feedstock, as well as the co-pyrolysis of two fuels. Typically, individual pyrolysis of OS and BM has been studied in inert atmospheres, such as N_2 and Ar. Using alternative atmospheres, such as CO_2, H_2O, H_2 or CH_4, can contribute to enhanced pyrolysis by improving product properties, enhancing devolatilization, and char reforming [17] through decreased char production, increasing condensable gas yield and improving bio-oil properties [18]. Particularly, in OS pyrolysis, CO_2 atmospheres are shown to decrease activation energy, increase interactions between the kerogen and mineral content, and decrease the yield of semicoke [19]. However, despite its potential benefits, CO_2 atmospheres have not been widely considered for OS and BM co-pyrolysis, and there have been only a few studies reported on BM and/or OS co-pyrolysis so far [13,20].

This paper studied the co-pyrolysis behaviour of Estonian woody BM and OS in N_2 and CO_2 atmospheres. The addition of small ratios of BM to OS pyrolysis was studied to determine the potential benefits of co-feeding both fuels while preserving the operational conditions typically used during individual OS and BM pyrolysis. The co-pyrolysis of OS and BM can potentially enhance the decomposition of OS while contributing to the reduction of environmental effects. In addition, the current study aimed to determine the effect of introducing CO_2 atmospheres to the co-pyrolysis process as a path to further improve the pyrolytic behaviour of OS, as well as increase the yields of usable products. The experiments were carried out in TGA equipment at temperatures up to 630 °C. A kinetic study using the Coats–Redfern and Kissinger methods and isoconversional Vyazovkin and Friedman methods were implemented to determine the kinetic parameters of OS:BM pyrolysis and co-pyrolysis. The kinetic parameters, calculated using isoconversional methods with values closest to those found in the literature, were utilised for modelling

the conversion of OS and BM and their blends, using Aspen Plus® software version 12.1. The novel aspect of this study includes making use of kinetic data obtained from TGA in the Aspen simulation, allowing for the incorporation of actual kinetic data to predict the co-pyrolytic behaviour of different blends. The obtained experimental and kinetic results plus the model will be used to continue further research on the co-pyrolysis of OS and BM in larger-scale equipment.

2. Materials and Methods

2.1. Materials

The wood of the trunks without bark of four of the most common Estonian BM species was used in co-pyrolysis: Norway spruce (*Picea abies*), grey alder (*Alnus incana*), Scots pine (*Pinus sylvestris*), and silver birch (*Betula pendula*). The chemical, physical, and thermodynamic properties of the BM species were previously obtained through elemental analysis, according to ISO 16948:2015 [21] and 16994:2016 [22], proximate analysis, based on ISO 18134-2:2017 [23] and 18122:2022 [24], and calorific values, according to ISO 18125:2017 [25,26], respectively. To obtain a representative sample of a mixture of Estonian BM species, each species was ground and sieved into a particle size below 0.125 mm, following ISO 14780:2017 [27]. The sieved samples were mixed in equal parts (25 wt% of each wood species). Estonian OS was characterized in terms of elemental analysis and calorimetry, according to ISO 29541:2010 [28] and ISO 1928:2020 [29], respectively. The ash content was determined following EVS 669:2022 [30]. The OS sample was sieved into a particle size below 0.125 mm. For the co-pyrolysis experiments, 6 ratios of OS-BM were prepared and mixed manually: 1:0, 9:1, 7:3, 1:1, 3:7, and 0:1 (100, 70, 50, 30, and 10 wt% BM) with a deviation of ±1%.

2.2. Experiment Set-Up

TGA co-pyrolysis experiments of BM and OS mixtures were conducted using a Netzsch STA 449F3 thermal analyser (NETZSCH Instruments North America, Burlington, United States). The equipment has a temperature resolution of 0.001 K and a balance resolution of 0.1 μg. The samples are pyrolyzed in aluminium oxide crucibles, using two gases, namely N_2 and CO_2, as the atmosphere, supplied with a flow rate of 0.05 L/min. The mass of the samples was 5 mg ±0.4 mg. The co-pyrolysis experiments were carried out with an initial purging stage from ambient temperature until 80 °C for 30 min, followed by the experimental segment with a heating rate of 10 °C/min, from 80 to 630 °C, for a total of 55 min, an isothermal segment of 20 min, and, finally, a cooling segment of around 60 min until the temperature of the samples was below 90 °C.

The residual mass curves of OS:BM 9:1, 7:3, 1:1, and 3:7 blends obtained experimentally were compared to the theoretical residual mass of OS:BM blends, calculated from the experimental TGA data for individual pyrolysis of OS and BM, which allowed us to determine the existence of interactions, including the inhibitory and promoting effects of co-processing OS and BM. The theoretical TGA curves of blends were calculated using Equation (1), where $m_{\%_{OS}}$ is the mass percentage of OS, $m_{\%_{BM}}$ is the mass percentage of BM, and x is the fraction of OS. The OS:BM blend ratios were selected to observe the effect of adding a share of BM in OS retorting in similar retorting conditions used in the industry, considering the calorific values and densities of each fuel.

$$m_{\%_{theo}} = m_{\%_{OS}}x + m_{\%_{BM}}(1 - x) \tag{1}$$

2.3. Kinetic Studies

The thermal decomposition of BM and OS can be studied through non-isothermal kinetic methods [31]. For the current research, kinetics methods were used to determine the apparent activation energy in the pyrolytic stage of BM and OS. The kinetic parameters were obtained using the TGA data in CO_2 atmospheres, at 10, 20, and 30 °C/min, from 200–520 °C. Based on these data, the conversion degree α was calculated. The conversion

degree is the ratio of actual mass loss to total mass loss, which was calculated using the mass loss data as shown in Equation (2):

$$\alpha = \frac{m_0 - m_t}{m_0 - m_\infty} \tag{2}$$

where m_0 is the initial mass of the sample, m_∞ is the final mass of the sample, and m_t is the actual mass of the sample at the time t. The rate of pyrolysis is a function of the reaction conversion function ($f(\alpha)$) (Equation (3)) and the temperature-dependent rate constant $K(T)$, as described by the Arrhenius equation (Equation (4)).

$$\frac{d\alpha}{dt} = K(T)f(\alpha) \tag{3}$$

$$K(T) = Ae^{-\frac{E}{RT}} \tag{4}$$

At a constant heating rate β for non-isothermal conditions, Equations (3) and (4) can be expressed as Equation (5):

$$\frac{d\alpha}{dT} = \frac{1}{\beta}K(T)f(\alpha) = \frac{A}{\beta}e^{-\frac{E}{RT}}f(\alpha) \tag{5}$$

A is the pre-exponential factor (min^{-1}), E is the activation energy (kJ/mol), R is the universal gas constant (kJ/mol K), and T is the temperature at time t. The integral form of Equation (5) can be solved through different approximations [32]. For the current study, the Coats–Redfern method [33] was implemented, describing the reaction conversion function ($f(\alpha) = (1 - \alpha)^n$), where n is the reaction order, as shown in Equation (6).

$$\frac{d\alpha}{dT} = \frac{A}{\beta}e^{-\frac{E}{RT}}(1 - \alpha)^n \tag{6}$$

The Coats–Redfern Equation (6) can be written for n = 1 and n ≠ 1, as follows (Equations (7) and (8)):

$$\ln\left(\frac{1 - (1-\alpha)^{(1-n)}}{T^2(1-n)}\right) = \ln\left(\frac{AR}{\beta E}\left(1 - \frac{2RT}{E}\right)\right) - \frac{E}{RT}, \; n \neq 1 \tag{7}$$

$$\ln\left(\frac{-\ln(1-\alpha)}{T^2}\right) = \ln\left(\frac{AR}{\beta E}\left(1 - \frac{2RT}{E}\right)\right) - \frac{E}{RT}, \; n = 1 \tag{8}$$

Equations (7) and (8) can be expressed as a linear regression y = mx + b, where the value of the activation energy E was calculated as the slope m of the equation. For Coats–Redfern, the reaction orders used for the calculations were from 0 to 2 at a step increase of 0.1. The reaction orders with the highest correlation coefficient R^2 in all heating rates were selected for the calculation of the activation energy E of the pyrolysis of all the OS:BM blends.

In addition to the Coats–Redfern method, isoconversional models including Friedman, widely used for BM kinetics, and Vyazovkin were used to evaluate the kinetics of BM and OS. The Kissinger model was also used as a first estimation of the kinetic parameters. The kinetic parameters for these models were determined using the free open-source thermokinetic software THINKS Version 31.10.21 for isoconversional analysis developed by Muravyev et al. [34]. These models are shown in Equations (9)–(11).

Friedman [35]

$$\ln\beta\left(\frac{\alpha}{dT}\right) = \ln(f(\alpha)A) - \frac{E}{RT} \tag{9}$$

Vyazovkin [36]

$$\sum_{i=1}^{n} \sum_{j \neq i}^{n} \frac{I(E, T_{\alpha,i}) \beta_j}{I(E, T_{\alpha,j}) \beta_i} \qquad (10)$$

$$\text{where } I(E, T(t_\alpha)) = \int_{t_\alpha - \Delta_\alpha}^{t_\alpha} \exp\left(\frac{-E}{RT(t)}\right) dt \qquad (11)$$

Kissinger [37]

$$\ln \frac{\beta}{T_p^2} = \ln\left(\frac{AR}{E}\right) - \frac{E}{RT_p} \qquad (12)$$

The Vyazoykin model is based on a minimisation procedure of Equation (10) for each value of α, using the temperature integral on Equation (11). For the Kissinger model, T_p is the temperature at the maximum of the reaction exothermic peak. For all four models, the temperature range considered was between 200 and 520 °C as the starting and ending temperatures for pyrolysis and co-pyrolysis.

2.4. Process Modelling

Based on the experimental TGA data and the kinetic analysis from OS and BM, a computational model was made, using Aspen Plus®. The model uses the activation energies, E and pre-exponential factors, A, for OS, and the BM structural components (i.e., hemicellulose, cellulose, and lignin). From TGA calculations, the E and A for the components can be estimated employing Equations (2) and (3), with the additional consideration of the mass of ash m_∞ as an inactive part of both materials. Based on this, the kinetic equation used for the model is shown in Equation (14).

$$-\frac{dm_t}{dt} = K(m_t - m_\infty) \qquad (13)$$

$$\frac{dm}{dt} = Km, \text{ considering ash as inactive} \qquad (14)$$

$$K = A \times \exp\left(-\frac{E}{RT}\right) \text{ and } m = m_t - m_\infty \qquad (15)$$

2.4.1. Oil Shale

OS decomposition is studied based on stoichiometry, using the dry ash-free (daf) basis results from the elemental and the proximate analyses. The chemical formula of OS is estimated as shown in Equation (16), calculated with stoichiometry based on the OS composition.

$$C_{4.265} H_{5.232} O_{2.472} N_{0.0134} S_{0.117} \qquad (16)$$

The proximate analysis (on a daf basis) is used to determine the molar amount of carbon that goes into char while the rest of the elemental components go into volatiles. The moles of C in char are derived from the mass fraction of fixed carbon, assuming a mass basis of 100 g. The stoichiometry of OS pyrolysis was based on the modification of the approach made by Baliban et al. [38], where OS decomposes into $C_{(s)}$, CO, CO_2, H_2, CH_4, N_2, H_2S, and NH_3. Water is assumed to exist only as free water (moisture) in the oil shale, and is therefore not considered among the products in the stoichiometric equation. The formulation of objective function and objectives was conducted as follows:

Sets: The set of all atoms $A_{\text{oil shale}}$ is

$$a \in A_{\text{oil shale}} = \{C, H, O, N, S\} \qquad (17)$$

The set of all gaseous species produced from the pyrolysis step is given as follows:

$$s \in S_{\text{oil shale}} = \left\{C_{(s)}, CO, CO_2, H_2, CH_4, N_2, H_2S, NH_3\right\} \qquad (18)$$

Assuming inter-relationships between gas species CO, CO_2, H_2, and CH_4, the following rations as shown in Equations (19)–(21) can be given. The ratios (1), (2), and (3) were estimated from the gas composition reported by Mozaffari et al. [39].

$$\text{ratio}(1) = CO/CO_2 \tag{19}$$

$$\text{ratio}(2) = CO_2/CH_4 \tag{20}$$

$$\text{ratio}(3) = CO/H_2 \tag{21}$$

Defining parameters are the following:

- $w_{a,\text{oil shale}}$—weight fraction of atom a in OS sample (daf);
- AW_a—atomic weight fraction of atom a;
- FC_a—fixed carbon weight fraction in OS sample (daf);
- $E_{a,S}$—number of a atoms in species s;
- x_s—moles of species s;
- $M_{\text{oil shale}}$—weight of OS (on daf basis);
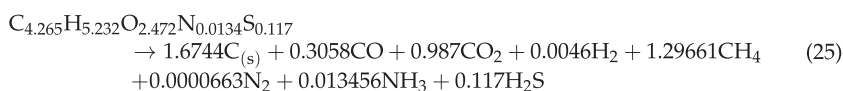- MW_s—molecular weight of species s.

Based on the formulation, the proposed model is a nonlinear optimisation model and takes the following form, as shown in Equation (22).

$$\min \left[M_{\text{oil shale}} - \sum_{s=1}^{s} MW_s \times x_s \right], \text{subject to :} \tag{22}$$

$$\text{C balance: } M_{\text{oil shale}} \left(\frac{w_{a \text{ oil shale}}}{AW_a} - \frac{FC_a}{AW_a} \right) = \sum_{s \in S_{\text{oil shale}}} (E_{a,s} x_s), \ a = C \tag{23}$$

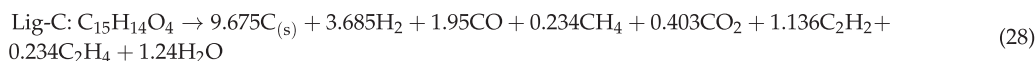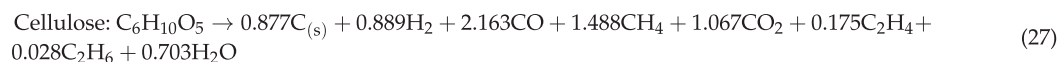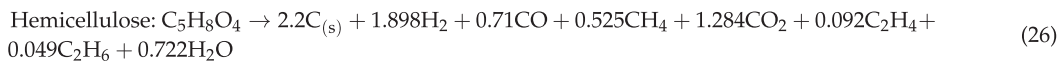$$\text{H and O balance: } M_{\text{oil shale}} \left(\frac{w_{a \text{ oil shale}}}{AW_a} \right) = \sum_{s \in} (E_{a,s} x_s), \ a \in A_{\text{oil shale}} (a \neq C), \ a \neq C \tag{24}$$

Solving the model in MATLAB results in the stoichiometric equation for the decomposition of the organic fraction of OS and becomes:

$$\begin{aligned} C_{4.265}H_{5.232}O_{2.472}N_{0.0134}S_{0.117} \\ \rightarrow 1.6744C_{(s)} + 0.3058CO + 0.987CO_2 + 0.0046H_2 + 1.29661CH_4 \\ + 0.0000663N_2 + 0.013456NH_3 + 0.117H_2S \end{aligned} \tag{25}$$

2.4.2. Biomass

The stoichiometry of BM is calculated based on the structural components: cellulose, hemicellulose, and lignin. The detailed derivation of the stoichiometric pyrolysis coefficients is based on Ranzi et al. and Baliban et al. [38,40]. This derivation considers BM components as cellulose ($C_6H_{10}O_5$), hemicellulose ($C_5H_8O_4$), and lignin monomers: Lig-C ($C_{15}H_{14}O_4$), Lig-H ($C_{22}H_{28}O_9$) and Lig-O ($C_{20}H_{22}O_{10}$), and models char as solid carbon, C, and considers all tar components to decompose into hydrocarbons. Based on this derivation, the stoichiometric equations for all components are as shown in Equations (26)–(30).

$$\text{Hemicellulose: } C_5H_8O_4 \rightarrow 2.2C_{(s)} + 1.898H_2 + 0.71CO + 0.525CH_4 + 1.284CO_2 + 0.092C_2H_4 + 0.049C_2H_6 + 0.722H_2O \tag{26}$$

$$\text{Cellulose: } C_6H_{10}O_5 \rightarrow 0.877C_{(s)} + 0.889H_2 + 2.163CO + 1.488CH_4 + 1.067CO_2 + 0.175C_2H_4 + 0.028C_2H_6 + 0.703H_2O \tag{27}$$

$$\text{Lig-C: } C_{15}H_{14}O_4 \rightarrow 9.675C_{(s)} + 3.685H_2 + 1.95CO + 0.234CH_4 + 0.403CO_2 + 1.136C_2H_2 + 0.234C_2H_4 + 1.24H_2O \tag{28}$$

$$\text{Lig-H: } C_{22}H_{28}O_9 \rightarrow 11C_{(s)} + 5.507H_2 + 4.9CO + 1.443CH_4 + 1.05CO_2 + 1.804C_2H_4 + 2H_2O \tag{29}$$

$$\text{Lig-O: } C_{20}H_{22}O_{11} \rightarrow 11C_{(s)} + 5.721H_2 + 4.9CO + 0.729CH_4 + 1.55CO_2 + 0.911C_2H_4 + 2H_2O \tag{30}$$

3. Results and Discussion

3.1. Fuel Characterisation

The composition of the studied samples of Norway spruce, grey alder, scots pine, silver birch, and OS are provided in Table 1, including elemental analysis, proximate analysis, and calorific values. As shown, the four studied BM samples have the same range of elemental composition, as well as ash content, moisture, heating values, and fixed carbon with the exception of silver birch, whose FC content is slightly lower than the rest (Table 1). On the contrary, the OS sample contains a significantly higher share of ash, with 52.5 wt% compared to 0.3 wt% for BM. Table 1 indicates how the OS's elemental composition in terms of C, H, and O differs from those of BM, as well as the share of volatiles, which are significantly lower.

Table 1. Elemental, proximate analysis, and calorific value for BM and OS.

Composition		Woody Biomass [26]				Oil Shale
		Norway Spruce	Grey Alder	Scots Pine	Silver Birch	
Elemental analysis [wt%]	C	50.3	49.9	50.1	49.3	27.2
	H	6.6	6.6	6.6	6.6	2.8
	N	0.1	0.2	0.2	0.1	<0.1
	S	n.d.	n.d.	n.d.	n.d.	2.0
	O *	42.7	43.0	43.1	44.0	15.4
Molar ratio	H/C	1.6	1.6	1.6	1.6	1.3
	O/C	0.6	0.6	0.6	0.7	0.4
Proximate analysis [wt%]	Ash content	0.3	0.3	0.3	0.3	52.4
	Moisture **	6.9	7.6	8.5	7.7	0.9
	Fixed carbon	14.2	14.0	14.5	12.8	1.5
	Volatile matter	85.5	85.7	85.2	86.9	46.1
Calorific value [MJ/kg]	LHV	18.6	18.5	18.4	18.0	8.7
	HHV	20.0	19.9	19.8	18.1	9.7

* Calculated, n.d.—not detected. ** Moisture content for room dry sample.

3.2. TGA Behaviour

The TGA behaviour of individual pyrolysis of OS and BM and OS:BM blends can be observed in Figure 1. The temperature range from 80 to 520 °C was selected according to the individual pyrolysis temperature of BM (250–500 °C) [2] and OS (350–550 °C) [41]. A temperature of 520 °C was chosen, as for both fuels a temperature greater than 550 °C favour more gas yield than oil [42].

The TGA curve of BM pyrolysis started with a pre-pyrolysis stage from 100 to 250 °C, followed by the most significant mass loss at the temperature range of 250–400 °C, with a smaller loss in mass continuing after 400 °C. As expected, there was no considerable mass loss between 80 and 120 °C. The BM pyrolysis temperature range is explained by its main components, cellulose, hemicellulose, and lignin, which decompose at 350–400 °C, 220–315 °C, and 250–800 °C, respectively [3]. The mass loss curve and temperature range in BM pyrolysis agreed with the decomposition pattern of its three major components: cellulose, hemicellulose, and lignin (40–50%, 15–30%, and 10–25% respectively). As observed, the majority of the mass loss occurred in the decomposition temperature range of cellulose and hemicellulose, and the partial decomposition of lignin [43]. At temperatures above 500–520 °C, the last stage of BM decomposition occurred, which included the decomposition of lignin and residues from incomplete pyrolysis. The final mass losses for BM were 79.5 to 78.8 wt% in N_2 and CO_2, respectively, which are comparable to mass losses obtained

in the TGA of woody BM at different heating rates studied by Garcia-Perez et al. [44], who also observed the minimal changes in the mass loss at temperatures above 450–500 °C.
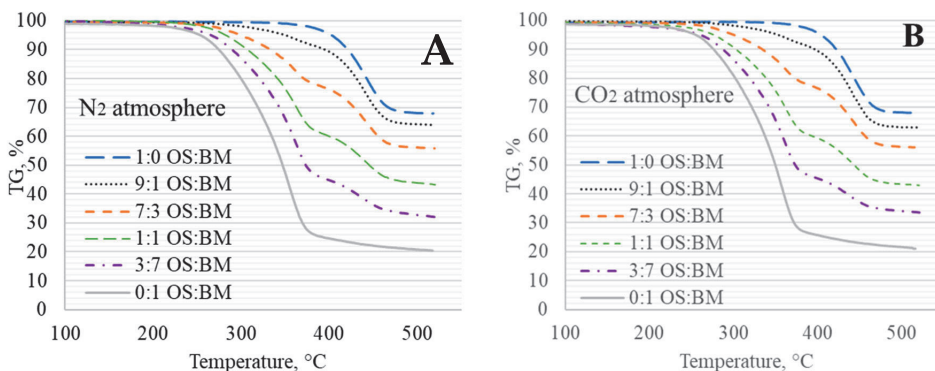

Figure 1. TGA curves of OS:BM co-pyrolysis in (**A**) N_2 atmosphere and (**B**) CO_2 atmosphere.

The individual pyrolysis of OS is shown in Figure 1A,B. The mass loss started at temperatures above 300 °C, having the highest mass loss at a range from 350 to 510 °C, which resulted in a final mass loss from 32.1 to 32.3 wt% in N_2 and CO_2, respectively. Likewise, with BM, there was no significant amount of moisture in the OS sample. A one-stage mass loss in the range of 350–510 °C can be attributed to the endothermic transformation of OS kerogen into volatile hydrocarbons and semicoke, as also observed by Wang et al. [45]. Decomposition above 600 °C, which was not covered in this study, would be related to the decomposition of inorganic matter, residual organic matter, and carbonates, as explained by Tiwary et al. [46] and Lin et al. [47]. Compared to OS, BM had a significantly higher share of mass loss (79 vs. 32 wt%). This was due to lower ash content in BM samples (0.3% in BM vs. 52.4% in OS) (Table 1).

The co-pyrolytic behaviour of OS and BM blends 9:1, 7:3, 1:1, and 3:7 in N_2 and CO_2 atmospheres is shown in Figures 1A and 1B, respectively. The experiments for all the samples including pyrolysis of only OS (1:0 OS:BM) and only BM (0:1 OS:BM) were carried out at a temperature range between 80 and 550 °C. For the 9:1 OS:BM blend, the TGA decomposition curve had a profile comparable to the curve of individual pyrolysis of OS. However, the addition of 10 wt% of BM accelerated the decomposition of the blend, reducing the initial pyrolysis temperature to around 260 °C for both gas atmospheres. Additionally, the presence of BM caused a higher mass loss in the range of 250–400 °C, resulting in 11–12 wt% mass loss, compared to 4–5 wt% in individual co-pyrolysis of OS. After 400 °C, the decomposition curve followed the same pattern of individual pyrolysis of OS, but the curve was shifted from 1 to 3 °C to the left, resulting in a decomposition of the blend at a slightly lower temperature. Overall, the 9:1 OS:BM blend resulted in a higher final mass loss (from 35.1–36.2 wt%). The 7:3 OS:BM blend had a more pronounced initial decomposition stage, which also started at a lower temperature, close to 250 °C, and increased the mass loss to 23.5–24 wt% in the range of 250–400 °C. At temperatures above 400 °C, the decomposition curve followed a similar behaviour to individual pyrolysis of OS and 9:1 OS:BM co-pyrolysis, but the curve was shifted around 3–5 °C to the left for both gas atmospheres. The 7:3 OS:BM blend had a final mass loss between 43.8–44.1 wt%. As the share of BM increased to 50 and 70 wt% (OS:BM 1:1 and 3:7), the main decomposition started between 200 and 220 °C, with a mass loss of 44 and 60 wt%, respectively, in the range of 250–400 °C. The share of OS decomposed above 400 °C, starting at 8–10 °C lower than individual OS pyrolysis. The final mass loss was 57.0–57.2 and 66.4–66.7 wt% for OS:BM 1:1 and 3:7, respectively. The residual mass of OS:BM blends are mostly composed of Char and ashes from BM pyrolysis and semicoke (char and organic matter) from OS [48].

The DTG curves in N_2 and CO_2 are shown in Figure 2A,B for OS and BM and OS:BM blends. The temperatures where the highest loss of mass occurred varied based on the TGA behaviour of each fuel and the blend ratio. Individual pyrolysis of BM had the highest DTG peak at 355–358 °C, while the same for OS reached 443–446 °C. The OS:BM blends had two temperature peaks as a result of an additive pyrolytic behaviour of both fuels. The higher ratios of BM shifted the TGA curve, and DTG peaks to the left up to 10 °C in OS:BM blends, towards a behaviour more similar to the pyrolysis of BM, including the temperature ranges where the most significant share of OS pyrolysis occurred. Therefore, the DTG peaks of OS:BM blends varied due to their combined thermal decomposition, and the heat transfer interactions between OS and BM. The addition of BM to OS contributed to enhanced pyrolysis. This was maybe due to and higher volatile content of BM (Table 1), which potentially led to the production of a higher yield of liquid (oil) and gaseous products [49]. The addition of BM and the pyrolysis temperature shift can reduce the activation energy [50]. Higher ratios of BM can increase the yield of products [51] and accelerate thermal decomposition [20]. A probable reason for the enhanced OS pyrolysis when adding BM is the catalytic effect of fuel elements, such as ash alkali and alkaline earth metals, which can promote pyrolysis, enhance organic matter decomposition, and promote the production of oil and gas [16,42,51]. Higher hydrogen content of BM (6.6 vs. 2.8 wt% in OS) can also contribute to an increased number of hydrogen-free radicals promoting OS pyrolysis and enhancing liquid and gaseous pyrolytic products [52].
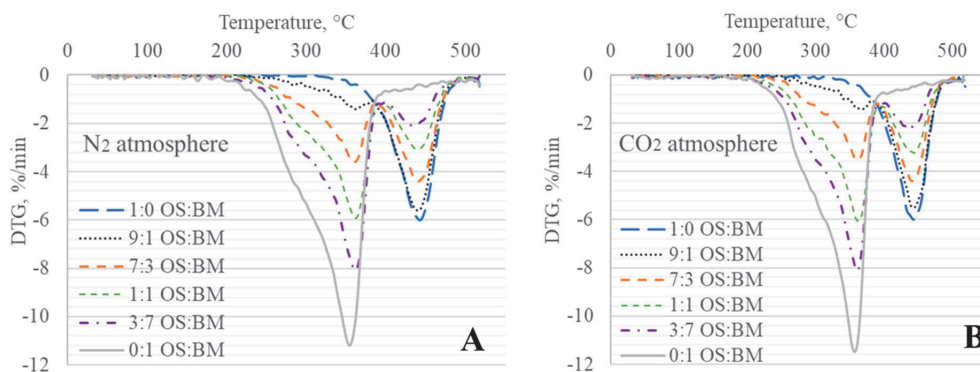

Figure 2. DTG curve of OS:BM co-pyrolysis in (**A**) N_2 atmosphere and (**B**) CO_2 atmosphere.

From the co-pyrolytic curves in Figure 1A,B and Figure 2A,B, it can be seen that the TGA decomposition was a result of an additive behaviour of individual pyrolysis of OS and BM, as the final weight loss increased with the addition of BM, as also observed by Kiliç et al. [53]. Figure 3 displays the residual mass vs. OS:BM blends in all N_2 and CO_2. For both gas atmospheres, the additive behaviour is evidenced by a linear increase in mass loss as the BM ratio increases, with a linear coefficient of determination R^2 from 0.994 to 0.996. The TGA behaviour of OS:BM blends follow a two-stage decomposition, the first stage from 200 to 380–400 °C, which is predominantly attributed to BM pyrolysis, and the second stage, from 380–400 to 490–500 °C, which primarily corresponds to OS pyrolysis. The temperature range, where the largest share of mass loss occurred for both pyrolysis blends, was from 200 to 500 °C, as also noted by Chen et al. [20]. An earlier thermal degradation occurred as the BM ratio increased, which was also noted by Dai et al. [51]. This was mainly due to a shift of the mass loss in all decomposition stages towards a lower temperature region, which can lead to improved pyrolysis characteristics of OS, as explained previously by Jiang, et al. [16].
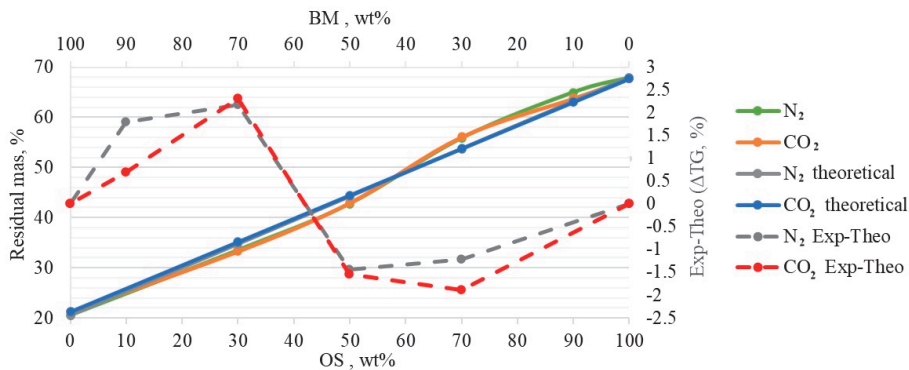
Figure 3. Final residual mass of OS:BM blends.

The co-pyrolytic behaviour of OS and BM is also shown in Figure 1A,B for pyrolysis in N_2 and CO_2 atmospheres. At first glance, it can be visualised that the TGA curves for individual pyrolysis, as well as for OS:BM blends, have almost identical behaviour under both gas atmospheres. There were few differences in pyrolysis in CO_2 atmospheres compared to N_2. The differences in the final residual mass between CO_2 and N_2 atmospheres for OS:BM 1:0, 9:1, 7:3, 1:1, 3:7, and 0:1 were 0.2, 1.2, 0.2, 0.2, 0.2, and 0.7 wt%, respectively. The effect of CO_2 could in all likelihood be more noticeable at higher temperatures (above 500 °C), as the gas can contribute to gasification reactions, enhancing thermal cracking and increasing the gas yield, while decreasing the solid yield [54,55]. Even though CO_2 atmospheres did not have considerable improvement in the pyrolysis of OS and BM from a TGA point of view, using CO_2 can be potentially beneficial, as the decomposition behaviour and the mass losses are not inhibited and the outcome is comparable to N_2 pyrolysis, while having the advantage of using this pollutant gas to be stored through Carbon Capture, Utilisation and Storage Technologies (CCUS) [56].

3.3. Interactions in Co-Pyrolysis

A detailed comparison is shown in Figure 4A,B, displaying the experimental and theoretical TGA (from Equation (1)) curves obtained for co-pyrolysis of OS:BM 9:1, 7:3, 1:1, and 3:7 blend ratios in N_2 and CO_2 atmospheres.
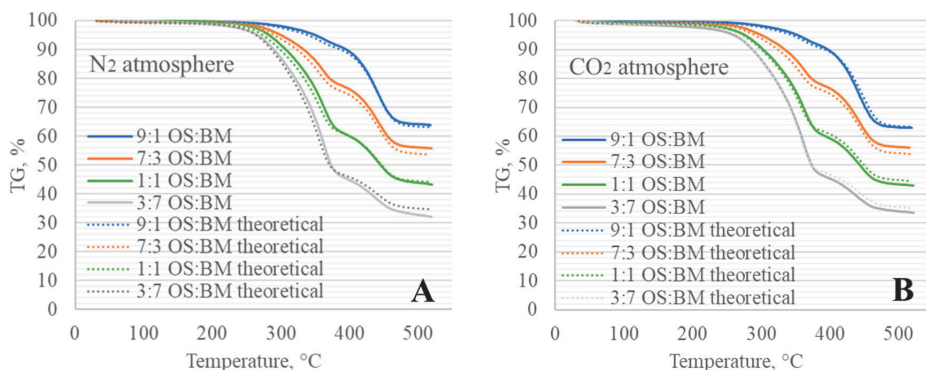

Figure 4. Comparison of theoretical and experimental TGA curves of OS:BM co-pyrolysis in (**A**) N_2 atmosphere and (**B**) CO_2 atmosphere.

The theoretical and experimental TGA curves of OS:BM co-pyrolysis displayed slight differences in the residual mass for all the OS:BM blends in both gas atmospheres. The TGA

curves shown in Figure 4A,B indicate that the experimental curves behaved as an additive process from individual pyrolysis of OS and BM, as also demonstrated in the theoretical curves, which had almost identical behaviour. However, there were some slight differences between the theoretical and experimental curves, which can be observed in Figure 5A,B. In the temperature range from 80 to 250 °C, the TGA experimental and theoretical residual mass differed by less than 0.5 wt% for all blends, with the majority of the experimental residual mass being higher than the theoretical for all blends in both gas atmospheres. The behaviour was different at temperatures from 250 to 370 °C, where most BM decomposition occurred. For N_2 pyrolysis, the experimental residual mass was higher than the theoretical residual mass, reaching the maximum difference at 350–360 °C, with up to 1.4, 2.8, 1.8, and 2.4 wt% difference for OS:BM 9:1, 7:3, 1:1, and 3:7, respectively. The blends in the CO_2 atmosphere at the same temperature range had higher experimental residual mass for OS:BM 9:1 and 7:3 (up to 1.0 and 2.8 wt% difference, respectively) and lower residual mass with less than 1 wt% difference for OS:BM 1:1 and 3:7. After 370–400 °C, OS:BM 1:1 and 3:7 blends had a final experimental residual mass of 2.2–2.3 and 0.7–1.8 wt% lower than the theoretical residual mass. The 9:1 and 7:3 blends had the opposite behaviour, with a higher experimental residual mass, from 1.2 to 1.9 and 1.4 to 1.5 wt%, higher than the theoretical residual mass. Overall, the residual mass difference between experimental and theoretical decomposition was no greater than 3 wt%, with an uncertainty of ± 1 wt%, with the highest differences at temperatures from 350 to 370 °C and >450 °C, and the lowest differences at temperatures below 250 °C.
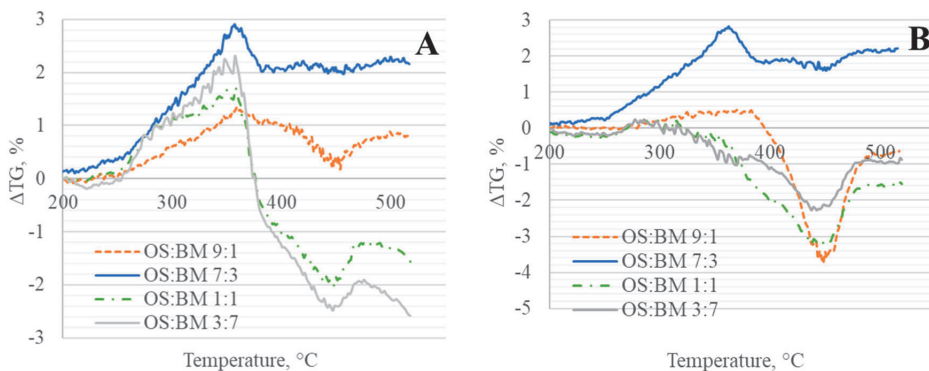

Figure 5. Difference between experimental and theoretical (Exp-Theo) TGA curves of OS:BM co-pyrolysis in (**A**) N_2 atmosphere and (**B**) CO_2 atmosphere (**right**).

From the comparison of experimental and theoretical TGA curves, it was observed that at temperatures below 250 °C there were negligible or no interactions between OS and BM. At temperature ranges of 350–370 °C and >450 °C, there were some slight interactions between OS and BM, with a predominantly inhibiting effect on the mass loss for OS:BM 9:1 and 7:3 blends, and a mass loss promoting effect for OS:BM 1:1 and 3:7 blends in both atmospheres, indicating improved pyrolysis as the BM ratio raised. The peaks of interactions were identified to coincide with the highest DTG temperature peaks, where BM and OS were going through the most significant stage of decomposition, indicating the existence of interactions during the main pyrolytic stage for each fuel. Nonetheless, in all cases, the promotion or inhibition effects were not too significant to conclude the presence of a strong synergistic effect during co-pyrolysis. Similar results have been obtained by Kiliç et al. [53] in the co-pyrolysis of OS and E.rigida, and Janik et al. [15] in the co-pyrolysis of OS and Terebinth berries, who noted an additive behaviour from individual pyrolysis of OS and BM. Johannes et al. [57] also noted minimal synergistic effects, only in the initial decomposition stage. On the contrary, other research has found promoting synergistic interactions between OS and different BM, which increased the

liquid product yields, decreased the solid yields and the activation energy, and improved the pyrolysis product properties [13,20,51]. It should be noted that, in most research, the synergistic effects were observed in the yields and/or composition of products and mostly in larger-scale equipment.

3.4. Kinetic Studies

The experimental and theoretical mass losses of OS, BM, and OS:BM blends in co-pyrolysis at 10, 20, and 30 °C/min are shown in Table 2, where it can be observed that the theoretical mass loss differs from the experimental mass loss in blends with larger ratios of BM. However, the differences are lower than 2 wt% in most blends and heating rates, except for the OS:BM blend 3:7 at 30 °C/min. The TGA data at heating rates of 10, 20, and 30 °C/min were used to calculate the apparent activation energy using the Coats–Redfern model, as shown in Table 3.

Table 2. Experimental (exp.) and theoretical (th.) mass losses of BM and OS blends at 10, 20, and 30 °C/min.

Blend OS:BM	Heating Rate, °C/min					
	10		20		30	
	Mass Loss, wt%		Mass Loss, wt%		Mass Loss, wt%	
	exp.	th.	exp.	th.	exp.	th.
0:1	78.8	-	79.7	-	80.9	-
3:7	66.7	64.8	65.4	66.0	62.3	66.9
1:1	57.1	55.5	58.7	56.9	54.9	57.1
7:3	43.9	46.2	48.2	47.8	46.9	47.3
9:1	36.2	36.9	39.3	38.7	37.7	37.5
1:0	32.3	-	34.1	-	32.6	-

Table 3. Activation energies of co-pyrolysis of BM and OS obtained through the Coats–Redfern method.

OS:BM	E, kJ/mol	RSD, %	R^2	n
0:1	96.73	1.82	0.9926	1.7–1.8
3:7	85.33	1.26	0.9945	1.6-1.7
1:1	77.44	1.47	0.9901	1.4–1.5
7:3	69.90	0.48	0.9878	1.0–1.2
9:1	66.13	2.50	0.9854	0.3–1.0
1:0	58.89	7.80	0.9388	0.1

From Table 3, the deviation in the activation energy for all OS:BM blends at different heating rates was below 2.5%, except for 7.8 for OS:BM 1:0. Therefore, the calculation of the activation energy is considered reliable as the deviation is well below 10%. It is also observed that the R^2 values are close to 1, especially for 100 wt% BM and for OS:BM blends with higher ratios of BM. As the BM ratio increased, the reaction order n that resulted in the best correlation was also raised. The activation energies obtained with Coats–Redfern agree with some other research, for BM [58,59] and OS [60]. It should be considered that the values of activation energies vary, depending on the temperature range studied. The current study calculated the activation energy for a temperature range where pyrolysis of BM and OS occurred, at 200–520 °C. However, the activation energies calculated using the Coat–Redfern model are considerably lower than those found in most of the results from the literature. Therefore, the Kissinger, Friedman, and Vyazovkin models were applied, and the results obtained through these methods are shown in Table 4.

Table 4. Activation energies of co-pyrolysis of BM and OS.

OS:BM	Coats–Redfern		Kissinger		Friedman			Vyazovkin	
	E, kJ/mol	R^2	E, kJ/mol	R^2	E, kJ/mol	R^2	A, min^{-1}	E, kJ/mol	Ω
0:1	96.7	0.9926	147.4	0.984	139.3	0.99101	2.95×10^9	140.4	30.0138
3:7	85.3	0.9945	179.4	0.997	154.7	0.97557	5.95×10^9	156.8	30.2506
1:1	77.4	0.9901	152.9	0.997	164.3	0.97786	5.25×10^{11}	163.1	30.1756
7:3	69.9	0.9878	145.9	0.947	197.3	0.89704	7.39×10^{11}	193.0	30.9744
9:1	66.1	0.9854	172.9	0.988	153.6	0.80934	2.94×10^8	153.4	21.1926
1:0	58.9	0.9388	160.2	0.979	167.4	0.95007	2.34×10^9	171.5	30.1077

While Coats–Redfern resulted in activation energies of 96.7 kJ/mol for BM and 58.9 kJ/mol for OS, the results from the Kissinger, Friedman, and Vyazovkin models shown in Table 4 are significantly different. Even though the Coats–Redfern model provided a higher R^2, Vyazovkin, and Friedman are advanced isoconversional models that determine the kinetic parameters at different stages of conversion, which resulted in a more detailed analysis of the pyrolysis and co-pyrolysis of OS and BM. From Kissinger, Friedman, and Vyazovkin models, the activation energy range was 139.3–147.4 kJ/mol for BM and 160.2–171.5 kJ/mol for OS. The apparent activation energy for OS:BM blends ranged from 145.9 to 197.3 kJ/mol. These values are in accordance with most studies from the literature on OS and BM [20,51,61–63]. The apparent activation energy for OS and BM and OS:BM blends at different stages of conversion based on the Friedman model are shown in Figure 6A,B and Figure 7, respectively.
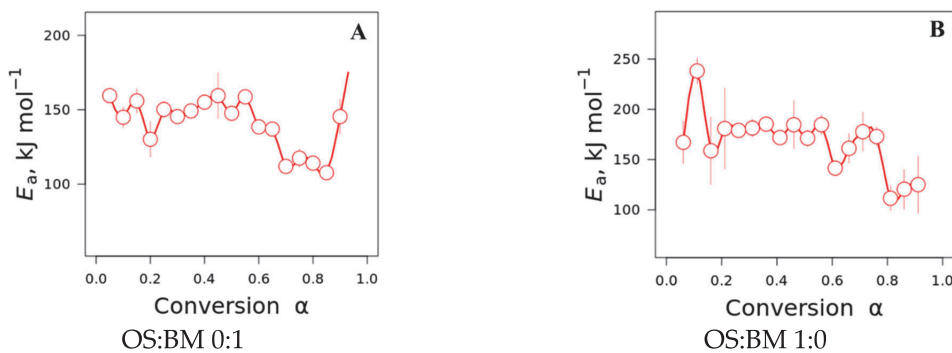

Figure 6. Friedman apparent activation energies of (**A**) OS and (**B**) BM at different conversion stages.
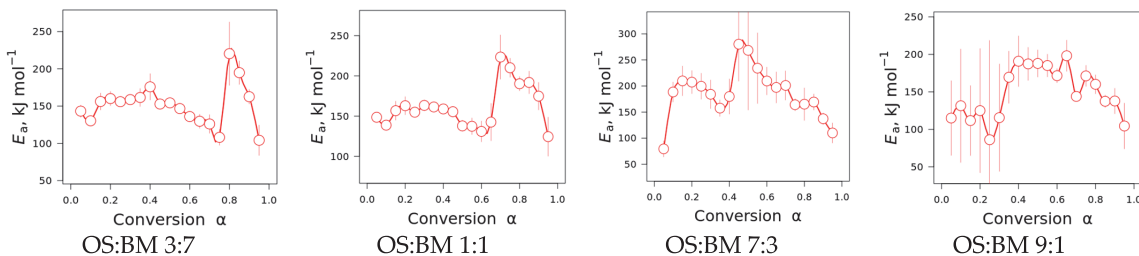

Figure 7. Friedman apparent activation energies of OS:BM blends at different conversion stages.

From the apparent activation energies shown in Figure 6A,B, it can be observed that both OS and BM have activation energy in the range of 100–200 kJ/mol at most degrees of

conversion, which tend to decrease as the conversion degree increases. However, the most significant result is observed in Figure 7. For all OS:BM blends, there is a clear two-stage decomposition based on the activation energy at different stages of conversion. Lower activation energy at the first stage corresponds mostly to BM pyrolysis, while the second stage of higher activation energy corresponds for the most part to OS pyrolysis. The two-stage decomposition varies based on the ratio of OS:BM. The higher ratio of OS results in a wider second stage of conversion, with a higher activation energy. These results agree with the additive behaviour obtained in the TGA analysis and the analysis of interactions between OS and BM in Section 3.2. A two-stage decomposition with two different sections of apparent activation energies could explain the additive behaviour and low interactions in the residual mass of OS:BM co-pyrolysis. Based on the kinetic results from the Friedman model from Figure 7, the average activation energy for OS and BM was calculated based on the conversion ranges of the two-stage decomposition observed. The results are shown in Table 5.

Table 5. Activation energies of co-pyrolysis of BM and OS at different stages of conversion.

Blend OS:BM	Feedstock	Conversion, α	Friedman E_a [kJ/mol]
3:7	BM	0.05–0.8	146.6
	OS	0.8–0.95	192.6
1:1	BM	0.05–0.7	150.1
	OS	0.7–0.95	198.1
7:3	BM	0.05–0.45	200.9
	OS	0.45–0.95	194.1
9:1	BM	0.05–0.25	114.0
	OS	0.8–0.95	170.1

3.5. Process Modelling

In the Aspen Plus® environment, OS was modelled as a non-conventional component, while the BM components (i.e., cellulose, hemicellulose, and lignin) were entered as conventional components, and their thermophysical properties were estimated using the approach proposed by Gorensek et al. [64]. The kinetic parameters used in the model for BM and OS are shown in Table 6. The biochemical composition of BM, i.e., cellulose, hemicellulose, lignin-C, lignin-H, and lignin-O, was estimated from the elemental analysis of wood using the method proposed by Debiagi et al. [65]. The Peng–Robinson Equation of State with Boston–Mathias (PR-BM) modification was used to estimate the thermodynamic properties of conventional components. Figure 8 displays the Aspen Plus® process schematics used.

Table 6. Kinetic parameters of BM and OS used in Aspen Plus® model.

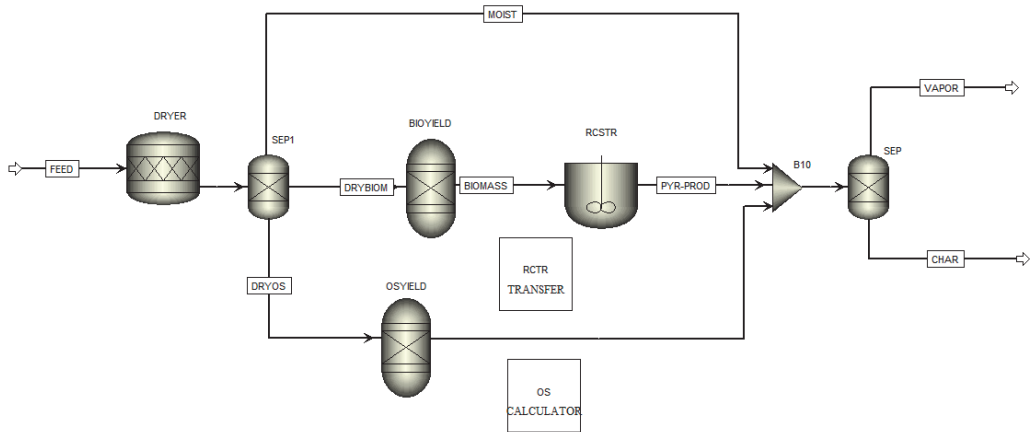|		A (s^{-1})	E (kJ/mol)
Biomass	Hemicellulose	2.41×10^8	141
	Cellulose	2.42×10^9	147
	Lignin	3.90×10^8	157
Oil shale	-	2.03×10^9	161

Figure 8. Process schematic in Aspen Plus®.

With the first-order reaction mechanism, the kinetic parameters estimated by the TGA kinetic models were optimised to fit with the experimental data as shown in Figure 9. There was a close match between the model prediction and the experimental TGA data of the individual pyrolysis of BM and OS, and the co-pyrolysis of BM and OS. The mean absolute errors for BM and OS of 3.78% and 1.81%, respectively, and 2.89, 2.60, 1.75, and 2.53% for OS:BM 9:1, 7:3, 1:1, and 3:7, were obtained by comparing the simulated and experimental TGA data. A sensitivity analysis revealed that the exponential factor, A, and reaction order, n, have a greater influence on the mass loss curve than the activation energy.
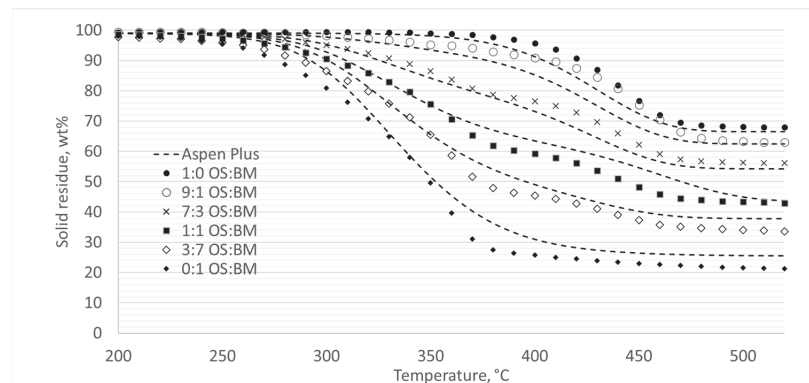

Figure 9. TGA behaviour vs. mass loss curve modelled in Aspen Plus®.

4. Conclusions

- The obtained TGA and DTG curves for OS:BM blends demonstrated an improved pyrolysis process, as the TGA curves were shifted from up to 10 °C to a lower temperature when the BM ratio increased. The addition of BM could enhance the pyrolysis of OS by increasing the mass loss and reducing the decomposition temperature. There was a linear relationship between the mass loss and the ratio of BM.
- The different two gas atmospheres resulted in an almost identical pyrolytic behaviour for all OS and BM blends. Nonetheless, the use of a CO_2 atmosphere resulted in the pyrolysis of OS and BM blends comparable to the N_2 atmosphere, showing its potential use in pyrolysis and co-pyrolysis as an alternative gas atmosphere obtained from CCUS technologies.

- The interactions between BM and OS were mostly negligible, particularly at low temperatures (<250 °C), while some slight interactions were observed at 350–370 °C and >500 °C, resulting in additive co-pyrolytic behaviour of OS:BM blends, which was further confirmed with the two-stage decomposition observed in the apparent activation energies at different stages of conversion.
- The Aspen Plus® model can be useful in optimising the TGA pyrolysis experiments, and further studies involving a comparison with experimental data from larger-scaled fixed-bed reactors would unlock the opportunity to directly apply TGA kinetic data in the reactor design.
- Experiments in larger-scale equipment, such as fixed beds or fluidized bed reactors, are proposed as a follow-up path to study the co-pyrolytic behaviour of OS and BM, possible interactions, and the effect of CO_2 as a gas atmosphere.

Author Contributions: Conceptualisation, A.L.C., S.S. and A.K.; methodology, A.L.C., R.O. and A.K.; software, R.O., S.S. and A.L.C.; validation, A.L.C., R.O. and A.K.; formal analysis A.L.C., R.O., S.S. and A.K.; writing—original draft preparation, A.L.C.; writing—review and editing, A.L.C., R.O., S.S., O.J. and A.K.; visualisation, A.L.C.; supervision, S.S. and A.K. All authors have read and agreed to the published version of the manuscript.

Data Availability Statement: Data are not publicly available due to the extensive nature of the dataset, which makes it impractical for direct public dissemination; the data may be made available on request from the corresponding author.

Conflicts of Interest: The authors declare no conflicts of interest.

References

1. Rogelj, J.; Den Elzen, M.; Höhne, N.; Fransen, T.; Fekete, H.; Winkler, H.; Schaeffer, R.; Sha, F.; Riahi, K.; Meinshausen, M. Paris Agreement climate proposals need a boost to keep warming well below 2 °C. *Nature* **2016**, *534*, 631–639. [CrossRef]
2. Uddin, M.N.; Techato, K.; Taweekun, J.; Rahman, M.M.; Rasul, M.G.; Mahlia, T.M.I.; Ashrafur, S.M. An overview of recent developments in biomass pyrolysis technologies. *Energies* **2018**, *11*, 3115. [CrossRef]
3. Akhtar, A.; Krepl, V.; Ivanova, T. A Combined Overview of Combustion, Pyrolysis, and Gasification of Biomass. *Energy Fuels* **2018**, *32*, 7294–7318. [CrossRef]
4. Han, X.; Kulaots, I.; Jiang, X.; Suuberg, E.M. Review of oil shale semicoke and its combustion utilization. *Fuel* **2014**, *126*, 143–161. [CrossRef]
5. Knaus, E.; Killen, J.; Biglarbigi, K.; Crawford, P. An overview of oil shale resources. *ACS Symp. Ser.* **2010**, *1032*, 3–20. [CrossRef]
6. Wang, Q.; Li, X.; Wang, K.; Zhu, Y. Commercialization and Challenges for the Next Generation of Biofuels: Biomass Fast Pyrolysis. In Proceedings of the 2010 Asia-Pacific Power and Energy Engineering Conference, Chengdu, China, 28–31 March 2010; IEEE: Piscataway, NJ, USA, 2010; pp. 1–4.
7. Pihu, T.; Konist, A.; Puura, E.; Liira, M.; Kirsimäe, K. Properties and environmental impact of oil shale ash landfills. *Oil Shale* **2019**, *36*, 257–270. [CrossRef]
8. Lees, H.; Järvik, O.; Konist, A.; Siirde, A.; Maaten, B. Comparison of the ecotoxic properties of oil shale industry by-products to those of coal ash. *Oil Shale* **2022**, *39*, 1–19. [CrossRef]
9. Baird, Z.S.; Oja, V.; Järvik, O. The composition of kukersite shale oil. *Oil Shale* **2023**, *40*, 25–43. [CrossRef]
10. Haykiri-Acma, H.; Yaman, S. Interaction between biomass and different rank coals during co-pyrolysis. *Renew. Energy* **2010**, *35*, 288–292. [CrossRef]
11. Quan, C.; Xu, S.; An, Y.; Liu, X. Co-pyrolysis of biomass and coal blend by TG and in a free fall reactor. *J. Therm. Anal. Calorim.* **2014**, *117*, 817–823. [CrossRef]
12. Lan, W.; Chen, G.; Zhu, X.; Wang, X.; Xu, B. Progress in techniques of biomass conversion into syngas. *J. Energy Inst.* **2015**, *88*, 151–156. [CrossRef]
13. Chen, B.; Han, X.; Tong, J.; Mu, M.; Jiang, X.; Wang, S.; Shen, J.; Ye, X. Studies of fast co-pyrolysis of oil shale and wood in a bubbling fluidized bed. *Energy Convers. Manag.* **2020**, *205*, 112356. [CrossRef]
14. Bai, F.; Sun, Y.; Liu, Y.; Li, Q.; Guo, M. Thermal and kinetic characteristics of pyrolysis and combustion of three oil shales. *Energy Convers. Manag.* **2015**, *97*, 374–381. [CrossRef]
15. Yanik, J.; Seçim, P.; Karakaya, S.; Tiikma, L.; Luik, H.; Krasulina, J.; Raik, P.; Palu, V. Low-temperature pyrolysis and co-pyrolysis of Göynük oil shale and terebinth berries (Turkey) in an autoclave. *Oil Shale* **2011**, *28*, 469–486. [CrossRef]

16. Jiang, H.; Deng, S.; Chen, J.; Zhang, L.; Zhang, M.; Li, J.; Li, S.; Li, J. Preliminary Study on Copyrolysis of Spent Mushroom Substrate as Biomass and Huadian Oil Shale. *Energy Fuels* **2016**, *30*, 6342–6349. [CrossRef]

17. Lee, J.; Yang, X.; Cho, S.H.; Kim, J.K.; Lee, S.S.; Tsang, D.C.W.; Ok, Y.S.; Kwon, E.E. Pyrolysis process of agricultural waste using CO_2 for waste management, energy recovery, and biochar fabrication. *Appl. Energy* **2017**, *185*, 214–222. [CrossRef]

18. Lee, J.; Oh, J.I.; Ok, Y.S.; Kwon, E.E. Study on susceptibility of CO_2-assisted pyrolysis of various biomass to CO_2. *Energy* **2017**, *137*, 510–517. [CrossRef]

19. Tang, L.; Yan, Y.; Meng, Y.; Wang, J.; Jiang, P.; Pang, C.H.; Wu, T. CO_2 gasification and pyrolysis reactivity evaluation of oil shale. *Energy Procedia* **2019**, *158*, 1694–1699. [CrossRef]

20. Chen, B.; Han, X.; Mu, M.; Jiang, X. Studies of the Co-pyrolysis of Oil Shale and Wheat Straw. *Energy Fuels* **2017**, *31*, 6941–6950. [CrossRef]

21. *ISO 16948:2015*; Solid Biofuels—Determination of Total Content of Carbon, Hydrogen, and Nitrogen. International Organization for Standardization: Geneva, Switzerland, 2015.

22. *ISO 16994:2016*; Solid Biofuels—Determination of Total Content of Sulfur and Chlorine. International Organization for Standardization: Geneva, Switzerland, 2016.

23. *ISO 18134-2:2017*; Solid Biofuels—Determination of Moisture Content—Oven Dry Method—Part 2: Total Moisture—Simplified Method. International Organization for Standardization: Geneva, Switzerland, 2017.

24. *ISO 18122:2022*; Solid Biofuels—Determination of Ash Content. International Organization for Standardization: Geneva, Switzerland, 2022.

25. *ISO 18125:2017*; Solid Biofuels—Determination of Calorific Value. International Organization for Standardization: Geneva, Switzerland, 2017.

26. Sulg, M.; Konist, A.; Järvik, O. Characterization of different wood species as potential feedstocks for gasification. *Agron. Res.* **2021**, *19*, 2021. [CrossRef]

27. *ISO 14780:2017*; Solid Biofuels—Sample Preparation. International Organization for Standardization: Geneva, Switzerland, 2017.

28. *ISO 29541:2010*; Solid Mineral Fuels—Determination of Total Carbon, Hydrogen, and Nitrogen Content—Instrumental Method. International Organization for Standardization: Geneva, Switzerland, 2010.

29. *ISO 1928:2020*; Coal and Coke—Determination of Gross Calorific Value. International Organization for Standardization: Geneva, Switzerland, 2020.

30. *EVS 669:2022*; Oil Shale. Determination of Ash Content. Estonian Centre for Standardisation (EVS): Tallinn, Estonia, 2022.

31. Li, J.; Dou, B.; Zhang, H.; Zhang, H.; Chen, H.; Xu, Y.; Wu, C. Pyrolysis characteristics and non-isothermal kinetics of waste wood biomass. *Energy* **2021**, *226*, 120358. [CrossRef]

32. Wahab, A.; Sattar, H.; Ashraf, A.; Hussain, S.N.; Saleem, M.; Munir, S. Thermochemical, kinetic and ash characteristics behaviour of Thar Lignite, agricultural residues and synthetic polymer waste (EVA). *Fuel* **2020**, *266*, 117151. [CrossRef]

33. Ebrahimi-Kahrizsangi, R.; Abbasi, M.H. Evaluation of reliability of Coats-Redfern method for kinetic analysis of non-isothermal TGA. *Trans. Nonferrous Met. Soc. China* **2008**, *18*, 217–221. [CrossRef]

34. Muravyev, N.V.; Pivkina, A.N.; Koga, N. Critical appraisal of kinetic calculation methods applied to overlapping multistep reactions. *Molecules* **2019**, *24*, 2298. [CrossRef]

35. Friedman, H. Kinetics of Thermal Degradation of Char-Forming Plastics from Thermogravimetry. *Appl. Phenolic Plastic. J. Polym. Sci. Part. C Polym. Symp.* **2007**, *6*, 183–195. [CrossRef]

36. Vyazovkin, S. Modification of the Integral Isoconversional Method to Account for Variation in Activation Energy. *J. Comput. Chem.* **2001**, *22*, 178–183. [CrossRef]

37. Kissinger, H.E. Reaction Kinetics in Differential Thermal Analysis. *Anal. Chem.* **1957**, *29*, 1702–1706. [CrossRef]

38. Baliban, R.C.; Elia, J.A.; Floudas, C.A. Toward novel hybrid biomass, coal, and natural gas processes for satisfying current transportation fuel demands, 1: Process alternatives, gasification modeling, process simulation, and economic analysis. *Ind. Eng. Chem. Res.* **2010**, *49*, 7343–7370. [CrossRef]

39. Mozaffari, S.; Järvik, O.; Baird, Z.S. Composition of gas from pyrolysis of Estonian oil shale with various sweep gases. *Oil Shale* **2021**, *38*, 215–227. [CrossRef]

40. Ranzi, E.; Cuoci, A.; Faravelli, T.; Frassoldati, A.; Migliavacca, G.; Pierucci, S.; Sommariva, S. Chemical kinetics of biomass pyrolysis. *Energy Fuels* **2008**, *22*, 4292–4300. [CrossRef]

41. Han, X.X.; Jiang, X.M.; Cui, Z.G. Studies of the effect of retorting factors on the yield of shale oil for a new comprehensive utilization technology of oil shale. *Appl. Energy* **2009**, *86*, 2381–2385. [CrossRef]

42. Hu, Z.; Ma, X.; Li, L. The synergistic effect of co-pyrolysis of oil shale and microalgae to produce syngas. *J. Energy Inst.* **2016**, *89*, 447–455. [CrossRef]

43. Wang, S.; Luo, Z. *Pyrolysis of Biomass*; GREEN—Alternative Energy Resources; Walter de Gruyter GmbH: Berlin, Germany, 2017; p. 268. [CrossRef]

44. Garcia-Perez, M.; Wang, X.S.; Shen, J.; Rhodes, M.J.; Tian, F.; Lee, W.J.; Wu, H.; Li, C.Z. Fast pyrolysis of oil mallee woody biomass: Effect of temperature on the yield and quality of pyrolysis products. *Ind. Eng. Chem. Res.* **2008**, *47*, 1846–1854. [CrossRef]

45. Wang, Q.; Sun, B.; Hu, A.; Bai, J.; Li, S. Pyrolysis characteristics of Huadian oil shales. *Oil Shale* **2007**, *24*, 147–157.

46. Tiwari, P.; Deo, M. Compositional and kinetic analysis of oil shale pyrolysis using TGA-MS. *Fuel* **2012**, *94*, 333–341. [CrossRef]

47. Liu, Q.Q.; Han, X.X.; Li, Q.Y.; Huang, Y.R.; Jiang, X.M. TG-DSC analysis of pyrolysis process of two Chinese oil shales. *J. Therm. Anal. Calorim.* **2014**, *116*, 511–517. [CrossRef]

48. Lyons Cerón, A.; Konist, A. Co-Pyrolysis of Woody Biomass and Oil Shale in a Batch Reactor in CO_2, CO_2-H_2O, and Ar Atmospheres. *Energies* **2023**, *16*, 3145. [CrossRef]

49. Li, S.; Chen, X.; Liu, A.; Wang, L.; Yu, G. Co-pyrolysis characteristic of biomass and bituminous coal. *Bioresour. Technol.* **2015**, *179*, 414–420. [CrossRef]

50. Özsin, G.; Pütün, A.E. TGA/MS/FT-IR study for kinetic evaluation and evolved gas analysis of a biomass/PVC co-pyrolysis process. *Energy Convers. Manag.* **2019**, *182*, 143–153. [CrossRef]

51. Dai, M.; Yu, Z.; Fang, S.; Ma, X. Behaviors, product characteristics and kinetics of catalytic co-pyrolysis spirulina and oil shale. *Energy Convers. Manag.* **2019**, *192*, 1–10. [CrossRef]

52. Bai, J.; Chen, X.; Shao, J.; Jia, C.; Wang, Q. Study of breakage of main covalent bonds during co-pyrolysis of oil shale and alkaline lignin by TG-FTIR integrated analysis. *J. Energy Inst.* **2019**, *92*, 512–522. [CrossRef]

53. Kiliç, M.; Pütün, A.E.; Uzun, B.B.; Pütün, E. Converting of oil shale and biomass into liquid hydrocarbons via pyrolysis. *Energy Convers. Manag.* **2014**, *78*, 461–467. [CrossRef]

54. Ye, J.; Xiao, J.; Huo, X.; Gao, Y.; Hao, J.; Song, M. Effect of CO_2 atmosphere on biomass pyrolysis and in-line catalytic reforming. *Int. J. Energy Res.* **2020**, *44*, 8936–8950. [CrossRef]

55. Farrow, T.S.; Sun, C.; Snape, C.E. Impact of CO_2 on biomass pyrolysis, nitrogen partitioning, and char combustion in a drop tube furnace. *J. Anal. Appl. Pyrolysis* **2015**, *113*, 323–331. [CrossRef]

56. Cheng, C.-Y.; Kuo, C.-C.; Yang, M.-W.; Zhuang, Z.-Y.; Lin, P.-W.; Chen, Y.-F.; Yang, H.-S.; Chou, C.-T. CO_2 Capture from Flue Gas of a Coal-Fired Power Plant Using Three-Bed PSA Process. *Energies* **2021**, *14*, 3582. [CrossRef]

57. Johannes, I.; Tiikma, L.; Luik, H. Synergy in co-pyrolysis of oil shale and pine sawdust in autoclaves. *J. Anal. Appl. Pyrolysis* **2013**, *104*, 341–352. [CrossRef]

58. Van de Velden, M.; Baeyens, J.; Brems, A.; Janssens, B.; Dewil, R. Fundamentals, kinetics and endothermicity of the biomass pyrolysis reaction. *Renew. Energy* **2010**, *35*, 232–242. [CrossRef]

59. Johannes, I.; Kruusement, K.; Veski, R. Evaluation of oil potential and pyrolysis kinetics of renewable fuel and shale samples by Rock-Eval analyzer. *J. Anal. Appl. Pyrolysis* **2007**, *79*, 183–190. [CrossRef]

60. Syed, S.; Qudaih, R.; Talab, I.; Janajreh, I. Kinetics of pyrolysis and combustion of oil shale sample from thermogravimetric data. *Fuel* **2011**, *90*, 1631–1637. [CrossRef]

61. Baqain, M.; Neshumayev, D.; Konist, A. TG-MS analysis and kinetic study of co-combustion of ca-rich oil shale with biomass in air and oxy-like conditions. *Carbon. Capture Sci. Technol.* **2024**, *10*, 100162. [CrossRef]

62. Ochieng, R.; Cerón, A.L.; Konist, A.; Sarker, S. A combined analysis of the drying and decomposition kinetics of wood pyrolysis using non-isothermal thermogravimetric methods. *Energy Convers. Manag. X* **2023**, *20*, 100424. [CrossRef]

63. Maaten, B.; Loo, L.; Konist, A.; Nešumajev, D.; Pihu, T.; Külaots, I. Decomposition kinetics of American, Chinese and Estonian oil shales kerogen. *Oil Shale* **2016**, *33*, 167–183. [CrossRef]

64. Gorensek, M.B.; Shukre, R.; Chen, C.C. Development of a Thermophysical Properties Model for Flowsheet Simulation of Biomass Pyrolysis Processes. *ACS Sustain. Chem. Eng.* **2019**, *7*, 9017–9027. [CrossRef]

65. Debiagi, P.E.A.; Pecchi, C.; Gentile, G.; Frassoldati, A.; Cuoci, A.; Faravelli, T.; Ranzi, E. Extractives Extend the Applicability of Multistep Kinetic Scheme of Biomass Pyrolysis. *Energy Fuels* **2015**, *29*, 6544–6555. [CrossRef]

Publication III

Lyons Cerón, Alejandro; Konist, Alar (2023). **Co-Pyrolysis of Woody Biomass and Oil Shale in a Batch Reactor in CO_2, CO_2-H_2O, and Ar Atmospheres.** Energies, 16 (7), #3145. DOI: 10.3390/en16073145.

Article

Co-Pyrolysis of Woody Biomass and Oil Shale in a Batch Reactor in CO_2, CO_2-H_2O, and Ar Atmospheres

Alejandro Lyons Cerón * and Alar Konist (ID)

Department of Energy Technology, Tallinn University of Technology, Ehitajate tee 5, 12616 Tallinn, Estonia
* Correspondence: allyon@taltech.ee

Abstract: The partial replacement of fossil fuels with biomass provides an alternative to producing cleaner and more sustainable energy and fuels. Conventional shale oil production infrastructure can potentially be used in co-pyrolysis with biomass to reduce the use of oil shale and decrease its environmental impact. The effect of adding 10 and 30 wt% woody biomasses (spruce, alder, pine, and birch) into oil shale was studied through intermediate co-pyrolysis. The experiments were carried out in a batch reactor at 520 °C, with a 20 min residence time, in CO_2, CO_2-H_2O 1:1, and Ar gas atmospheres. The solid products were collected and analyzed for elemental composition and surface area, while the composition of the gases was determined through gas chromatography. The difference in experimental and theoretical mass balances of fuel blends was lower than 2.5 wt% in all gas environments, indicating slight interactions between the fuels. CO_2 atmospheres contributed to increased decomposition, with up to 2.6 wt% lower solid products. Biomass increased the production of combustible gases, especially CO yields, from 0.42 to 1.30 vol%. The addition of biomass and the use of alternative atmospheres can improve pyrolysis through increased fuel decomposition and a lower share of residual mass from 74.4 wt% for oil shale to 58–70 wt% for oil shale and biomass blends.

Keywords: co-pyrolysis; batch reactor; oil shale; woody biomass

1. Introduction

The use of conventional fossil fuels for energy solutions has produced a direct impact on the environment, increasing the emissions of greenhouse gases. This threatens to raise global temperatures above 1.5 °C by 2030 and 2050 [1]. Alternative and clean energy solutions can mitigate the environmental impact by reducing the emissions of pollutant gases and the depletion of non-renewable resources. The co-conversion of two types of resources such as biomass, a carbon-neutral renewable resource, and oil shale (OS), an alternative fuel, is proposed as a solution for the generation of more sustainable liquid, gaseous, and solid products through the partial replacement of OS with biomass in co-pyrolysis. Co-pyrolysis, a thermochemical conversion process, can produce valuable products (bio-oil, gas, porous char) for the energy sector and other industrial applications [2].

Biomass is a renewable non-fossil resource with a high carbon content, low ash content, high volatile matter, and a lower calorific value of 15–19 MJ/kg [3]. Its utilization can potentially provide 3000 TWh of energy and save 1.3 billion tons of CO_2 [4]. Biomass is composed of hemicellulose, cellulose, and lignin. Woody biomass (WB) is mostly composed of hemicellulose and cellulose (50–80 wt%) [5], which decompose at 220–315 °C and 350–400 °C [6], and the remaining component, lignin, decomposes at a temperature above 400 °C. The thermochemical conversion of WB through gasification or pyrolysis results in valuable products, such as bio-oil, gas, and porous char. From these processes, pyrolysis of biomass produces high yields of liquid (up to 75%), solid (10–25%), and gaseous products (20%) [7]. Intermediate pyrolysis is a relatively new conversion method, with a longer residence time, which yields around 40, 40, and 20 wt% of liquids, solids, and gas, respectively.

This process has been observed to have beneficial effects on reducing char cracking and a more stable bio-oil, while different research has proven beneficial effects of intermediate pyrolysis, including catalytic pyrolysis [8], and char with high thermal stability in N_2/CO_2 atmospheres [9]. However, there are some challenges in the individual conversion of WB. These are mostly due to its high moisture content and comparatively lower energy density than other fuels. WB energy density can be as low as one-tenth of a conventional fuel [10].

OS is an alternative fossil fuel obtained from geological formations in various locations around the world. It is characterized by its high share of organic matter (kerogen), which allows its use as an energy source through direct combustion, or as a source of valuable products, including shale oil, shale gas, and semi-coke. Depending on its type, OS has a lower calorific value in the range of 5–20 MJ/kg. The thermochemical conversion of OS results in up to 20% shale oil, 5–20% shale gas, and around 60% semi-coke [11]. During pyrolysis, OS kerogen is transformed into bitumen and further into liquid and gas products, such as volatile hydrocarbons, and solid products, such as semi-coke [12]. However, OS conversion also comes with environmental and technological challenges, such as reducing CO_2 emissions as well as NO_x and SO_x [13]. Various efforts have been made to transition from OS combustion to the production of shale oil [14], as its production is more profitable than the use of OS in power production.

Thermochemical conversion through co-pyrolysis involves two or more fuels, which undergo degradation in an oxygen-free atmosphere under specific thermal conditions, including temperature, residence time, and heating rate. This thermal degradation breaks the fuels' large molecules through different chemical reactions, producing liquid, solid, and gaseous products with combined properties from the pyrolyzed fuels [15]. Co-pyrolysis has been studied to determine the interactions between fuels, produce solid, liquid, and gaseous products with combined and/or improved properties, reduce the environmental effect of fossil fuels, and make use of waste residues [16]. The co-pyrolysis of fossil fuels, including OS, with shares of biomass, decreases the consumption of fossil fuels along with the emissions of pollutant gases from their individual conversion [17]. Due to its low ash content and high volatile matter, the addition of biomass to OS in co-pyrolysis can decrease the yields of solid products while increasing the yields of liquid and gaseous products [15]. Moreover, the high hydrogen content and H/C ratio of biomass can promote decomposition and thermal cracking in co-pyrolysis [18].

Possible interactions between biomass and other fuels have been observed to improve the pyrolytic behavior, shifting the pyrolysis temperature, reducing the activation energy of the process [19], and increasing the energy density [20]. Previous research on OS and biomass co-pyrolysis have found improvements in the decomposition and cracking of fuels, higher yields of pyrolysis products with enhanced properties, and lower CO_2 emissions [21]. The interactions and pyrolysis behavior of biomass and OS have been studied in TGA and different types of reactors in temperature ranges of 400–600 °C in inert atmospheres [22]. Some studies of OS co-pyrolysis have used OS and wheat straw [23], OS, and spirulina [24]. The effect of other atmospheres, such as CO_2 and steam, has been studied in gasification for biomass [25,26] but has not been studied in co-pyrolysis, even though such atmospheres have been demonstrated to have potential benefits in the decomposition of fuels, such as the pyrolysis of biomass in CO_2 [27]. Some of these benefits include enhanced pyrolysis [28], promotion of the liquid and gas product yields, prevention of secondary cracking (to produce more liquid products) [29], a decrease in the activation energy, a reduction of semi-coke and char yields, and bio-oil with improved properties [30].

Considering the possible advantages of the partial replacement of OS with biomass in co-pyrolysis and its potential to contribute to a path for cleaner energy solutions, the addition of shares of WB to OS in co-pyrolysis was studied using OS and forestry WB. For this purpose, experiments were carried out in a prototype batch reactor at isothermal conditions, at 520 °C for OS:WB blend ratios of 1:0, 9:1, 7:3, and 0:1. Different gas atmospheres, including Ar, CO_2, and an $H_2O:CO_2$ blend were used to test their effect on the yield, elemental composition and surface area of solid products, and the concentration of

product gases, including CO, H_2, and CH_4. Solid products were collected to determine the residual mass, composition, and BET surface area, while the concentration of gas species was determined with gas chromatography with a thermal conductivity detector. Additionally, the individual pyrolysis of OS and WB was carried out at different residence times to study the decomposition of both fuels and determine the most suitable residence time for co-pyrolysis in the batch reactor to minimize the yield of solid products. The current study focused on solid and gaseous products, using a batch reactor designed for the production and collection of these products. The reactor's design does not allow an accurate collection of a representative sample of liquid products. Future work is required considering a larger-scale reactor to focus on liquid production and analysis.

2. Materials and Methods

2.1. Feedstock Characterization

The intermediate co-pyrolysis of biomass and OS was conducted using a blend of WB species; spruce, alder, pine, and birch from Estonian forests, and OS, a light-brown OS type also found in Estonia. The WB species were previously characterized [31] in terms of elemental and proximate composition and calorimetry according to ISO 16948, 16994, 18134-2, and 18122. OS was similarly characterized to obtain its elemental and proximate composition and calorific values according to ISO 29541:2015 and ISO 1928:2016 and EVS 669:1996 for the ash content. Details on the equipment used for elemental and proximate analysis and calorimetry are found in ref. [27]. The OS and the four types of WB species were individually sieved to a particle size between 0.5 and 1 mm, following the ISO 14780:20 (Solid biofuels—sample preparation) as a guideline. After sieving, the WB and OS samples were dried in a Nabertherm L9 furnace sourced from Nabertherm GmbH Lilienthal, Germany. The drying conditions were 105 °C for 3 h to remove moisture. Once the samples' moisture was removed, all WB samples were mixed in equal parts (25 wt% each) to obtain a blend of WB species. This WB blend was used to manually prepare blends of OS and WB with the following OS:WB ratios: 1:0, 9:1, 7:3, and 0:1 (0, 10, 30, and 100 wt% WB). The preparation of blends, as well as the storage in air plastic bags, was carried out following ISO 14780:20 guidelines. The analyses were conducted for WB, OS as raw feedstock and products of WB, OS, and blends after pyrolysis. After pyrolysis, the analysis was focused on the co-pyrolytic behavior of both feedstock and the composition of the solid products, including OS, WB, and OS-WB blends.

2.2. Experiment Set Up

The co-pyrolysis of blends of OS and WB was conducted in a prototype batch reactor, with a capacity of 1–5 g of fuel, at a reaction temperature of 520 °C in isothermal conditions. This temperature was chosen as it is the optimal temperature to obtain the highest yields of liquid products for OS and WB, or OS:WB blends [32]. The experiments were carried out in different gas atmospheres: Ar as an inert atmosphere, CO_2, and a blend of equal volumetric parts of CO_2 and H_2O (steam), with a total flow rate of 0.3 L/min. For each parameter, the experiment and 2 replicates were conducted to ensure reproducibility. The system used for the co-pyrolysis experiments (Figure 1) consisted of a batch reactor, a gas cleaning system, a gas analysis system, and a steam generator. The prototype batch reactor was composed of a balance chamber, where the sample holder containing the sample was inserted, and a reaction zone made of an internal heater with a precision of ±10 °C. A quartz cylindrical glass in the reaction zone contained the sample during the co-pyrolysis. A gas input supplied the gas atmosphere, controlled by Alicat Scientific Mass Flow controllers, with a precision of ±0.8%. A gas exhaust was used for the pyrolytic gas generated. The gas input and exhaust were externally heated to 150 °C to prevent condensation of volatiles in the system. Once the pyrolysis gas exited the reactor, it passed through a cooling and cleaning system operating at 4–6 °C to condensate volatiles. A Cole Parmer Steam Generator, sourced from Antylia Scientific in Vernon Hills, Illinois, United

States, was used to produce and deliver the steam for the CO_2:H_2O 1:1 atmosphere. The steam generator used N_2 as the carrier gas.
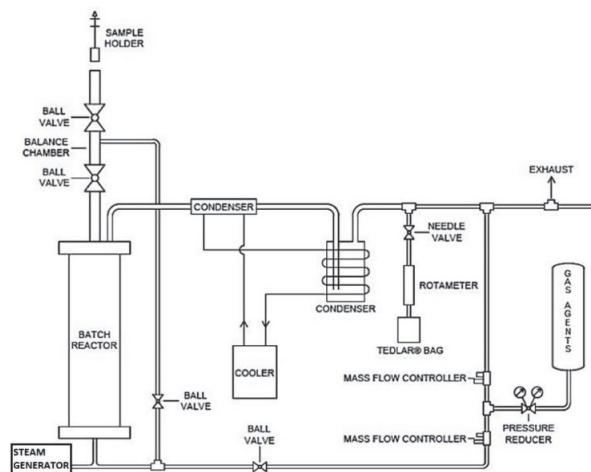

Figure 1. Pyrolysis system (modified from reference [33]).

Two types of experiments were conducted, both at 520 °C in isothermal conditions. The first type consisted of individual pyrolysis in an Ar atmosphere of 2.0 g $\pm$ 2.7% of OS and 1.5 g $\pm$ 1.1% of WB at different residence times in the reaction zone to study the evolution of the pyrolytic decomposition over time. For WB and OS, the residence times were 0.5, 1, 3, 5, 7, 10, and 20 min, and 2, 5, 10, 15, and 20 min, respectively. The second type of experiment was carried out in Ar, CO_2, and CO_2:H_2O 1:1 gas atmospheres to study co-pyrolysis of OS and WB, using 1.5 g $\pm$ 5.5% of OS:WB at 1:0, 9:1, 7:3, and 0:1 ratio. For the co-pyrolysis experiments, the residence time in the reaction zone was 20 min. Additionally, for both types of experiments, the samples were kept in the balance chamber before and after the reaction zone for 5 min to ensure an inert or clean atmosphere.

A comparison of the theoretical and experimental residual mass during the co-pyrolysis of OS:WB 9:1 and 7:3 was obtained from a linear correlation of OS and WB shares, based on the experimental residual mass of the individual pyrolysis of WB and OS (Equation (1)). m_{th} is the theoretical residual mass of OS:WB blends, m_{OS} and m_{WB} are the experimental residual mass of OS and WB, respectively, and x is the share of OS.

$$m_{th} = m_{OS}x + m_{WB}(1 - x)$$
(1)

2.3. Gas Products Analysis

The volumetric concentration of combustible gases H_2, CO, and CH_4 was measured using a gas chromatography with thermal conductivity detector (GC-TCD) and a Gazohrom 3101 gas analyzer. The analyzer was composed of two packed columns of 2.5 m in length and 3.6 mm in diameter and used air at 70 L/min as a carrier gas. The pyrolytic gas was collected in Tedlar bags after it exited the batch reactor and passed through the cleaning system. The GC-TCD was calibrated for the measured gas species, and the concentration in vol% was calculated using the chromatogram function of Clarity Software. The calibration of the GC-TCD is described in previous works with the same equipment [34].

2.4. Solid Product Analysis

The solid products obtained from the pyrolysis of OS and WB and OS:WB were evaluated for their elemental composition, using a Vario MACRO CHNS analyzer to determine the concentration of C, H, N, and S. The surface area of the solid products was

determined using a Quantachrome Autosorb iQ-C surface area and pore size analyzer, sourced from Anton Paar in Boynton Beach, Florida, United States, which determines the BET specific surface area, through physisorption. For these analyses, samples of 0.1–1.0 g of solid product were used. Firstly, the samples were put into degassing at 300 °C for 20 h to prepare, clean, and remove any volatiles from the samples. After degassing, the surface area was determined by recording 40 adsorption and 40 desorption points to obtain the isotherms, using N_2 as adsorbent gas.

3. Results and Discussion

3.1. Feedstock Properties

Table 1 displays the main properties of the WB and OS samples used, including elemental and proximate composition in terms of C, H, N, S, O, ash content, moisture content, fixed carbon, and volatile matter, as well as higher and lower calorific values (HHV and LHV, respectively). The values from the elemental analysis of WB and the organic part of OS were determined on a dry basis. All WB samples have a similar composition, making them suitable for studying their co-pyrolysis behavior as one blend of WB. As seen from Table 1, OS and WB differ in various aspects, particularly in their heating values, being over two-fold times higher for WB compared to OS, and the ash content, 0.3 wt% for WB and 52.5 wt% for OS. Therefore, it is expected to have a different pyrolytic behavior as well as residual mass for OS and WB and a combined pyrolytic behavior for OS:WB blends, according to the blend ratio.

Table 1. WB and OS feedstock properties.

		WB **				OS **
		Spruce	Alder	Pine	Birch	
Elemental composition [wt%]	C	50.3	49.9	50.1	49.3	27.2
	H	6.6	6.6	6.6	6.6	2.8
	N	0.1	0.2	0.19	0.08	<0.1
	S	n.d.	n.d.	n.d.	n.d.	2.0
	O *	42.7	43.0	43.1	44.0	21.0
Proximate analysis [wt%]	Ash content	0.3	0.3	0.3	0.3	52.5
	Moisture	6.9	7.6	8.5	7.7	0.9
	Fixed carbon	14.2	14.0	14.5	12.8	2.0
	Volatile matter	85.5	85.7	85.2	86.9	45.5
Heating value [MJ/kg]	LHV	18.4	18.5	18.6	18.1	8.7
	HHV	19.8	19.9	20.0	19.9	9.7

* Calculated, ** dry-basis, n.d. not detected.

3.2. Pyrolysis at Different Residence Times

The pyrolytic behavior of WB and OS at 520 °C in the Ar atmosphere at different residence times is shown in Figure 2. The residual mass measurements obtained from pyrolysis experiments of WB and OS had a relative standard deviation of up to 2.88% and 2.29% for WB and OS, respectively, between each parameter and its replicates. Figure 2 indicates the difference in decomposition between WB and OS. WB samples were inserted in the reactor and removed after a residence time of 0.5, 1, 3, 5, 7, 10, and 20 min, as most of the reaction occurred during the initial 5 min. The residence time for OS samples was 2, 5, 10, 15, and 20 min, considering the slower decomposition of OS. The results shown in Figure 2 were used to set the most suitable residence time for the co-pyrolysis of OS and WB so that the blend of fuels achieved a complete decomposition for the pyrolysis temperature considered (520 °C).
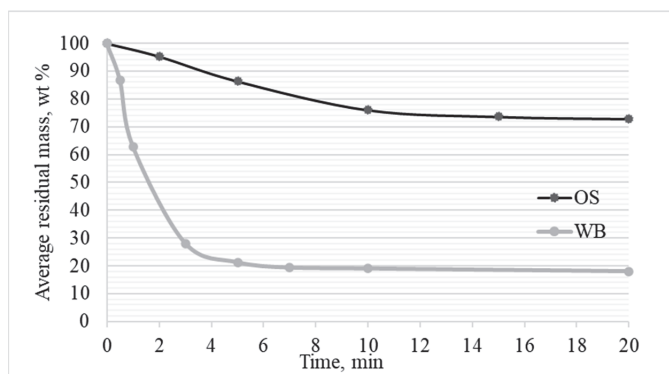
Figure 2. Residual mass from individual pyrolysis of OS and WB.

The pyrolysis of WB at different resident times indicated that over 95% of the decomposition occurred during the first 5 min of the reaction process, where WB lost over 78 wt% of its mass, reaching a residual mass of 21.2 wt%. After 5 min, the mass loss only increased by 3.2 wt% in 15 min, reaching a residual mass of 18.0 wt% at a residence time of 20 min. This residual mass after 20 min consisted of char, ashes, and some residual mass from incomplete pyrolysis (4 wt%). This behavior showed that during the first 5 min of the reaction, the WB samples reached temperatures close to 400 °C, where its main components decomposed, starting with cellulose and hemicellulose from 0–5 min and lastly lignin, which likely occurred within 3–5 min of the reaction. The composition of WB in terms of cellulose, hemicellulose, and lignin explains the reason most of WB mass was decomposed within the first 7 min of the pyrolysis, as the sample reached the temperature of the reactor (520 °C). At this temperature, the WB samples underwent most of the pyrolysis due to the decomposition temperatures of these three components. Mass losses occurring after 5–7 min (below 2.0 wt% mass loss) can be considered decomposition from incomplete pyrolysis of hemicellulose and cellulose of the WB samples; with the decomposition of lignin, the complete decomposition of WB occurs at 800–900 °C [5]. Similar observations have been noted by refs. [35,36]. Based on these results, it is observed that WB in the batch reactor requires a residence time of no less than 7 min. Residence times above 10 min will not increase the mass loss by more than 1–2 wt%. Additional evidence of this behavior is shown in Appendix A.1, which visually displays the solid residues of WB after different residence times. The residues indicate that after 3–5 min, most of the residue is char, while before 3 min, there is still a share of unreacted WB.

The case for OS differs from WB pyrolytic behavior. As Figure 2 shows, OS has a linear decomposition during 0–10 min of the reaction, where it is subject to a mass loss of 23.9 wt%, reaching 76.1 wt% residual mass at a 10 min residence time. This mass loss represents over 86% of the total maximum mass loss during pyrolysis at 20 min residence time. After 10 min, OS lost 3.2 wt% of its mass in the remaining 10 min. The residual mass from OS pyrolysis is composed of semicoke, which is OS that has lost a portion of hydrocarbons; moreover, the complete decomposition of OS occurs within the range of 540–900 °C [37]; therefore, the residual mass of 72.9 wt% is higher than the ash + fixed carbon of OS from the elemental analysis. Unlike WB, OS decomposition was slower, indicating that the fuel required more time to reach the temperature range where most of the decomposition occurs (350–510 °C). During the first 10 min of the reaction, OS Kerogen was transformed into its products: shale oil, gas, and semi-coke. Further decomposition can be attributed to the completion of pyrolysis, and the decomposition of incomplete pyrolysis, after which the fuel reaches the operating temperature of the reactor (520 °C). This behavior agrees with observations by refs. [11,38,39], who studied the kinetic and thermogravimetric behavior of OS. Therefore, for the pyrolysis of OS in the batch reactor, it is required that the residence time is greater than 15 min to achieve maximum decomposition for the selected

operating temperature. Residence times above 15 min will not increase the mass loss by more than 1–2 wt%. Appendix A.2 contains visual evidence of the OS decomposition at different residence times, indicating the required residence time above 15 min to transform OS into semi-coke. Based on the obtained results, a residence time of 20 min was chosen for the co-pyrolysis of OS and WB to ensure maximum decomposition of both fuels.

3.3. OS-WB Co-Pyrolysis

Figure 3 displays the residual mass from individual pyrolysis of OS and WB and co-pyrolysis of OS:WB 9:1 and 7:3 in Ar, CO_2, and $H_2O:CO_2$ 1:1 atmospheres. The residual mass measurements obtained from co-pyrolysis experiments of WB and OS had a relative standard deviation from 0.35% up to 3.99% between each parameter and its replicates. The addition of 10 and 30 wt% WB to OS (blends 9:1 and 7:3) decreased the residual mass as the share of WB rose. This resulted in a residual mass of 57.4–60.0 wt% and 68.2–71.6 wt% for OS:WB blends of 7:3 and 9:1, respectively, in all gas atmospheres. The results were compared to the theoretical curves of OS:WB co-pyrolysis formulated using Equation (1), as shown in detail in Figure 3 for all the tested gas atmospheres. Overall, the comparison of residual masses evidences the additive decomposition behavior of OS:WB in co-pyrolysis, as the experimental results share a linear decrease in residual mass as the ratio of WB increases.
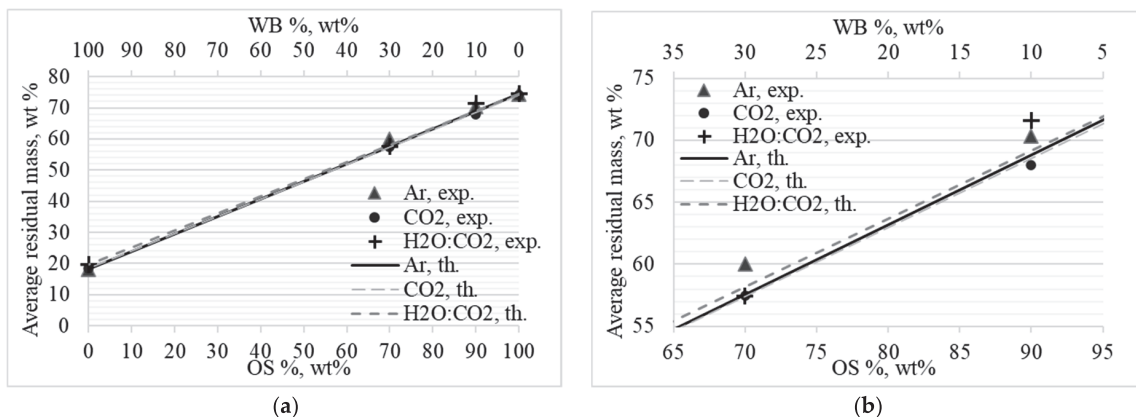

Figure 3. (**a**) Theoretical (th.) co-pyrolysis curves and experimental results (exp.). (**b**) Detail of theoretical (th.) and experimental (exp.) residual mass for co-pyrolysis blends.

The experimental residual mass obtained had a behavior comparable to the theoretical curves, with a difference lower than 2.5 wt%, indicating the absence of strong promoting or inhibiting effects between the two fuels. This absence of strong interactions was also observed by refs. [40–42]. Johannes et al. [40] co-pyrolyzed OS and pine sawdust, resulting in a synergistic effect in the yield of oil (21% more); however, this was observed only during incomplete pyrolysis at temperatures below 360 °C, where the pyrolysis process is still ongoing. At higher temperatures, there was no synergy in co-pyrolysis. Yanik et al. [41] found that the co-pyrolysis of OS with berries had an additive result in the total extract yield. At 400 °C, the yield of organic residue was 41.47 and 32.47 wt%, respectively, for OS and berries, while the co-pyrolysis yield was 36.46 wt%, which is almost identical to the theoretical yield of 36.97%. Kılıç et al. [42] conducted co-pyrolysis of OS with Euphorbia rigida, resulting in no significant synergistic effect. The solid yields at 550 °C were 26.87 and 16.66% for OS and E.rigida, respectively. The co-pyrolysis yield was from 20–22%, which is not different from the theoretical yield of 21.76%. Additionally, the liquid product was an additive result of both feedstocks.

Despite the absence of strong interactions between OS and WB in the current experiments, the addition of WB to OS pyrolysis has the potential to improve the decomposition of OS as well as improve its products. In co-pyrolysis with WB, OS decomposition is shifted to a lower temperature region, resulting in earlier decomposition due to the lower temperatures required to pyrolyze WB components, which products can interact with OS. Some of the WB components that interact with OS include hydrogen-free radicals (considering the higher H content of biomass, shown in Table 1). These radicals can promote kerogen and bitumen cracking and WB inorganic elements, which can produce a catalytic effect on OS and enhance its decomposition. From the current experiments, a direct advantage is observed with the addition of 30 wt% WB to OS in co-pyrolysis, as the residual mass decreases the most with this WB share. Higher shares of WB decrease the share of semi-coke produced from OS retorting and the environmental effects of OS pyrolysis, such as emissions of NO_x, SO_x, and CO_2, as also observed by ref. [42]. Other studies with biomass in co-pyrolysis with coal have observed strong interactions, especially in the devolatilization rate, the generation of CO_2, and improved pyrolysis through volatile–char interactions [43]. Moreover, benefits are also observed for WB in co-pyrolysis, as blends of OS and WB result in fuel mixtures with a higher energy density and lower moisture content than the individual pyrolysis of WB.

Figure 3 also displays the differences in residual mass as the gas atmosphere varies in Ar inert atmosphere, CO_2, and the $H_2O:CO_2$ 1:1 blend. It was observed that the co-pyrolysis of OS:WB in all gas environments followed a linear behavior, decreasing the residual mass as the WB share increased, with a linear coefficient of determination R^2 in the range of 0.997–0.999 for all gas atmospheres. On average, the residual masses were 18.8, 58.3, 70.0, and 74.4 wt% for OS:WB blends of 0:1, 7:3, 9:1, and 1:0, respectively, with an RSD between gas atmospheres in the range of 0.3 to 4.6%. This indicates slight differences in the decomposition of OS:WB blends as the gas atmosphere varied. Nevertheless, the co-pyrolysis in non-inert atmospheres resulted in a lower residual mass for OS:WB blends 7:3, 9:1, and 1:0 in CO_2 and for OS:WB blends 7:3 in $H_2O:CO_2$. Non-inert atmospheres, such as CO_2 and $H_2O:CO_2$ blends, have led to a pyrolytic decomposition comparable to or, in some cases, improved compared to Ar as an inert atmosphere. This is likely due to the role of CO_2 and H_2O in pyrolysis. CO_2 can enhance thermal efficiency, cracking, and improve decomposition, while H_2O can act as a reactive agent and promote secondary cracking and provide free hydrogen radicals. For the experimental conditions used, CO_2 and H_2O did not promote gasification reactions, as the reaction temperature was below 700 °C. Above 700 °C, CO_2 and H_2O play a major role in the process, specifically in the Boudouard, water–gas, and water–gas shift reactions [34]. The similarities and improvements in the co-pyrolytic decomposition of OS:WB blends allow the implementation of CO_2 and H_2O atmospheres as a feasible alternative to inert atmospheres in the co-pyrolysis of OS:WB blends. Using such gas atmospheres, especially CO_2, can potentially make use of CO_2 emissions captured through carbon capture and storage (CCS) technologies [44], addressing the environmental impact of CO_2 emissions.

3.4. Gas Composition

The concentration of H_2, CO, and CH_4 obtained from the co-pyrolysis gas is shown in Table 2. Every Tedlar gas sample for a single experiment was measured three times with an average error from 0.9–12.9%, 0.7–15.4%, 1.8–12.8%, and 1.5–12.1% for WB, OS, OS:WB 7:3, and OS:WB 9:1, respectively. Every experiment was conducted three times, with an average standard deviation between parallel experiments of 1.6–25.0%, 2.7–24.1%, and 2.7–27% for H_2, CO, and CH_4, respectively. Other uncertainties in GC-TCD can be related to the injection of the gas, measurement repeatability, column temperature [45], and the collection of the gas sample from the reactor, among others. Higher deviation in the gas analysis is related to the lower concentration of gases obtained rather than the reproducibility of the experiment. Evidence of this is the low deviation in the yield of solid products (lower than 5%). The presence of the three combustible gases was significantly

low in comparison to other thermochemical conversion processes, such as gasification. This is due to the lower decomposition temperature selected, aimed to decrease secondary cracking. Higher pyrolysis temperatures could have increased the H_2, CO, and CH_4 due to reduction reactions occurring above 600 °C, converting more fuel into gas products and transforming CO_2 into CO [46]. In general, the concentration of H_2, CO, and CH_4 was higher in the individual pyrolysis of WB, especially that of CO and CH_4, due to the elemental composition of the fuel. There was no clear correlation between the concentration of gas species and the ratio of OS:WB blends. Nonetheless, the concentration of gas species was in a low range to provide any clear relation. The effect of the gas atmosphere on the produced gases had no clear trend or difference between CO_2, $H_2O:CO_2$ 1:1, and Ar atmospheres. The gas concentration of H_2, CO, and CH_4 is not significantly different between atmospheres due to the low pyrolysis temperature, where the atmospheres do not have a strong interaction with the feedstock [34]. The largest share of gas species in the pyrolysis gas was the species used as the gas atmosphere (Ar, CO_2, or $H_2O:CO_2$). It should be noted that during pyrolysis, other gas species are produced, including CO_2, NO_x, SO_x, and other hydrocarbons. The equipment used had calibration and capabilities to measure only H_2, CO, and CH_4.

Table 2. Concentration of H_2, CO, and CH_4 in the co-pyrolysis gas.

OS:WB Ratio	Gas Atmosphere, 0.3 L/min	Gas Species Concentration, vol%		
		H_2	CO	CH_4
0:1	CO_2	0.08	1.19	0.15
	$H_2O:CO_2$ 1:1	0.06	1.01	0.14
	Ar	0.08	1.30	0.14
7:3	CO_2	0.05	0.56	0.06
	$H_2O:CO_2$ 1:1	0.07	0.87	0.04
	Ar	0.05	0.82	0.07
9:1	CO_2	0.05	0.31	0.08
	$H_2O:CO_2$ 1:1	0.05	0.37	0.04
	Ar	0.06	0.65	0.06
1:0	CO_2	0.06	0.42	0.06
	$H_2O:CO_2$ 1:1	0.1	0.75	0.06
	Ar	0.04	0.42	0.05

3.5. Solid Products

Table 3 displays the characteristics of the solid products obtained from individual pyrolysis and co-pyrolysis of OS and WB and OS:WB blends. It is observed how the composition of the solid products is directly related to the elemental composition of WB and OS, with WB char having a higher content of C, H, and N, which gradually decreases as the share of WB decreases. In parallel, the share of S is only observable in blends with OS due to the high sulfur content of OS. It should also be considered that from individual pyrolysis, the share of residual mass is close to 19 and 74 wt% for WB and OS, respectively. This means that for the OS:WB blends studied, most of the residual mass is composed of OS semi-coke, which explains why the elemental composition of these blends is similar to the composition of OS semi-coke. Therefore, OS has a more significant contribution in the composition of the solid products in OS:WB co-pyrolysis, while WB has a larger contribution in the production of gaseous and liquid products. The blend of OS:WB should then be selected based on what type of product needs to be obtained in the co-pyrolysis process. Similarly, the BET-specific surface areas obtained through physisorption are shown in Table 3. The BET surface area results show how considerably higher values for WB solid products (127–173 m^2/g) compared to OS and OS:WB blends (4–46 m^2/g). It is known that biochar, obtained from biomass, usually has a surface area ranging from 8–132 m^2/g [47], while OS semi-coke has a surface area of around 4–50 m^2/g [48]. As with the elemental

composition of solid products, the surface area of OS:WB blends is comparable to the one obtained from individual pyrolysis of OS due to the higher contribution of OS semi-coke in the blend. The effect of the gas atmosphere on the elemental composition and surface area of the solid residues did not show a clear difference or trend in the results obtained in CO_2, H_2O:CO_2 1:1, and Ar atmospheres. As with the solid yields in co-pyrolysis, the similarities of the results in all atmospheres are related to the lower pyrolysis temperature used, at which the CO_2 and H_2O gases have low interaction with the feedstock, as explained by the main reduction reactions of CO_2 and H_2O [34]. Future suggestions for increasing the specific surface area of the blends include pyrolyzing blends with higher shares of WB and optimizing the pyrolysis parameters, including temperature, heating rate, pressure, residence time, and post-treatments [47].

Table 3. Elemental composition of OS, WB, and OS:WB solid products, BET surface area of solid products.

OS:WB Ratio	Gas Atmosphere, 0.3 L/min	C, wt%	H, wt%	N, wt%	S, wt%	BET, m²/g
0:1	CO_2	78.92	3.26	0.40	n.d. *	127.9
	H_2O:CO_2 1:1	78.86	3.47	0.38	n.d.	173.8
	Ar	77.29	3.39	0.43	n.d.	175.9
7:3	CO_2	15.03	0.27	0.05	0.69	17.8
	H_2O:CO_2 1:1	15.87	0.40	0.04	0.69	19.5
	Ar	14.39	0.27	0.05	1.09	6.1
9:1	CO_2	12.00	0.15	0.02	0.72	19.1
	H_2O:CO_2 1:1	12.64	0.20	0.02	0.95	29.3
	Ar	11.77	0.19	0.02	1.87	45.7
1:0	CO_2	11.39	0.22	0.02	1.12	11.4
	H_2O:CO_2 1:1	11.25	0.20	0.01	0.94	28.8
	Ar	11.55	0.20	0.01	0.90	4.3

* n.d. not detected.

4. Conclusions

This work studied the effect of adding shares of woody biomass to oil shale pyrolysis using a batch reactor in isothermal conditions and with various gas atmospheres. The residual masses yields, composition, surface area, and produced gas yields were analyzed to determine the interactions and effects of both fuels in co-pyrolysis.

An optimal residence time of 20 min for co-pyrolysis was defined through the results of individual pyrolysis of each fuel. Due to its higher pyrolysis temperature, OS decomposition occurred slower than WB (90% decomposition in 15 min compared to 95% in 5 min for the reactor used). As WB reaches the isothermal temperature faster, it can contribute to the pyrolysis of OS, accelerating its decomposition.

The residual mass of OS:WB co-pyrolysis indicates an additive behavior, as it linearly decreases as the share of WB raises, with less than a 2.5 wt% difference between theoretical and experimental yields of solid products. Despite the evidence of strong interactions, adding WB to OS results in lower production of solids compared to individual pyrolysis of OS, reducing its environmental impact, while similarly, adding OS to WB increases the energy density of the blend.

All gas atmospheres had a comparable linear behavior, decreasing the residual mass as the WB ratio increased. Despite improvements in non-inert atmospheres (<2.6 wt% difference) compared to Ar co-pyrolysis, CO_2 and H_2O:CO_2 proved to yield solid products as low or lower than pyrolysis in Ar inert atmosphere, indicating its potential to use CO_2 from CCS in co-pyrolysis.

The BET-specific surface area was observed to be higher for WB solid products and comparable to OS semi-coke for OS:WB blends. To increase the surface area in blends, it would be necessary to use higher shares of WB, optimize the pyrolysis parameters, or use post-treatment methods.

Future research can address the effect of OS:WB co-pyrolysis in the yield and composition of liquid products, considering their potential use as valuable biofuels. Additionally, OS:WB blend ratios with higher shares of WB and the characterization of the liquid products could contribute to a better understanding of the co-pyrolytic behavior. Future experimental arrangements in larger scale reactors and/or prototype reactors can contribute to the state of the art of co-pyrolysis, leading to valuable results for industrial applications.

Author Contributions: Conceptualization, A.L.C. and A.K.; methodology, A.L.C. and A.K.; software, A.L.C.; validation, A.L.C. and A.K.; formal analysis A.L.C. and A.K.; writing—original draft preparation, A.L.C.; writing—review and editing, A.L.C. and A.K.; visualization, A.L.C.; supervision, A.K. All authors have read and agreed to the published version of the manuscript.

Data Availability Statement: Data are not publicly available; the data may be made available upon request from the corresponding author.

Conflicts of Interest: The authors declare no conflict of interest.

Nomenclature

BET	Brunauer, Emmett, and Teller surface area
CCS	Carbon capture and storage technologies
GC-TCD	Gas chromatography with thermal conductivity detector
HHV	Gross or higher heating value
LHV	Net or lower heating value
OS	Oil shale
TGA	Thermogravimetric analysis
WB	Woody biomass

Appendix A

Appendix A.1

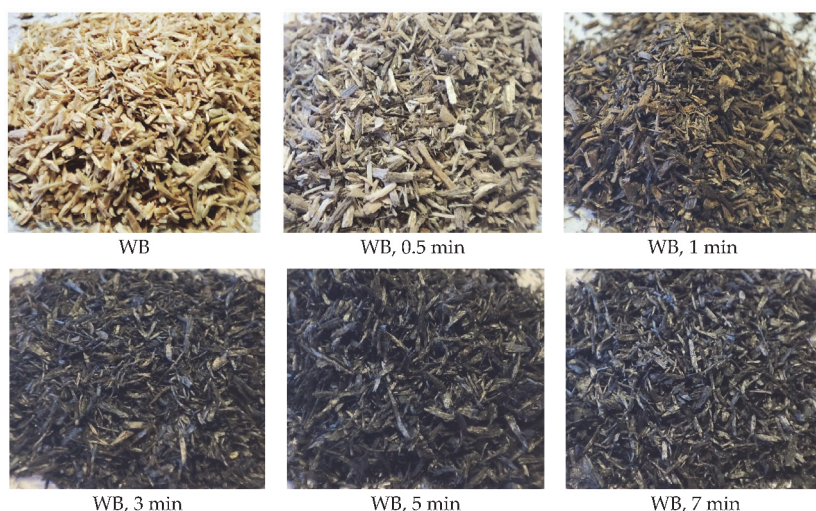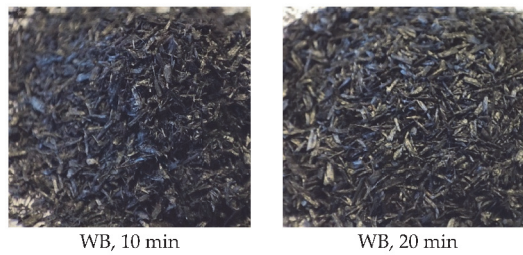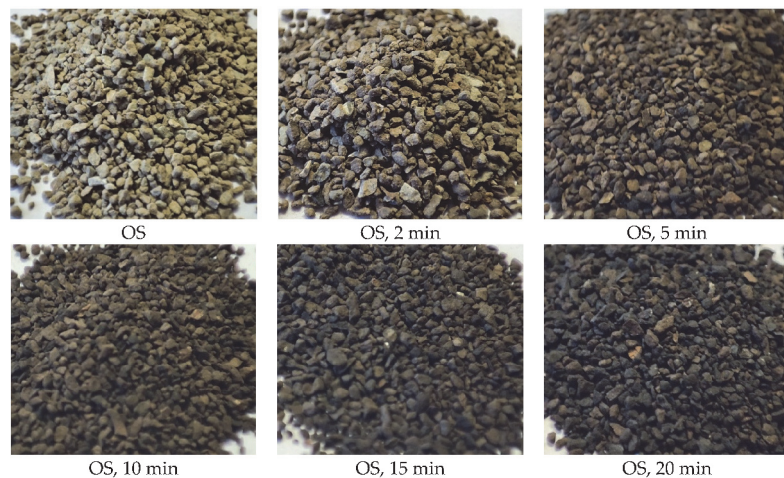Raw WB and WB residues after decomposition in the batch reactor, with different residence times.

WB   WB, 0.5 min   WB, 1 min

WB, 3 min   WB, 5 min   WB, 7 min

Figure A1. *Cont.*

WB, 10 min

WB, 20 min

Appendix A.2

Raw OS and OS residues after decomposition in the batch reactor, with different residence times.

OS

OS, 2 min

OS, 5 min

OS, 10 min

OS, 15 min

OS, 20 min

References

1. Rogelj, J.; Den Elzen, M.; Höhne, N.; Fransen, T.; Fekete, H.; Winkler, H.; Schaeffer, R.; Sha, F.; Riahi, K.; Meinshausen, M. Paris Agreement climate proposals need a boost to keep warming well below 2 °C. *Nature* **2016**, *534*, 631–639. [CrossRef] [PubMed]
2. Mariyam, S.; Shahbaz, M.; Al-Ansari, T.; Mackey, H.R.; McKay, G. A critical review on co-gasification and co-pyrolysis for gas production. *Renew. Sustain. Energy Rev.* **2022**, *161*, 112349. [CrossRef]
3. Zhang, L.; Xu, C.; Champagne, P. Overview of recent advances in thermo-chemical conversion of biomass. *Energy Convers. Manag.* **2010**, *51*, 969–982. [CrossRef]
4. Antar, M.; Lyu, D.; Nazari, M.; Shah, A.; Zhou, X.; Smith, D.L. Biomass for a sustainable bioeconomy: An overview of world biomass production and utilization. *Renew. Sustain. Energy Rev.* **2021**, *139*, 110691. [CrossRef]
5. Wang, S.; Luo, Z. *Pyrolysis of Biomass*; GREEN—Alternative Energy Resources; Walter de Gruyter GmbH: Berlin, Germany, 2017; p. 268.
6. Akhtar, A.; Krepl, V.; Ivanova, T. A combined overview of combustion, pyrolysis, and gasification of biomass. *Energy Fuels* **2018**, *32*, 7294–7318. [CrossRef]
7. Uddin, M.N.; Techato, K.; Taweekun, J.; Rahman, M.M.; Rasul, M.G.; Mahlia, T.M.I.; Ashrafur, S.M. An overview of recent developments in biomass pyrolysis technologies. *Energies* **2018**, *11*, 3115. [CrossRef]
8. Jerzak, W.; Gao, N.; Kalemba-Rec, I.; Magdziarz, A. Catalytic intermediate pyrolysis of post-extraction rapeseed meal by reusing ZSM-5 and Zeolite Y catalysts. *Catal. Today* **2022**, *404*, 63–77. [CrossRef]
9. Ibrahim, M.D.; Abakr, Y.A.; Gan, S.; Lee, L.Y.; Thangalazhy-Gopakumar, S. Intermediate Pyrolysis of Bambara Groundnut Shell (BGS) in Various Inert Gases (N_2, CO_2, and N_2/CO_2). *Energies* **2022**, *15*, 8421. [CrossRef]
10. Wang, Q.; Li, X.; Wang, K.; Zhu, Y. Commercialization and challenges for the next generation of biofuels: Biomass fast pyrolysis. In Proceedings of the 2010 APPEEC Conference, Chengdu, China, 28–31 March 2010; IEEE: Piscataway, NJ, USA, 2010; pp. 1–4.
11. Bai, F.; Sun, Y.; Liu, Y.; Li, Q.; Guo, M. Thermal and kinetic characteristics of pyrolysis and combustion of three oil shales. *Energy Convers. Manag.* **2015**, *97*, 374–381. [CrossRef]

12. Raja, M.A.; Zhao, Y.; Zhang, X.; Li, C.; Zhang, S. Practices for modeling oil shale pyrolysis and kinetics. *Rev. Chem. Eng.* **2017**, *34*, 21–42. [CrossRef]

13. Ristic, N.D.; Djokic, M.R.; Konist, A.; Van Geem, K.M.; Marin, G.B. Quantitative compositional analysis of Estonian shale oil using comprehensive two dimensional gas chromatography. *Fuel Process. Technol.* **2017**, *167*, 241–249. [CrossRef]

14. Maaten, B.; Järvik, O.; Pihl, O.; Konist, A.; Siirde, A. Oil shale pyrolysis products and the fate of sulfur. *Oil Shale* **2020**, *37*, 51–69. [CrossRef]

15. Jin, Q.; Wang, X.; Li, S.; Mikulčić, H.; Bešenić, T.; Deng, S.; Vujanović, M.; Tan, H.; Kumfer, B.M. Synergistic effects during co-pyrolysis of biomass and plastic: Gas, tar, soot, char products and thermogravimetric study. *J. Energy Inst.* **2019**, *92*, 108–117. [CrossRef]

16. Ganev, E.; Ivanov, B.; Vaklieva-Bancheva, N.; Kirilova, E.; Dzhelil, Y. A multi-objective approach toward optimal design of sustainable integrated biodiesel/diesel supply chain based on first-and second-generation feedstock with solid waste use. *Energies* **2021**, *14*, 2261. [CrossRef]

17. Li, S.; Chen, X.; Liu, A.; Wang, L.; Yu, G. Co-pyrolysis characteristic of biomass and bituminous coal. *Bioresour. Technol.* **2015**, *179*, 414–420. [CrossRef] [PubMed]

18. Krerrkkaiwan, S.; Fushimi, C.; Tsutsumi, A.; Kuchonthara, P. Synergetic effect during co-pyrolysis/gasification of biomass and sub-bituminous coal. *Fuel Process. Technol.* **2013**, *115*, 11–18. [CrossRef]

19. Özsin, G.; Pütün, A.E. TGA/MS/FT-IR study for kinetic evaluation and evolved gas analysis of a biomass/PVC co-pyrolysis process. *Energy Convers. Manag.* **2019**, *182*, 143–153. [CrossRef]

20. Kong, L.; Li, G.; Jin, L.; Hu, H. Pyrolysis behaviors of two coal-related model compounds on a fixed-bed reactor. *Fuel Process. Technol.* **2015**, *129*, 113–119. [CrossRef]

21. Jiang, H.; Deng, S.; Chen, J.; Zhang, L.; Zhang, M.; Li, J.; Li, S.; Li, J. Preliminary study on co-pyrolysis of spent mushroom substrate as biomass and Huadian oil shale. *Energy Fuels* **2016**, *30*, 6342–6349. [CrossRef]

22. Cerón, A.L.; Konist, A.; Lees, H.; Järvik, O. Current status of co-pyrolysis of oil shale and biomass. *Oil Shale* **2021**, *38*, 228–263. [CrossRef]

23. Chen, B.; Han, X.; Mu, M.; Jiang, X. Studies of the co-pyrolysis of oil shale and wheat straw. *Energy Fuels* **2017**, *31*, 6941–6950. [CrossRef]

24. Dai, M.; Yu, Z.; Fang, S.; Ma, X. Behaviors, product characteristics and kinetics of catalytic co-pyrolysis spirulina and oil shale. *Energy Convers. Manag.* **2019**, *192*, 1–10. [CrossRef]

25. Nowicki, L.; Siuta, D.; Markowski, M. Carbon Dioxide Gasification Kinetics of Char from Rapeseed Oil Press Cake. *Energies* **2020**, *13*, 2318. [CrossRef]

26. Nowicki, L.; Siuta, D.; Markowski, M. Pyrolysis of rapeseed oil press cake and steam gasification of solid residues. *Energies* **2020**, *13*, 4472. [CrossRef]

27. Ye, J.; Xiao, J.; Huo, X.; Gao, Y.; Hao, J.; Song, M. Effect of CO_2 atmosphere on biomass pyrolysis and in-line catalytic reforming. *Int. J. Energy Res.* **2020**, *44*, 8936–8950. [CrossRef]

28. Giudicianni, P.; Cardone, G.; Ragucci, R. Cellulose, hemicellulose and lignin slow steam pyrolysis: Thermal decomposition of biomass components mixtures. *J. Anal. Appl. Pyrolysis* **2013**, *100*, 213–222. [CrossRef]

29. Kantarelis, E.; Yang, W.; Blasiak, W. Production of liquid feedstock from biomass via steam pyrolysis in a fluidized bed reactor. *Energy Fuels* **2013**, *27*, 4748–4759. [CrossRef]

30. Lee, J.; Yang, X.; Cho, S.H.; Kim, J.K.; Lee, S.S.; Tsang, D.C.W.; Ok, Y.S.; Kwon, E.E. Pyrolysis process of agricultural waste using CO2 for waste management, energy recovery, and biochar fabrication. *Appl. Energy* **2017**, *185*, 214–222. [CrossRef]

31. Sulg, M.; Konist, A.; Järvik, O. Characterization of different wood species as potential feedstocks for gasification. *Agron. Res.* **2021**, *19*, 276–299.

32. Chen, B.; Han, X.; Tong, J.; Mu, M.; Jiang, X.; Wang, S.; Shen, J.; Ye, X. Studies of fast co-pyrolysis of oil shale and wood in a bubbling fluidized bed. *Energy Convers. Manag.* **2020**, *205*, 112356. [CrossRef]

33. Cascante Cirici, P. Biomass and Oil Shale Co-Pyrolysis. Master's Thesis, Tallinn University of Technology, Tallinn, Estonia, 2019.

34. Cerón, A.L.; Konist, A.; Lees, H.; Järvik, O. Effect of woody biomass gasification process conditions on the composition of the producer gas. *Sustainability* **2021**, *13*, 11763. [CrossRef]

35. Garcia-Perez, M.; Wang, X.S.; Shen, J.; Rhodes, M.J.; Tian, F.; Lee, W.J.; Wu, H.; Li, C.Z. Fast pyrolysis of oil mallee woody biomass: Effect of temperature on the yield and quality of pyrolysis products. *Ind. Eng. Chem. Res.* **2008**, *47*, 1846–1854. [CrossRef]

36. Grieco, E.; Baldi, G. Analysis and modelling of wood pyrolysis. *Chem. Eng. Sci.* **2011**, *66*, 650–660. [CrossRef]

37. Syed, S.; Qudaih, R.; Talab, I.; Janajreh, I. Kinetics of pyrolysis and combustion of oil shale sample from thermogravimetric data. *Fuel* **2011**, *90*, 1631–1637. [CrossRef]

38. Tiwari, P.; Deo, M. Compositional and kinetic analysis of oil shale pyrolysis using TGA-MS. *Fuel* **2012**, *94*, 333–341. [CrossRef]

39. Tiwari, P.; Deo, M. Detailed kinetic analysis of oil shale pyrolysis TGA data. *AIChE J.* **2012**, *58*, 505–515. [CrossRef]

40. Johannes, I.; Tiikma, L.; Luik, H. Synergy in co-pyrolysis of oil shale and pine sawdust in autoclaves. *J. Anal. Appl. Pyrolysis* **2013**, *104*, 341–352. [CrossRef]

41. Yanik, J.; Secim, P.; Karakaya, S.; Tiikma, L.; Luik, H.; Krasulina, J.; Raik, P.; Palu, V. Low-temperature pyrolysis and co-pyrolysis of Göynük oil shale and terebinth berries (Turkey) in an autoclave. *Oil Shale* **2011**, *28*, 469–486. [CrossRef]

42. Kiliç, M.; Pütün, A.E.; Uzun, B.B.; Pütün, E. Converting of oil shale and biomass into liquid hydrocarbons via pyrolysis. *Energy Convers. Manag.* **2014**, *78*, 461–467. [CrossRef]
43. Tian, B.; Wang, J.; Qiao, Y.; Huang, H.; Xu, L.; Tian, Y. Understanding the pyrolysis synergy of biomass and coal blends based on volatile release, kinetics and char structure. *Biomass Bioenergy* **2023**, *168*, 106687. [CrossRef]
44. Cheng, C.-Y.; Kuo, C.-C.; Yang, M.-W.; Zhuang, Z.-Y.; Lin, P.-W.; Chen, Y.-F.; Yang, H.-S.; Chou, C.-T. CO_2 capture from flue gas of a coal-fired power plant using three-bed PSA process. *Energies* **2021**, *14*, 3582. [CrossRef]
45. Xie, W. Uncertainty analysis and evaluation of calibration results of meteorological chromatograph. In Proceedings of the 2022 IEEE 10th Joint International Information Technology and Artificial Intelligence Conference (ITAIC), Chongqing, China, 17–19 June 2022; pp. 1158–1161.
46. Quan, C.; Xu, S.; An, Y.; Liu, X. Co-pyrolysis of biomass and coal blend by TG and in a free fall reactor. *J. Therm. Anal. Calorim.* **2014**, *117*, 817–823. [CrossRef]
47. Leng, L.; Xiong, Q.; Yang, L.; Li, H.; Zhou, Y.; Zhang, W.; Jiang, S.; Li, H.; Huang, H. An overview on engineering the surface area and porosity of biochar. *Sci. Total Environ.* **2021**, *763*, 144204. [CrossRef]
48. Pikkor, H.; Maaten, B.; Baird, Z.S.; Järvik, O.; Konist, A.; Lees, H. Surface area of oil shale and its solid pyrolysis products depending on the particle size. *Chem. Eng. Trans.* **2020**, *81*, 961–966.

Publication IV

Co-pyrolysis of biomass woodchips with Ca-rich oil shale fuel in a continuous feed reactor

Alejandro Lyons Ceron*, Tõnu Pihu, Alar Konist

Department of Energy Technology, Tallinn University of Technology, Ehitajate tee 5, 12616, Tallinn, Estonia
* corresponding author: allyon@taltech.ee

Co-pyrolysis of woodchips and oil shale was conducted in a continuous reactor at 520 °C in a CO_2 atmosphere. The experimental yields of products and an analysis of the liquid products were conducted, using gas chromatography, infrared spectroscopy, and physicochemical analysis. A maximum yield of liquids and gases was obtained as the share of biomass increased (43.9 and 35.1 wt% respectively), The product characterization confirmed an additive behavior in co-pyrolysis. The liquid products from co-pyrolysis blends had lower oxygenated compounds, derived from biomass, and lower aromatic compounds, derived from oil shale. Co-pyrolysis liquids had abundant aliphatic hydrocarbons (C_6 to C_{11}).

1. Introduction

Utilizing alternative and clean energy solutions offers the potential to mitigate the environmental impact of using conventional fossil fuels for energy production by decreasing pollutant gas emissions and reducing reliance on non-renewable resources [1]. An approach to a carbon-neutral transition is the co-conversion of renewable resources, such as biomass, and fossil resources such as oil shale. Both fuels are utilized in thermochemical conversion processes to produce solid, liquid, and gaseous products with valuable applications in the energy sector and the chemical industry [2].
Biomass has been widely used and studied as a resource to produce energy and valuable products. It stands as a renewable and carbon-neutral resource, with the potential of supplying 14 % of the world's energy needs [1]. The use of biomass as an energy resource can save above one billion tons of carbon dioxide [2], contributing to the reduction of the environmental impact of the utilization of conventional fossil fuels [3, 4]. The high content of volatile matter (60-85 wt%) and low ash content (1-20 wt) [5, 6] makes biomass types, such as woody biomass [7] suitable to produce bio-oil, absorbent materials, and chemical products among others [8, 9]. Biomass has a biochemical composition of hemicellulose, cellulose, and lignin, components that define its thermochemical behavior, and the yield and quality of products obtained during pyrolysis [10]. A temperature of 520 °C has been proven to be the optimal pyrolysis temperature for the highest yield of bio-oil, resulting in a high yield of liquid and gaseous products (40-70 wt% and 20-30 wt % respectively) and a low yield of char (10-25 wt%) [11]. At 500-550 °C not only the yields of bio-oil increase, but also the quality, with a lower moisture content and oxygen content, and higher heating values, carbon content, and viscosity [12]. The study of bio-oil production is significant in identifying its potential utilization as a fuel or chemical. Bio-oil is dark and viscous and has a high share of water (15-35 wt%) and a significant share of oxygenated compounds, acids, ethers, and sugars [13]. However, bio-oil is not stable, requiring additional reforming to address the high corrosiveness, chemical instability, and viscosity [14, 15]. The lower toxicity and biodegradability of bio-oil make its potential use as a valuable resource, in various applications, including as engine fuel, chemicals including phenols, resins, and fertilizers.
Oil shale (OS) is a non-conventional fossil fuel extracted from geological deposits found in diverse regions worldwide [16]. Notably, its composition is distinguished by a significant proportion of organic material known as kerogen and a share of inorganic matter and ash. Kerogen, the organic part of OS can be converted into valuable products, such as shale oil and shale gas, through thermochemical conversion processes [17]. Pyrolysis is typically implemented for OS retorting and the production of shale oil. Typically, OS retorting yields, 5–20 wt% of shale oil, 5–20 wt% of shale gas, and >60 wt% of semicoke [18, 19]. Temperatures from 450-550 °C have been proven to yield the highest shares of shale oil [20], however, the yield and quality of OS pyrolysis depend on the type and composition of the OS, whose organic matter content and heating value can vary from 5 to 80 % [21] and 5-20 MJ/kg respectively. The operational parameters and the type of reactor used will also have a direct impact on the yields and quality of the pyrolysis products [22]. The most significant challenges in OS utilization include environmental impacts such as CO_2, NO_x, and SO_x emissions [23]. Additionally, OS pyrolysis can result in a shale oil with high molecular weight and viscosity, as well as high sulfur content and low stability [23]. As for bio-oil, shale oil may require additional upgrading for its use as a fuel or chemical [24, 25]. The reduction of the yields of solid products (semicoke) is also a challenge to overcome in OS pyrolysis.
Due to the similarity in the operational and thermal conditions required for the degradation of OS and biomass, both fuels can be co-fed in co-pyrolysis to study the thermal degradation and the combined co-pyrolytic properties and yields of the solid, liquid, and gaseous products [26]. The co-pyrolysis of Ca-rich OS and biomass can potentially result in a more environmentally friendly alternative for the production of energy and chemicals, such as the reduction of emissions from

OS utilization, and the use of biomass waste resources [27]. In co-pyrolysis, biomass and OS can interact through chemical reactions or heat transfer mechanisms, resulting in higher yields of products with enhanced properties. Even though biomass and OS pyrolysis occur at the same temperature range [28], the most significant degradation of biomass occurs faster and in a lower temperature region, which can result in heat transfer interactions that enhance OS pyrolysis [29]. Moreover, biomass has a higher hydrogen content, which can act as a hydrogen donor to improve OS thermal cracking and reduce the activation energies of co-pyrolytic blends [30]. Studies in co-pyrolysis of OS and biomass have shown to result in improved properties of solid, liquid, and gaseous products [31, 32] as well as enhanced cracking of the fuels and higher product yields [33].

The present study investigates the yields and composition of the products obtained from the intermediate co-pyrolysis of biomass woodchips (WC) and Ca-rich OS in a continuous feed reactor in optimized operational parameters for the highest yields of liquids, at 520 °C in a CO_2 atmosphere. Various blends of OS:WC were pyrolyzed to obtain liquid, gaseous, and solid products. The liquid and solid products were characterized in terms of yields, and elemental composition, and a comprehensive physicochemical analysis was conducted for the liquid products, including, density, viscosity, refractive index, Fourier-transform Infrared spectroscopy (FTIR), and Gas Chromatography with mass spectrometer detector (GC-MS) to identify the most common chemical compounds and functional group in the pyrolytic and co-pyrolytic liquids. A detailed comprehensive analysis of the yields and composition of products allowed the identification of the potential benefits of co-pyrolysis, in terms of interactions that can enhance the fuels decomposition, and the quality of the products, or reduce the environmental impact of conventional retorting processes. The study includes an analysis of the GC-MS and FTIR and elemental analysis characteristics of the liquid products, to identify what elements and compounds are present in individual pyrolysis, and in co-pyrolysis, which can result in a co-pyrolysis liquid fuel with improved properties. The identification of co-pyrolytic products and their composition with improved or combined properties can highlight the potential of co-pyrolysis as a sustainable and efficient method for biomass and oil shale valorization.

2. Materials and methods

2.1. Fuel preparation and characterization

Two different fuels were used in pyrolysis and co-pyrolysis, WC and OS. The WC consisted of a mix of spruce (*Picea abies*), alder (*Alnus incana*), pine (*Pinus sylvestris*), and birch (*Betula pendula*) from Estonian forests. The OS used is a brown type of OS found in Estonia. The preparation of the fuels consisted of grinding to the required particle size, sieving, drying, and preparation of blends. OS and WC samples were grounded in a ball mill (Pulverisette 5 model, Laval Lab, Quebec, Canada) to a particle size below 1 mm, following ISO 14780:20 standards. The grounded particles were sieved to obtain particle sizes between 0.25 and 1.3 mm using Analysette 3 Pro Sieve (Fritsch GmbH, Germany). The sieved particles were dried at 105 °C for 3 h, using a Muffle furnace L9 (Nabertherm GmbH, Lilienthal, Germany) to remove moisture.

WC and OS were characterized in terms of chemical, physical, and thermodynamic properties through elemental analysis, proximate analysis, and calorimetry, respectively. For WC, the elemental analyses were conducted using the Vario MACRO CHNS Cube system (Elementar Analysensysteme GmbH, Langenselbold, Germany), according to ISO 16948 and 16994. The proximate analysis to obtain the share of volatile matter, moisture, and ash content was conducted following ISO 18122:2015, 18134:2017, and 18122:2015, respectively. The thermodynamic properties of WC were determined according to ISO 18125, using bomb calorimeters, IKA 2000C, and IKA 5000C (IKA-Werke GmbH & Co. KG, Staufen, Germany). Using the abovementioned equipment, OS elemental analysis was conducted according to ISO 29541:2015, the proximate analysis followed EVS 669:1996 for determining the ash content, and the upper and lower calorific values were determined following ISO 1928:2016.

Six different samples of WC, OS, and OS:WC blends were prepared: OS:WC 0:1, 7:3, 1:1, 3:7, and 1:0, to obtain samples of 100, 70, 50 and 30 wt% WC, and 100 wt% OS. The blends were manually prepared, using the coning and quartering mixing method, according to ISO 14780:20, and stored in airtight plastic bags, following ISO 14780:20. The prepared mixtures of samples had an average deviation of ±2 %.

2.2. Experiment set up

Pyrolysis and co-pyrolysis of WC, OS, and OS:WC blends were conducted using a prototype continuous feed reactor. The reactor consists of a retort, a feed hopper, a screw conveyor, a heating system, and a cooling and condensing system. The schematic of the reactor is shown in Figure 1. The continuous feed reactor, where the pyrolysis reactions occur, consists of a cylindrical tank retort, with 85 and 130 mm of diameter and height respectively, and a capacity of 460 cm^3. The retort is equipped with a cylindrical heater Omega CRFC-46/240-A, 240 V, 900 W (Omega Engineering Inc., Norwalk, United States), which can heat the reactor to temperatures of 982 °C. The fuels (WC, OS, or blends) are stored in feed hopper tanks (560 cm^3) with a conical bottom. These tanks count on an agitator to avoid clogging and feed the fuel to the screw feeder. The agitators function using an electric stepper motor OMC Stepper Online 23HS32-4004S, 48 V, 2.4 Nm, 1.8° step (Stepperonline Inc., New York, United States). From the hopper, the fuel is fed to the screw feeder, driven by a stepped motor (the same type as the one used in the agitator). The fuel is then fed through the screw feeder that discharges the material parallel to the screw axis directly into the retort, which gives the screw greater thrust and prevents blockages.

In the retort, the fuel undergoes a set of chemical reactions at a controlled temperature. The retort counts with a supply of carrier gas to prevent air from entering the system and ensure pyrolysis. Additionally, the retort counts with two cassette heaters IHP 270-08100200, 240 V, 200 W (IHP AB, Stenkullen, Sweden), on top of the lid and one cartridge heater on the exhaust. These heaters contribute to minimizing condensation at the exhaust and maintaining the desired temperature in the whole retort. The retort cylindrical heater and the cassette and cartridge heaters are controlled through an Omega CN7523 PID controller (OMEGA Engineering Inc., Norwalk, United States), which receives feedback from two TC Direct 405-016, and 405-017 (TC Ltd., Uxbridge, United Kingdom) K-type thermocouples. Lastly, the reactor also counts with a cooling and condensing system, where the condensable and non-condensable are cooled down, using a coolant bath, through a Huber TC40E recirculating chiller (Peter Huber Kältemaschinenbau SE, Offenburg, Germany) condensing system which uses ethylene glycol as a cooling agent, kept at -30 °C recirculated through a glass thermosensor containing a finger chiller for oil vapor condensation.

The current research used the continuous feed reactor and fuel blends of OS and WC (OS:WC 0:1, 7:3, 1:1, 3:7, and 1:0) to conduct co-pyrolysis with CO_2 as the gas carrier (50 ml/min), in isothermal conditions at 520 °C. This pyrolysis temperature was chosen as it results in the highest production of liquid products for WC, OS, and the OS:WC blends [28]. The cartridge and cassette heaters were also heated to 520 °C. The experiments started when the fuel was fed to the retort from the feed hopper (motor at 10 rpm) to the screw feeder (motor at 5 rpm), with an average feeding rate of 0.05 kg/h for WC, 0.2 kg/h for OS, and 0.05-0.2 kg/h for OS:WC blends. The variable feeding rate was due to the difference in densities, with WC having a lower density than OS. The fuel was fed into the retort for approximately 40-60 min, assuring the production of enough liquid products for analysis. Before each experiment, the retort was heated and purged for 30 min with CO_2, to ensure a homogeneous pyrolysis atmosphere, while a leak test was conducted, to ensure proper collection of products. After the pyrolysis, solid and liquid products were collected. Solid products (Char, ash, and semicoke) were collected from the cylindrical retort, while liquid products were collected from the condenser. All components, including the retort, the outlet pipes, and the condenser were weighed previous and after the experiment to obtain a proper mass balance of products. The solid products were stored in airtight bags, and the liquid products were stored in a fridge in airtight containers, to prevent evaporation. Each blend of OS:WC was pyrolyzed, with 2 parallel experiments, to ensure a low deviation.
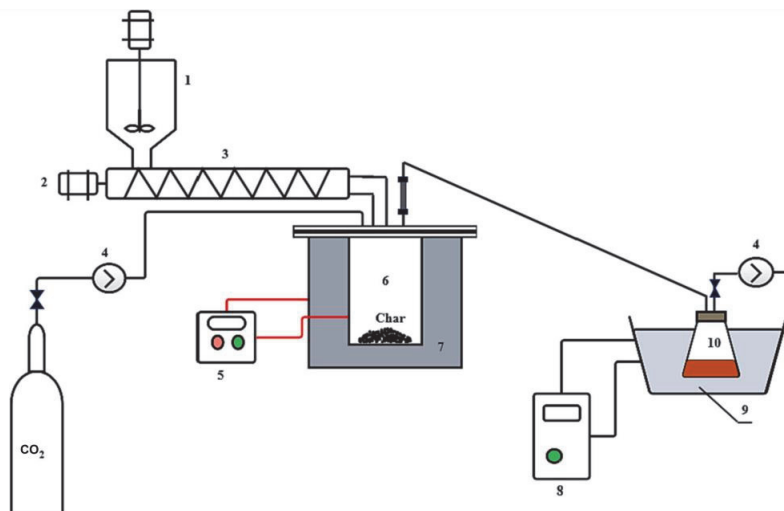
Figure 1. Schematic of continuous feed reactor (from reference [34]) (1. Feed hopper, 2. Stepped motor, 3. Screw feeder, 4. Carrier gas, 5. PID controller, 6. Retort reactor, 7. Cylindrical heater, 8. Chiller, 9. Coolant bath, 10. Condenser)

The estimated and experimental yields of liquids, solids, and gaseous products from the co-pyrolysis of OS:WC 3:7, 1:1, and 7:3 were derived through the application of a linear correlation involving the shares of OS and WC. This correlation was established based on the experimental yields obtained from individual pyrolysis of both OS and WC as shown in Equation (1), where m_{theo} is the estimated yields of OS:WC blends, m_{OS} and m_{WB} are the experimental yields, and x is the share of OS.

$$m_{est} = m_{OS}x + m_{WC}(1 - x) \tag{1}$$

2.3. Mass balance

For all pyrolysis and co-pyrolysis scenarios, the yields of products were determined by mass balance. At the beginning of the experiment the initial mass of WC and OS and OS:WC blends was recorded. The amount of fuel consumed was calculated by the difference between the initial fuel fed and the mass of fuel left in the hopper after the experiment. This amount of fuel consumed was considered as 100 wt% for calculating the product yields. The yield of solids was determined by the difference in the initial and final mass of the reactor, as all solid products from pyrolysis remained in the reactor. For the liquid products, the yield was calculated using the mass of liquids collected in the condenser (final-initial weight of condenser), additionally, the increase of weight in the exhaust prices, and all outlet components was added to the yield of liquids, as these correspond to condensed deposits in the component's walls. The gas products' yield was calculated by difference, assuming minimal losses, due to a low gas flow rate and the leak tests.

2.4. Characterization of solid products

The solid products from the pyrolysis and co-pyrolysis of OS and WC and OS:WC blends were characterized in terms of elemental composition, proximate composition, and calorific values. The elemental analysis was conducted using the Vario MACRO CHNS Cube system (Elementar Analysensysteme GmbH, Langenselbold, Germany) and the calorific values were determined using IKA 2000C and IKA 5000C (IKA-Werke GmbH & Co. KG, Staufen, Germany).

2.5. Characterization of liquid products

The liquid products were characterized in terms of elemental composition, using a Vario MACRO CHNS Cube system Thermal analyzer (Elementar Analysensysteme GmbH, Langenselbold, Germany). Additional physicochemical characteristics of the liquid products were measured, including density, viscosity, and refractive index. The density of the liquid samples was measured at 21°C, using a DMA 5000 M density meter (Anton Paar GmbH, Graz, Austria). The viscosity was determined using a Modular Compact Rheometer, MCR 72 (Anton Paar GmbH, Graz, Austria), with a cone plate spindle at 40 °C. The refractive index was determined using an Abbemat HT refractometer (Anton Paar GmbH, Graz, Austria), at a temperature of 20 °C and a wavelength of 589.3 nm. The density, viscosity, and refractive index of water were determined before and after each measurement of oil samples, to verify the correct performance of the devices.

2.6. Liquid products analysis

The liquid samples were analyzed using FTIR and GC-MS. The IR spectra of the liquid products from pyrolysis and co-pyrolysis were obtained using an Interspec 301-X portable spectrometer (Interspectrum OU, Tartu, Estonia), with an ATR (Attenuated Total Reflection), a wavelength range from 7000 to 400 cm^{-1}, a resolution of 1 cm^{-1}, and an S:N ratio up to 12000:1. For the pyrolysis liquid products, the samples were analyzed in the wavelength range from 600-4000 cm^{-1} and at a resolution of 1 cm^{-1}

The chemical composition of the liquid products of pyrolysis and co-pyrolysis was analyzed with GC-MS (Gas Chromatography with Mass Spectrometer detector) to identify different compounds present in the oil. The equipment used was an Agilent 7890B Gas Chromatograph (Agilent Technologies, Inc., Santa Clara, United States) connected to an Agilent 5975C Inert MSD mass spectrometer (Agilent Technologies, Inc., Santa Clara, United States). The gas carrier was Helium with a purity of 99.9999 % and at a flow rate of 0.9 ml/min. The samples were injected using a CTC Combi/GC-PAL 80 autosampler (Agilent Technologies, Inc., Santa Clara, United States). 1 µl of the sample was injected with a 10:1 split ratio and an injector temperature of 300 °C. The initial temperature was programmed to start at 40 °C, held for 10 min, followed by a temperature rise to 160 °C, with a heating rate of 3 °C/min. The temperature was then raised to 320 °C with a heating rate of 15 °C/min. The temperature was then kept at 320 °C for 5 min. Each analysis had a total time of 66 min. The liquid products from pyrolysis and co-pyrolysis were analyzed. The GC used a DB Petro column of 100 m x 250 µm x 0.5 µm. The MS capillary dimensions are 1 m x 250 µm x 0 µm. All the samples were dissolved in acetone, with an average share of sample 15 % ± 0.8 %, two samples of each pyrolysis oil were measured. The NIST1.4L library and the Agilent MassHunter Qualitative Analysis Software were used to identify the chromatographic peaks and for the identification of compounds. Each sample had one more parallel run.

3. Results and discussion

3.1. Fuel properties

The composition in terms of C, H, N, S, O, the ash and moisture content, fixed carbon, volatile matter, and calorific values (HHV and LHV) of WC and OS are shown in Table 1. WC composition is similar to the composition of woody biomass species [35], with a high content of carbon and oxygen, over 80 wt % volatile matter, and low ash content (below 2 wt%). Table 1 displays the composition of the organic part of OS. OS compared to WC has a considerably higher ash content (above 50 wt%), higher density, and lower calorific value. In terms of elemental composition WC and OS have a

significantly different composition, especially of C, H, and O, while oil shale has a high content of sulfur. The share of volatiles for OS is lower than WC, which will result in a lower yield of oil and gas products. The pyrolytic behavior and yields of products from WC and OS are then expected to differ, while the co-pyrolysis is expected to produce oil, gas, and char with additive yields of products [36].

Table 1. WC and OS properties

Composition		Wood chips (WC)	Oil shale (OS)
Elemental analysis [wt%]	C	51.68	27.00
	H	6.44	2.46
	N	0.35	0.06
	S	<0.10	1.65
	O*	41.53	15.40
Proximate analysis [wt%]	Ash content	1.54	51.42
	Moisture	6.40	0.90
	Fixed carbon*	10.58	1.48
	Volatile matter	81.48	47.10
Calorific value [MJ/kg]	LHV	18.76	8.72
	HHV	20.16	9.73

* Calculated

3.2. Pyrolysis and co-pyrolysis yields

The yields of gas, solid and liquid products from pyrolysis, and co-pyrolysis at 520 °C of OS and WC are illustrated in Figure 2. The measured yields of liquid and solid products had a relative standard deviation of 1.43-6.88 % and 3.41-8.73 % for each parameter and its replicates, respectively. As expected, WC yields a higher share of gas and liquid products, with 43.9 wt% of liquids (oil+water), 35.1 wt% of gas, and 21.0 wt% of solids, from which the majority is composed of pyrolysis char. These product yields are consistent with the expected yields of woody biomass in intermediate pyrolysis [6, 10, 11, 37] as also observed in studies of various types of woody biomass as shown in Table 2. From the current study and the studies displayed in Table 2, it is shown that the yields of products obtained match well with the yields obtained in other studies of intermediate pyrolysis at 450-650 °C, with average product yields of 35-62 wt% of liquids, 22-41 wt% of gas, and 21-37 wt% of solids. A higher yield of liquids and gas, and a lower yield of solids (21.0 wt%), indicate the pyrolysis was complete, based on elemental composition from Table 1, with a low share of unreacted fuel.
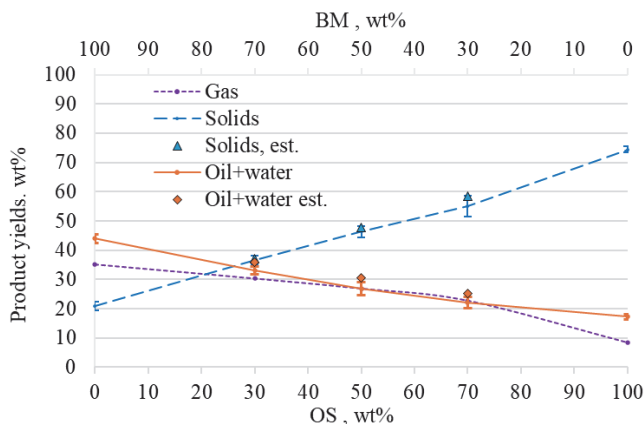

Figure 2. Experimental and estimated yields of products from co-pyrolysis of OS and WC

OS yielded a higher share of solid products, with 74.3 wt%, and a lower yield of liquids 17.3 wt% and gas 8.4 wt% products. The higher yield of solids is due to the considerably higher share of ashes in OS, compared to WC, as shown in Table 1. The lower volatile content of the OS results in a lower yield of liquid and gas products. The pyrolysis yields of OS are consistent with the expected pyrolytic yields of OS, 5–20 wt% liquids (shale oil), 5–20 wt% gas (shale gas), and >60 wt% of solids (semicoke) [22]. Table 3 shows a comparison of the yields of products from pyrolysis at 420-600 °C of diverse types of OS. The yields of products obtained from pyrolysis of OS match well with the yields obtained in other studies, with 7-46 wt% of liquids, 5-31 wt% of gas, and 37-76 wt% of solids. The wide range of yields of products in the

comparative analysis from Table 3 is due to the different types of OS used, which contain different shares of organic matter. The OS used in the current study yielded 74.3 wt% of solids due to the higher ash content of the fuel, this share of solids is composed of semicoke, which is composed of ash and organic matter that did not pyrolyze [18, 19].

Table 2. Comparative analysis of yields of woody biomass intermediate pyrolysis

Biomass type	Experiment type	Operating temperature [°C]	Residence time [min]	Particle size [mm]	Liquids yield (oil+water) [wt%]	Gas yield [wt%]	Solid yield [wt%]
Woodchips (WC), current study	**Continuous feed reactor**	**520**	**40-60**	**0.25-1**	**44**	**35**	**21**
Pine sawdust [38]	Fixed bed reactor	550	30 min	1	45	26	28
Paulonwnia wood [39]	Fixed bed reactor	500	-	0.22-0.42 0.42-1.1 1.1-1.8	25-30	22-27	26
Beech and spruce [40]	Tubular reactor	427	-	1.0-2.5	36-38	-	34-37
Beech and pine pellets [41]	Stainless steel capsule	670-970	25	11-13 diameter 60 length	53-62	17-21	21-27
Pinewood [42]	Rotary kiln reactor	500	30 min	4	35	41	24
Spruce and pine sawdust [43]	Furnace	500	-	0.5-2	50	25	25
Pine sawdust [44]	Screw reactor	600	6 min	1-2	52	22	20
Spruce [45]	Cylindrical reactor	525	-	-	45	30-35	28
Silver birch [46]	Batch retort	450	-	-	38-43	18-22	34

Table 3. Comparative analysis of yields of OS pyrolysis

OS	Experiment type	Operating temperature [°C]	Residence time [min]	Particle size [mm]	Liquids yield (oil+water) [wt%]	Gas yield [wt%]	Solid yield [wt%]
Oil shale (OS), current study	**Continuous feed reactor**	**520**	**40-60**	**0.25-1**	**17**	**8**	**74**
Goynuk OS[47]	Autoclave	420	120	<0.12	37-46	10-16	37-52
Huadian OS[33]	Retorting reactor	490-590	-	<0.9	7-19	15-20	65-76
Huadian OS [31]	Cylindrical retort	520	20	<3	32	5	66
Huadian OS [28]	Bubbling fluidized bed reactor	430-600	-	3	21	13	67
Kukersite OS [22]	Fischer assay	520	-	0.04-0.1	34	8	58
Goynuk OS [48]	Fixed bed reactor	600	60	1	30	32	38

Figure 2 displays the yields of co-pyrolysis products from OS:WC 7:3, 1:1, 3:7 blends. There is an evident additive relation between the yields of products and the blend ratio of OS:WC. The yields of liquids rise as the share of WC is increased, with 17.3 wt% for OS:WC 1:0, increasing to 22.2, 26.9, 33.1, and 43.9 wt% for OS:WC 7:3, 1:1, 3:7 and 0:1, respectively. The case is similar for Gas products, starting with 8.4 wt% for OS:WC 1:0, increasing to 22.7, 26.8, 30.3, and 35.1 wt% for OS:WC 7:3, 1:1, 3:7, and 0:1, respectively. On the other hand, the yield of solid products decreases as the share of WC is raised. OS:WC 1:0 yielded 74.4 wt% of solids, while the yield decreased to 55.1, 46.3, 36.6, and 21.0 for OS:WC 7:3, 1:1, 3:7 and 0:1, respectively. The yields of products from co-pyrolysis indicate a linear behavior as the ratio of WC

increases. With a linear increase in yields of liquid , with a coefficient of determination R^2 of 0.9704, and a linear decrease in the yields of solids, with a coefficient of determination R^2 of 0.9955.

Figure 2 also shows a comparison of experimental yields and estimated yields of co-pyrolysis products based on Equation (1). Overall, for solid and liquid products from co-pyrolysis, the experimental yields were lower than the estimated yields. The estimated yields resulted in 0.4-3.7 wt% higher than the experimental yields, this could indicate some interactions between the fuels in co-pyrolysis. However, considering the deviation of up to 9 % between parallel experiments, and the sample mixing deviation of ±2 wt%, the difference in experimental and estimated yields is in all likelihood due to uncertainties in experimentation, including the collection of liquid and solid products. The yield of products in co-pyrolysis follows instead an additive linear relation, increasing the yields of liquids and gas and decreasing the yield of products as the share of WC rises. Other research has also observed additive behavior and low or no interactions [24, 47, 49] in the co-pyrolysis of OS and biomass. However, the addition of WC to OS improved the pyrolysis process, with a reduction in the yield of solid products and a higher yield of oil and gas [31, 32, 50] WC pyrolysis starts at a lower temperature region due to its biochemical composition [10]; therefore, the products of WC pyrolysis can interact with OS through heat transfer or chemical reactions, enhancing the pyrolysis process for OS. The higher H content of WC (Table 1) and alkali and alkaline earth metals [33] can promote the decomposition of OS through a catalytic effect [32, 33, 51, 52].

3.3. Solid products

The characteristics of the solid products from OS and WC pyrolysis and co-pyrolysis are shown in Table 4. The elemental composition, proximate composition, and calorific values had a relative standard deviation of 0.21-10.28 %, 0.12-6.72 %, and 1.00-6.31 % for each parameter and its replicates, respectively. Experimental analysis of solid products indicates how the Carbon and hydrogen content and calorific values of OS:WC blends increase as the share of WC rises. On the other hand, sulfur content and ash content decrease as the share of WC rises. The solid products from WC pyrolysis consist mostly of char (81.1 wt% C), with below 8 wt% of ashes, which agrees with the composition of char from intermediate pyrolysis of woody biomass [53, 54]. The OS pyrolysis solid products consist mostly of ashes (67.7 wt%), and a low fraction of char, below 13 wt%, which agrees with the composition of semicoke from OS pyrolysis [55]. The solid products from OS:WC mixtures have a composition in between the composition of WC and OS. The volatile matter in the chars indicates that there was incomplete degradation during pyrolysis and co-pyrolysis [44] for blends containing shares of OS. The addition of WC to OS in co-pyrolysis contributes to solid products of higher calorific values, higher C and H content, and lower ash and S content. These properties result in an improved char with enhanced thermal properties, for example, higher C and H content increase the heating value of the char, while lower ash and S decrease possible environmental effects of using the solid products from co-pyrolysis of OS and WC. According to literature, the chars obtained co-pyrolysis at 520 °C of WC, OS, and OS:WC have higher aromaticity and thus higher stability, allowing its applications as absorbent materials, a pollutant sorbent, and biochar [13, 56], especially for chars from WC and OS:WC blends with high shares of WC.

Table 4. Composition of solid products from pyrolysis and co-pyrolysis of OS and WC

	Blend OS:WC	WC	3:7	1:1	7:3	OS
Elemental analysis [wt%]	C	81.10	31.74	23.26	18.76	12.90
	H	3.12	1.08	0.70	0.50	0.28
	N	0.58	0.19	0.11	0.08	0.04
	S	0.15	1.13	1.32	1.36	1.53
Proximate analysis [wt%]	Ash content	7.44	49.86	58.09	62.1	67.74
	Moisture	11.41	5.54	2.93	1.73	0.73
	Fixed carbon*	62.45	15.00	10.17	9.50	5.32
	Volatile matter	18.70	29.59	28.81	26.67	26.21
Calorific value [MJ/kg]	LHV	29.54	9.07	5.66	3.84	1.89
	HHV	30.23	9.31	5.82	3.96	1.96

* Calculated

3.4. Liquid products characterization

Table 5 summarizes the properties of the raw liquid products from the pyrolysis and co-pyrolysis of OS, WC and OS:WC, with a relative standard deviation for viscosity, density, refractive index, and elemental composition of 6.35-11.51 %, 0.37-0.67 %, 0.18-0.35 % and 1.07-10.10 % for each parameter and its replicates, respectively.

The WC (OS:WC 0:1) pyrolysis oil is viscous, dense, and of brown color, with a characteristic pungent-like barbecue odor [57]. In the pyrolysis with 100 wt% WC, the composition of the liquid part agrees with the typical composition of the pyrolytic liquids from woody biomass, pyrolysis, with C, H, N ranging from 54.0-58.0, 5.5-7.0, and 0.0-0.2 wt % respectively [58]. A higher share of H (8.85 wt%) in the current results may be due to a higher share of water in the liquid part, which can contain up to 35 wt% of water [13]. The physicochemical properties of the liquid products of WC are also in agreement with other studies, with literature values of viscosity ranging from 40-100 mPa·s, and densities of 1.0-1.2 kg/m^3 [45, 57, 59, 60]. The bio-oil viscosity is relatively high, due to the high molecular weight of the lignin-derived compounds, this can affect the bio-oil operating temperature, as well as combustion efficiency and emissions [45]. The density is also relatively higher than conventional liquid fuels [58]. As with all bio-oils, the current bio-oil requires upgrading and refining [58].

The OS pyrolysis oil (OS:WC 1:0) is lighter and of a dark brown color. Pyrolysis of 100 wt% OS resulted in elemental composition and physicochemical properties comparable to other literature studies, with C, H, and N 78-82 9-11 and 0.03-2.2 wt % respectively [23, 61, 62]. The sulfur content of Shale oil is relatively high compared to sulfur content in bio-oil, however, the sulfur content is comparable to or lower than most crude oils' sulfur content (0.01-4.20 wt %). The shale oil obtained had a higher C/H ratio than crude oil (5.28-7.73), even though the difference is not significantly higher, it causes fouling during processing [23, 58]. The density, viscosity, and refractive index of OS are also in agreement with the literature, with observed densities from 0.89 to 0.99 g/cm^3, [62, 63]. The shale oil analyzed is of low density and low viscosity compared to petroleum-derived oils [58].

The characteristics of the liquids obtained from co-pyrolysis of OS and WC (OS:WC 3:7, 1:1, and 7:3) range in between the ones of individual pyrolysis of OS and WC. The co-pyrolysis of OS and WC also results in oils with enhanced properties. The oil blends of OS:WC result in oil with a lower content of sulfur (0.43-0.82 wt%) and a lower C/H ratio (7.74-8.38), due to the WC properties, while at the same time, a higher content of C (58.52-78.74 wt %), and lower viscosity (17.28-38.79 mPa·s) and density (1.01-1.05 g/cm^3). These combined properties allow the production of pyrolysis oil with properties more similar to the ones of conventional petroleum-derived oils. The refractive index remained almost the same for all OS:WC blends (1.52-1.54).

Table 5. Composition of liquid products from pyrolysis and co-pyrolysis of OS and WC

Blend OS:WC		WC	3:7	1:1	7:3	OS
Viscosity [mPa·s]		51.08	38.79	29.5	17.28	12.30
Density [g/cm^3]		1.06	1.05	1.02	1.01	0.95
Refractive index [n.D.]*		1.52	1.54	1.54	1.53	1.53
Elemental analysis [wt%]	C	58.52	68.27	65.79	78.74	80.64
	H	8.85	8.82	8.48	9.40	9.25
	N	0.35	0.32	0.32	0.28	0.17
	S	0.33	0.43	0.71	0.82	0.85
C/H [wt%/wt%]		6.62	7.74	7.76	8.38	8.72

* Dimensionless

3.5. Liquid products analysis

3.5.1. GC-MS analysis

The GC-MS spectra were obtained for the liquid products from pyrolysis and co-pyrolysis of OS, WC and OS:WC. The Chromatograms obtained using Agilent MassHunter Qualitative Analysis Software are shown in Figure 3, indicating the identified peaks, their abundance, and retention times. At first glance, there is an evident difference between the chromatogram of WC and OS pyrolysis liquid products, with larger peaks for WC at lower retention times (15-25 min), while larger peaks for OS at higher retention times (30-50 min). The co-pyrolysis liquid products OS:WC 3:7, 1:1, and 7:3 have a chromatogram that indicates a combination of the OS and WC chromatograms. Based on the observations a qualitative analysis was made, using the compounds identified by the NIST1.4L library. The selection of the compounds was based on the score given by the MassHunter Qualitative Analysis Software, which is based on the coelution score, which calculates a score based on abundance, peak symmetry, width, and retention time. The selected compounds were chosen if the score was above 70, with an obtained average score of 84.6, 80.2, 78.8, 79.3, and 83.3 for OS:WC 0:1, 3:7, 1:1, 7:3, and 1:0, respectively. Based on a comparison of the score obtained, and a comparison of the parallel runs of liquid products analysis, the compounds with high scores and also detected in both parallel measurements were selected for qualitative analysis. As a result, there were 21, 25, 30, 39, and 42 compounds identified for the OS:WC 0:1, 3:7, 1:1, 7:3,

and 1:0, respectively. It is immediately observed that OS:WC ratios with higher shares of OS had more compounds identified. For all OS:WC ratios, the identified compounds with their chemical formula were organized by abundance and retention time in Figure 4 and Figure 5.
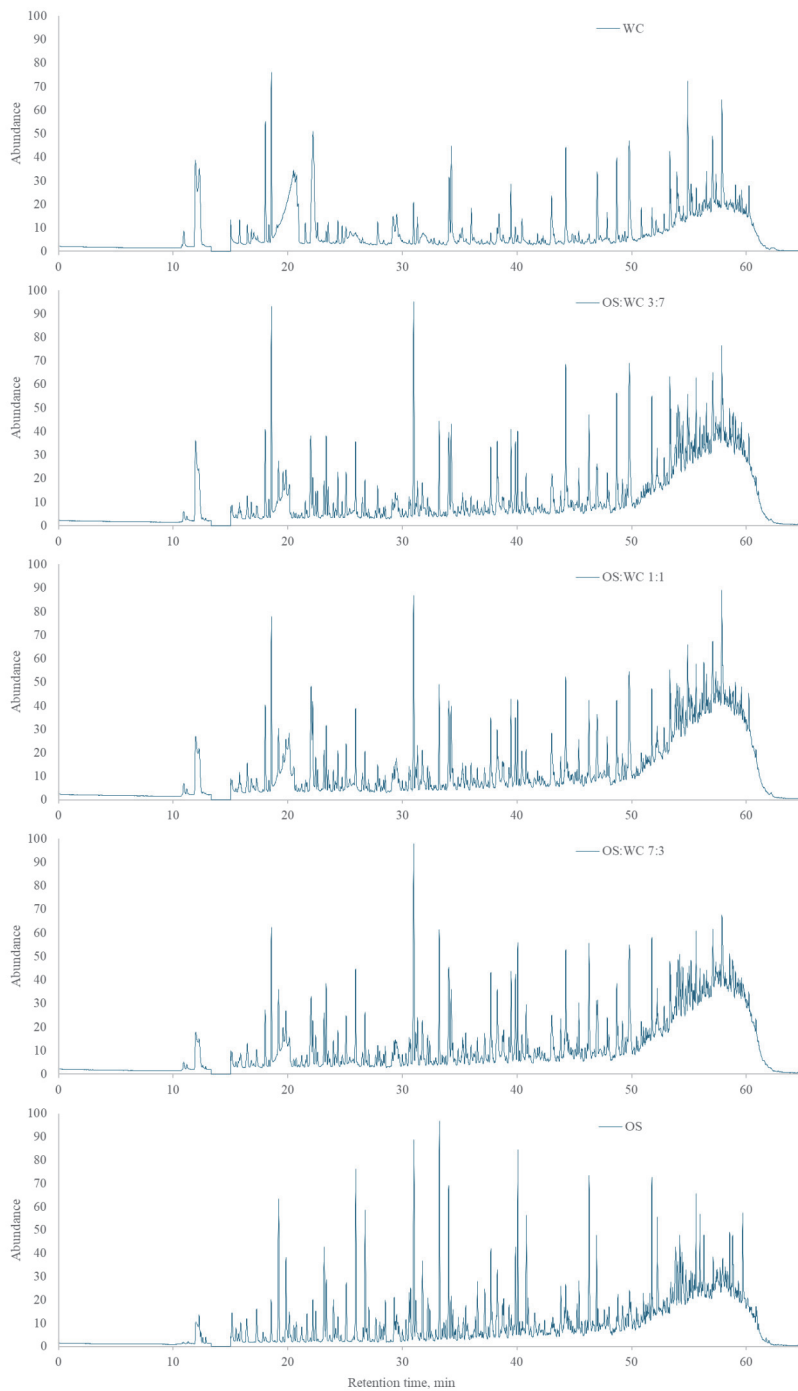

Figure 3. GC-MS chromatogram of liquid products from pyrolysis of OS:WC 0:1, 3:7, 1:1, 7:3 and 1:0

Figure 4 displays the identified compounds for the WC liquid products. Overall, the compounds identified are from Functional groups of ketones, carboxylic acids, siloxanes, aromatic hydrocarbons, aldehydes, phenols, and dihydrobenzenes. Ketones (C=O) and phenols (OH) were the most common groups identified. From the ketone Functional group, some compounds identified include 2-butanone, and cyclic ketones. From the phenol group, the compounds identified include phenol, phenol with two methyl, and phenol with ethyl. Other compounds identified include benzenediols, esters, carboxylic acids, and aldehydes. From the chromatogram of WC, only one aromatic hydrocarbon was identified, toluene. For WC liquid products, most compounds were oxygen-containing compounds, and had a relatively small number of carbon atoms, from C_2 to C_8 analysis. The characterization obtained from GC-MS spectra of WC liquid products agrees with other studies in literature, with a large number of phenols and ketones [38, 64] low molecular-weight oxygenated organic compounds [39, 65–67], and less acidic compounds [68]. However, studies by Yorgun, et.al [39] and Suguraman, et. al [69] identified phenols and ketones, but also aliphatic and aromatic hydrocarbons, such as heavier alkanes and alkenes C_{14} to C_{20}, which were not identified in WC liquid products in the current study. These compounds identified for WC, including cyclic ketones and phenols with multiple substituents, as well as others like benzenediols, esters, and carboxylic acids, contribute to challenges in refining and utilization of the bio-oil. Additionally, the predominance of oxygen-containing compounds can reduce the energy density and overall efficiency as a fuel.

The compounds identified from the OS liquid products (Figure 4) are significantly different than WC liquid compounds. The compounds belong to Functional groups including aromatic hydrocarbons, aliphatic hydrocarbons, aliphatic alcohols, cycloalkanes, polycyclic compounds, phenols, and ketones. Most compounds present in the OS liquid products were aromatic hydrocarbons, aliphatic hydrocarbons, and cycloalkanes. The most abundant were aliphatic hydrocarbons, including, alkenes, alkanes, and alkynes, ranging from C_6 to C_{11}. Some aromatic hydrocarbons identified include benzene, toluene, and o-xylene, ranging from C_6 to C_{11}. Various cycloalkanes were identified from C_6 to C_{12}. Few oxygen-containing compounds were identified, including ketones, phenols, polycyclic compounds, and aliphatic alcohols. Compared to WC, the OS liquid products were composed mostly of compounds with a larger number of carbon atoms, from C_4 to C_{12}, heavier aromatic and aliphatic hydrocarbons, both cycloalkanes and alkenes, and less oxygen-containing compounds. The functional groups identified for the liquid products of OS pyrolysis agree with other studies, with the presence of larger chains [24] of aliphatic and aromatic hydrocarbons including alkenes and alkanes [61], monocyclic and polycyclic hydrocarbons [47]. Similar to the current study, Jiang, et.al [33] found a large proportion of aliphatic hydrocarbons. The abundant aliphatic hydrocarbons, including alkenes, alkanes, and alkynes are an advantage of the shale oil obtained, with great potential for liquid fuel applications. Their high energy density and compatibility with existing infrastructure make shale oil a candidate for meeting energy demands. Moreover, the presence of cycloalkanes enhances its suitability for refining into valuable liquid fuels.
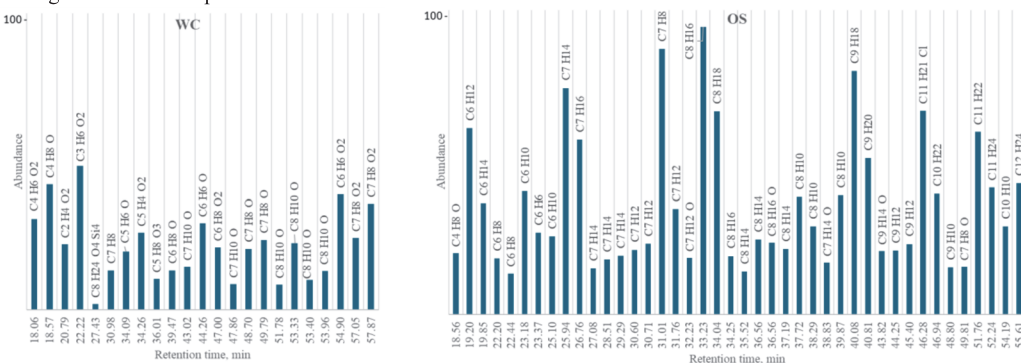

Figure 4. Most abundant compounds in the liquid products of pyrolysis of OS and WC

The compounds identified for the liquid products from co-pyrolysis of OS:WC 3:7, 1:1, and 7:3 are shown in Figure 5. The liquid products of OS:WC blends were mostly composed of compounds from the same Functional groups identified on individual pyrolysis of OS and WC, such as ketones, carboxylic acids, siloxanes, aromatic hydrocarbons, aliphatic hydrocarbons, aldehydes, phenols, and aromatic carboxylic acids. All OS:WC blends containing WC had the same type of compounds identified from the ketones and phenols Functional groups, including 2-butanone, ketones with hydroxyl, cyclic ketones, phenols, phenols with methyl, and phenols with ethyl. As the OS ratio increased, there amount of aromatic and aliphatic hydrocarbons identified increased. From the aromatic hydrocarbons, the compounds identified ranging from C_6 to C_{11} include benzene, ethyl, and methyl with benzene rings and o-xylene. The aliphatic hydrocarbons identified ranging from C_7 to C_{11} include alkenes, alkanes, and alkynes, as well as methyl group alkanes. A comparison of the Functional group distribution of the compounds identified for liquid products from the OS:WC mixture is shown in Table 6.
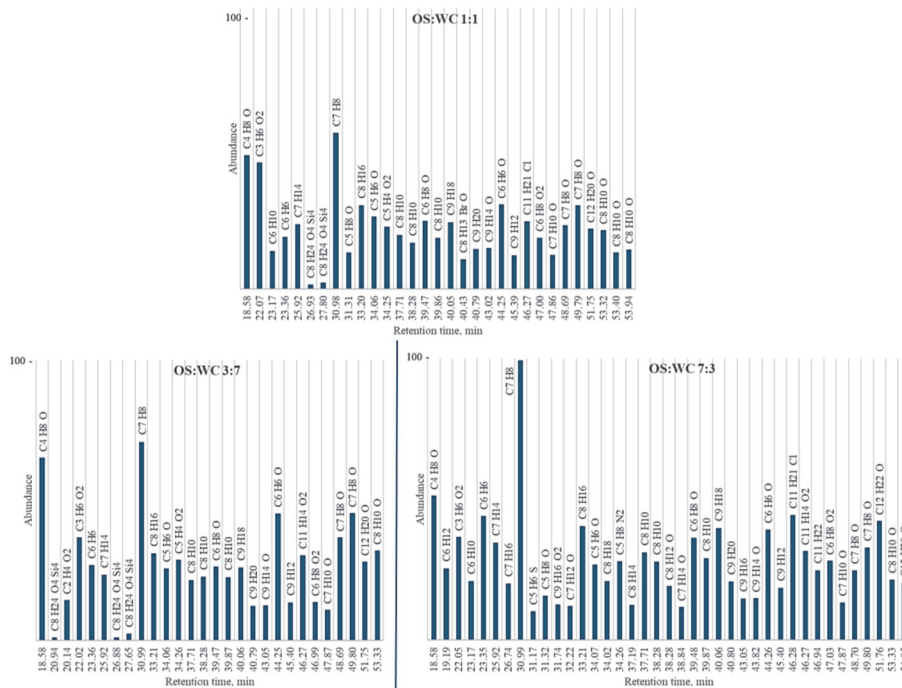
Figure 5. Most abundant compounds in the liquid products of co-pyrolysis of OS:WC 3:7, 1:1, and 7:3

As shown in Table 6, the co-pyrolysis of OS and WC resulted in the production of liquid products with compounds from both OS and WC, including mostly Ketones and Phenols from WC, and aliphatic and aromatic hydrocarbons from OS. Based on this composition, and the yields and composition of the liquid products shown in Figure 2 and Table 5, the co-pyrolysis products appear to be a result of an additive mixture from OS and WC, rather than a synergistic promoting or inhibiting effect. This has also been observed in the co-pyrolysis of *E.Rigida* and OS, where the co-pyrolytic liquid products contained oxygenated and acid-based compounds produced from *E.Rigida*, and hydrocarbons from OS [24]. The co-pyrolysis of OS and Terebinth berries identified a higher share of polycyclic and monocyclic hydrocarbons in OS products than in Terebinth Berries products, resulting in an additive composition for the co-pyrolysis liquid products. Despite the lack of synergistic effects, the co-pyrolysis results in improved liquid products, from the WC side, the addition of OS reduces the production of ketones, which are considered undesirable due to low stability and heating value [33], while the addition of WC to OS decreases the aromatic hydrocarbons. The higher number of oxygenated compounds in WC liquid products is also explained by the larger content of oxygen in WC compared to OS as shown in the elemental composition in Table 1, while more hydrocarbons detected in OS liquid products can be due to the higher content of oxygen and hydrogen in the OS liquids as shown in Table 4. The co-pyrolysis of OS and WC presents an opportunity to make use of the favorable properties of shale oil to enhance the quality of bio-oil. By combining OS and WC, the resulting liquid products benefit from the composition of shale oil, characterized by its abundance of aliphatic hydrocarbons that contribute to the improved properties of the co-pyrolysis liquid products, offering higher energy density, improved stability, and enhanced suitability for various applications, including liquid fuels. The addition of OS to the co-pyrolysis process decreases the presence of oxygenated compounds (with low stability and heating value), thus enhancing the overall quality of the resulting co-pyrolysis oil. Moreover, the reduction in aromatic hydrocarbons present in shale oil, further improves the liquid products, with a reduction of pollutants caused by the combustion of aromatic hydrocarbons.

Table 6. Comparison of Functional Group Distribution in the liquid products of pyrolysis and co-pyrolysis of OS and WC

Functional group	WC	OS:WC 3:7	OS:WC 1:1	OS:WC 7:3	OS
Ketones	8	7	7	6	2
Aromatic Hydrocarbons	1	7	9	9	10
Aliphatic Hydrocarbons	0	5	6	9	19
Phenol	8	6	6	6	1

3.5.2. FTIR analysis

The FTIR spectra of the pyrolysis and co-pyrolysis products of OS and WC are shown in Figure 6. The spectra in Figure 6 are divided by wavenumber sections which indicate the presence of different functional groups. The wavenumber ranges from 3200-3600 cm^{-1} caused by O—H stretching vibrations indicating the presence of phenols, alcohols, and other OH functional groups. Aliphatic hydrocarbons such as alkanes are identified by C—H stretching vibrations in the range of 2800-3000 cm^{-1}, and C—H bending in the range of 1325-1490 cm^{-1}. The peaks present in the range of 1650-1775 cm^{-1} indicate C=O stretching vibration from ketones, esters, and carboxylic acids. The range from 1575 to 1680 cm^{-1} identifies alkenes with C=O stretching. The lower range from 950-1300 cm^{-1} indicates C—O stretching vibrations from alcohols and phenols. Similar to the results obtained from the GC-MS analysis, the IR spectra show a clear difference between the WC and OS liquid products due to the diverse types of compounds produced on the individual pyrolysis of each fuel. The IR spectra are in agreement with the GC-MS results, as for the WC liquid products, the IR peaks are stronger in the 950-1300, 1650-1775, and 3200-3600 cm^{-1}, due to the larger presence of oxygenated compounds, phenols, and ketones. On the other hand, IR spectra of OS liquid products resulted in larger peaks, in the 2800-3000 cm^{-1} range, and more bent peaks 1325-1490 cm^{-1} range due to the larger presence of aliphatic hydrocarbons as also detected by the GC-MS. The co-pyrolysis liquid products resulted in IR spectra with combined characteristics and peaks from the spectra of OS and WC, reiterating the additive behavior of OS and WC co-pyrolysis. Similar results for IR spectra are observed by Kiliç et. al [24], Jiang et.al [33] for OS and biomass co-pyrolysis, and Mozaffari et. al [62] for shale oil pyrolysis.
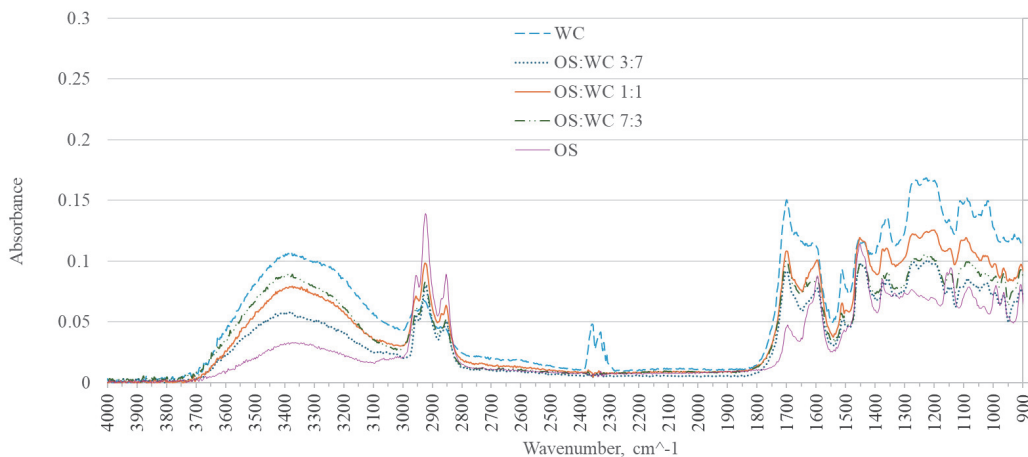

Figure 6. Infrared spectra of the liquid products from pyrolysis and co-pyrolysis of OS and WC

Conclusions

- This work studied the yield and composition of the products from the co-pyrolysis of oil shale and woodchips. The elemental composition of the fuel, solid, and liquid fractions, as well as the functional groups, most relevant organic compounds, and the physicochemical properties of the liquid fraction, were analyzed using GC-MS, FTIR, and other analytical equipment.
- The yields of products, as well as the elemental composition of the liquid and solid fraction, demonstrated an additive behavior in co-pyrolysis, with no synergistic or inhibiting effect in co-pyrolysis. The functional groups present in co-pyrolysis liquid fractions corroborated the additive behavior, with oxygenated compounds derived from biomass bio-oil and aromatic and aliphatic hydrocarbons derived from shale oil.
- Biomass pyrolysis liquid fraction was composed of oxygenated compounds such as ketones and phenols, while shale oil was composed of aromatic, aliphatic hydrocarbons, and cycloalkanes. The co-pyrolytic liquid fraction was composed of an additive mixture of bio-oil and shale oil compounds. The addition of oil shale to biomass resulted in a reduction in oxygenated compounds, while the addition of biomass to oil shale resulted in a reduction in aromatic compounds. Thus, yielding a liquid fraction with enhanced properties, such as higher stability and heating value, for its potential use as a fuel or chemical.
- Future research could involve exploring variations in process parameters such as temperature, residence time, and catalyst usage. Additionally, conducting detailed quantitative analysis of the composition of the liquid fraction, as well as the gaseous fraction. Economic and environmental assessments could help evaluate the feasibility and sustainability of scaling up co-pyrolysis of oil shale and biomass for commercial applications.

Nomenclature:

ATIR   Attenuated Total Reflection
FTIR   Fourier-transform Infrared Spectroscopy
GC-MS   Gas Chromatography/Mass Spectrometry
HHV   Gross Calorific Value
IR   Infrared
LHV   Net Calorific Value
OS   Oil Shale
WC   Woodchips

References

1. Mehmood, M. A., Ye, G., Luo, H., Liu, C., Malik, S., Afzal, I., et al. Pyrolysis and kinetic analyses of Camel grass (Cymbopogon schoenanthus) for bioenergy. *Bioresour. Technol.*, 2017, **228**, 18–24. https://doi.org/10.1016/j.biortech.2016.12.096

2. Antar, M., Lyu, D., Nazari, M., Shah, A., Zhou, X., Smith, D. L. Biomass for a sustainable bioeconomy: An overview of world biomass production and utilization. *Renew. Sustain. Energy Rev.*, 2021, **139**(April 2020), 110691. https://doi.org/10.1016/j.rser.2020.110691

3. Erkiaga, A., Lopez, G., Amutio, M., Bilbao, J., Olazar, M. Influence of operating conditions on the steam gasification of biomass in a conical spouted bed reactor. *Chem. Eng. J.*, 2014, **237**, 259–267. https://doi.org/10.1016/j.cej.2013.10.018

4. Van de Velden, M., Baeyens, J., Brems, A., Janssens, B., Dewil, R. Fundamentals, kinetics and endothermicity of the biomass pyrolysis reaction. *Renew. Energy*, 2010, **35**(1), 232–242. https://doi.org/10.1016/j.renene.2009.04.019

5. Wang, X., Deng, S., Tan, H., Adeosun, A., Vujanović, M., Yang, F., et al. Synergetic effect of sewage sludge and biomass co-pyrolysis: A combined study in thermogravimetric analyzer and a fixed bed reactor. *Energy Convers. Manag.*, 2016, **118**, 399–405. https://doi.org/10.1016/j.enconman.2016.04.014

6. Zhang, L., Xu, C. (Charles), Champagne, P. Overview of recent advances in thermo-chemical conversion of biomass. *Energy Convers. Manag.*, 2010, **51**(5), 969–982. https://doi.org/10.1016/j.enconman.2009.11.038

7. Smołka-Danielowska, D., Jabłońska, M. Chemical and mineral composition of ashes from wood biomass combustion in domestic wood-fired furnaces. *Int. J. Environ. Sci. Technol.*, 2022, **19**(6), 5359–5372. https://doi.org/10.1007/S13762-021-03506-9

8. Demirbas, M. F., Balat, M. Recent advances on the production and utilization trends of bio-fuels: A global perspective. *Energy Convers. Manag.*, 2006, **47**(15–16), 2371–2381. https://doi.org/10.1016/j.enconman.2005.11.014

9. Singh, R. K., Ruj, B. Time and temperature depended fuel gas generation from pyrolysis of real world municipal plastic waste. *Fuel*, 2016, **174**, 164–171. https://doi.org/10.1016/j.fuel.2016.01.049

10. Wang, S., Luo, Z. Pyrolysis of biomass. In: *GREEN Alternative Energy Resources*. Walter de Gruyter GmbH, 2017, 268. https://doi.org/10.1515/9783110369632-001

11. Uddin, M. N., Techato, K., Taweekun, J., Rahman, M. M., Rasul, M. G., Mahlia, T. M. I., et al. An overview of recent developments in biomass pyrolysis technologies. *Energies*, 2018, **11**(11), 3115. https://doi.org/10.3390/en11113115

12. Garcia-Perez, M., Wang, X. S., Shen, J., Rhodes, M. J., Tian, F., Lee, W. J., et al. Fast pyrolysis of oil mallee woody biomass: Effect of temperature on the yield and quality of pyrolysis products. *Ind. Eng. Chem. Res.*, 2008, **47**(6), 1846–1854. https://doi.org/10.1021/ie071497p

13. Igliński, B., Kujawski, W., Kiełkowska, U. Pyrolysis of Waste Biomass: Technical and Process Achievements, and Future Development—A Review. *Energies*, 2023, **16**(4). https://doi.org/10.3390/en16041829

14. Wang, Q., Li, X., Wang, K., Zhu, Y. Commercialization and Challenges for the Next Generation of Biofuels: Biomass Fast Pyrolysis. In: *2010 Asia-Pacific Power and Energy Engineering Conference*. IEEE, 2010, 1–4.

15. Sharifzadeh, M., Sadeqzadeh, M., Guo, M., Borhani, T. N., Murthy Konda, N. V. S. N., Garcia, M. C., et al. The multi-scale challenges of biomass fast pyrolysis and bio-oil upgrading: Review of the state of art and future research directions. *Prog. Energy Combust. Sci.*, 2019, **71**, 1–80. https://doi.org/10.1016/j.pecs.2018.10.006

16. Oil, T. R. S., U.S. Energy Information Administration. *Shale Gas Resources: An Assessment of 137 Shale Formations in 41 Countries Outside the United States*. 2013.

17. Foltin, J. P., Lisboa, A. C. L., De Klerk, A. Oil Shale Pyrolysis: Conversion Dependence of Kinetic Parameters. *Energy and Fuels*, 2017, **31**(7), 6766–6776. https://doi.org/10.1021/acs.energyfuels.7b00578

18. Boak, J. Shale-Hosted Hydrocarbons and Hydraulic Fracturing. In: *Future Energy: Improved, Sustainable and Clean Options for Our Planet*. 2013, 117–143. https://doi.org/10.1016/B978-0-08-099424-6.00006-5

19. Speight, J. G. *Origin and Properties of Oil Shale*. 2012. https://doi.org/10.1016/b978-0-12-401721-4.00001-1

20. Bai, F., Sun, Y., Liu, Y., Li, Q., Guo, M. Thermal and kinetic characteristics of pyrolysis and combustion of three oil shales. *Energy Convers. Manag.*, 2015, **97**, 374–381. https://doi.org/10.1016/j.enconman.2015.03.007

21. Urov, K., Sumberg, A. Characteristic of oil shales and shale-like rocks of known deposits and outcrops. *Oil Shale*, 1999, **16**(3), 1–64.

22. Luik, H., Luik, L., Tiikma, L., Vink, N. Parallels between slow pyrolysis of Estonian oil shale and forest biomass residues. *J. Anal. Appl. Pyrolysis*, 2007, **79**(1-2 SPEC. ISS.), 205–209. https://doi.org/10.1016/j.jaap.2006.12.003

23. Ristic, N. D., Djokic, M. R., Konist, A., Van Geem, K. M., Marin, G. B. Quantitative compositional analysis of Estonian shale oil using comprehensive two dimensional gas chromatography. *Fuel Process. Technol.*, 2017, **167**, 241–249. https://doi.org/10.1016/j.fuproc.2017.07.008

24. Kiliç, M., Pütün, A. E., Uzun, B. B., Pütün, E. Converting of oil shale and biomass into liquid hydrocarbons via pyrolysis. *Energy Convers. Manag.*, 2014, **78**, 461–467. https://doi.org/10.1016/j.enconman.2013.11.002

25. Nazzal, J. M. The influence of grain size on the products yield and shale oil composition from the Pyrolysis of Sultani oil shale. *Energy Convers. Manag.*, 2008, **49**(11), 3278–3286. https://doi.org/10.1016/j.enconman.2008.03.028

26. Jin, Q., Wang, X., Li, S., Mikulčić, H., Bešenić, T., Deng, S., et al. Synergistic effects during co-pyrolysis of biomass and plastic: Gas, tar, soot, char products and thermogravimetric study. *J. Energy Inst.*, 2019, **92**(1), 108–117. https://doi.org/10.1016/j.joei.2017.11.001

27. Ganev, E., Ivanov, B., Vaklieva-Bancheva, N., Kirilova, E., Dzhelil, Y. A multi-objective approach toward optimal design of sustainable integrated biodiesel/diesel supply chain based on first-and second-generation feedstock with solid waste use. *Energies*, 2021, **14**(8). https://doi.org/10.3390/en14082261

28. Chen, B., Han, X., Tong, J., Mu, M., Jiang, X., Wang, S., et al. Studies of fast co-pyrolysis of oil shale and wood in a bubbling fluidized bed. *Energy Convers. Manag.*, 2020, **205**(September 2019), 112356. https://doi.org/10.1016/j.enconman.2019.112356

29. Lyons Cerón, A., Ochieng, R., Sarker, S., Järvik, O., Konist, A. Co-Pyrolysis of Woody Biomass and Oil Shale—A Kinetics and Modelling Study. *Energies*, 2024, **17**(5), 1055.

30. Krerkkaiwan, S., Fushimi, C., Tsutsumi, A., Kuchonthara, P. Synergetic effect during co-pyrolysis/gasification of biomass and sub-bituminous coal. *Fuel Process. Technol.*, 2013, **115**, 11–18. https://doi.org/10.1016/j.fuproc.2013.03.044

31. Chen, B., Han, X., Mu, M., Jiang, X. Studies of the Co-pyrolysis of Oil Shale and Wheat Straw. *Energy and Fuels*, 2017, **31**(7), 6941–6950. https://doi.org/10.1021/acs.energyfuels.7b00871

32. Dai, M., Yu, Z., Fang, S., Ma, X. Behaviors, product characteristics and kinetics of catalytic co-pyrolysis spirulina and oil shale. *Energy Convers. Manag.*, 2019, **192**(March), 1–10. https://doi.org/10.1016/j.enconman.2019.04.032

33. Jiang, H., Deng, S., Chen, J., Zhang, L., Zhang, M., Li, J., et al. Preliminary Study on Copyrolysis of Spent Mushroom Substrate as Biomass and Huadian Oil Shale. *Energy and Fuels*, 2016, **30**(8), 6342–6349. https://doi.org/10.1021/acs.energyfuels.6b01085

34. Ochieng, R., Cerón, A. L., Konist, A., Sarker, S. Experimental and modeling studies of intermediate pyrolysis of wood in a laboratory-scale continuous feed retort reactor. *Bioresour. Technol. Reports*, 2023, **24**(August). https://doi.org/10.1016/j.biteb.2023.101650

35. Cerón, A. L., Konist, A., Lees, H., Järvik, O. Effect of woody biomass gasification process conditions on the composition of the producer gas. *Sustainability (Switzerland)*. 2021. https://doi.org/10.3390/su132111763

36. Lyons Cerón, A., Konist, A. Co-Pyrolysis of Woody Biomass and Oil Shale in a Batch Reactor in CO2, CO2-H2O, and Ar Atmospheres. *Energies*, 2023, **16**(7). https://doi.org/10.3390/en16073145

37. Bridgwater, A. V. Review of fast pyrolysis of biomass and product upgrading. *Biomass and Bioenergy*, 2012, **38**, 68–94. https://doi.org/10.1016/j.biombioe.2011.01.048

38. Özbay, G. Catalytic Pyrolysis of Pine Wood Sawdust to Produce Bio-oil: Effect of Temperature and Catalyst Additives. *J.

Wood Chem. Technol., 2015, **35**(4), 302–313. https://doi.org/10.1080/02773813.2014.958240

39. Yorgun, S., Yildiz, D. Slow pyrolysis of paulownia wood: Effects of pyrolysis parameters on product yields and bio-oil characterization. *J. Anal. Appl. Pyrolysis*, 2015, **114**, 68–78. https://doi.org/10.1016/j.jaap.2015.05.003

40. Demirbas, A. Effect of temperature on pyrolysis products from biomass. *Energy Sources, Part A Recover. Util. Environ. Eff.*, 2007, **29**(4), 329–336. https://doi.org/10.1080/009083190965794

41. Grieco, E., Baldi, G. Analysis and modelling of wood pyrolysis. *Chem. Eng. Sci.*, 2011, **66**(4), 650–660. https://doi.org/10.1016/j.ces.2010.11.018

42. Pistis, A., Tugulu, C., Floris, F., Asquer, C., Scano, E. A. Fast pyrolysis of pine wood at pre-industrial scale: Yields and products chemicalphysical characterisation. *Eur. Biomass Conf. Exhib. Proc.*, 2017, **2017**(25thEUBCE), 1198–1204.

43. Zhou, C., Yang, W. CHARACTERIZATION OF THE PRODUCTS FROM SPRUCE AND PINE SAWDUST PYROLYSIS AT. In: *21st European Biomass Conference and Exhibition*. 2013, 3–7.

44. Ningbo, G., Baoling, L., Aimin, L., Juanjuan, L. Continuous pyrolysis of pine sawdust at different pyrolysis temperatures and solid residence times. *J. Anal. Appl. Pyrolysis*, 2015, **114**, 155–162. https://doi.org/10.1016/j.jaap.2015.05.011

45. Demirbas, M. F. Characterization of bio-oils from spruce wood (Picea orientalis L.) via pyrolysis. *Energy Sources, Part A Recover. Util. Environ. Eff.*, 2010, **32**(10), 909–916. https://doi.org/10.1080/15567030903059970

46. Fagernäs, L., Kuoppala, E., Tiilikkala, K., Oasmaa, A. Chemical composition of birch wood slow pyrolysis products. *Energy and Fuels*, 2012, **26**(2), 1275–1283. https://doi.org/10.1021/ef2018836

47. Yanik, J., Seçim, P., Karakaya, S., Tiikma, L., Luik, H., Krasulina, J., et al. Low-temperature pyrolysis and co-pyrolysis of Göynük oil shale and terebinth berries (Turkey) in an autoclave. *Oil Shale*, 2011, **28**(4), 469–486. https://doi.org/10.3176/oil.2011.4.02

48. Bozoglu, C., Karayildirim, T., Yanik, J. Utilization of products obtained from copyrolysis of oil shale and plastic. *Oil Shale*, 2009, **26**(4), 475–490. https://doi.org/10.3176/oil.2009.4.04

49. Johannes, I., Tiikma, L., Luik, H. Synergy in co-pyrolysis of oil shale and pine sawdust in autoclaves. *J. Anal. Appl. Pyrolysis*, 2013, **104**, 341–352. https://doi.org/10.1016/j.jaap.2013.06.015

50. Li, S., Chen, X., Liu, A., Wang, L., Yu, G. Co-pyrolysis characteristic of biomass and bituminous coal. *Bioresour. Technol.*, 2015, **179**, 414–420. https://doi.org/10.1016/j.biortech.2014.12.025

51. Bai, J., Chen, X., Shao, J., Jia, C., Wang, Q. Study of breakage of main covalent bonds during co-pyrolysis of oil shale and alkaline lignin by TG-FTIR integrated analysis. *J. Energy Inst.*, 2019, **92**(3), 512–522. https://doi.org/10.1016/j.joei.2018.04.007

52. Hu, Z., Ma, X., Li, L. The synergistic effect of co-pyrolysis of oil shale and microalgae to produce syngas. *J. Energy Inst.*, 2016, **89**(3), 447–455. https://doi.org/10.1016/j.joei.2015.02.009

53. Bieniek, A., Jerzak, W., Magdziarz, A. Experimental studies of intermediate pyrolysis of woody and agricultural biomass in a fixed bed reactor. *E3S Web Conf.*, 2021, **323**, 1–6. https://doi.org/10.1051/e3sconf/202132300003

54. Yang, Y., Brammer, J. G., Mahmood, A. S. N., Hornung, A. Intermediate pyrolysis of biomass energy pellets for producing sustainable liquid, gaseous and solid fuels. *Bioresour. Technol.*, 2014, **169**, 794–799. https://doi.org/10.1016/J.BIORTECH.2014.07.044

55. Maaten, B., Järvik, O., Pihl, O., Konist, A., Siirde, A. Oil shale pyrolysis products and the fate of sulfur. *Oil Shale*, 2020, **37**(1), 51–69. https://doi.org/10.3176/oil.2020.1.03

56. Wiedemeier, D. B., Abiven, S., Hockaday, W. C., Keiluweit, M., Kleber, M., Masiello, C. A., et al. Aromaticity and degree of aromatic condensation of char. *Org. Geochem.*, 2015, **78**, 135–143. https://doi.org/10.1016/j.orggeochem.2014.10.002

57. Okoroigwe, E., Li, Z., Stuecken, T., Saffron, C., Onyegegbu, S. Pyrolysis of Gmelina arborea wood for bio-oil/bio-char production: Physical and chemical characterisation of products. *Journal of Applied Sciences*. 2012, 369–374. https://doi.org/10.3923/jas.2012.369.374

58. Lachos-Perez, D., Martins-Vieira, J. C., Missau, J., Anshu, K., Siakpebru, O. K., Thengane, S. K., et al. Review on Biomass Pyrolysis with a Focus on Bio-Oil Upgrading Techniques. *Analytica*, 2023, **4**(2), 182–205. https://doi.org/10.3390/analytica4020015

59. Tinwala, F., Mohanty, P., Parmar, S., Patel, A., Pant, K. K. Intermediate pyrolysis of agro-industrial biomasses in bench-scale

pyrolyser: Product yields and its characterization. *Bioresour. Technol.*, 2015, **188**, 258–264. https://doi.org/10.1016/J.BIORTECH.2015.02.006

60.   Yadykova, A. Y., Ilyin, S. O. Compatibility and rheology of bio-oil blends with light and heavy crude oils. *Fuel*, 2022, **314**, 122761. https://doi.org/10.1016/J.FUEL.2021.122761

61.   Olukcu, N., Yanik, J., Saglam, M., Yuksel, M. Liquefaction of beypazari oil shale by pyrolysis. *J. Anal. Appl. Pyrolysis*, 2002, **64**(1), 29–41. https://doi.org/10.1016/S0165-2370(01)00168-1

62.   Mozaffari, S., Järvik, O., Baird, Z. S. Effect of N2 and CO2 on shale oil from pyrolysis of Estonian oil shale. *Int. J. Coal Prep. Util.*, 2021, **00**(00), 1–15. https://doi.org/10.1080/19392699.2021.1914025

63.   Järvik, O., Oja, V. Molecular weight distributions and average molecular weights of pyrolysis oils from oil shales: Literature data and measurements by size exclusion chromatography (SEC) and atmospheric solids analysis probe mass spectroscopy (ASAP MS) for oils from four different deposits. *Energy and Fuels*, 2017, **31**(1), 328–339. https://doi.org/10.1021/ACS.ENERGYFUELS.6B02452/SUPPL_FILE/EF6B02452_SI_001.PDF

64.   Jin, F., Liu, P., Chen, L., Hua, D., Yi, X. Study on the thermal stability of the bio-oil components by Py-GC/MS. *Energy Reports*, 2023, **9**, 280–288. https://doi.org/10.1016/j.egyr.2023.04.001

65.   Zandersons, J., Dobele, G., Jurkjane, V., Tardenaka, A., Spince, B., Rizhikovs, J., et al. Pyrolysis and smoke formation of grey alder wood depending on the storage time and the content of extractives. *J. Anal. Appl. Pyrolysis*, 2009, **85**(1–2), 163–170. https://doi.org/10.1016/j.jaap.2008.11.036

66.   Zhang, L., Shen, C., Liu, R. GC-MS and FT-IR analysis of the bio-oil with addition of ethyl acetate during storage. *Front. Energy Res.*, 2014, **2**(JAN), 75175. https://doi.org/10.3389/FENRG.2014.00003/BIBTEX

67.   dos Santos, A. L., Lucas, A. N. L., da Mota, I. D. P., Schneider, J. K., Polidoro, A. S., Pinho, A. R., et al. Quantitative GC-MS Analysis of Sawdust Bio-Oil. *J. Braz. Chem. Soc.*, 2023, **34**(11), 1581–1591. https://doi.org/10.21577/0103-5053.20230060

68.   Patra, S. C., Vijay, M., Panda, A. K. Production and characterisation of bio-oil from Gold Mohar (Delonix regia) seed through pyrolysis process. *Int. J. Ambient Energy*, 2017, **38**(8), 788–793. https://doi.org/10.1080/01430750.2016.1222958

69.   Sugumaran, V., Prakash, S., Ramu, E., Arora, A. K., Bansal, V., Kagdiyal, V., et al. Detailed characterization of bio-oil from pyrolysis of non-edible seed-cakes by Fourier Transform Infrared Spectroscopy (FTIR) and gas chromatography mass spectrometry (GC–MS) techniques. *J. Chromatogr. B*, 2017, **1058**, 47–56. https://doi.org/10.1016/J.JCHROMB.2017.05.014

Curriculum vitae

Personal data

Name:	Alejandro Lyons Cerón
Date of birth:	18.12.1992
Place of birth:	Bogota, Colombia
Citizenship:	Colombian

Contact data

E-mail:	allyon@taltech.ee

Education

2020–2024	Tallinn University of Technology, PhD
2018–2020	Tallinn University of Technology, University of Tartu, Materials and processes of sustainable energetics, MSC
2010–2016	Universidad Nacional de Colombia, Mechanical Engineering, BSC
2006–2009	Colegio Anglo Americano, High school

Language competence

English	Fluent
Spanish	Native

Professional employment

2020–…	Tallinn University of Technology, School of Engineering, Department of Energy Technology, early stage researcher

Elulookirjeldus

Isikuandmed
Nimi: Alejandro Lyons Cerón
Sünniaeg: 18.12.1992
Sünnikoht: Bogota, Kolumbia
Kodakondsus: Kolumbialane

Kontaktandmed
E-post: allyon@taltech.ee

Hariduskäik
2020–2024   Tallinn University of Technology, PhD
2018–2020   Tallinn University of Technology, University of Tartu,
                    Materials and processes of sustainable energetics, MSC
2010–2016   Universidad Nacional de Colombia, Mechanical Engineering,
                    BSC
2006–2009   Colegio Anglo Americano, High school

Keelteoskus
Inglise keel   Kõrgtase
Hispaania keel   Emakeel

Teenistuskäik
2020–…   Tallinna Tehnikaülikool, Inseneriteaduskond,
                    Energiatehnoloogia instituut, doktorant-nooremteadur